ZANCO Journal of Pure and Applied Sciences

The official scientific journal of Salahaddin University-Erbil
ZJPAS (2018), 30 (s1); s1-s15
http://dx.doi.org/10.21271/ZJPAS.30.s1.1

Erbil City Household Water Consumption Data Collection Utilizing Smart Metering System

[1]Ali Kattan, [2]Reem A. Alrawi

[1]Information Technology Department, Ishik University, Erbil, Kurdistan Region, Iraq.

[2]Dams & Water Resources Department, College of Engineering, Salahaddin University, Erbil, Kurdistan Region, Iraq

ARTICLE INFO

Article History:
Received:14 /05/2017
Accepted: 12 /04/2018
Published: 01/06/2018

Keywords:
water consumption;
smart metering;
neural networks;
fuzzy systems.

***Corresponding Author:**
Email:
alikattan@hotmail.com

ABSTRACT

Understanding water consumption patterns would offer a viable tool for sustainable development. The accuracy and quality of the collected water consumption data would be vital for the prediction of future water supply demand and thus enabling the planning and development of relevant projects. This paper presents a study of the different factors affecting household water consumption and the diverse methods used to collect and analyze water consumption data. The per capita household water consumption is subject to many factors that include socio-economic aspects, household characteristics, number of occupants, seasonal temperature, humidity and others. The paper also highlights water supply and demand issues related to Erbil City and proposes a design for a household smart metering system that could provide high resolution data to compute the liter per capita. A pilot plant is used to test and verify the designed system functionality and a complementary survey is suggested to provide more relevant data considering other factors. This work represents an important preliminary step for more in depth analysis of water consumption patterns using artificial neural network models and fuzzy inference systems that would serve as tools for decision making.

1. INTRODUCTION

Kurdistan represents the northern part of Iraq having an independent reginal government (KRG) with Erbil City as its capital as shown in Figure 1. Erbil City is about 15,000 km2 with a population of more than 2 million people in7 2015. Springs, streams, rivers and ground water constitute its major water resources .

There are also reservoirs such as Dohuk, Derbandikhan and Dokan. However, rainfall is still considered as the most important water resource. In recent years, the amount of rainfall has decreased and an exaggerated drought conditions resulted from the increased water consumption

due to the expansion in industrial and domestic sectors (Hameed, 2013).

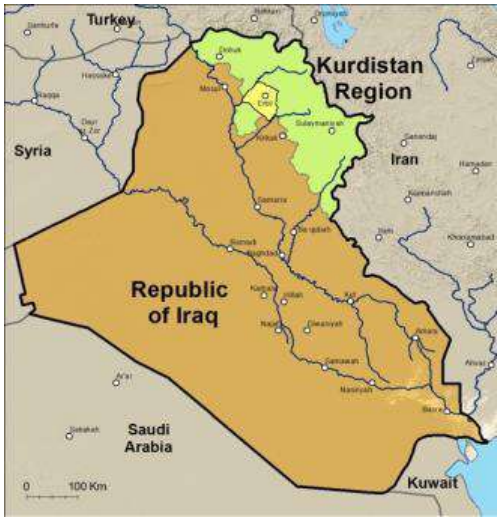

Figure 1. Kurdistan region and the capital of Erbil City

In 2011, a project was financed by the Swedish International Development Cooperation Agency (SIDA) and implemented from mid 2008 to mid 2010 by Erbil's Directorate of Water (DOW) (Andersson and Ryan, 2011). The project aimed to study water management in the city in order to develop sustainable and safe supply of drinking water to the population of Erbil City. A small pilot area in the Kwestan quarter was initially targeted by this project. Creating awareness and eventually reduce water consumption was a major objective of this project but unfortunately, SIDA's report concluded that there was no evidence that such objective was ever achieved. The report attributed this to the lack of an effective tariff system where the current system applies a flat rate tariffs for households that is simply based on the household plant size (m2). In a special issue of the Kurdistan Review (Kudistan Review, 2015), it was indicated that "The KRG Ministry of Planning estimates that individual water usage within the Kurdistan Region is approximately four times higher than the World Bank standard". The article highlighted major issues related to water overuse and declining availability. One of the viable resources for planning future water supply and management projects is the provision of accurate and reliable water consumption data.

Household water consumption represents one of the important sectors that needs more attention as indicated by SIDA (Andersson and Ryan, 2011). In this work, the different factors affecting household water consumption and the diverse methods used to collect and analyze water consumption data are discussed considering examples from other countries. Many of the reviewed data collection and analysis methods would incorporate the use of artificial intelligence (AI) technologies that relies on smart metering devices to provide high resolution data.

Water consumption studies are often domestic and geospatial in nature targeting either a country (Donnelly and Cooley, 2015, Morgenroth, 2014, Shan et al., 2015) or a specific city or region (Otaki et al., 2008, Lu, 2007, Fan et al., 2014, Loh and Coghlan, 2003, Grech, 2014). The overexploitation of water resources would cause breaks in the balance of the ecosystem and eventually result in many environmental problems (Lu, 2007). Due to a large number of interacting parameters, forecasting and predicting water demand cannot be described by using mathematical function since such function would be a very complicated function (Tabesh and Dini, 2009).

Household water supply would meet the four basic human needs; drinking, hygiene, sanitation and cooking. Water consumption is measured in liter "per capita", which is litres/person.day (lpd). The basic water requirements is proposed to be a minimum of 50 lpd noting that more than 70% of the countries worldwide are able to provide just less than 30 lpd (Butler and Memon, 2006). Thus, this work aims to study of the factors influencing household consumption and how to obtain realistic figures about the per capita water consumption targeting the City of Erbil. A smart metering system is presented, which could be utilized by the relevant governing

authorities, such as the DOW, to acquire a more accurate picture of water consumption patterns in the city enabling the better planning of future water supply and management projects.

1.1 Water Consumption Data Collection

There are generally two water consumption data collection methods; estimation methods and direct measurements (Otaki et al., 2008). The former, which is based on surveys and questionnaires, has the disadvantage of not being able to provide the deemed accuracy but has the advantage of relative easiness to obtain the data. The latter method, uses different metering devices to provide accurate data but is criticized that it is relatively expensive due to the cost involved in installing and maintaining such meters in households. Both methods could be used at the same time to provide even more authentic data since domestic water consumption varies based on diverse factors. Such data would consider economic well-being, traditional habits regarding sanitation, availability of freshwater resources, political willingness to improve water efficiency and most importantly the pace of population growth and emerging socio-economic trends providers (Butler and Memon, 2006). Collecting water usage data from variety of sources is an effort exerted by many developed countries, such as the United States, as a continuous effort aiming to improve the efficiency of water use (Donnelly and Cooley, 2015). A more rigorous data collection could target household micro-component consumption. The aim is to scrutinize consumption patterns to understand more deeply the individual uses within a household such as total amount of water used for washing, toilets, laundry, etc. (Butler and Memon, 2006). Thus, the use of metering devices would be recommended for the collection of such high-resolution data. Yet, some other studies would rely only on surveys and questionnaires in order to estimate such micro-components (Otaki et al., 2008). However, and in order to provide some accurate high-resolution data, some smart metering methods were also used such that conducted in Ningxiang County in China (Fan et al., 2014). It considered factors such as household income, number of occupants, the age group and gender of occupants, as well as their level of education in 776 households.

In Europe, a survey-based study that comprised a total of 118 households from Greece and was conducted to address the question of how the water was used within households in Greece and Poland (Shan et al., 2015). The same factors mentioned preciously were considered including psychosocial constructs such as attitudes and beliefs. The results showed a discrepancy in the estimated data from the two counties. This was attributed to existing differences between the two countries in terms of issues related to demographical factors, legislations, and of availability of resources. It is a proof that water consumption is strongly affected by demographic factors.

A larger scale study carried out by the Irish Water targeted a total of 1650 households over a three-month period based on meter readings (Morgenroth, 2014). Similar factors were considered and it was indicated that the analyzed data are not normally distributed and the existing skew in the distribution is attributed to significant heterogeneity existing across households. Results showed an average of about 120 lpd. This would indicate that even within the same demographic area water consumption is affected by other factors. One important outcome of this study concluded that the per capita consumption decreases with increased occupancy, a nonlinear relationship, as shown in Figure 2.

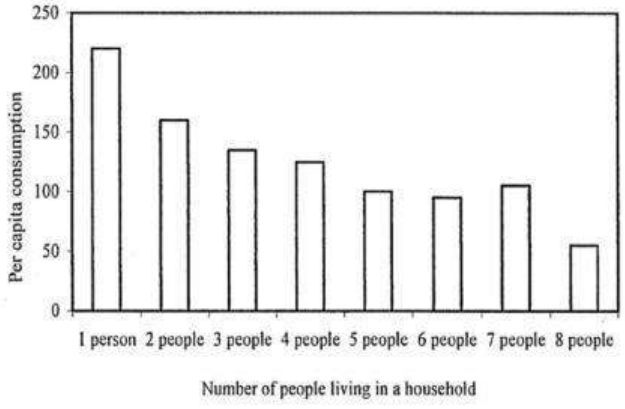

Figure 2. Impact of occupancy on per capita consumption (Butler and Memon, 2006)

Another important factor relevant to the household characteristics is the existence of a garden where households that are characterized by having a garden could constitute of up to 40% of total water consumption especially during the summer season (Butler and Memon, 2006).

Data collection methods pertinent to surveys and/or questionnaires would require further effort to validate the data and the manual entry of such data for further computer-based analysis. A more convenient approach would opt for using digital data collection methods such as the study conducted by the Water Corporation of Western Australia in Perth (Loh and Coghlan, 2003). The study rigorously targeted about 1000 households to determine the major factors and variables affecting water consumption. Two main objectives were identified: data collection of water usage and the identification of water use patterns and trends. Data logging devices (i.e. digital) capable for retaining timing data, total usage and so on were employed. Such data included two basic categories to address consumption: In-house and ex-house. The parameters considered by these two categories are shown in Figure 3.

In addition, the study also used the survey/questionnaires methods to collect data considering many factors such as occupancy, age groups, income, and "socio-economic level" related to the area in which a household is located as well as the household characteristics. The study found that per capita water consumption is around 376 lpd and 350 lpd for detached households and multi-residential houses (flats and apartments) respectively. A summary of all the major factors considered by the studies presented earlier is outlined in Table 1.

The interest in household water consumption within Erbil City is reflected also by some of the postgraduate studies within the Kurdistan Region universities such as that conducted by (Maroof, 2016). Although the proposed system utilizes smart metering, it only accounts for the in-house consumption represented by the amount of water consumed from the reservoir tanks using a water level metering technique. The system connects to a Cloud-based service to monitor water levels in the reservoir tanks of several households but does not account for per capita or any of the other factors stated in Table 1. Hence, estimation was used to label the data collected as the amount of actual water supplied is not considered.

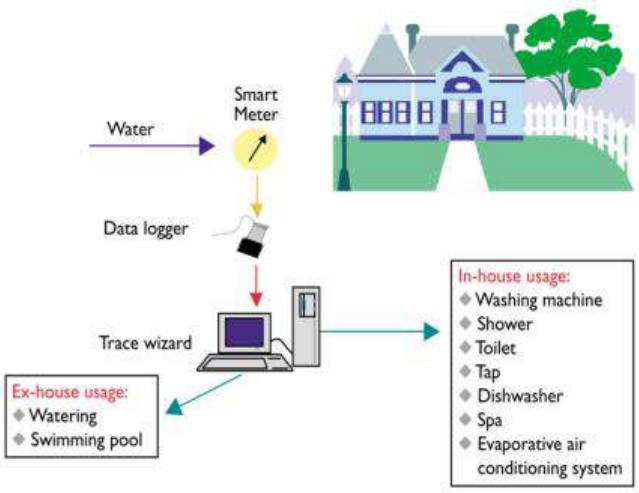

Figure 3. Smart Metering in a Household (Loh and Coghlan, 2003)

Table 1. Summary of Water Consumption Factors Reviewed

Household Factor	Description
Property type	Detached, with garden, non-detached, etc.
Property location	Area & demographic factors
Occupancy	Total number of residents
Occupants' Data	Gender, Age Group, Education, Beliefs/Religion
Household Income	Total monthly income.
Temporal Data / Season	Month, day of week, hour
In-house baths/toilets/showers	Total number
In-house basins/taps	Total number
In-house appliances (total number)	Washing machines, Dishwashers, etc.
In-house cooling/heating	Evaporative air-conditioning systems, water heaters.
Ex-house consumption	Taps, Garden sprinkling systems, swimming pools, etc.
Weather Data	Temperature & Humidity

1.2 Analysis using AI techniques

The provision of high-resolution water consumption data would enable the use of AI techniques such as artificial neural networks (ANN), fuzzy inference systems (FIS) and Adaptive-Neuro Fuzzy Inference System (ANFIS), which is a combination of the former two. Such techniques would be implemented in the last two stages of Figure 4, namely the data processing and analysis to provide feedback for decision making. Such methods would provide an invaluable tool to analyse water consumption trends and patterns to predict and forecast future water consumption.

There are many applications that utilizes ANN targeting decision systems. Such systems would require the use of sets of digital data in order to perform classification or clustering based on their adaptability at modelling nonlinear relationships (Saad and II, 2007). ANN models' implementation techniques are grouped based on the method the model is trained were training methods are either supervised learning or unsupervised learning methods. This depend on the availability of the input data sets whereby a class-label exists. If this is the case then the supervised method is preferred to match the input to the desired label output (Kattan et al., 2011). In the absence of such class-label data the unsupervised method is used to deal with unlabelled data (Zaidi and Rasmani, 2016). Both techniques could be potentially used to categorize water consumption data.

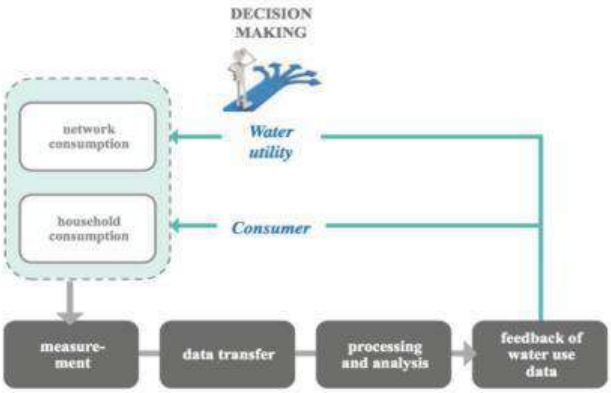

Figure 4. Intelligent water metering system (Loh and Coghlan, 2003)

The iWIDGET project of the European Union aimed for the extraction of useful information from vast amounts of high-resolution consumption data using a supervised training ANN to predict future water consumption (Ribeiroa et al., 2015). Additional statistical techniques were used to add more value to the collected consumption data (Walker et al., 2015). Another example involved using unsupervised ANN learning algorithm, based on Kohonen Self-Organized Maps, to analyze water consumption patterns for a group of household residents in the Greek island of Skiathos (Laspidou et al., 2015). Although ANN approaches were successfully deployed in many water consumption studies, it was indicated that due to the uncertainties that exist with water management problems, the use of FIS would be preferred over the use of ANN since it can be adopted for spatial decision support systems in urban water management (Zaidi and Rasmani, 2016). Fuzzy C-Means (FCM) clustering algorithm was used in the process of classifying excessive water consumption. FIS, like ANN, would also require the availability of consumer data over a time period in terms of days, weeks or months to provide the necessary data sets. A similar approach was used to predict water consumption in the Yelahanka City in the state of Karnataka of India based on climate variables (J and Deka, 2014).

The above techniques could be combined by using ANFIS models offering advantages of both ANN and FIS. Such model provides the "learning" capability and the ability for generalization using ANN and the inferencing rules uses the FIS (Corona-Nakamura et al., 2008). Such system was used in Istanbul City of Turkey for the prediction of future monthly water consumption (Altulkaynak et al., 2005) as well as in in Tehran City of Iran for short-term water demand forecasting (Tabesh and Dini, 2009).

Based on the arguments presented earlier, household water consumption data collection is an essential task that must be undertaken before being able to arrive at the analysis stage from which good predictions, forecasting and decisions could be made. High-resolution data involve the use of smart metering systems to provide accurate digital data sets and the use of questionnaires and surveys would be complementary task that would add more value to data collected.

2. MATERIALS AND METHODS

Due to the intermittent water supply, households in Erbil City make use of reservoir tanks that are usually placed at the household's roof to collect water. The reservoir tanks are mostly cylindrical in shape and made from tin to account for weather conditions, such as the ones shown in Figure 5. The water supply system setup might also include the use of electric water pumps attached to the main household inlet water supply pipe, such as the one shown in Figure 6. This will provide the necessary pressure required to pump water to the reservoir tanks at the roof. The material, size and the number of interconnected reservoir tanks varies from one household to another. However, they are usually identical in shape

and use a float ball type valve for water supply control.

Figure 5. Interconnected tin made reservoir tanks at household roof

Figure 6. Electric water pump installed on the household water supply inlet.

2.1 Modelling the Smart Metering System Operation

Based on the previously described households water supply setup, equation (1) below describes the relation between supplied, collected and consumed water.

$$S(t) = nR_V(t) + C_1(t) + C_2(t) \quad (1)$$

where $S(t)$ represents the supplied water from the household main inlet pipe, R_V is the size of the reservoir tank, n is the total number of interconnected identical tanks, C_1 is the in-house water consumption via the reservoir tanks and C_2 is the ex-house water consumption representing taps existing before the reservoir tanks. These parameters are function of the time period t, representing the accumulated supply & usage values. The proposed smart metering systems model is depicted in Figure (7).

The system makes use of two water flow sensors. The first (wfs1), measures S, the inlet supply water, while the second (wfs2), measures C_1, the consumed water from the reservoir tanks. The cylindrical tank's measurements include the diameter d, and the height h. There will be a free board distance, which is the space kept between the top of water level and the bottom of the roof slab of the water tank. Thus, $'h$ represents the actual tank's height represented by the maximum water level for a full tank. Equation (2) gives the current volume of water in one reservoir tank with g representing the distance measured by the water level sensor (wls) attached to the bottom of the roof slab of the water tank. The sensor should be adjusted so that the reading of g would account for some separation distance from the maximum water level given by $'h$.

Since there is usually one in-house outlet point represented by C_1 but there could be more than one ex-house outlet points represented by taps, it would be more convenient to calculate C_2 as a function of S and C_1 rather installing multiple water flow sensors for each tap. Using equation (1) we can find C_2 as in equation (3)

$$R_V = (\acute{h} - g) * \pi(\tfrac{d}{2})^2 \quad (2)$$

$$C_2 = S - (C_1 + nR_V) \quad (3)$$

The per capita water consumption is given by equation (4)

$$Per\ Capita = \sum_{t=1}^{k}(C_1(t) + C_2(t)) \div P \quad (4)$$

were k is the total number of readings taken per day and P represents the total number of household occupants.

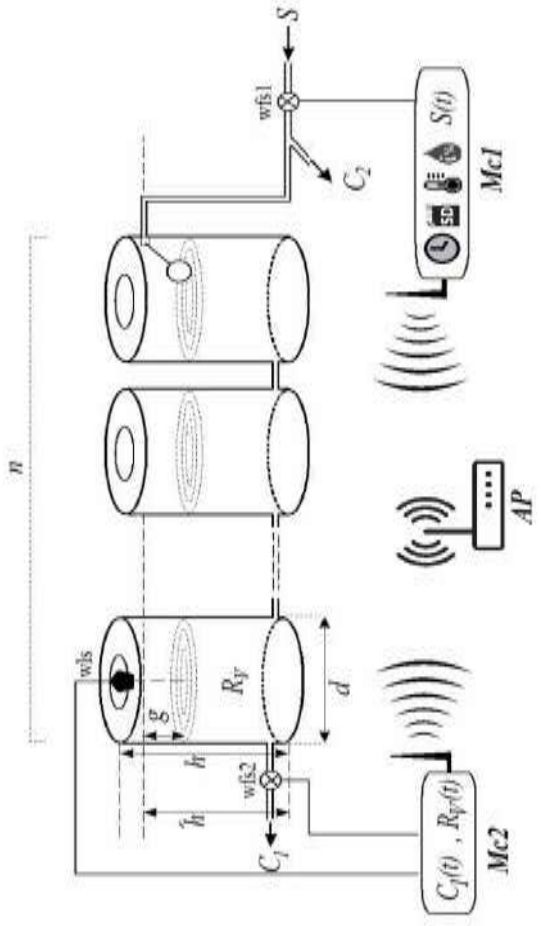

Figure 7. Proposed household smart metering system

Two low powered microcontrollers, *Mc1* and *Mc2* are used in this system. These microcontrollers are equipped with wireless network connectivity with *Mc1* as the master and *Mc2* as the slave. An access point wireless router (*AP*) is utilized to establish the wireless connection between the two. The first microcontroller, namely *Mc1*, uses real-time battery backed clock that would generate interrupts every *t* minutes to acquire the accumulated readings form the sensors including the current value of the supplied water *S*, current humidity and temperature as well as the data recorded by the second *Mc2* slave microcontroller. *Mc2* would make use of the two sensor readings of wls and wfs2 to computes the current volume of water in the reservoir tank R_V and the total in-house consumption C_1 respectively. C_2 would be computed using equation (3) and all logging data are saved as a file entry on the SD memory card of *Mc1*. The sensors readings are then reset to start the computations again for another *t* time period. There will be a total of *k* readings per day and the data logging file would be then closed. Each file represents one day and the per capita could be calculated using equation (4). Time-series data would be provided by the set of files stored in the SD card representing daily usage over a period of time.

The system would be initialized by reading a text-based setup file that is stored on the SD card. This setup file contains the predefined parameters values of *n*, *d*, *'h*, *t*, *k* and *P*. The setup would also include the IP addresses used for the wireless connection of *Mc1* and *Mc2*. The proposed Smart Metering System would use two cooperating control algorithms for the two microcontrollers. As the case with all microcontrollers, the control algorithm is characterized by having a main loop that goes indefinitely to carry out the tasks assigned. Table 2 lists all the parameters involved in the proposed Smart Metering System and Figure 8 gives the algorithms used by the two microcontrollers.

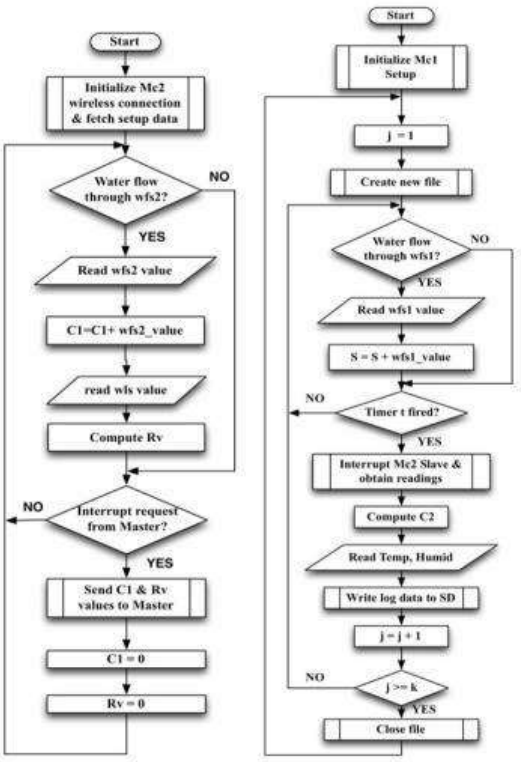

Figure 8. Smart Metering System algorithms for master (right) & slave (left) microcontrollers

Table 2. Smart Metering System Parameters

Factor		Description / Unit
Occupants	P	Total number of people, constant value
Reservoir height & diameter	'h, d	cm (cylindrical), constant value
Total number of reservoirs	n	Interconnected tanks
Total readings per day	k	Total readings per day, constant value (affects t)
Reservoir water level	g	cm as read by the water level sensor
Reservoir water volume	R_V	Current volume (L)
Temporal Date	***tms***	Timestamp data and timer data
Supplied Water Volume	***S***	Inlet water supply (L)
Ex-House Consumption	***C2***	Outlet from taps (L)
In-House Consumption	***C1***	Outlet from reservoir (L)
Temperature	***T***	C^o
Humidity	***H***	%RH

The two algorithms are self-explanatory. The Mc1 algorithm, on right, would create a data logging file per day. The total number of readings is set by k. The interrupt time t is chosen by dividing the total number of minutes per day, i.e. 1440 minutes (i.e. 24 times 60), by the total number of readings required represented by k. In the Mc1 algorithm, j is the counter used to determine when to close the current file and start a new one. The data collected from both Mc1 and Mc2 are stored on the SD card using a (.csv) format file. This format is basically a coma-delimited text file and each line, terminated by CR, represents one log entry. Applications such as MS Excel© and MATLAB© among many others can directly read such files without any modification. The format of each line entry, for a time interval t, would include a time stamp (tms), total supply (S), total in-house consumption (C1), total ex-house (C2), current reservoir tank water volume (nRV), current temperature (T) and current humidity (H).

2.2 PROPOSED COMPLEMENTARY SURVEY

Based on the studies presented previously, it would be recommended to collect some demographics and socio-economic data to complement the digital data obtained. Hence, a complementary survey would be recommended for the actual implementation. The authors, who are themselves residents of Erbil City, opted to consider some of the parameters outlined earlier in Table 1, excluding those that are of socio-economic nature for the time being. The rationale behind this is that at this stage the main goal is to have an accurate figure regarding the person per capita and hence the focus would be on property characteristics, occupancy and the use of some water appliances such as evaporation coolers and heaters. Table 3 lists the recommended data items that the survey should include to augment the digital data collected by the Smart Metering System.

Table 3. Proposed complementary survey data required

Household Factor	Description
Property type	With / Without Garden
Property location	Area & Quarter
Property plant size	In m2
Occupancy	Total number of residents
Occupants' Data	Total number of adults, children (<15) & senior (>65)
In-house cooling/heating	Total heaters/air coolers

2.3 PILOT PLANT IMPLEMENTATION

A pilot plant is constructed to verify the functionality of the proposed Smart Metering System presented in the previous section. The algorithms were written using standard Arduino V1.65 and testing was carried out using serial output interface (via USB) that would generate output from the microcontroller to the connected computer screen. The pilot plant is based on the model presented earlier and shown in Figure 7. However, a smaller scale is considered in what regards to the overall water volume used by the system. A snapshot of the pilot plant implemented is shown in Figure 9 were the system utilizes small plastic containers with rubber tubes to simulate household setup. The major system components used for the implementation of this pilot plant are shown in Figure 10 (numbered from 1 to 8). In this figure, a pen is shown next to the photo of each component to give a sense of each component size. The electronic circuit of both controllers are placed in a plastic housing enclosure at the back the system shown in Figure 9. Each controller was assigned a static IP address, and the connection was established by the access point wireless router. The wireless router used is capable of 3G Internet connectivity. However, only WiFi local wireless mode was used to test the system in this pilot plant by creating a password free local wireless network to simply implementation.

It is worth to mention that the components used to build the system are relatively cheap and available commercially from many online shopping websites. All the components shown in Figure 10, apart from component 3 and 8 are the same ones to use for an actual household implementation. Component 3, the ½“ plastic water flow sensor, would be replaced by the ½” copper water flow sensors adhering to ROHS testing standards since the latter would bear

more water pressure for an actual installation in a household. Component 8 is the pilot plant plastic setup utilizing rubber tubes and DC water pump, would not be required as these are merely used for simulation. A small modification was carried on component 4 of Figure 10, the data logger shield with real-time clock, whereby a more powerful battery was used to support the real-time clock circuitry. Considering that this is a pilot plant implementation, both microcontrollers are powered using 5v DC power supplies. An actual implementation would consider the use of power units equipped with rechargeable batteries for both microcontrollers and the wireless access point to account for any power interruption.

The setup file of the master microcontroller was initialized with n=1, d=16cm, 'h=25cm, t=60s, k=15 and P=1. These values are proposed only for simulation and thus the t time period was set to a lower value of one minute with k set to 15 so that each experiment would last for 15 minutes only. Testing involved starting the system and using pre-measured volumes of water in a bucket that was placed under the system whereby the electric pump is used to supply the system. The process of consumption was simulated by opening the outlets from valves representing C1 and C2 to a discharge tank used to collect the water. This tank is shown at the base of the pilot plant snapshot of Figure 9 to the left of the water pump.

The water level sensor, wls, would account for a small free board distance of 2cm and also a safety distance of 1.5cm so that water does not touch the sensor's circuit. This was reflected in the program used to read data from this wls whereby suitable calculations are considered to adjust the read values. A similar technique is to be used for an actual implementation.

3. RESULTS & DISCUSSION

The system is started by starting the wireless router first and then powering up both microcontrollers. The connection between the two was established after a short dely. After conducting multiple simulations for water supply and consumption on the pilot plant, the resultant data files on the SD card were checked. Having all the data items in each entry of a log file would indicate successful readings form sensors and successful network connection between the two microcontrollers. These values are then compared to the actual volumes of water used for the supply and the those collected in the discharge tank.

Verification based on the records obtained from several cases by pumping and consuming varied amounts of water and compare the amount pumped/consumed with the obtained readings. Generally, all the readings were very consistent but exhibits some error in the range of 3% to 9% between the actual volumes and those recorded by the Smart Metering System. Other readings involving temperature and humidity were accurate reflecting the conditions of the room for which the pilot plant was tested. The overall size of each file is relatively very small in comparison to the storage capacity of the SD card used.

As indicated by the sensors' manufacturer data sheets, there might be a 5% error associated with the sensor's readings. Some of the other factors contributing to errors is that the plastic reservoir tank used for the pilot plant does not have an optimal cylindrical shape. A discrepancy between the proposed model and the designed pilot plant. The results obtained from the pilot plant are consistent and are considered acceptable. This is consistent with results obtained from other studies utilizing digital data and AI for water consumption data processing where it was stated that if the error is in terms of 10% or less then this is

practically acceptable (Altulkaynak et al., 2005, Zaidi and Rasmani, 2016).

The proposed Smart Metering System household water consumption would offer relatively high resolution data for the hourly water consumption and enable the collection of time-series readings over an extended period of time. For an actual implementation, the use of more accurate sensors would be recommended to reduce the overall error to a marginal value. However, this would probably incur higher cost. It should be also noted that in the case of actual implementation another problem would surface; leakages. The overall consumed water might not reflect the actual total consumed water if such leakages exist in the household. However, the proposed system could give an indication for such leakages based on comparisons against data collected from other households with similar household characteristics and occupancy. The design could be extended further to include more microcontrollers to account for micro-component readings and as discussed in the literature review section. More water flow sensors would be installed around the household to account for each micro-component such washing machines, showers, toilets, kitchen sinks, etc.

Some of the other anticipated problems are related to wireless connectivity between the two devices. In an actual implementation, the wireless signal power could be affected by range and the existence of many obstacles in between the units since the first would be usually near to the household entrance, while the second would be on the household's roof near the reservoir tanks. This issue is non-existent with the current pilot plant presented in this work since all the units are adjacent to each other making the wireless signal the strongest. The proposed pilot plant relied only on the WiFi connectivity without using the 3G internet feature of this router. It would be interesting to use 3G internet connectivity to connect the microcontrollers as such feature as it would not only solve the wireless signal power issue but also offers Cloud connectivity providing direct Internet access to the system data and parameters.

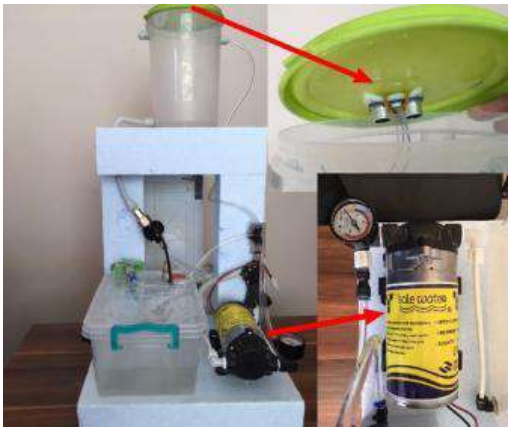

Figure 9. Pilot Plant of the Smart Metering System

2) ReadBearLab CC3200 Dual core MCU with Antenna (Mc2).

1) RealTek Ameba RTL8195 Arduino Wireless Board with Antenna (Mc1).

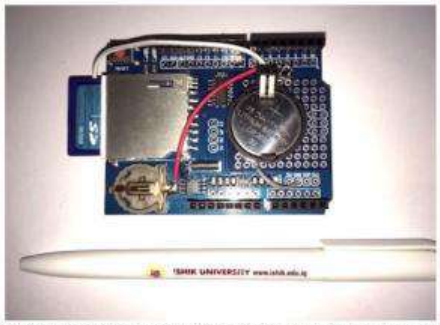

4) Gikfun Data Logger for Arduino Data Logging Shield EK1439 with 2GB SD card (Mc1)

3) ½" Plastic Water Flow Sensor, Model: YF-S201, NPS Threaded (x2). (wfs1 and wfs2 for Mc1 and Mc2 respectively).

6) Ultrasonic Module HC-SR04 (Mc2)

5) Smakn HT21 AM2301 Digital Temperature Humidity Sensor module Arduino (Mc1)

8) System simulation using a set of plastic containers, rubber tubes, valves with small 12v DC water pump with AC-DC adapter.

7) EnGenius 3G Wireless Router ESR6650. Represents the AP used to establish the wireless connection between the two microcontrollers.

Figure 10. Pilot plant components

4. CONCLUSION

The quality and accuracy of the collected household water consumption data would be vital for the prediction of future water supply demand and thus enabling the planning and development of relevant projects. This paper presented a proposed Smart Metering System for Erbil City households considering the common water supply setups used in households around the city. The system would collect time-series data with different parameters to compute the per capita value for several readings throughout the day. The microcontrollers were programmed using cooperating algorithms to achieve its goal. The system setup is relatively simple requiring only the installation of the water flow sensor on the household's water supply inlet and reservoir tanks outlet. However, the proposed design does not account for errors that could result from leakages and water evaporation during summer season. Considering that the aim of this work is to provide essential time-series data, the proposed design in this work would be sufficient since the overall error is acceptable as stated by other studies. The proposed complementary survey would collect additional data to add value to the overall data collected.

The system could be improved potentially by connecting it to the Internet and utilizing a Cloud-based application to obtain the readings from multiple households with multiple sensor readings without the need to collect the stored data manually by retrieving it from the SD cards. A Cloud-based application could also incorporate data processing and analysis further to study consumption patterns and trends making use of appropriate ANN, FIS and ANFIS models for decision making output. The first author is on the process of developing such system making use of Cloud service.

ACKNOWLEDGMENT

The first author would like to thank the following students of the 4th year Information Technology Department of Ishik University for assembling and building the pilot plant piping system and containers used for this experiment. These students are, in random order, Ms. Samiha Osama, Mrs. Mariam Bakhtyre, Ms. Avin Saeed, Mr. Alan Saleh and Mr. Rebin Tahsin.

REFERENCES

ALTULKAYNAK, A., ÖZGER, M. & ÇAKMAKCI, M. 2005. Water Consumption Prediction of Istanbul City by Using Fuzzy Logic Approach. Water Resources Management, 19, 641-654.

ANDERSSON, B. & RYAN, T. 2011. Evaluation of the Water Network Management Programme in Erbil, Iraqi Kurdistan, Final Report. Sida Review 2011:5 ed.

BUTLER, D. & MEMON, F. A. 2006. Water Demand Management, London, UK, IWA Publishing.

CORONA-NAKAMURA, M. A., RUELAS, R., OJEDA-MAGANA, B. & ANDINA, D. Classification of domestic water consumption using an Anfis model. 2008 World Automation Congress, 2008 Waikoloa, HI, USA. IEEE, 1-9.

DONNELLY, K. & COOLEY, H. 2015. Water Use Trends in the United States. Pacific Institute.

FAN, L., WANG, F., LIU, G., YANG, X. & QIN, W. 2014. Public Perception of Water Consumption and Its Effects on Water Conservation Behavior. Water, 6, 1771-1784.

GRECH, A. 2014. Household water consumption in the Maltese islands : an analytical study. M.Sc., University of Malta.

HAMEED, H. M. 2013. Water harvesting in Erbil Governorate, Kurdistan region, Iraq Detection of suitable sites using Geographic Information System and Remote Sensing. M.Sc., Lund University.

J, S. H. & DEKA, P. C. 2014. Development of a Fuzzy Logic Based Model using different Membership and Rules criteria for predicting water consumption using Climatic variables. International Journal of Scientific & Engineering Research, 5, 1293-1301.

KATTAN, A., ABDULLAH, R. & GEEM, Z. W. 2011. Artificial Neural Network Training & Software Implementation Techniques, USA, Nova Science Publishers Inc.

KUDISTAN REVIEW 2015. Agriculture & Water. Kurdistan Review - Special Issue 2015. Erbil: Invest in Group

LASPIDOU, C., PAPAGEORGIOU, E., KOKKINOS, K., SAHU, S., GUPTA, A. & TASSIULAS, L. 2015. Exploring patterns in water consumption by clustering. Elsevier Procedia Engineering, 119, 1439-1446.

LOH, M. & COGHLAN, P. 2003. Domestic Water Use Study In Perth, Western Australia 1998-2001.

LU, T. 2007. Research of domestic water consumption: a field study in Harbin, China. M.Sc., Loughborough University.

MAROOF, H. H. 2016. Water Level Estimation & Monitoring System in Erbil City. M.Sc., University of Kurdistan Hewler.

MORGENROTH, E. 2014. Final Report on Household Water Consumption Estimates. Irland: Economic and Social Research Institute.

OTAKI, Y., OTAKI, M., PENGCHAI, P., OHTA, Y. & ARAMAKI, T. 2008. Micro-components survey of residential indoor water consumption in Chiang Mai. Drinking Water Engineering and Science, 1, 17-25.

RIBEIROA, R., LOUREIROA, D. L., BARATEIROA, J., SMITHB, J. R., REBELOA, M., KOSSIERISC, P., GERAKOPOULOUC, P., MAKROPOULOSC, C., VIEIRAA, P. & MANSFIELD, L. 2015. Framework for technical evaluation of decision support systems based on water smart metering: the iWIDGET case. Elsevier Procedia Engineering, 119, 1348-1355.

SAAD, E. W. & II, D. C. W. 2007. Neural network explanation using inversion. Neural Networks, 20, 78-93.

SHAN, Y., YANG, L., PERREN, K. & ZHANG, Y. 2015. Household Water Consumption: Insight from a Survey in Greece and Poland. Elsevier Procedia Engineering, 119, 1409-1418.

TABESH, M. & DINI, M. 2009. Fuzzy and Neuro-Fuzzy Models for Short-Term Water Demand Forecasting in Tehran. Iranian Journal of Science & Technology, Transaction B, Engineering, 33, 66-77.

WALKER, D., CREACO, E., VAMVAKERIDOU-LYROUDIA, L., FARMANI, R., KAPELAN, Z. &´, D. S. 2015. Forecasting Domestic Water Consumption from Smart Meter Readings using Statistical Methods and Artificial Neural Networks. Elsevier Procedia Engineering, 119, 1419-1428.

ZAIDI, A. Z. & RASMANI, K. A. 2016. Classification of excessive domestic water consumption using Fuzzy Clustering Method. Journal of Physics: Conference Series, 738.

ZANCO Journal of Pure and Applied Sciences
The official scientific journal of Salahaddin University-Erbil
ZJPAS (2018) **30**(s1) s16-s23
http://dx.doi.org/10.21271/ZJPAS.30.s1.2

Simulation of Downpull Forces of Leaf Gate in High Dams

Bashir Thabit Mohammed*

*Professor in Department of Dam and Water Resources Engineering, College of Engineering, Salahaddin University-Erbil

Binahi Mohammad Amin Said Ali**

**Lecturer in Department of Dam and Water Resources Engineering, College of Engineering, Salahaddin University-Erbil

ARTICLE INFO

Article History:
Received: 14/05/2017
Accepted: 12/04/2018
Published:01/06/2018

Keywords:
downpull forces
turbulence model
ANSYS fluent
piezometric head

**Corresponding Author:*
Email: alkadibashir@hotmail.com
Email: binahimuhamad@yahoo.com

ABSTRACT

The downpull forces on high head leaf gates due to underflow conditions are of paramount importance in the design of gate hoist, especially during opening and closing operation. Hence, there is a need to enrich the concept of estimating the hydrodynamic forces caused by the deflection of streamlines along the bottom side of the gate. In this research, bottom downpull force coefficient of leaf gate in high dams was estimated by the solution of two dimensional Navier-Stokes equations using standard k-ε turbulence model. The equations were solved by ANSYS FLUENT software using finite volume techniques. Experimental investigations in the hydraulic laboratory in College of Engineering/ University of Salahaddin were also conducted so as to calibrate and verify the numerical results. The evaluated model was used to predict the distributions of the piezometric head on the inclined gate lip surface, top and bottom tunnel walls, and predict the distributions of bottom downpull coefficient in the gate lip considering the effects of many geometric and hydraulic parameters.

INTRODUCTION

Vertical lift gates are among the most widely used high head gates for flow regulation or emergency closure of large outlets and conduit. One case of gates is the tunnel- leaf gate which goes through a gate shaft located within the tunnel conduit. Nevertheless, it may be subjected to large downpull forces that are resulting from two military units, one resulting from the flow passing over the top gate surface through the upstream and downstream gate clearances, whereas the other results from pressure exerted on the bottom gate surface by the flow issuing beneath the gate. The resulting pressure difference between the top and bottom induces an unbalanced force which may be in the down wards direction, known as the hydraulic downpull, or in the upward direction termed negative downpull or uplift force. Because of magnitude of downpull force that affects by the design of the gate-hoisting equipment. Its prediction is of major importance to hydraulic engineering and designers. And severe vibration as a consequence of high velocity fluid around the gate lip and low pressure due to suction

induced by high momentum fluid downstream of the control section,(Aydin ,2002).

Many surveys are taken to find the magnitude of downpull and looked into some relevant parameters. A linear figure that can be utilized for estimating downpull force acting on high head leaf gate taking into account the issue of flow parameters and boundary geometry on it,(Naudascher et.al,1964). An experimental model study was directed on a 3-leaf powerhouse intake gate system for TVA'S Melton Hill Dam and conducted to develop a gate design that would effectively shut off the turbine flow for all discharges up to 5700cfs. Tests on five proposed gate lip shapes and on nine other basic shapes failed to produce a satisfactory gate design. The reasons were of excessively large hydraulic force included with the lip forms, oscillation of the gate during closure and, in several of the designs, failure of the leaves to close. The tests finally led to the development of an acceptable design, (Elder and Jack ,1964)(quoted in Al-Kadi 1997). A model study of hydraulic downpull on a high – leaf gate for powerhouse emergency closure was conducted. The downpull forces were measured while the initial discharge, the gate closure speed, the gate slot head wall geometry, and the bottom shape of the gate were varied. The downpull on the top and bottom beams of the gate with eight bottom shapes and the discharge rating of the gate were presented in a generalized form for use in the design of similar gates. Another result was that a properly designed head wall minimized the downpull on the top seal of the gate,(Smith ,1964) (cited in Al-kadi ,1997)..

General studies were made to determine design parameters for hydraulic downpull on downstream seal, roller-mounted gates located in entrance transition of large conduits. Data were presented in both dimensional and non-dimensional form on the effects of gate leaf and gate shaft geometry and on air vent size. The results indicated a maximum downpull force about (710 kips) would occur during the emergency closure of the gates if free discharge conditions occur in the downstream gate frame, (Murray and Simmons, 1966). A random hydraulic model was constructed to investigate the effect of fourteen gate lip shapes on the value of downpull force. The study included the investigation of the effect of the gap width ratio and gate lip geometry on the magnitude of top downpull coefficient. The results indicate that the top downpull coefficient was sensitive to the change in gap width ratio but not changes with gate lip geometry. On the other hand, the bottom downpull coefficient was influenced effectively by the gate lip geometry, (Ahmed ,1999). The effect of downpull on tunnel type-high head gate using a hydraulic model was investigated, According to the tail water conditions free surface flow and submerged flow have occurred, (Drobir et.al.,2001).

In the present study, the water flow controlled by leaf gate in dams under high pressure had been modeled using “FLUENT” software to estimate the bottom downpull force coefficient on the gate lip. The model was calibrated and verified using laboratory results.

2.THEORETICAL CONSIDERATIONS

2.1. Hydraulic Downpull Force

The downpull force is influenced by various parameters, which may be classified into three groups, (Sagar ,1978). The first group: The flow characteristics which include the operating head on the gate flow conditions which contain whether free or submerged flow exists and aeration downstream the gate. The second group: Includes the flow properties such as the specific weight of water, dynamic viscosity, and vapor pressure. The third group: Is the geometry of gate installation, including conduit height upstream the gate shaft, gate opening, gate thickness, gate shaft dimensions, angle inclinations of gate bottom with horizontal, geometry of other lip shapes, and

location and thickness of the skin plate. See Figs. (1) and (2) (Sagar, 1978).

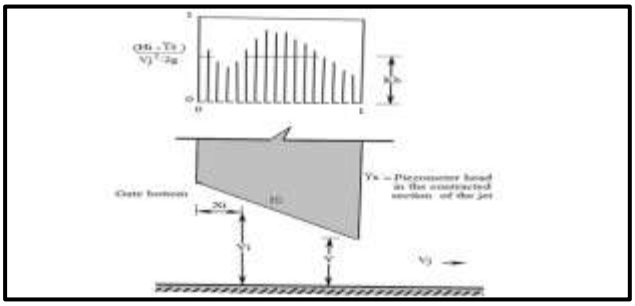

Fig.1.Definition sketch for k_b

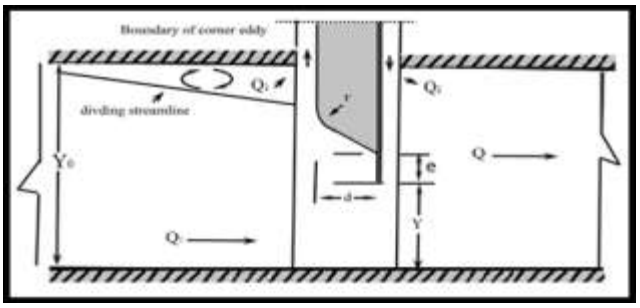

Fig.2.Geometric configurations

2.2. Bottom Downpull Coefficient

The bottom downpull coefficient can be estimated as follows :

$$k_b = \frac{H_i - Y_s}{\frac{v_j^2}{2g}} \qquad (1)$$

And $\frac{v_j^2}{2g} = H_u - Y_s + \frac{v_\circ^2}{2g}$

Where: H_i = Piezometric head at specific points on the bottom surface of gate,

Y_s = Piezometric head downstream the gate at contracted jet,

V_j =Velocity of the contracted jet issuing from underneath the gate, which is obtained from the results of model,

H_u= Piezometric head upstream of the gate, and

$V_\circ$ = Average velocity of the flow in the conduit upstream the gate, (Naudascher ,1964).

2.3. Governing Equations

2.3.1.The standard K-Epsilon model

The model is based on the solution of two transport equations, namely one equation for the turbulence kinetic energy k and one for the rate of dissipation of turbulence energy ε these equations are solved simultaneously with other governing equations of fluid motion. The standard form of the model is applicable to high Reynolds number flows where the effect of molecular viscosity is negligible. The model also provides good economy and reasonable accuracy for a wide range of turbulence flows, (Launder and Spalding, 1974).

The equations for k and ε are written as :

k- Equation

$$\rho\frac{Dk}{Dt} = \frac{\partial}{\partial x_i}\left[(\mu + \frac{\mu_t}{\sigma_k})\frac{\partial k}{\partial x_i}\right] + P_k - \rho\varepsilon \qquad (2)$$

ε- Equation

$$\rho\frac{D\varepsilon}{Dt} = \frac{\partial}{\partial x_i}\left[(\mu + \frac{\mu_t}{\sigma_\varepsilon})\frac{\partial \varepsilon}{\partial x_i}\right] + C_{1\varepsilon}\frac{\varepsilon}{k}P_k - C_{2\varepsilon}\rho\frac{\varepsilon^2}{k} \qquad (3)$$

Where:c_1, c_2, σ_k and σ_ε are constants. The term is the generation of turbulence kinetic energy k due to the interaction between the Reynolds stresses and mean velocity gradients, which can be written as:

$$P_k = -\rho\overline{\acute{u}_i\acute{u}_j}\frac{\partial U_i}{\partial x_j} \qquad (4)$$

Since

$$\tau_{ij} = \mu e_{ij} \qquad (5)$$

Where: $\mu =$ the laminar viscosity and $e_{ij} = \left(\frac{\partial U_i}{\partial x_j} + \frac{\partial U_j}{\partial x_i}\right)$ is the rate of strain tensor.

Substituting Eq. (5) into Eq. (4), yields

$$P_k = \mu_t\frac{\partial U_i}{\partial x_j}\left(\frac{\partial U_i}{\partial x_j} + \frac{\partial U_j}{\partial x_i}\right) \qquad (6)$$

The model uses Eq. (6) to determine the eddy-viscosity(μ_t). The standard k-ε model employs values for the constants that are arrived at by comprehensive data fitting for a

$C_\mu = 0.09;\ \sigma_k = 1;\ \sigma_\varepsilon = 1.3;\ C_{1\varepsilon} = 1.44;\ C_{2\varepsilon} = 1.92$, (Piradeepan, 2002).

2.3.2.Setting Boundary Data for the Present CFD Analysis

Appropriate condition must be specified at domain boundaries depending on the nature of the flow. In the simulation performed in the present study

1. Inlet boundary: inlet boundary condition is specified pressure; the distribution of pressure inlet values is taken from experimental study.

2. Outlet boundaries: outlet boundary conditions its defined Outlet pressure with a known value.

3. Wall boundaries: the solid boundaries of the fluid domain are defined as smooth and non-slip walls. Non-slip wall is the most common type of wall boundary condition implementation, in which the fluid immediately next to the wall assumes the velocity of the wall, which is zero by default (ANSYS Help, 2011). The interior cell zones are defined as a fluid and the faces of gate are taken to be interior wall boundaries, see Fig (3) and (4).

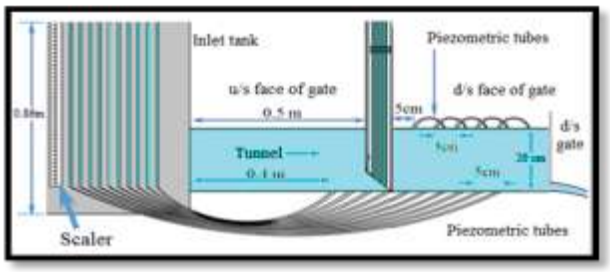

Fig (3): General sketch of the tunnel.

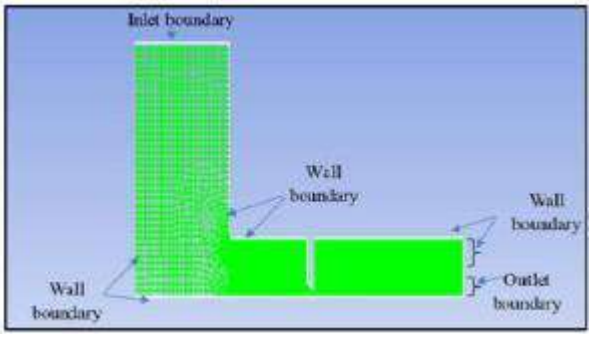

Fig (4): Boundary condition of mesh

3.EXPERIMENTAL WORK AND EQUIPMENT

The inlet tank was manufactured from Perspex sheets had one tunnel had square cross section 0.2×0.2 m with 1.5m length. The end of the tunnel was provided by a slide gate to control the flow condition. Fifteen piezometric tubes with 6mm diameter were fixed at several locations along the center line of the top and bottom of the tunnel with 5cm interval. Five of them were fixed on the top of the tunnel at a distance 5cm from the downstream face of the gate and the other were fixed in the bottom at a distance 40cm from the upstream end of the tunnel. All piezometric tubes were fixed on the side inlet tank with a metric scale. This tunnel was connected to the inlet tank has 0.86m height with a square cross section bed of 0.61m×0.61m. The gate was manufactured, 5cm thickness, and 20cm width with 45^o inclined lip angle. It was located at a distance 0.5m from the tank. Two rows of piezometric tube, with 4mm diameter and 2.5cm away from the center line were fixed on the gate lip. Each row had four piezometers with 12mm interval. The first piezometer was fixed at 6mm from the vertical upstream face of the gate. All piezometers were 12mm apart. Three pumps were set up near the tunnel to feed the tunnel from the pipe via the inlet tank into the sump tank. Details of the experimental are shown in fig (5) and Photo. (1). the flow rate that passing via the tunnel was measured using volumetric flow rate tank. At the beginning of experiment, both the two gates were closed (model gate and d/s gate). The water started to be circulated by three pumps to feed the tunnel by inlet tank. The gate was opened gradually at a certain height. After a sufficient operating time, in order to gain fully submerged condition, the d/s gate would be gradually opened in order to get constant flow rate. All piezometers were checked to be free of bubbles. The readings were taken for every run from all piezometers. The gate was opening at (y=1 cm, 2cm, 3cm, 4cm, and 5cm).

Photo. (1). The tunnel with its own service

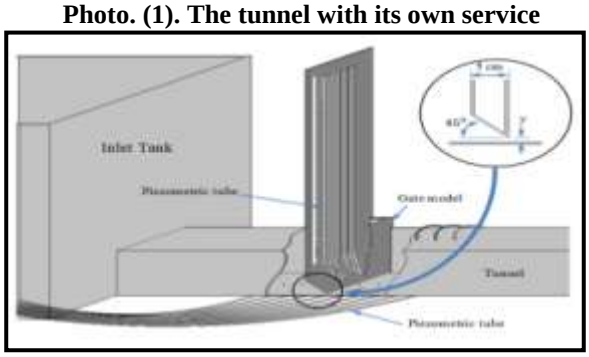

Fig.(5).Construction of the model System

4. RESULTS AND DISCUSSION

4.1. Test the Validity of ANSYS FLUENT Model

Usually any numerical model should be verified using reliable experimental data in order to test the validity of the model for the considered problem. ANSYS-FLUENT program was verified using experimental data that were read in certain positions in flow field.

4.1.1. Piezometric Head Positions Used in the Test

The following three positions were considered for the comparison between experimental and numerical models:

Position (Ht) which indicated the distribution of piezometric head on the downstream top of the tunnel wall. Position (Hb) which indicated the distribution of piezometric head along the bottom of tunnel wall. Position (Hi) which indicated the distribution of piezometric heads on the gate lip. The distribution of piezometric head on top, bottom of the tunnel wall, and along the inclined gate lip surface (θ=45°) were obtained by piezometric tubes used in the model. The readings were plotted and compared with those obtained by ANSYS FLUENT program. Figs. (6 to 10) showed a comparison between numerical and experimental results of piezometric head for different gate opening ratios (YY0⁄= 5%, 10 %, 15%, 20%, and 25%), where Y was height of the gate opening and Y0 is height of the tunnel. "x1" was a top or bottom distance measured horizontally from the first point of piezometric tubes fixed on the tunnel wall, or "x1" was a distance measured horizontally from the leading edge of the gate lip toward trailing edge of gate, and d1 was total horizontal distance. Figs. (6 to 10) showed good agreement between numerical and measured piezometric head values. The correlation coefficients for the comparison of numerical and experimental piezometric head values showed that the maximum and minimum correlation coefficient (R) were 0.9737 and 0.84 at gate opening ratios 20% and 10% respectively.

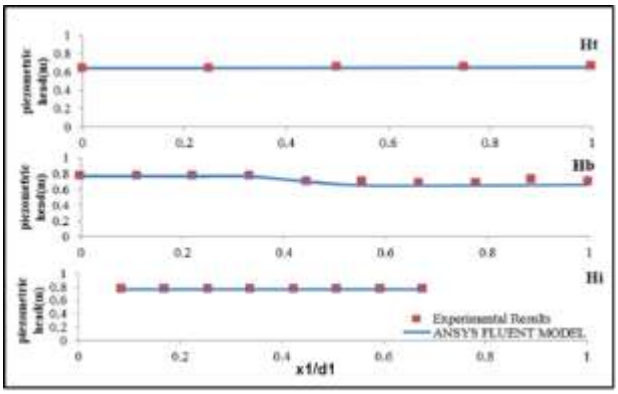

Fig. (6): Comparison between numerical and experimental values of piezometric head for Ht, Hb and Hi positions at gate opening ratio (Y/Y_0=5%)

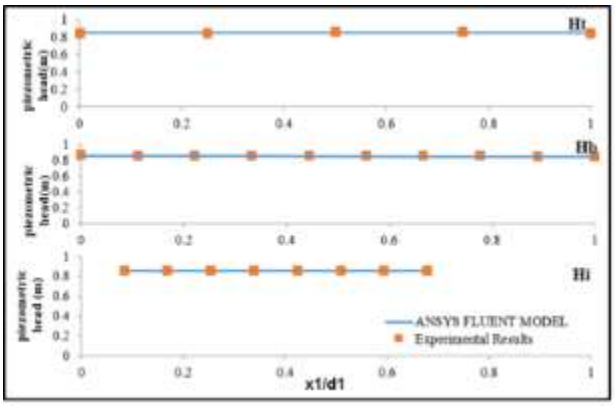

Fig. (7): Comparison between numerical and experimental values of piezometric head for Ht, Hb and Hi positions at gate opening ratio (Y/Y_0=10%)

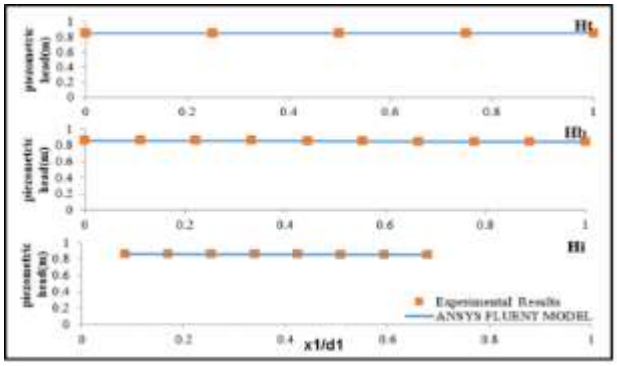

Fig. (8): Comparison between numerical and experimental values of piezometric head for Ht, Hb and Hi positions at gate opening ratio (Y/Y_0=15%)

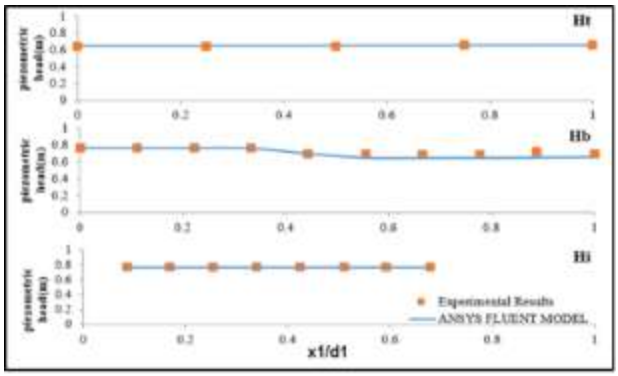

Fig. (9): Comparison between numerical and experimental values of piezometric head for Ht, Hb and Hi positions at gate opening ratio (Y/Y_0= 20%)

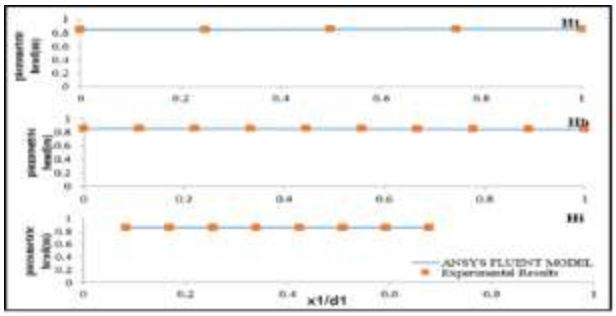

Fig. (10): Comparison between numerical and experimental values of piezometric head for Ht, Hb and Hi positions at gate opening ratio (Y/Y_0= 25%)

4.2.Bottom Downpull Coefficient k_b

The bottom down pull coefficient along the gate width could be computed by Eq. (1):

$$k_b = \frac{H_i - Y_s}{\frac{v_j^2}{2g}}$$

Where: (H_i) was the local piezometric head at specific points on the bottom surface of gate, (Y_s) was the piezometric head downstream the gate at contracted jet and (V_j) was the mean jet velocity below the gate. The variation of piezometric head along the bottom of gate was presented as non-dimensional term (k_b) plotted versus the distance along the gate thickness (x/d) for various gate opening. "X" was a distance measured horizontally from the leading edge of the gate lip toward trailing edge of gate, and d was the gate thickness. The basic objective of prediction (k_b) at various points along the bottom surface of gate was to understand and analyze the flow pattern under the gate and to correlate it with the fluctuating pressure on the gate bottom. Thus, the observation of the separation and reattachment points along the gate lip were useful in the present investigation due to their importance in describing the behavior of the flow beneath the gate and hence to reveal whether the separated flow from the leading edge of the gate lip would reattach or remain separated from the gate bottom. The location of reattachment zone was indicated by a sudden increase in (k_b) followed by a maximal positive pressure whereas the separation zone could be pointed as a region of low constant pressure head followed by sudden rise in pressure. The fact that (k_b) remains particularly constant over the gate thickness indicates that the flow was completely separated from the gate bottom

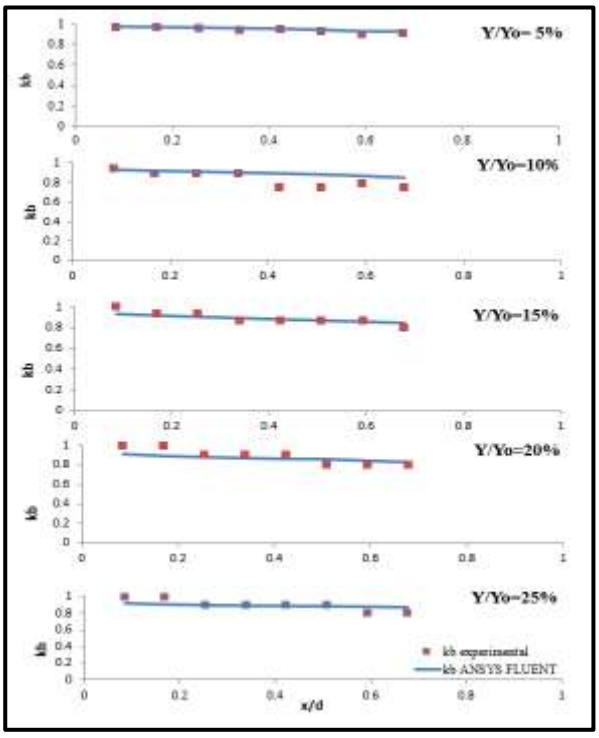

Fig. (11): Comparison between numerical and experimental values of (k_b) for different gate opening ratios

surface, (Reynolds, 1974). The distribution of bottom down pull coefficient along the gate lip surface obtained from Eq.(1) were plotted and compared with those obtained by the ANSYS FLUENT program for different gate opening ratios was shown in Fig (11). Fig (11) revealed good agreement between numerical and experimental values. It means no reattachment appeared in Fig (11) since there is no rapid increase in k_b values. Fig (12) showed the ANSYS FLUENT results of velocity vectors, pressure contours and velocity streamlines for the flow field with opening gate ratio (Y/Y_0 = 5%). Fig (12) observed that the maximum velocity reached 2.448 m/s at control gate in the downstream end of the tunnel. Figure (12) also illustrated that the piezometric pressure changed from7552.9 pa near upstream of the gate to about 6713.8 pa downstream the gate within the gate opening.

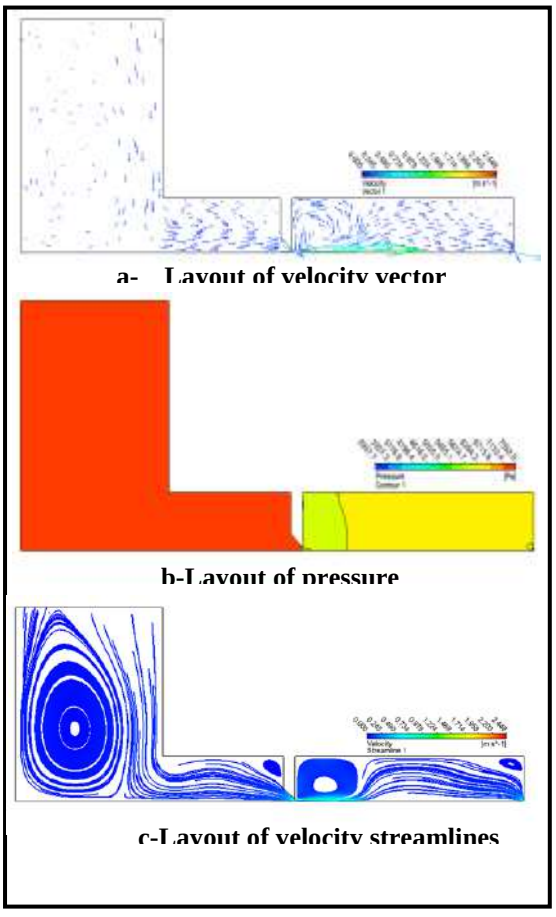

Fig. (12) Layout of velocity vector, pressure contour and velocity streamline of the tunnel gate model with gate opening ratio ($Y/Y_0 = 5\%$)

5. Conclusions

ANSYS FLUENT V14 was used to estimate the downpull forces on tunnel gates for high dams. Laboratory model was conducted to investigate the bottom downpull coefficient for vertical leaf gate. Several runs were conducted to find the piezometric head distribution and water discharge. The bottom downpull coefficient (k_b) was calculated from measurements of piezometric head on the bottom gate surface for different gate opening and for the fully submerged (pressurized) flow condition. The (k_b) values obtained from experimental measurements were used to calibrate and verify ANSYS FLUENT program.

The following conclusions can be outlined:

1. The comparison between numerical and experimental results of piezometric head for different gate opening ratios (Y/Y_0= 5%, 10 %, 15%, 20%, and 25%) showed good agreement between numerical and measured piezometric head values.
2. The comparison between distribution of bottom downpull coefficient along the gate lip surface obtained from experimental value and with those obtained by the ANSYS FLUENT program for different gate opening ratios was shown good agreement between of them.

REFERENCES

- Ahmed, T.1999.*Effect of Gate Lip Shapes on the Downpull Force in Tunnel Gates.* Ph. D Thesis Submitted to the College of Engineering, University of Baghdad.
- Al-Kadi, B.1999..*Numerical Evaluation of Downpull Force in Tunnel Gates*.Ph. D Thesis Submitted to the College of Engineering, University of Baghdad.
- Ansys Help, 2011.
- Aydin, I.2002.*Air Demand behind High Head Gates.* Journal of Hydraulic Research, Vol. 40, No. 4.
- Drobir, H., Volker, K., and Johannes, S. 2001. *Downpull and Tunnel Type High Head Leaf Gates*. Iahr/Airh Hydraulic Report, Balkema, Rotter Dam.

- Elder, R.,and Garrison, J.1964. *Flow Induced Hydraulic Forces on Three Leaf Intake Gates.*ASCE, Vol. 90, No. 3.
- Launder, B., Spalding, D.1974.*The Numerical Computation of Turbulent Flow*.In Computer Methods Applied Mechanics and Engineering 3, Pp. 269-289.
- Murray, R., And Simmons, W.1966.*Hydraulic Downpull Forces on Large Gates*. Water Resources Technical Publication, No. 4.
- Naudascher, E., Rao, P., Richter, A., Vargas, P., and Wonik, G. 1986.*Prediction and Control of Downpull on Tunnel Gates.* Hydraulic Engineering, Vol. 112, No. 5, Pp. 392-416.
- Naudascher, E., Kobus, H., and Rao, R. 1964.*Hydrodynamic Analysis for High- Head Leaf Gates.* ASCE, Journal of the Hydraulic Division. Vol. 90, No. 3, Pp. 155-192.
- Piradeepan,N.2002.*An Experimental and Numerical Investigation of a Turbulent Airfoil Wake in* 90°*Curved Duct*, Ph.D , Thesis Submitted to Department, Mechanical Engineering and University of Brunel.
- Reynolds,A.,1974.*Turbulent Flow in Engineering*. John Wiley & Sons.
- Sagar, B.1978.*Prediction of Gate Shaft Pressure in Tunnel Gate*, Water Power and Dam Construction, March.
- Smith, M.1964.*Hydraulic Downpull on Ice Harbor Powerhouse Gate*, Journal of Hydraulic Division, Vol. 90, No. 3, Pp. 193-213.

ZANCO Journal of Pure and Applied Sciences
The official scientific journal of Salahaddin University-Erbil
ZJPAS (2018) **30**(s1) s24-s31
http://dx.doi.org/10.21271/ZJPAS.30.s1.3

Discharge Coefficients for Different Types of Side Weirs

***Bruska S. Mamand[1], Adil M. Raheem[2]**

[1]Assistant Lect., College of engineering, Salahaddin University-Erbil

[2]Assistant Prof., College of engineering, Salahaddin University-Erbil

A R T I C L E I N F O

Article History:
Received:14 /05 /2017
Accepted:12 /0 4 /2018
Published:01/06/2018

Keywords:
Side weir
Discharge coefficient
Labyrinth weir
Open channel flow

**Corresponding Author:*
Email:
bruska.sardar@gmail.com

A B S T R A C T

Side weirs are extensively used with open channel structures for different purposes such as; raising water level for irrigation and drainage purposes, also to divert a course of excess flow from rivers or channels during the occurrence of flood which is consider the main problem during the wet seasons. In the present study a series of 18 manufactured laboratory models of different types of side weirs are investigated through a total of 160 test runs. Subcritical flow regime was tested on the side weirs that installed inside the prismatic rectangular main channel. Five different types of side weirs are used namely linear crest of normal rectangle with ($\theta = 90^o$), an oblique rectangle which inclined its crest with flow direction by ($\theta = 75^o$, 60^o and 45^o), Triangular labyrinth with apex angles ($\delta = 90^o$ and 120^o), Semi-hexagonal labyrinth with wall angles ($Z = 30^o$ and 64.7^o) and Semi-circular labyrinth side weirs. Dimensional analysis for different parameters which influence the behavior of models were carried out, then the equations outlined from multivariable regressions. For this purpose a statistical software called (SPSS V.22.0) was applied. Finally De Marchi's assumption of constant specific energy along the side weir was checked and approved, moreover the results shows that the coefficient of discharge in labyrinth side weir cross–sections are greater than of the linear crests of rectangular models.

INTRODUCTION

Free surface flow are affected by the value of Froude number, if this value is changed gradually then the phenomenon is called spatially varied flow (SVF). Side weir is a hydraulic structure used for diverting flow from the main channel into the side channel whenever the water surface rises above the side weir crest, and the flow overflows over it freely under gravity. Their hydraulic behavior is complex and exhibition to change due to different free surface profiles along the side weir. (De Marchi, 1934) is one of the earliest investigators who gave equations for the flow over side weirs on the basis of a constant specific energy along this structure. (Collinge, 1957) studied experimentally the discharge capacity of side weirs. (Subramanya and Awasthy,1972) and (Ranga Raju *et al.*, 1979) concluded that the De Marchi equation can be used and they presented different equations for calculation of discharge coefficient in terms of upstream Froude number for subcritical flow conditions. (May *et al.*, 2003) indicated that the flow condition in the main channel at the upstream and downstream of a side weir can have a major influence on the behavior of the flow on the weir itself. There are numerous application that related to the side weirs can

commonly highlighted in hydraulic engineering applications namely irrigation systems such as flood control structure, and in sanitary engineering practice to disperse storm flow in the combined sewer system. The main purpose of this study is to predict the discharge coefficient for different types of side weirs especially when the weir length increased while the width of the lateral opening is kept constant.

Theoretical Consideration:

The SVF equation can be derived basing on energy or momentum principle which described the flow condition within the main channel, dynamic equation for SVF is expressed by:

$$\frac{dy}{dx} = \frac{S_o - S_f - \frac{\alpha Q\, dQ}{g A^2 dx}}{1 - \frac{\alpha Q^2 T}{g A^3}}$$

where; y is the depth of flow, x is the distance along the side weir from upstream end, S_o is the main channel slope, S_f is friction slope, α is kinetic energy correction factor, Q is discharge in channel, dQ/dx is discharge per unit length of side weir, g is the acceleration due to gravity, A is the cross sectional area of flow and T is the top width of the channel section.

In accordance of De Marchi's approach of constancy in specific energy between upstream and downstream ends of the side weir, the parameters that affected on the flow over rectangular cross-section was explained in Figure (1). The discharge through an elementary strip (dx) was:

$$\frac{-dQ}{dx} = \frac{2}{3} C_m \sqrt{2g}\,(y-p)^{\frac{3}{2}}$$

Discharge coefficient for flow passing over the side weir was proposed as:

$$C_m = \frac{3B}{2L}(\emptyset_2 - \emptyset_1)$$

In which $\emptyset_1$&$\emptyset_2$ are varied flow functions at sections 1& 2 expressed as:

$$\emptyset_1 = \frac{2E_1 - 3p}{E_1 - p}\sqrt{\frac{E_1 - y_1}{y_1 - p}} - 3\sin^{-1}\sqrt{\frac{E_1 - y_1}{E_1 - p}}$$

$$\emptyset_2 = \frac{2E_2 - 3p}{E_2 - p}\sqrt{\frac{E_2 - y_2}{y_2 - p}} - 3\sin^{-1}\sqrt{\frac{E_2 - y_2}{E_2 - p}}$$

Where : B is main channel width, E_1&E_2 is specific energy heads at upstream and downstream ends of the side weir respectively (i.e. sections 1&2) ,y_1&y_2 is water depths at upstream and downstream ends of the side weir respectively, L is length of the side weir, and p is side weir height.

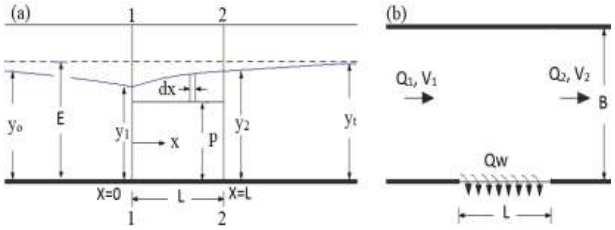

Fig.1. Sketch of flow over rectangular side weir in: (a) Longitudinal section, (b) Top view.

Buckingham's π- theorem was used for evaluation of the variables controlled the flow over the side weir. As sketched in Figure (2), the expected factors which affecting the discharge coefficient for different types of side weirs was expressed in general relation as:

$C_m = f$ (L, Lc, p, B, V_1, y_1, ρ, g, Θ, δ, Z).

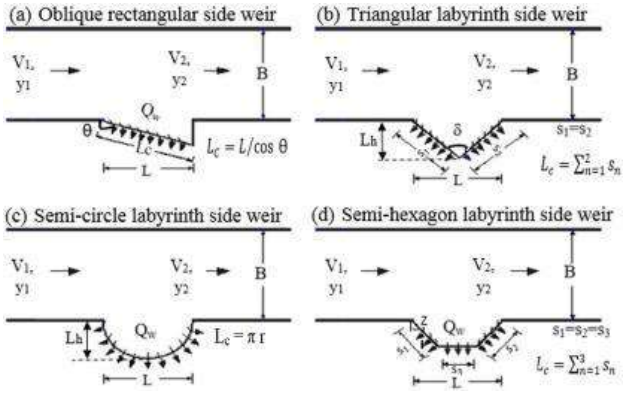

Fig.2. Definition sketch for different side weir models.

Discharge coefficient for different type of side weirs in term of dimensionless pi terms was expressed as:

$$C_m = f\left(Fr_1, \frac{P}{y_1}, \frac{L}{B}\right) \quad \text{. . . . . Normal Rectangular.}$$

$$C_m = f\left(Fr_1, \frac{P}{y_1}, \frac{L}{B}, \frac{L}{Lc}, \Theta\right) \quad \text{. . . . . Oblique Rectangular.}$$

$$C_m = f\left(Fr_1, \frac{p}{y_1}, \frac{L}{B}, \frac{L}{Lc}, \delta\right) \quad \text{. . . Triangular Labyrinth.}$$

$$C_m = f\left(Fr_1, \frac{p}{y_1}, \frac{L}{B}, \frac{L}{Lc}, Z\right) \text{. .Semi-hexagon Labyrinth.}$$

$C_m = f\left(Fr_1, \frac{p}{y_1}, \frac{L}{B}, \frac{L}{Lc}\right)$ . . . Semi-Circular Labyrinth.

MATERIALS AND METHODS

Methodology of experimental program was conducted in the laboratory of civil engineering department belonging to the college of engineering/Salahaddin University. The laboratory flume has a rectangular prismatic section which its dimensions were 12m length, 0.5m wide and 0.5m deep. The width of the flume was divided into two passage channels as shown in Figure (3), one for the main channel of width (B=0.2m) while (B=0.294m) was the side channel width and the lateral openings of the side weir was taken as (L= 0.2, 0.25 and 0.3m), the side weirs are usually considered as short structures with (L/B ≤ 3.0), and the longitudinal slope of the flume was set to zero (horizontal) for all tests.

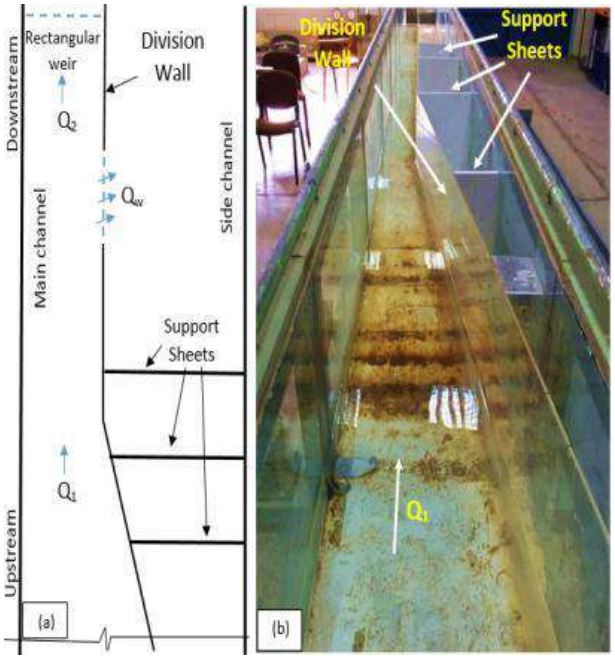

Fig.3. Flume dividing: a) Top view, b) laboratory view.

The experimental program was carried out through investigation on five different types of side weirs as shown in Figure (4). The weirs were normal rectangular (θ=90°), oblique rectangular (θ=75°, 60° and 45°), triangular labyrinth (δ=120° and 90°), semi-hexagonal labyrinth (Z=64.5° and 30°), and semi-circular labyrinth (r = L/2). Side weirs were installed at a distance of 2.2m from the downstream end of the main channel. These models were investigated through 160 test runs with different flow rates, the flow starting from very low rate controlled via a manually operated small valve, and the flow rate was gradually increased. Eight to ten runs was conducted on each side weir models.

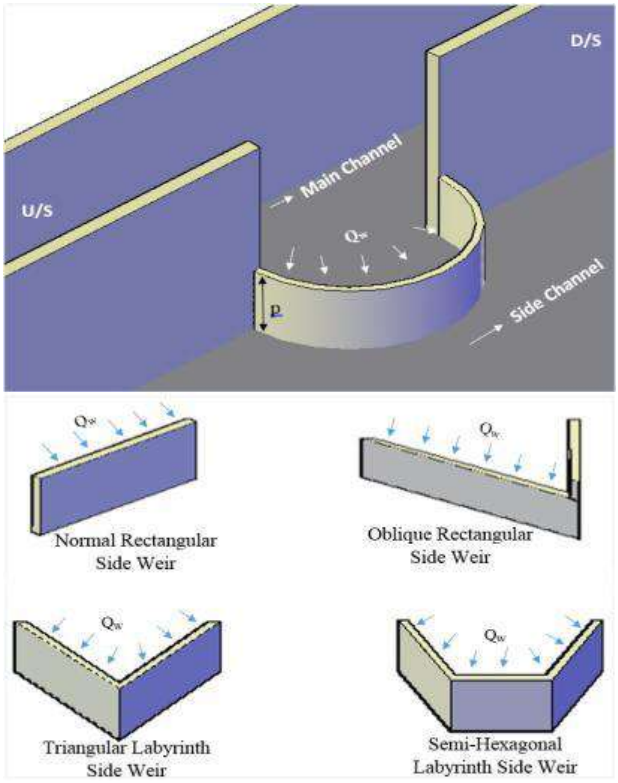

Fig.4. Different side weir models and their position.

Total discharge entering the main channel (Q_1) was measured through a v-notch weir equation (Q_1=0.0194 $h^{2.4015}$) which calibrated by (Bahar, 2015) and a point gauge of a vernier scale with an accuracy of 0.05mm was used to measure the water depth(h) above the v-notch weir. It was fixed to zero level corresponding to the level of v-notch weir crest. Whereas the discharge (Q_2) at the downstream of the main channel was measured by installing the standard rectangular weir at 2.2m away from downstream end of the side weir. According to (British standard institute, 1965) for a rectangular weir, the discharge at the downstream of the main channel can be calculated by Rehbock formula: ($Q_2 = \frac{2}{3} C_d \sqrt{2g}\ b\ he^{1.5}$). The coefficient of

discharge was determined:($C_d = 0.602 + 0.083\frac{h_d}{p}$), and $h_e = h_d + 0.0012$

Where: C_d is the discharge coefficient, p is the weir height, h_e is the effective head above the standard rectangular weir and h_d is the depth of water measured at the upstream of standard rectangular weir.

In order to check the accuracy of the above standard equation, the flow through the side weir was sited to be turn off and the results of mass balance for several test runs shows that the maximum error in the discharge measurements between inlet and outlet of the main channel not exceeded 6.04%. Then the flow passing over the side weir (Q_w) was measured as ($Q_w=Q_1-Q_2$).

RESULTS AND DISCUSSION

Specific energy values at the side weir entry (E_1) and side weir exit (E_2) was calculated and plotted in Figure (5) which illustrated that the specific energy between two ends of side weirs has a linear variation. The best intercept fit line among all models includes high correlation coefficient. This finding means that the energy differences was a small fraction which considered as no significant effect. (Jaafar, 2010) estimated the energy difference to be less than 1% in for the rectangular cross-section of side weirs with different crest lip shapes, while (Raju *et al.*, 1979) obtained mean value of 2%, (Khameneh *et al.*, 2014) obtained the energy difference to be less than 1% for semi-circle labyrinth side weir. In the present study, the average error of energy difference was found to be between (1-2) %. This finding was adopted with De Marchi's assumption in which the specific energy should be considered as constant in the main channel between upstream and downstream ends of the side weir.

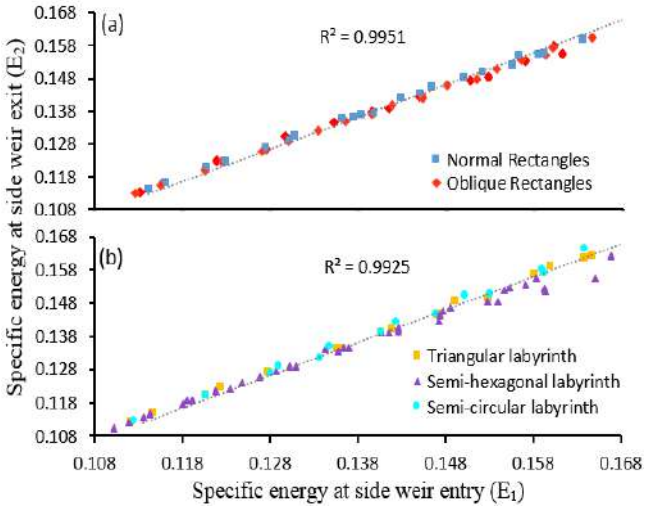

Fig.5. Specific energy variation along rectangular and Labyrinth side weirs.

Variations of De-Marchi's discharge coefficient (C_m) with upstream Froude number (Fr_1) for different side weir models was shown in Figure (6), which revealed that by increasing the Fr_1 a decrease in C_m values will produced. This pattern was familiar by (Subramanya and Awasthy, 1972) were obtained a similar tendency for the aforementioned relation. Flow with low velocity value, good efficiency of the side weir flow was obtained, while increasing the flow velocity leads to creating vortexes which made a return flow area especially in labyrinth side weirs were consequently decreased the flow capacity over the side weirs. For an oblique rectangular side weir (Fig.6.a) with different inclination angles as ($\theta = 45^o$, 60^o and 75^o), and (L/Lc) ratio as (0.707, 0.866 and 0.966) with keeping the side weir height as 0.1m. It was noted that the lowest oblique angle ($\theta = 45^o$) will give higher value of Cm in comparison with the other oblique angles due to its longer crest length which leads to serve more lateral flow above the side weir. Similar results was founded for triangular and semi-hexagonal labyrinth side weirs (Fig.6.b,c), in which the longer side weir crest length provide greater efficiency than the other crest lengths.

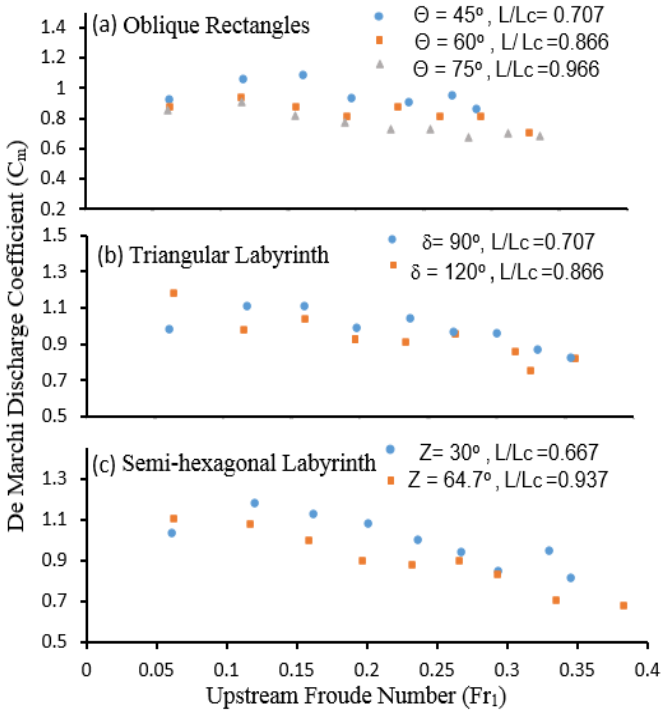

Fig.6. Variation (C_m) with (Fr_1).

The relations of C_m against ratio of p/y_1 for different side weirs was shown in Figure (7). Results pointed out grow up in C_m values with increasing the ratio of p/y_1. This revealed the majority and sensitivity of the measurement of upstream side weir water depth (y_1).

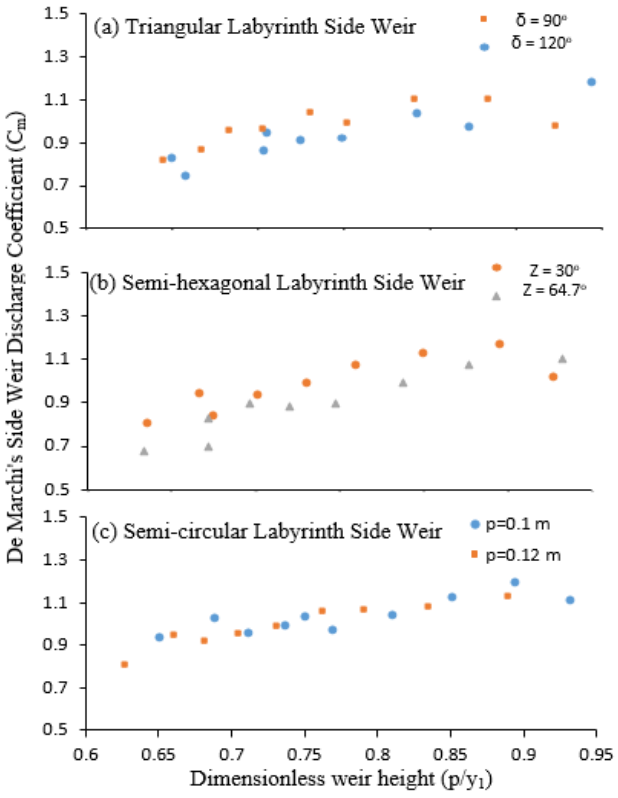

Fig.7. Variation (C_m) with (p/y_1).

In the Figure (8), the variation of L/B ratio on C_m values was revealed. For different lateral openings of rectangular and triangular side weirs, a slight effect was seen. In other words, the lateral opening inside channel width has no significant effect on the performance of the side weir in terms of discharge coefficient.

Comparison between different types of side weirs was shown in Figure (9), results indicated that for different lateral openings (L= 0.2,0.3m) the normal rectangular side weir has lower efficiency in terms of its discharge capacity, while the semi-hexagonal model provided higher C_m values when (Fr_1<0.2). Increasing flow rate (Fr_1>0.2), leads the triangular labyrinth weir to be a little bit performance. In other words, the discharge passed over labyrinth weirs was greater than that discharge over the normal and oblique rectangular weirs, this was due to longer crest length that allow more lateral flow into the side channel.

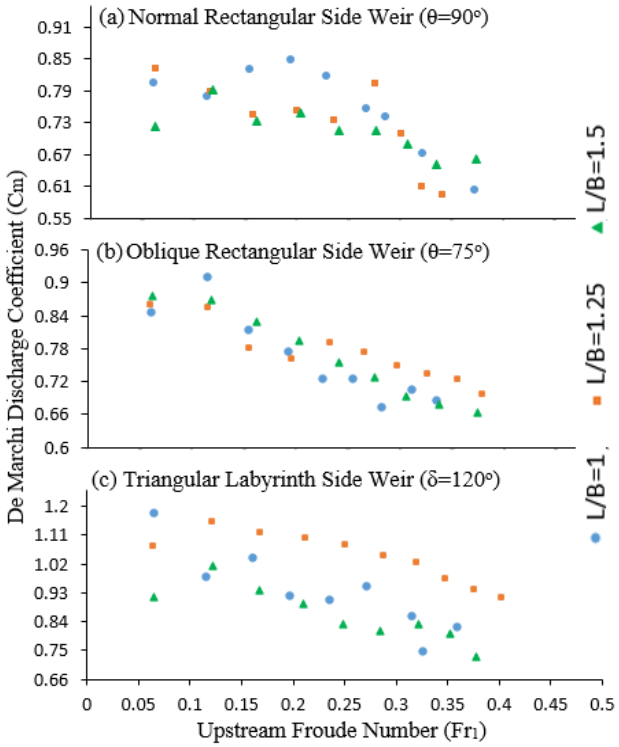

Fig.8. Effect of dimensionless (L/B) on the (C_m) value.

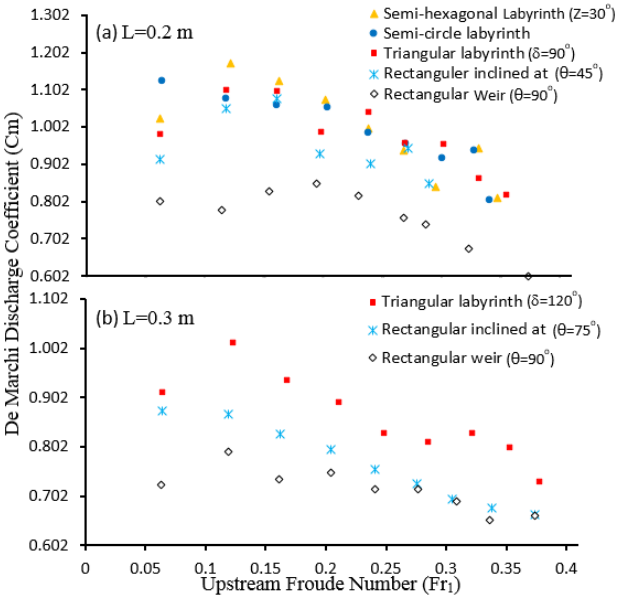

Fig.9. Comparison of different types of side weirs.

In order to find which shape of labyrinth weirs was better, taking into account the increasing of the weir crest length (Lc), the head length (L_h) should be focused on and considered as an important parameter in the hydraulic design aspects. Therefore semi-hexagonal labyrinth side weir model was found to be better than the other models due to its smaller head length (L_h= 0.086m). Whereas, semi-circle and triangle weirs has longer head lengths as (both L_h =0.1m). Similarly, the same conclusion for the side weirs with the lateral opening L=0.3m was adopted. Additionally, the labyrinth side weirs capacity were founded to be 1.27 times higher than the capacity of rectangular side weir.

In order to find the relation between the dependent and the independent dimensionless parameters, SPSS software was applied for each weir geometry and two empirical equations as multivariable linear and multivariable power regressions was examined as shown in Tables (1&2) respectively. The calculated values of C_m from the empirical equation was compared with actual C_m values of experimental runs as shown in Figure (10).

Table (1) Multivariable Linear Regression for different side weir models.

Side Weir Name	Multivariable Linear Regression $C_m = c + a_1(Fr_1) + b_1(p/y_1) + c_1(L/B) + d_1(L/L_c) + e_1(sine\theta, \delta, Z)$	R^2
Normal & Oblique Rectangular	$C_m = 0.955 + 0.062(Fr_1) + 0.666(p/y_1) - 0.064(L/B) + 29.354(L/L_c) - 30.002(sin\theta)$	0.7540
Triangular Labyrinth	$C_m = 5265.403 - 0.04(Fr_1) + 0.977(p/y_1) - 2.9650(L/B) - 2774.8190(L/L_c) - 3299.78(sin\delta)$	0.7952
Semi-hexagonal Labyrinth	$C_m = 1.462 - 0.935(Fr_1) + 0.337(p/y_1) - 0.31(L/B) - 0.247(L/L_c) - 0.068(sinZ)$	0.8241
Semi-circular Labyrinth	$C_m = 0.106 + 1.057(Fr_1) + 2.061(p/y_1) - 2.994(L/B) + 3.306(L/L_c)$	0.8498

Table (2) Multivariable power Regression for different side weir models.

Side Weir Name	Multivariable Power Regression $C_m = c + a_1(Fr1)^{a2} + b_1(p/y_1)^{b2} + c_1(L/B)^{c2} + d_1(L/L_c)^{d2} + e_1(sine\theta, \delta, Z)^{e2}$	R^2
Normal & Oblique Rectangular	$C_m = 0.704 - 0.014(Fr_1)^{-0.846} - 0.123(p/y_1)^{-2.741} - 0.024(L/B)^{2.57} + 0.217(L/L_c)^{-1.015} + 0.219(sin\theta)^{-0.957}$	0.8071
Triangular Labyrinth	$C_m = -73.165 - 3.799(Fr_1)^{-0.05} - 5.682(p/y_1)^{-0.311} - 1.5980 * 10^{-14}(L/B)^{74.485} + 2.6560(L/L_c)^{-9.982} + 0.2(sin\delta)^{-41.054}$	0.8817
Semi-hexagonal Labyrinth	$C_m = -0.783 + 9.295(Fr_1)^{0.024} - 6.061(p/y_1)^{-0.324} - 0.574(L/B)^{0.001} - 0.001(L/L_c)^{-6.012} + 0.006(sinZ)^{-3.995}$	0.8827
Semi-circular Labyrinth	$C_m = 10.615 - 15.443(Fr_1)^{-0.007} - 25.603(p/y_1)^{-0.047} + 10.532(L/B)^{0.001} + 0.106(L/L_c)^{-11.746}$	0.8584

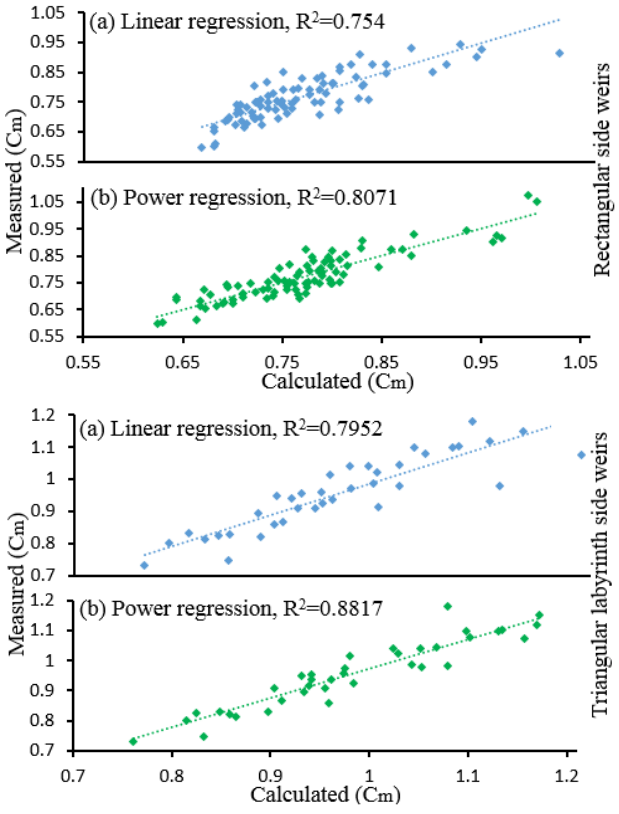

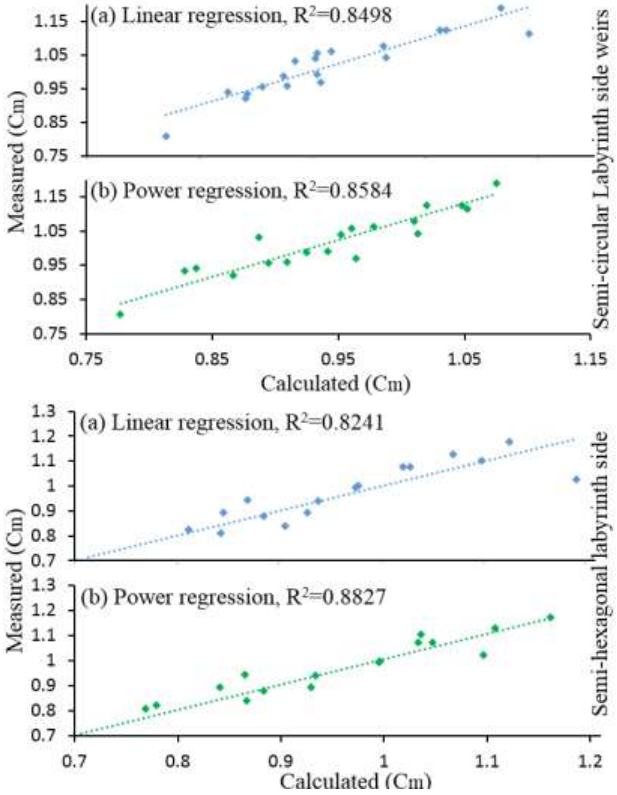

Fig.10. Calculated against measured C_m values of multivariable linear and power equations for different side weirs.

Multivariable power regressions was found to be more suitable with higher correlation coefficient than the linear one. Therefore the equations of this regression was used for calculating C_m of different side weir geometries then compared with the other investigator as shown in Figure (11). Results of the discharge coefficient (C_m) value in the present study was found to be higher than the values obtained by (Subramanya and Awasthy, 1976) for normal rectangular side weir. While it was found to be lower than that of (Kaya N., 2010) values for triangular labyrinth side weir and the experimental discharge coefficient (C_m) value was found to be almost in agreement with the obtained values by (Khameneh *et al.*, 2014).

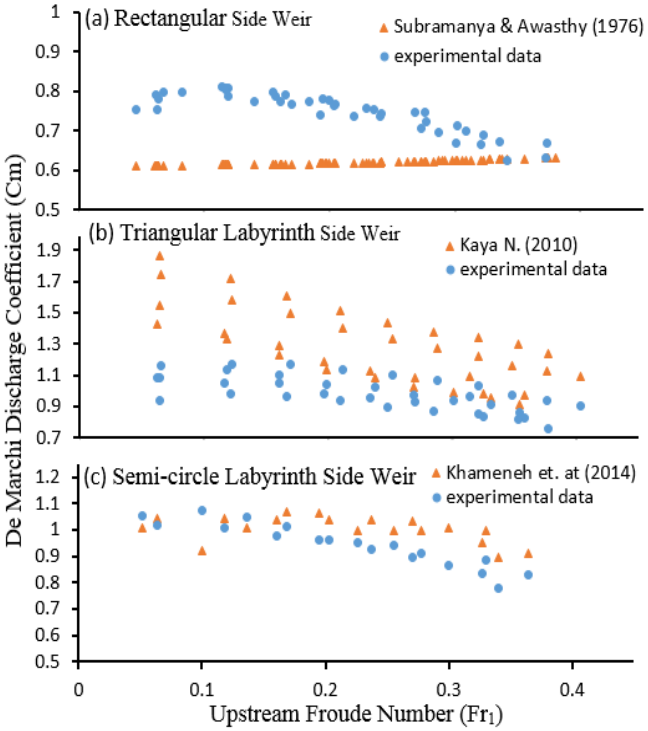

Fig.11. Comparison of (C_m) between present study and other researchers for different side weirs.

CONCLUTIONS

The conclusions was summarized as:

1. Results of this study were coincide with De Marchi assumption for constant specific energy between side weir entry and exit. The maximum value of average error in energy difference for different types of side weirs was found to be not more that 1.56%.
2. De Marchi's discharge coefficient (C_m) was found to be decreased with the increasing in (Fr_1) values and decreased with decreasing in (p/y_1) values. Whereas (C_m) increased with decreasing an oblique angle of rectangle weir (θ), apex angle of triangular labyrinth weir (δ) and side wall angle for semi-hexagonal labyrinth side weirs (Z).
3. Experimental tests show that the labyrinth side weirs had better performance due to its longer weir crests and the discharge coefficient of labyrinth side weir was found to be 1.27 times more than that of the rectangular side weir.
4. Several empirical equations for discharge coefficient for different types of side weirs

were predicted. Multivariable power regression models with higher correlation coefficient (R^2) was found to be more applicable than the multivariable linear regressions.

REFERENCES

Bahar, M. (2015). 'Hydraulic performance of single step broad crested weir', MSc thesis, university of salahaddin, Dept. of dams water resources engineering.

British Standards Institution (1965), " method of measurement of liquid flow in open channels ", part 4A, Bs3680, BsI, London, England.

Bruska ,S.,M.(2016). 'Flow over different types of side weirs in channels', MSc thesis, university of salahaddin, Dept. of dams water resources engineering.

Collinge V.K. (1957) 'The Discharge Capacity of Side Weirs' Proceedings, Institution of civil engineering, London, 6, pp. 288-304.

De Marchi, G. (1934). 'Saggio di teoria de funzi on a mented eglistra mazzi Laterali' Energ. Elettr, 11(11), 849–860.

Emiroglu, M., Kaya, N. and Agaccioglu, H. (2010). 'Discharge capacity of labyrinth side weir located on a straight channel ', J. of irrigation and drainage engineering, ASCE, 136 (1), p. 37-46.

Jaafar, R. (2009). 'Laboratory study of lip shape effect on the performance of side weir ', MSc thesis, university of Duhok, Dept. of water resources engineering.

Kaya, N. (2010). ' Effect of upstream crest length on flow characteristics and discharge capacity of triangular labyrinth side weirs ',Firat University, Civil Engineering Department, Turkey, 5 (13), p. 1702-1712.

Kaya, N., Emiroglu, M. and Agaccioglu, H. (2010). 'Discharge coefficient of a semi-elliptical side weir in subcritical flow ', J. of flow measurement and instrumentation, 22, p. 25-32.

Khameneh, H., Khodashenas, SR. and Esmaili, K. (2014). 'The Effect of Semicircular Side Weirs on Hydraulic Properties and Discharge Coefficient of Side Weirs ' J. of river engineering, Vol.2.

May, R., Bromwich, B., Gasowski, Y. and Richard, C. (2003). 'Hydraulic design of side weirs ', Thomas telford publishing, heron quay, London E14 4JD.

Raju, G., Parasad, B., and Gupta, K. (1979). 'Side weir in rectangular weir ' J. of irrigation and drainage engineering, ASCE, 105 (5), p. 457-554.

Subramanya, K. and Awasthy, S.C, (1972).'Flow over side weirs ', Indian institute of technology, p. 328-334.

ZANCO Journal of Pure and Applied Sciences

The official scientific journal of Salahaddin University-Erbil

ZJPAS(2018)30(s1) s32-s41

http://dx.doi.org/10.21271/ZJPAS.30.s1.4

RISK MANAGEMENT IN CONSTRUCTION PROJECTS: A CASE STUDY OF GOVERNMENTAL INSTITUTIONS IN KIRKUK

Gzing Adil Mohammed*

General Directorate of water resource, Ministry of Agriculture and water resource, Erbil, Kurdistan region, Iraq

A R T I C L E I N F O

Article History:
Received:14/05/2017
Accepted:12/04/2018
Published: 01/06/2018

Keywords: *risk management; building construction; governmental organizations; uncertainties; Iraq.*

Corresponding Author:
Email:
gzingadil87@gmail.com

A B S T R A C T

In this study, the risk factors in building construction are investigated, ranked and analyzed from the governmental institutions point of view in Iraq. A categorization method for these factors are addressed to environment sustainability, material availability, design , logistical problem, physical provision, political situation, dispute over ownership, management and legal groups. Therefore, 42 risk factors have been investigated and presented. These factors were derived from nine major groups. The ranking process is based on weighted mean (severity) and frequencies in order to get the importance of each risk factor. Kruskal-Wallis test has implemented to examine the mean homogeneity of the risk groups. Furthermore, multi comparison between the groups was performed by Post-Hoc test for non-parametric variables. Prevention, mitigation and analysis methods were also ranked according to its effectiveness and usage. The percentage importance 73.34%, 71.13% and 70.19% represent rapid design, disputes over land ownership and lack of security and stability of project region, respectively. As a result of non-parametric test, variation in groups mean were obtained at level of significant α=0.05. The higher ranking based on mean plot of the groups are going to be considered in design group.

INTRODUCTION

Construction in building projects is generally a creation of structure for any system. This creation is companied by risks that synchronize with project phases. Managing the project is not easy professional especially in construction projects due to the changing natural of the risks. For many years the risk is handled by reductionist approach through the application of contingency money or floats (time) which produce cost overrun and late in the project (Alfredo et al., 2014).The professionals such as contractor and supplier must provide a suitable risk management team to make a good management strategy to identify and control the discrete sources which made risks to the project (Flanagen & Norman, 1993). Risk management is a regular process of identifying, analyzing, qualifying, quantifying and corresponding to the project risks (A Guide by APM The Association of Project Management, 2000).complying with (B.A.K.S. et al., 2014)risk management is defined as the whole activities synchronized whith developing

stratigies that taken inorder to reduce the probability of occurance and impacts of risks.

Effective risk management is obtained by balance between cost of managing risk and estimated benefits from taking that risk. To obtain that balance identifying the risks that impact the project and document their characteristics and a proper risk identification is required which obtained from practical experience and training in using the techniques (Satyendra & Niranjan, 2011). The risk event identified from the first stage of risk management (Crawford, 2002). Risk treatment strategies according to (Cooper et al., 2005) are retention, reduction, transferring and avoidance. The effective treatment results come by applying two or more of this risk treatment strategies (Satyendra & Niranjan, 2011). The major important points from the institutions view are cost, time and quality. The governmental organizations need to be sure that the project start and finish throughout the entire amount of money and the sufficient time to achieve the project objective within the quality standards. Governmental institutions perspective is the angle in which the study spotting light on it. Only buildings are included in this study regardless of (Dams, Infrastructure, Bridge…) project.

The research is tried to answer the following questions regarding to risk management in building constructions projects:

- What the term "RISK" or uncertainties refer to?
- Who Risks and Risk management are sensed in the construction projects?
- What are the Risk factors that can affect the project with its significance?
- What actions can be taken in order to minimize the effects of the Risks and uncertainties during the project?

MATERIAL AND METHODS

i. Questionnaire writing, distributing and collecting:

The main purpose of organizing the questionnaire is to investigate and rank the essential factors that affect the project objectives before and after the project performance in construction sector. The questionnaire consisted of Cover tittle, Letter to the respondent: to explain what is the purpose of the research, Organization profile and the final section includes 42 factors that bring risks to the construction projects with questions for methods to mitigate and prevent the risks and ways to analysis the risks. Among 81 questionnaires only 43 questionnaires took into consideration. Participant's response rate was 53%. Despite of the small sample size but it still meets the central limit theorem that statistical analysis holds true with sample size greater than 30 subjects (Zhao et al., 2012). Difference expertise, years of work and positions of respondents may lead to undesirable results, so it is important to mention that these factors relate to the respondents in the questionnaire. The questionnaires have been distributed among engineers in different educational level, position title, Difference expertise, years of work and positions as shown in the Figure 1-(a), (b), (c), (d).

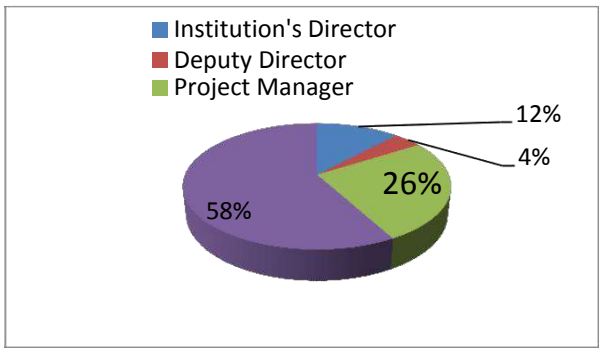

Figure 1-(a): Position of the respondent.

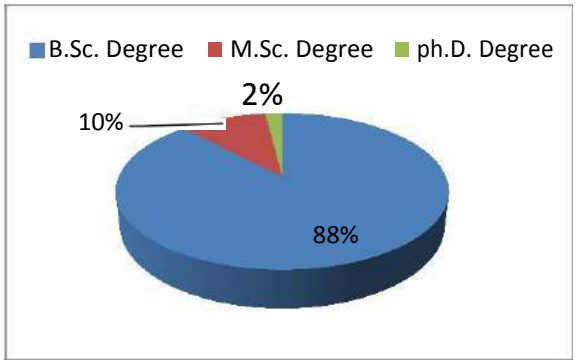

Figure 1-(b): Respondents qualifications and academic achievements.

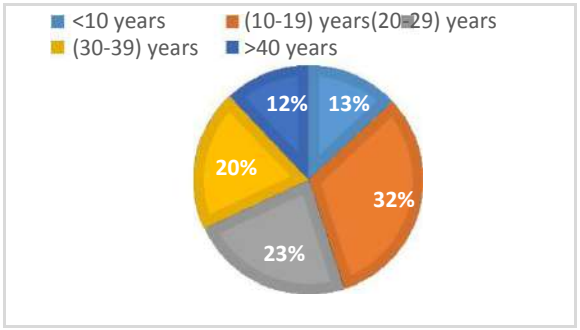

Figure 1-(c): Respondent Experience in Construction Projects.

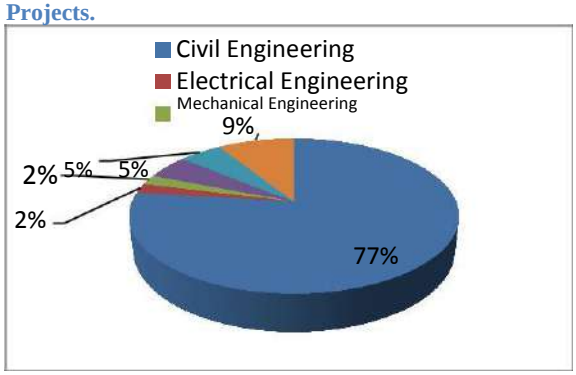

Figure 1-(d): Engineering specialists who contributed in filling questionnaire

ii. The research validity and reliability:

Joope (2000, as citied in Golafshani, (2003)) Described the word "validity" as measurement which "determines whether the research truly measures that which it was intended to measure or how truthful the research results are". Similarity aspects between Iraq and Palestine in construction sector permit the researcher to depend on thesis by (Mousa & Hmaid, 2005)

The extent to which data results consist over time and represent accurately of the total population under study is referred to reliability Joope (2000, as citied in Golafshani, (2003)). Cronbach's Alpha test by using Software of Statistical Package for Social Science (SPSS) is used to calculate the reliability of the data to measure the internal consistency or reliability and to determine whether the series of scales are measured the same construct.

Cronbach's Alpha's value is (0.84) as it is shown in Table 1 .That means 84% of the series of a scales measured the same construct, and this percentage is greater than the acceptable value which is 0.7, so the research data are adequately reliable. It is essential to mention, the more respondents are contributed the greater alpha value are obtained.

Case Processing Summary

		N	%
Cases	Valid	267	98.5
	Excluded[a]	4	1.5
	Total	271	100.0

a. Listwise deletion based on all variables in the procedure.

Reliability Statistics

Cronbach's Alpha	N of Items
.849	2

Table 1 Reliability test

iii. Data analysis:

Weighted mean was the base method to quantitate each of the (42) risk. The (42) risk factors are extracted from the questionnaire. The weighted means are evaluated from 1 to 10 depending on the impaction degree. The total weights are calculated by multiplying the number of the respondents with the rating scale of each factor. The significant of each risk factor (severity) is founded by the equation below.

$$\frac{\Sigma_{\varepsilon}}{}$$

Where = No. of respondents pick the specify rate for each risk factor, = weight of each rating number per each risk factor(ranges from 1 to 10 for sever) and = total weight of rate weights per risk factor.

Also the risk factors frequency index has been calculated from the below equation:

$$\frac{\Sigma_{\varepsilon}}{}$$

Where = No. of respondents pick the specify rate for each risk factor, = weight of each rating number per each risk factor(ranges from 1 to 10 for frequency) and = total weight of rate weights per risk factor.

The importance factor is calculated as a function of severity and frequency indices as follow:

The same equation of severity is used to determine the effectiveness for each of risk prevention, mitigation and usage of analysis technic with the ranges from (1 to 5) for effectiveness and usage.

iv. NPR (Nonparametric test) (kruskal-wallis) test:

Software of Statistical Package for Social Science (SPSS) is used to find the weighted mean of the major nine of risk factor groups. Nonparametric test is used as it does not require the normality distribution of the data and homogeneity of variance between the groups. Kruskal-Wallis test is the most suitable test to check the null hypothesis H0 (the risk factor groups have the same mean) regarding to the independency, sample randomly and the measurement per sample. Moreover, 95% confident interval is specified to clarify the level of confident. Level of significant which denoted by α was 5%. According to the probability α (0.05) mean that 5 chances in 100 that we would reject the hypothesis when it should be accepted i.e. we are about 95 confident that we have made the right decision. In order to examine the hypothesis and rank the mean, the following procedures have been done. Filing /organizing the data: in order to be ready for entering to the scheme, coding and defining each variable and entering the data into the work sheet and run the analysis of the data from the SPSS program.

v. Post Hoc test for NPR (Dunnett test):

Multi comparison test has used when significant is appeared. Comparison is performed to investigate the significant positions between the groups.

RESEARCH RESULTS AND DISCUSSION

i. Significant of Risk Factors in Construction Projects:

Safety provision is ranked within the most seven significant key risks factors with its importance index (51.49%) and first factor entire its group as shown in Table 2.

Governmental organizations want to finish its work with minimum budget. Therefore considering safety is wasting money rather than considering risk hazards. . To be honest, the governmental institution transfers the responsibility of the mentioned factors to the contractor in order to be in safe side.

Dealing with political factors is critical. Such factors are recorded as the high frequency occurrence comparing with the other risk groups. The series of wars that the Iraq passes through affect negatively on the country's economy, thus construction sector in Iraq. After the regime is extinct in 2003, Iraq becomes a hometown of the most terroristic organizations. "Explosion and instability of project regions" is in the head of risk factors list from the governmental organizations perspective. The governorate in this situation must cooperate with both owner and contractors and share the responsibility of facing the risk if any unexpected reaction happened. Poor managing the resource has a moderate risk while changing ways of management and delay in resolving problems have less significant impacts on construction projects from the client perspective. Among the legal factors, disputes over the land ownership is recorded the highest risk factor with importance (71.13%) as shown in Table 2. According to (Zou et al., n.d.) Study, the reasons of uncompleted approval work order and difficulty to obtain necessary permits to work return to missing management and bureaucracy of government. The government institution should establish a good foundation with efficient manager in order to issue the approval work order. Risk factors, that are related to design group, occupied the first rank among the risk groups. The best solution is to choose a reasonable and experienced designer. The other factors that related to environmental, logistic and construction are illustrated in Table 2.

ii. Data Analysis Results:

Kruskal-Wallis test was implemented to mean rank the risk groups and check the null hypothesis. As a result, design group factors evaluate as a first rank as it is shown in Figure 2.

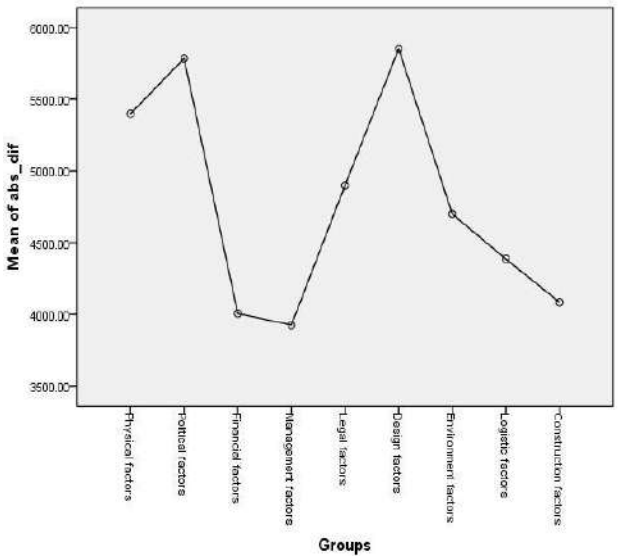

Figure 2 Post Hoc test (Mean Plot)

The statistical significances were shown between the nine risk groups at α=0.05. In this section, the test only checks the statistical significance and provides the mean rank per each risk group. The importance of Kruskal-Wallis test states in the chi-square value. Dividing the obtained Chi-Square value by the total number of observations ((N)-1) result the dependency of mean rank for each group factor. Table 3 illustrates the mean rank of each risk group and the chi-square value.

Risk factors item no.	RISK FACTORS	Frequency		Severity		Importance	
		Index	Ranking	Index	Ranking	Index	Ranking
R1	flash design(Rapid design cause mistakes)	88.37	1	83.00	3	73.34	1
R2	Disputes over land ownership	85.59	2	83.10	2	71.13	2
R3	lack of security and stability of project region	85.29	3	82.30	4	70.19	3
R4	Explosion and IED(improvised explosive device)	74.82	5	86.70	1	64.87	4
R5	giving the design into inefficient designer	80.34	4	77.80	6	62.50	5
R6	errors in estimating quantities	71.43	6	77.20	7	55.14	6
R7	lack of safety provision	67.04	8	76.80	9	51.49	7
R8	insolvency of main contractor	61.88	12	76.50	10	47.34	8
R9	incompatibility between the bell of quantities, designs and standards	62.54	11	73.60	14	46.03	9
R10	change the productivity capacity of worker and equipment	65.40	9	69.00	19	45.13	10
R11	lack in presence arbitrators specialist in conflict resolution engineering	57.53	15	75.40	11	43.38	11
R12	variation in actual and contract quantities	63.09	10	64.50	28	40.69	12
R13	inflation raising above the allowance in estimated cost	54.60	19	74.30	12	40.56	13
R14	competition in bidding	67.87	7	58.40	33	39.64	14
R15	incorrect design details	50.84	26	76.50	10	38.89	15
R16	late delivery of material mysteriously	54.52	20	69.40	17	37.84	16
R17	confusion between design's charts and specifications which cause variance between the actual executed work and specification	50.94	25	73.70	13	37.54	17
R18	Environment factors (earthquake, floods,….)	47.75	32	78.60	5	37.53	18
R19	legal controversial among project parties during project execution	50.75	27	73.10	15	37.10	19
R20	changing order	58.11	14	63.80	30	37.08	20
R21	lack in number of workers, equipment and resources	54.32	21	64.10	29	34.82	21
R22	low quality of works because of the constrains available	50.65	28	68.00	21	34.44	22
R23	difficulty to reach the project site	58.61	13	57.50	34	33.70	23
R24	instability of exchange rate	53.87	22	61.80	32	33.29	24
R25	urgent awarding of tenders	51.15	24	65.00	26	33.25	34

R26	poor managing the resources	48.52	30	68.20	20	33.09	26
R27	code and taxation changing in building sector	48.98	29	67.50	22	33.06	27
R28	unmanaged cash flow	45.19	35	72.00	16	32.54	28
R29	the lack of information mysteriously	46.04	33	69.20	18	31.86	31
R30	unforeseen weather conditions	56.14	16	56.20	35	31.55	30
R31	blurred planning because of complexity of the project	45.52	34	69.20	19	31.50	29
R32	inaccurate program for the project	39.30	41	76.90	8	30.22	32
R33	the delay in resolving problems	55.06	18	53.60	36	29.51	33
R34	no documentary changing order	44.67	36	65.00	26	29.04	25
R35	the monopoly of materials because of the unexpected political factors	42.37	37	65.90	24	27.92	35
R36	lack in communication between the site and managers	42.08	38	65.70	25	27.64	36
R37	rush bidding	52.04	23	52.00	38	27.06	37
R38	lack in defining project objective	40.68	39	64.60	27	26.28	38
R39	delay payments on contracts	40.53	40	63.60	31	25.78	39
R40	the difficulty in obtaining some of the necessary permits to work	55.11	17	46.20	39	25.46	40
R41	changing ways of managing the project	47.96	31	52.40	37	25.13	41
R42	blurred works law	35.96	42	66.30	23	23.84	42

Table 2 Risk factors Ranking According to severity Where: R= HIGH RISK and R= LOW RISK

Ranks

	Groups	N	Mean Rank
abs_dif	Physical factors	752	5161.07
	Political factors	829	5422.84
	Financial factors	1237	4509.33
	Management factors	1031	4231.03
	Legal factors	1085	4734.08
	Design factors	1437	5537.54
	Environment factors	623	4609.02
	Logistic factors	1284	4406.01
	Construction factors	1232	4289.98
	Total	9510	

Test Statistics[a,b]

	abs_dif
Chi-Square	287.720
Df	8
Asymp. Sig.	.000

a. Kruskal Wallis Test

b. Grouping Variable: Groups

Table 3 Kruskal Wallis Test

The core disadvantage of Kruskal-Wallis test doesn't clarify the significant position between the groups. Dunett test for multi comparison shows that the design and political risk groups does not have significant as p=1.00 (where P> α, α=0.05), while it has significant with other groups and so on.

iii. Effective Prevention Methods Used in Construction Projects:

One of the highest weighted mean of risk prevention methods is review of past and ongoing similar project as shown in Table 4. So, enhancing the management system with data and expecting situations from the similar historical projects is essence. This support will help the managers to activate the managing strategies for better returns. The more risks estimated, the less project failure is expected.

The methods to prevent the risks that face the project with its weights and significant are illustrated in the table 4.

PREVENTIVE METHOD	TOTAL WEIGHTED SCORES	rank	Effectiveness %
Create an effective schedule for the project and through the development of the employment relationships and renewal of project information	174	1	85.06
Review of past and ongoing similar project in order to establish an effective project program	161	2	81.36
Use personal experience to arbitration situation and the formation of a successful program for the project	138	3	73.914
Make alternative plans in case of failure of the ongoing implement of the plan for managing the risk	132	4	70.3
Adding an extra time as a result of errors or risks from inaccurate estimated project time	126	5	67.94
utilize analytic method such as precise quantitative risk analysis to compute the accurate estimated project time	109	6	53.4
Using traditional risk prevent method by transferring the risk to other parties or sharing it with theme	143	7	45.46

Table 4 Risk prevent actions in construction projects

iv. Effective Mitigation Method Used in Construction Projects:

Six risk mitigate methods are presented to the governmental institutions as illustrated in Table 5. The methods are scaled and calculated as the prevent methods. risk mitigation method are often used with risk prevention methods in order to complement the function of each other. While the prevention methods decreased the the liklihood of risk factors, the mitigation methods reduce the impact of the uncontrollable risk factors.

mitigation methods	total weighted scores	rank	Effectiveness %
Supervise with subordinator to reduce the wrong works	140	1	84.198
Make harmony of action with subcontractors	125	2	82.128
Augmentation in manpower and equipment	130	3	70.16
Working in more than one shift which mean extra working hours	132	4	67.88
Fast tracking the construction activities	128	5	67.5
Modify and change the method of project construction	122	6	48.78

Table 5 Risk mitigate action in construction projects

v. Usage of Qualitative and Quantitative Analysis Techniques:

The methods to prevent the risks that face the project with its weights and usage are illustrated in the Table 6.

Analysis methods	Total weighted scores	Rank	Usage%
Using experience and personal skills to direct judgment	168	1	87
Comparison analysis: by comparing analysis between similar projects	150	2	77.6
Probability analysis by using historical data	127	3	69.2
Using new and appropriate computer program system	113	4	65.4
Using sensitivity analysis	80	5	49
software computer package content simulation analysis	66	6	38.8

Table 6 Risk analysis methods in construction projects

CONCLUSION

Based on this study, the government institutions considerations against uncertainties can be recognized further more. The effective management is achieved through investigating and evaluating the key risk factors with corresponding to delay the project implementation. Therefore, the owner decision should be taken into account. According to the analysis of the results, the most significant risk factors (R1-R7) are highlighted individually starting with rapid design importance=73.34 and ending with lack of safety provision importance=51.49.

The government institutions and organizations are ranked for the risk factors as:

- 17% of the risk factors are assigned as high ranked;
- 60% of the risk factors have moderate; effect on construction projects; and
- 23% of the risks are considered as low risk factor.

These results indicate that the organizations recognized the most risky key factor but without knowing the effective management ways and using the analytic technique methods to control and eliminate it.

Based on Kruskal-Wallis test results, the design factors group is ranked to be the first risk group which affects the risk factors in practical point of view. Rapid design, errors in estimating quantities and incorrect design details are due to given the design into inefficient designers. The governmental organizations have to put qualified rules for the designers. Years of experience and the participated training should be taken into consideration.

The effective risk prevention method used in the government institutions in Iraq is created an effective schedule for the project and through the development of the employment relationships and renewal of project information. This method is common and its effectiveness is about 85%. The state institutions ranked the mitigation method (by supervise with subordinator to reduce the wrong works) as the first mitigation risk factor in construction projects with effectiveness of about 84%.

Regarding to the usage of the analysis techniques, using experience and personal skills (to direct judgment) is ranked as the first and its usage is about 87%. The state institutions prefer the traditional methods for making decision

rather than using computer software package to estimate accurately the projects time.

ACKNOWLEDGMENT

The author would like to thank Assoc. Prof. Dr. Kabir sadeghi for his support. Many thanks to directorate of planning and monitoring in governmental directorate in Kirkuk city on generalizing an official letter for all directorates and institutions concerned in building construction projects to show contribution with me for filling the questionnaire and data collection stage.

REFERENCES

A Guide by APM The Association of Project Management, 2000. *Project Risk Analysis and Management*. 85 Oxford road, high wycombe, London: Tha Association of Project Management.

Alfredo, F., Ximena, F., Rodolfo, H. & Larissa, R., 2014. Risk management in construction projects: a knowledge-based approach. *ELSEVIER*, 119, pp.653-62.

B.A.K.S., P., Raufdeen, R., Nicholas, C. & Reza, H., 2014. Enhancing the effectiveness of risk management practices in Sri Lanka road

construction projects:A Delphiapproach. *International Journal of Construction Management*, 14, pp.1-14.

Cooper, F.., Grey, S., Raymond, G. & Wallker, P., 2005. *Managing Risk in large projects and complex procurements*. England: Hohn Wiely & Sons.

Crawford, K.J., 2002. *Project Management Maturity Model: Providing a Proven Path to Project Management Excellence*. New York: Marcel Dekker.

Flanagen, H. & Norman, G., 1993. *Risk Management and Construction*. London: Blackwell science.

Golafshani, N., 2003. *Understanding Reliability and Validity in Qualitative Research*. Canada: The Qualitative Report.

Mousa, A. & Hmaid, J., 2005. *Risk Management in Construction Projects from Contractors and Owners perspectives*. [Online] Palestine: The Islamic University of Gaza Available at: library.iugaza.edu.ps/thesis/63916.pdf.

Satyendra, K. & Niranjan, S., 2011. Risk Management in Construction Projects. *Asia-Pacific Journal of Management Research and Innovation*, VII, pp.107-20.

Zhao, X., Hwang, B.G. & Yu, G.S., 2012. Identifying the critical risks in underground rail international construction project. *Construction Engineering Management*.

Zou, W.X., Zhang, G. & Wang, J.-Y., n.d. Identifying Key Risks in Construction Projects: Life Cycle and Stackehoklder Perspectives.

ZANCO Journal of Pure and Applied Sciences
The official scientific journal of Salahaddin University-Erbil
ZJPAS (2018) 30 (s1) s42-s49
http://dx.doi.org/10.21271/ZJPAS.30.s1.5

Water Surface Profile along Different Side Weirs in Subcritical Flow Regime

***Bruska S. Mamand[1], Adil M. Raheem[2]**

[1]Assistant Lect., College of engineering, Salahaddin University-Erbil

[2]Assistant Prof., College of engineering, Salahaddin University-Erbil

ARTICLE INFO

Article History:
Received: 14 / 05 /2017
Accepted: 12 /04 /2018
Published:01/06/2018

Keywords:
Side weir.
Fluent.
k-ε Turbulent Model.
Water Surface Profiles.

**Corresponding Author:*
Email:

bruska.sardar@gmail.com

ABSTRACT

Side weir was hydraulic structure used to divert flow from the main channel into the side channel whenever the water surface rise above the side weir crest. In the present study FLUENT code that interfaced on ANSYS (V.14.0) was used to examine the computational domain in subcritical flow condition. Five different types of side weirs installed inside the horizontal prismatic rectangular main channel. Models were normal rectangular with ($\theta = 90^o$), oblique rectangular in which its crest is inclined with the flow direction by ($\theta = 75^o$, 60^o and 45^o), triangular labyrinth with apex angles ($\delta = 90^o$ and120^o), semi-hexagonal labyrinth with wall angles ($Z = 30^o$ and 64.7^o) and semi-circular labyrinth side weirs. The volume of fluid method (VOF) provided to truck the free surface profiles. The computational code is validated against the experimental models. Three different k- ε turbulent models were tested namely re-normalized group (RNG k-ε), standard k-ε and realizable k-ε. Free surface flow profile for three dimensional (3D) subcritical flow condition at the centerline of the main channel and near side weir bank were measured and plotted for different side weir models, the longitudinal water surface profile in the main channel was found to be increased from upstream end towards the downstream end of the side weirs. Result for aforementioned turbulent models was compared with the experimental data and it was found that the RNG k-ε turbulent model provide more accurate results compared with other turbulent model examined in the present study.

INTRODUCTION:

The flow condition in the main channel at the upstream and downstream end of a side weir (i.e. Fr_1, Fr_2 respectively), have a major influence on the behavior of the flow over the weir itself. (May *et al.*, 2003) stated that the flow conditions at side weir was very complex issue due to many principal factors which were difficult to be analyse. Flow at the side weir section was strongly considered to be three dimensional flow passing over the weir crest crosses at an inclined angle rather than at right angle and the water level in the main channel does not remains constant but may rise and fall along the length of the side weir. Generally subcritical flow occur in the main channel with the existence of the side weirs. Using the principle of the energy in which developed by (De Marchi, 1934) considering the specific energy to be constant between upstream and downstream ends of the side weirs, the dynamic equation of spatially varied flow (SVF) can be obtained as:

$$\frac{dy}{dx} = \frac{S_0 - S_f - \frac{\alpha Q}{g A^2}\frac{dQ}{dx}}{1 - \frac{\alpha Q^2 T}{g A^3}}$$

where; y is depth of flow, x is the distance along the side weir from upstream end, S_o is the main channel slope, S_f is friction slope, α is kinetic energy correction factor, Q is discharge in channel, dQ/dx is discharge per unit length of side weir, g is the acceleration due to gravity, A is cross-sectional area of flow and T is the top width of the channel section.

Most of investigations carried out on the flow over side weirs, (Swamee *et al.*, 1994) analyzed the discharge coefficient using fourth order range kutta method. (Uyumaz, 2007) numerically investigated the flow over the side weirs in triangular main channel for both subcritical and supercritical flow regimes. Investigation both experimentally and numerically the flow over the rectangular side weir with zero sill height located in a horizontal rectangular channel was done by (Mangarulkar, 2010). Simulation experimentally water surface profile along 1m length of side weir using the ANSYS CFX code by (Martins, 2011). (Aydin, 2011) used ANSYS FLUENT code for model runs to simulate the free surface flow over triangular labyrinth side weir under subcritical flow condition. (Mahmodinia *et al.*, 2012) were investigated the effects of Froude number on the upstream side of the weir on the free surface flow over the side weir. (Namaee, 2014) applied ANSYS FLUENT code to investigate the flow over broad crested side weir having a longitudinal inclined ramp and water surface profiles of k-ε turbulence model was compared with an experimental profiles. (Hoseini *et al.*, 2013) investigated the discharge coefficient of rectangular broad crested side weir located on trapezoidal channel. One can notice that the flow over side weir was complex hence understanding its behavior and characteristics is essential to improve the design of such kind of hydraulic structure. For this purpose the computational FLUENT code is applied to predict the water surface profile along the side weirs for different flow conditions and flow rates in the main channel.

Navier-Stokes Equation:

Navier–Stokes equations are the governing equations for the fluid motion which numerically can be solve for the models of flow through different boundary conditions for a known geometry. These equations in three dimensional form for unsteady viscous fluid were presented by (Desai and Patil, 2015) as follows:

$$\frac{\partial u}{\partial t} + \frac{1}{V_F}\left(uA_x\frac{\partial u}{\partial x} + vA_y\frac{\partial u}{\partial y} + wA_z\frac{\partial u}{\partial z}\right) = -\frac{1}{\rho}\frac{\partial p}{\partial x} + G_x + f_x$$

$$\frac{\partial v}{\partial t} + \frac{1}{V_F}\left(uA_x\frac{\partial v}{\partial x} + vA_y\frac{\partial v}{\partial y} + wA_z\frac{\partial v}{\partial z}\right) = -\frac{1}{\rho}\frac{\partial p}{\partial y} + G_y + f_y$$

$$\frac{\partial w}{\partial t} + \frac{1}{V_F}\left(uA_x\frac{\partial w}{\partial x} + vA_y\frac{\partial w}{\partial y} + wA_z\frac{\partial w}{\partial z}\right) = -\frac{1}{\rho}\frac{\partial p}{\partial z} + G_z + f_z$$

It was supplemented by the mass conservation equation:

$$\frac{\partial u}{\partial x}A_X + \frac{\partial v}{\partial y}A_y + \frac{\partial w}{\partial z}A_z = 0$$

Where, V_F is the fractional volume open to flow, ρ is fluid density, (u,v,w) are velocities in (x,y,z) direction respectively, t is time, (Ax,Ay,Az) are fractional areas open to flow in direction (x,y,z), (G_x,G_y,G_z) are body accelerations and (f_x,f_y,f_z) are viscous accelerations. These are the simplified equations for incompressible free surface flow with constant viscosity. Fluid configuration was defined in terms of volume of fluid (VOF).

MATERIALS AND METHODS

Experimental models were constructed for different types of side weirs then their geometries numerically were created by using FLUENT workbench. It was consisted of a solid domain of horizontal 3D rectangular main channel. The dimensions of the channel was 0.2m width, 0.3 m deep, and 2.2m downstream length which starts from the end of the side weir crest toward the downstream end of the

channel and the upstream length 1.4 m starts from the inflow boundary (inlet) of the main channel to the upstream end of the side weir. For diverting a part of the flow laterally, side weirs was placed at one side of the main channel as shown in Figure (1). This figure describes the definition sketch of different side weir models tested in the current study.

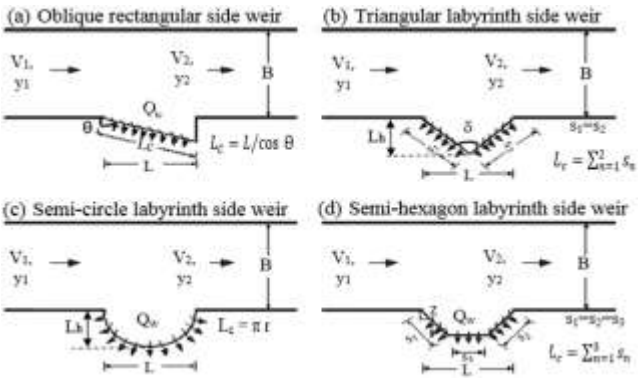

Fig.1. Definition sketch for different side weir models examined in the present work.

The geometric domain for triangular and semi-circular side weirs was shown in Figure (2). The computational area for all models was divided into a collection of cells which addressed as grids through set of points distributed on the geometry region. In the present study, the automatic mesh method used to calculate mesh grids throughout a solid domain as shown Figure (3). Mesh size should be fine enough to ensure the flow features spread out through all fields. Therefore the suitability of the mesh cells for all side weir models was checked from mesh metric option through a main key measurement named as skewness, the skewness should not exceed 0.85 for hexahedra, quadrilateral and triangular cells, while 0.90 for tetrahedral cells.

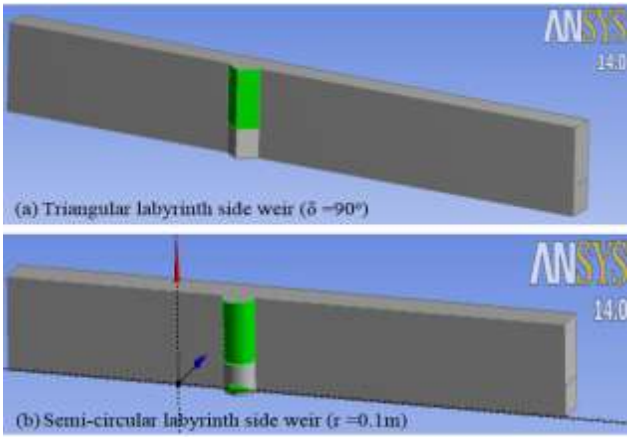

Fig.2. Isometric veiw for side weir geomerty.

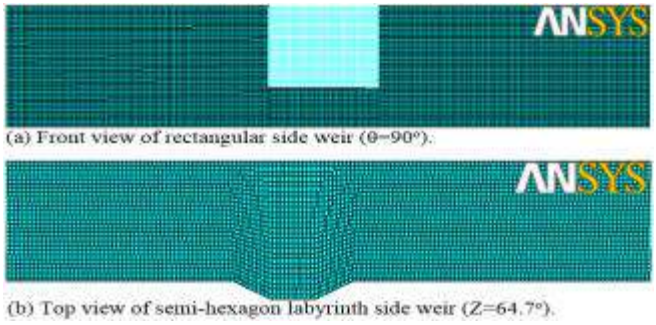

Fig.3. Displaying mesh density for different side weirs.

Boundary conditions are usually set to identify the physics of the flow passed over the side weirs. Their locations was divided into; Inlet: which water flows only into the channel with a known inlet water depth and the magnitude of inlet velocity that measured from the experiments. Side weir outlet: where fluid from the domain is exited out and Cartesian coordinate system (x, y, and z) for direction vectors was used. Ambient boundary: Top surface of the channel and walls were set as impermeable to flow, smooth and slipping did not occur. k-ε was selected as a specification method for inlet and outlet boundaries. Also second-order upwind scheme were set for mass, momentum and turbulence models. Mass imbalance for assessing the convergence criteria was checked via solver flux report with the actual experimental data.

RESULTS AND DISCUSSION

To produce more accurate computational results in term of water surface profiles along the channel centreline, the mesh dependence

was checked for several element sizes as shown in table (1). During all runs for meshes the RNG k- ε turbulence model was used.

Table (1) Four mesh sizes examined in the study.

Grid Name	No. of Elements	No. of Nodes
Mesh (A4)	62400	70854
Mesh (A3)	218400	237615
Mesh (A2)	427500	457314
Mesh (A1)	519480	553336

Mesh quality plays a significant role in the accuracy and stability of the numerical tests. The longitudinal water surface profiles for each mesh grid was measured at the centreline of the main channel along the side weir section. Figure (4) illustrated the quite difference between mesh four mesh grids in comparing with experimental water surface profile. In other words, Mesh (A1) was in agreement with experimental data therefore this mesh size was allowed in the present work.

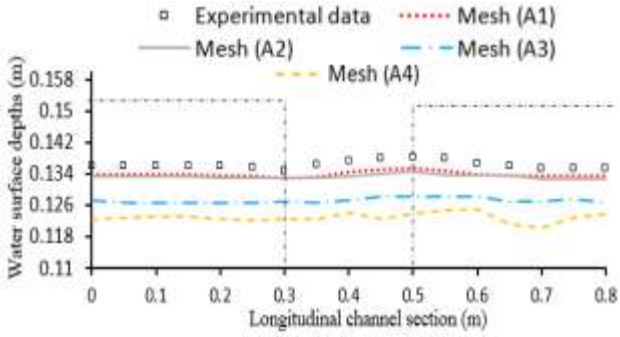

Fig.4. Comparison between experimental & numerical water profiles along the main channel centreline for different mesh sizes.

Three different k-ε turbulence models as (Standard, Realizable and RNG) were applied in this study to identify the numerical model that increase the accuracy of the numerical results. Figure (5) shows the error percentage for the flow passing over the side weirs (Q_w) using experimental flowrate ($Q_{w\ exp.}$). Average error obtained for three models (standard, realizable and RNG) models were (8.75%, 6.99% and 6.85%) respectively. This result demonstrate that the standard k-ε turbulence model provide higher percentage of error compared with the other two models. This may be due to the fact that the flow condition near the wall regions cannot be solved by this type of turbulence model. It can also be observed that the percentage of error produced by the other two models was identical. RNG model was more responsive to the effects of streamline curvature and treating sensitively near wall regions, and the profiles of RNG k- ε model at both positions (at centreline of the channel and near the side weir) was in agreement with the experimental profiles.

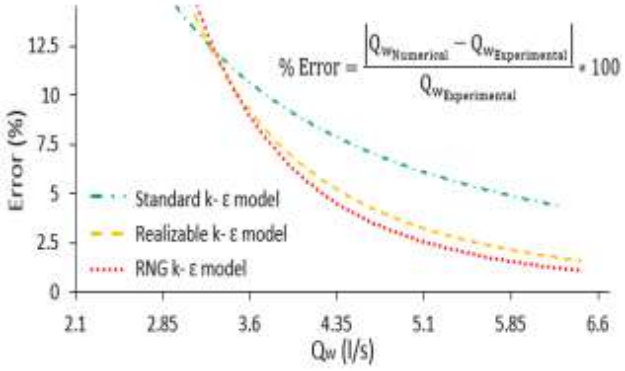

Fig.5. Error comparison of three types of k- ε turbulence models.

The aforementioned errors may be due to surface waves especially near the weir bank which was experimentally difficult to be measured exactly.

The longitudinal water surface profile for different side weir models as mentioned above were drawn experimentally and numerically. Two positions for profiles was selected, one at centerline of the main channel and the other near the side weir bank by a distance 0.05m. For this purpose a plane of the water-volume fraction was set as shown in Figure (6).

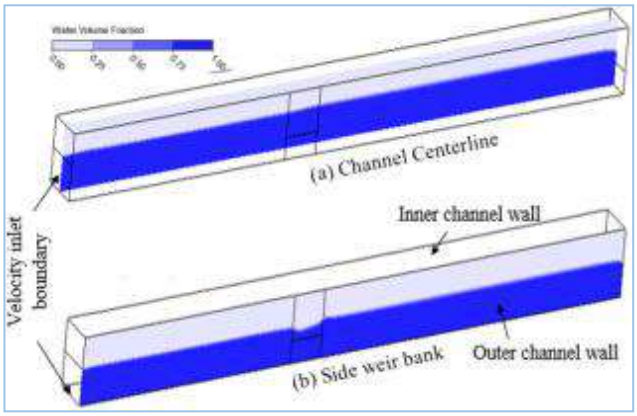

Fig.6. Longitudinal water surface profiles along centreline and near side weir bank.

Figure (7-A) indicates that for subcritical flow condition inside the main channel, the longitudinal water surface levels at both positions increase from the side weir entry towards the weir exit, due to the increase of the water depth in the downstream side of the weir ($y_2>y_1$). Water levels near the weir bank drop slightly at side weir entry with a small distance (x_1) and this phenomenon has been attributed to the side weir entrance effect at the upstream end near weir crest. Afterwards a gradual increase of water levels can be observed towards the middle of the crest. Finally, the water level rapidly rises by a distance (x_2) reaching its maximum level near the weir exit and parallel flow to the channel bed was observed at the downstream of the side weir. On the other side, the water profiles at the centreline of the channel was found to be smoother than the profiles along the side weir due to the absent of the side weir entrance effect at the channel centreline.

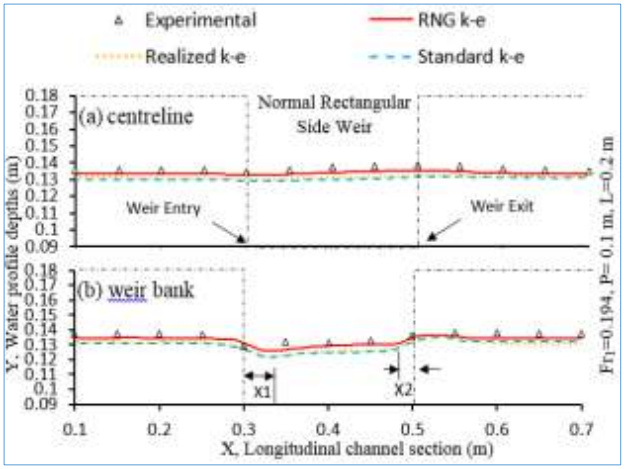

Fig.7-A. Water surface profiles along the centerline and banks of rectangular side weir ($\theta=90^o$).

Similar profiles was drawn for other types of the side weirs as shown in Figure (7-B). The tendency of surface profiles was slightly changed for different side weir geometric shape, dimensions, and channel inflow discharge. For furthermore on the free surface profiles the (SURFER V.08) software was used to plot their 3 dimensional view of elevations inside the main channel. Different types of side weirs were installed and their crests was taken as a reference datum for measuring the depth of water. For this purpose the same inlet discharge was tested for all type of the side weirs and a slight differences in Fr_1 values noted. Figure (8) revealed that the dropped flow toward the side weir was clearly noted.

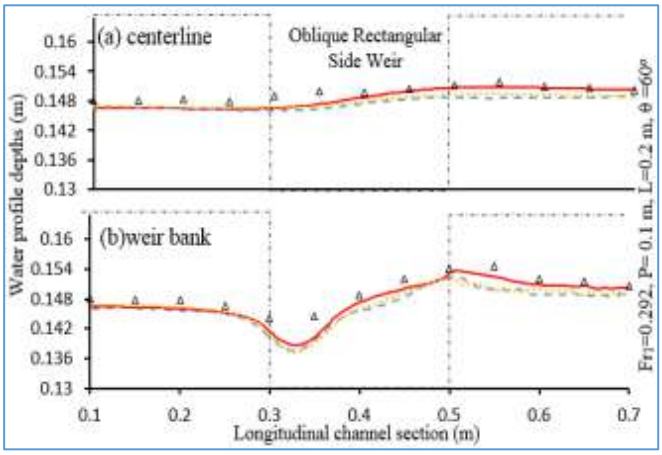

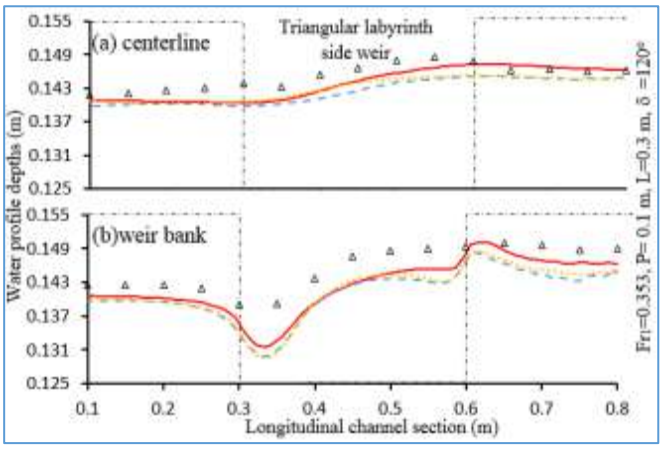

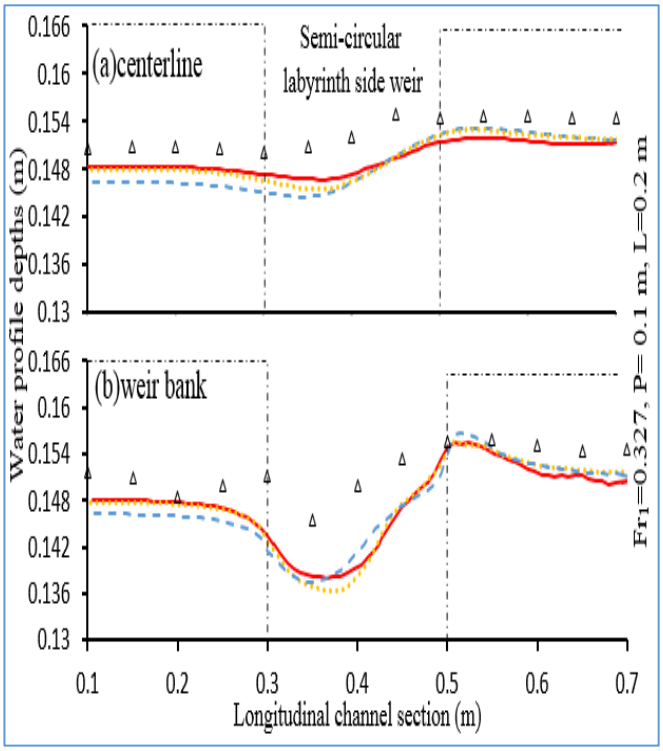

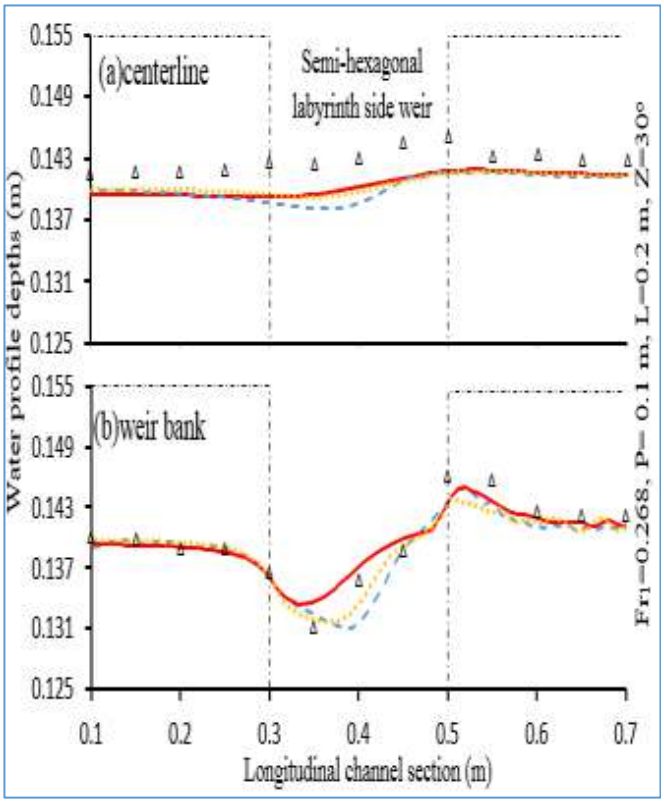

Fig.7-B. Water surface profiles along the centerline and banks of different side weir models.

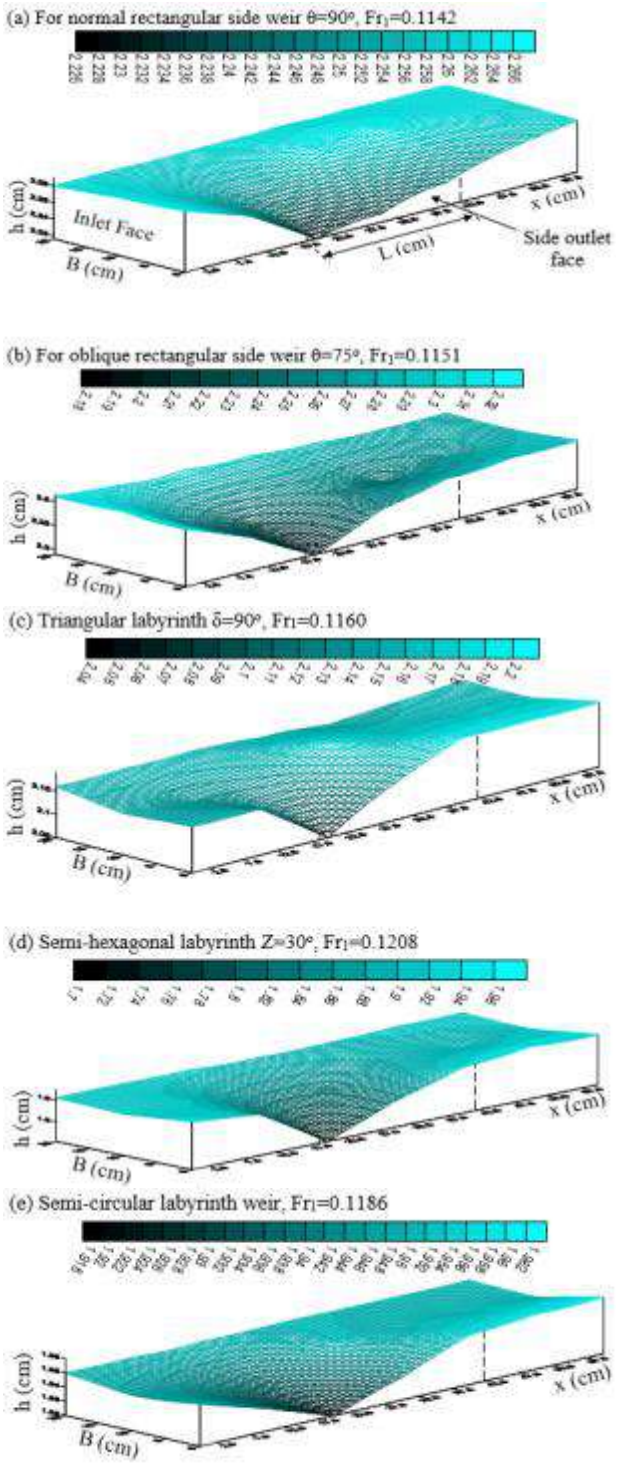

Fig.8. 3-D view of water surface elevations inside the main channel

The presence of lateral flow created by side weir overflow in the main channel causes the flow to separate from inner channel wall which forms a separation flow region as shown in Figure (9). The location of separation region, its length (S_L) and width (S_w) depend on the upstream Froude number, as well as on the shape and overflow length of the side weir. Results shows that length of separation flow

region decreases with increasing in Fr_1 value, the same result was obtained by Mangarulkar (2010), Rao (1968) and Emiroglu et al. (2010). While maximum width of this zone(S_w) was measured approximately to be less than 0.25 times the width of the main channel in comparing with Mangarulkar (2010) who showed S_w= 0.3 B.

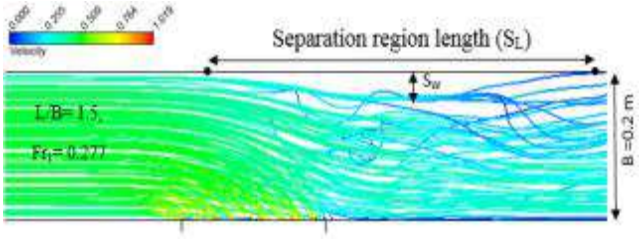

Fig.9. Top view of separation flow streamlines for Normal rectangular side weir.

Another main feature that occurred in labyrinth and an oblique rectangular side weirs was the formation of depression zone. This phenomenon was appeared near the upstream crest of the inner face of side weirs, it was due to contacting bed streamlines with side weir wall which causing the flow to re-circulate then either reversed to main channel (especially bed streamlines) or passed over the side weir into the side channel. As shown in Figure (10), the velocity streamlines at the inner side of upstream semi-circular side weir face developed an approximate elliptical rotation of streamlines due to weir circular bend. While at the downstream half of weir face larger amount of water was diverted to the side channel over its crest as their upstream portion is blocked by the return flow zone.

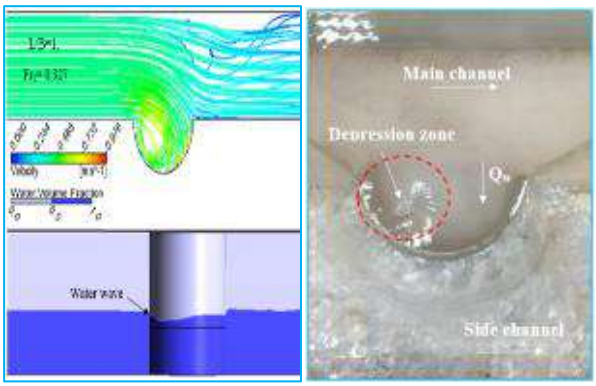

Fig.10. Depression zone of circular labyrinth side weir.

For different side weir models, Figure (11) demonstrate the size and shape of the return flow area for different weir geometry, upstream Froude number (Fr_1) and dimensionless (L/B) term.

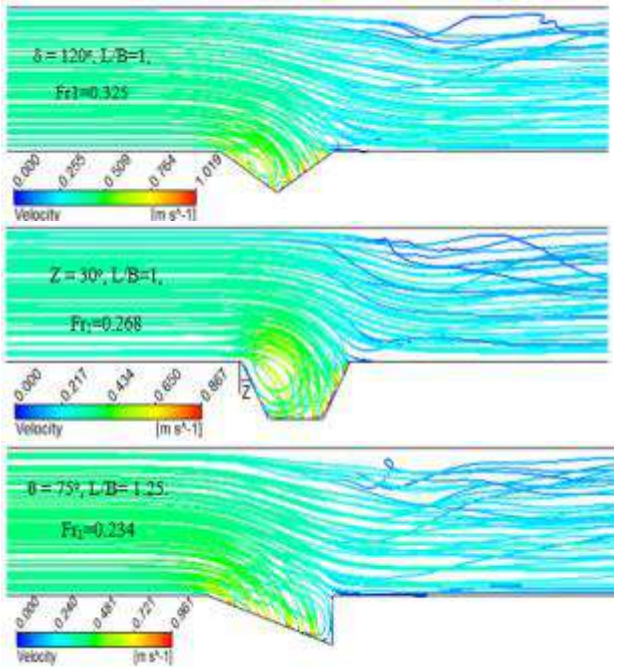

Fig.11. Return flow area for other side weir models.

CONCLUSION:

1. Experimental and numerical water surface profile inside the main channel was investigated for different types of side weirs. For subcritical flow condition the water depth at upstream end of the side weir was greater than the depth at downstream end ($y_2>y_1$).
2. Different mesh sizes were used and examined to determine the size that produces more accurate computational results compared with experimental data. Three difference k-ε turbulent models (Standard, realizable and RNG) were applied to identify the accuracy of the numerical models, the percentage of errors between the experimental and the numerical results for the flow passing over the side weirs (Q_w) for (standard, realizable and RNG model) were found to be (8.75%, 6.99% and 6.85%) respectively. RNG model was more responsive to the effects

of streamline curvature and treating sensitively near walls regions, the profiles of RNG k- ε model at both positions (at centreline of the channel and near the side weir) was in agreement with the experimental profiles.

3. The presence of lateral flow created by side weir overflow in the main channel causes the flow to separate from inner channel wall which forms a separation flow region, location of separation region, its length (S_L) and width (S_w) depend on the upstream Froude number. The length of separation flow region decreases with increasing in Fr_1 value the maximum width of this zone (S_w) was measured approximately to be less than 0.25 times the width of the main channel. Formation of depression zone appeared near the upstream crest of the inner face of the side weirs, which cause the flow to be re-circulate. Size and shape of the return flow area for different weir geometry, upstream Froude No ($Fr_{1)}$ and dimensionless (L/B) term were also investigated.

REFERENCES:

ANSYS FLUENT 12.0, tutorial guide (2009). Certified to ISO 9001: 2008 and ANSYS FLUENT 14.0, Solver and theory helps.

Aydin, M. (2011). 'CFD simulation of free-surface flow over triangular labyrinth side weir ', Department of Civil Engineering, BitlisEren University.

De Marchi, G. (1934). 'Saggio di teoria de funzionamentedeglistramazziLaterali' Energ. Elettr, 11(11), 849–860.

Desai, R. and Patil, L. (2015). 'Performance Comparison of Various Labyrinth Side Weirs ', International Journal of Application or Innovation in Engineering & Management (IJAIEM), 4 (6), p.68-73.

Hoseini, S., Jahromi, S. and Vahid, M. (2013). 'Determination of Discharge Coefficient of Rectangular Broad-Crested Side Weir in Trapezoidal Channel by CFD ', J. of Hydraulic Engineering, 2 (4), p. 64-70.

Emiroglu ,M.,Kaya,N. and Agaccioglu ,H.(2010) 'Discharge capacity of labyrinth side weir located on a straight channel',J. of irrigation and drainage engineering ,ASCE.136(1),P.37-46.

Mahmodinia, S., Javan, M. and Eghbalzadeh, A. (2012). ' The Effects of the Upstream Froude Number on the Free Surface Flow over the Side Weirs ' , International Conference on Modern Hydraulic Engineering, Vol.28, p. 644-647.

Mangarulkar, K. (2010). 'Experimental and numerical study of the characteristics of side weir flows ', MSc thesis, University of Concordia, Quebec, Canada.

Martins, J. (2011). 'Analysis of hydraulic performance of a side weir by CFD ', MSc thesis, Polytechnic school, University of Sao Paulo, Dept. of civil engineering, Sao Paulo, Portugal.

May, R., Bromwich, B., Gasowski, Y. and Richard, C. (2003). 'Hydraulic design of side weirs ', Thomas telford publishing, heron quay, London E14 4JD.

Namaee, M. (2014). 'Numerical Investigation of a Side Weir with an Inclined Ramp ', J. of World Applied Sciences, 31 (10), p. 1759-1766.

Rao N., Sridharan K., and Baig M. (1968). 'Experimental study of the division of flow in an open channel', India institute of science,p.139-142.

Subramanya, K. and Awasthy, S.C, (1972). 'Flow over side weirs ', Indian institute of technology, p. 328-334.

Swamee, P., Pathak, T. and AlP, M. (1994). 'Side-weir analysis using elementary discharge coefficient ', J. of irrigation and drainage engineering, ASCE, 120 (3), p. 742-755.

Uyumaz ,A.,2007. 'Discharge control by a side weir in a triangular main channel ' University of technical Istanbul,p.12451-1258.

ZANCO Journal of Pure and Applied Sciences
The official scientific journal of Salahaddin University-Erbil
ZJPAS (2018) **30**(s1)s50-s61
http://dx.doi.org/10.21271/ZJPAS.30.s1.6

Stochastic Models for the Maximum and Minimum Daily Flows of Tigris and Khabur Rivers

Dr.Khalid M.Khadir * Dr. Adil M. Raheem Mrs. Syran A. Ibrahim*****

*Assistant prof., college of engineering- University of Duhok.
**Assistant prof., college of engineering- University of Salahaddin
***Assistant Lecturer, college of engineering- University of Duhok.

A R T I C L E I N F O

Article History:
Received: 14/05/2017
Accepted: 12/04/2018
Published:01/06/2018

Keywords:
Stochastic model
Time series
SARIMA model
Matalas model

**Corresponding Author:*
Email:
adil.raheem@su.edu.krd

A B S T R A C T

In this paper, time series for the available recorded data of Tigris and Khabur Rivers at Tusan and Zakho stations were analyzed, stochastic models were investigated for both stations using several time intervals (maximum and minimum daily flow in a month), normality was tested using Kolmogrov-Smirnov approach, series transformation to normal distribution was carried out using Box-Cox method , Split-Sample method and Kendall's Correlation tests were used to check and remove the jump and trend components from the series of the two rivers, and the periodicity component also was detected.

Stochastic models, SARIMA (Seasonal Autoregressive Integrated Moving Average) and Matals (multisite), were used for forecasting and generating the time series for the above two mentioned rivers. Autocorrelation Function (ACF) and Partial Autocorrelation Function (PACF) were used to identify the suitable SARIMA model. The Akaike Information Criteria (AIC) formula was used to find the suitable model for the series with the time intervals as described previously.

SARIMA models of order SARIMA$(1,0,0)(0,1,1)_{12}$ and SARIMA$(1,0,0)(0,1,1)_{12}$ were found to be suitable for maximum and minimum daily flow in a month time series for Zakho station respectively, SARIMA$(1,1,1)(0,1,1)_{12}$ and SARIMA$(1,0,0)(0,1,1)_{12}$ were found to be suitable for maximum and minimum daily flow in a month time series for Tusan station respectively .Matalas model of first order AR(1) was applied for the time series of both stations.

INTRODUCTION

Stochastic simulation methods were first introduced in hydrology in the reservoir design. The required capacity of a reservoir depends on the sequence of flows, especially a sequence of low flows (**Lenseley, 1982)**.

Stochastic generation techniques can be used to generate time series that differ from the observed time series but retain many properties of the original series. This time series can be divided into different sequences and each one should have the same length of the recorded one. In each sequence, the events will have the same probability of occurrence as the observed sequence.

The technique of time series analysis used for the estimated statistical parameters (from

historical series) is to build a mathematical model capable of describing the evolution of possible sequences of events in time at the site of observations, which have the same statistical properties as the historical sample, this model can then be used to synthesis stream flow sequences. There are varieties of available methods for forecasting stream flows. However, to build a forecasting model is not an easy task to choose a suitable model because none of them is powerful and general enough every model has some degrees of structure and uncertainty parameters(**Al-Suhaili, 1985)**.

Due to lack of the recorded data for Tigris River and its tributaries, two stochastic models were used as SARIMA (Seasonal Auto Regressive Integrated Moving Average) and Matalas models for analyzing the available data of a long period, since the two models have wide applications for different types of hydrological time series.

In order to investigate the performance and evaluate the ability and efficiency of these two stochastic models for forecasting and generating different type of series, the time series of different intervals for the two discharges sites was used as maximum and minimum daily flow.

The Study Area:

The present paper deals with the investigation of the two stations, Zakho and Tusan, which are located on Khabur and Tigris Rivers respectively. Khabur River is one of the tributaries feeding Tigris River at the north of Iraq. The total length of Khabur River is about 160 km which feeds Tigris River about 1.6 million cubic meter of water yearly. Tigris River also flows out from the Turkish lands. The total length of Tigris River is about 1900 km where about 1415 km is inside the Iraqi lands, while the remaining length is inside the Turkish lands. Zakho station is located at Lat. 37^0 $8'$ North and Long. $42^0 41'$ East, elevation approximately equals 440m above the mean sea level .The drainage area was equal to 3500 km^2 and the available discharge was recorded for the period (1959 to 1982). The maximum daily discharge recorded was 1270 m^3/sec on 11 April 1963, while the minimum daily discharge recorded was 8 m^3/sec for the 1^{st} to 7^{th} October 1975. The drainage area was about 3500km^2.Tusan station is located at Lat 37^0 North and Long.$42^0 28'$ East. Its elevation is approximately equal to 330m above the mean sea level. The drainage area was equal to 46700 square kilometers and the available discharge was recorded for the period (1959 to 1975). The maximum daily discharge was 7050 m^3/sec on the 2nd April, 1969, while the minimum daily discharge was 53 m^3/sec on 7th to 30th September, 1971. The two rivers and stations was shown in **Figure 1**.

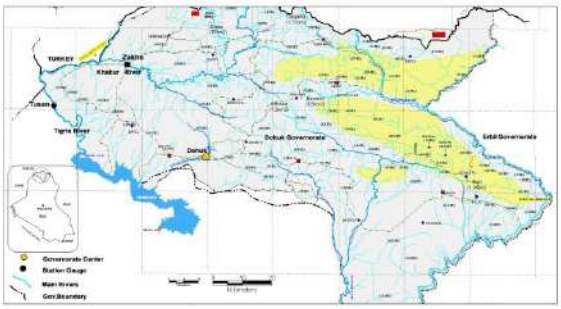

Figure 1 location of Zakho and Tusan stations

SARIMA and Matalas Models:

The general form of seasonal Autoregressive Integrated Moving Average SARIMA (p, d, q)*(P, D, Q)s can be expressed in the following form **(Wang, 2006)**:

$$\phi(B)\Phi(B^s)(w_t - \overline{X}) = \theta(B)\Theta(B^s)\xi_t \quad ...(1)$$

Where

$$\phi = 1 - \sum_{i=1}^{p} \phi_i B^i \quad ..... (2)$$

$$\Theta = 1 - \sum_{i=1}^{q} \Theta_i B^i \quad ..... (3)$$

$$\Phi = 1 - \sum_{i=1}^{P} \Phi_i B^i \quad \text{..... (4)}$$

$$\Theta = 1 - \sum_{i=1}^{Q} \Theta_{is} B^{is} \quad \text{..... (5)}$$

$$BX_t = X_{t-1} \quad \text{..... (6)}$$

$$w_t = \left((1-B)^d (1-B^s)^D X_t \right) \quad \text{..... (7)}$$

With $\overline{X}$: Average of Recorded time series, ϕ : Coefficient of Autoregressive (AR), θ : Coefficient of Moving Average (MA),p : Order of Autoregressive ,q : Order of Moving Average ,Φ:Coefficient of seasonal Autoregressive, Θ : Coefficient of seasonal Moving Average ,P : Order of seasonal Autoregressive, Q : Order of seasonal Moving Average, s : Season length, d : Order of de seasonality difference and D:Order of seasonality difference.

The most common Multisite model used was the first order auto-regressive model which was initiated in hydrology by Matalas (1967). This model assumed that the series of the recorded data at each site was normalized and standardized after removing the non homogeniety components (jump and trend) and seasonality.The Matalas model can be builted by normalyzing each time series by Box-Cox Transformation ,checking the stationary and homogeneity of each time series (Jump and Trend) ,and then standardizing the time series . After the previos steps were satisfied, the Matalas model can be used for any numbers of gauging stations (ns), where (ns) in this study equal to 2.

The form of the first order AR(1) of multisite model was(**Al-Mousawi, 2003**)::

$$X_t = \boldsymbol{A} X_{t-1} + \boldsymbol{B} \zeta_t \quad \text{..... (8)}$$

Where

X_t, X_{t-1} are (ns) - dimensioned column vectors representing the standardized flows corresponding to (ns) sites at time t and t-1. ζ_t is the column vector of (ns) serially and mutually uncorrelated independent variables at time t with zero mean and unit variance.

$$X_t = \begin{bmatrix} X(1,t) \\ X(2,t) \\ . \\ . \\ X(i,t) \\ . \\ . \\ X(ns,t) \end{bmatrix}, \quad X_{t-1} = \begin{bmatrix} X(1,t-1) \\ X(2,t-1) \\ . \\ . \\ X(i,t-1) \\ . \\ . \\ X(ns,t-1) \end{bmatrix},$$

$$\zeta_t = \begin{bmatrix} \xi(1,t) \\ \xi(2,t) \\ . \\ . \\ \xi(i,t) \\ . \\ . \\ \xi(ns,t) \end{bmatrix} \quad \text{..... (9)}$$

($\boldsymbol{A}$) and ($\boldsymbol{B}$) are coefficient of the matrices of size (ns x ns) which can be determined as :

$$\boldsymbol{A} = M_1 M_0^{-1} \quad \text{..... (10)}$$

$$\boldsymbol{B}\boldsymbol{B}^T = M_0 - \boldsymbol{A}\, M_1^T \quad \text{..... (11)}$$

M_0 : Lag-zero cross- correlation matrix

M_1 : Lag-one cross correlation matrix

M_0^{-1} : Inverse matrix of M_0

M_1^T : Transposed matrix of M_1

The matrix ($\boldsymbol{A}$) can be evaluated directly using equation (10), but the matrix ($\boldsymbol{B}$) can be evaluated from the Matrix ($\boldsymbol{B}\boldsymbol{B}^T$) using equation (11) **(Tahrir ,1984 as cited in Yong,**

1968) assumed the matrix ***B*** triangular as shown below:

$$\boldsymbol{B}=\begin{bmatrix} b_{11} & 0 & \dots & 0 \\ b_{21} & b_{22} & \dots & 0 \\ . & . & \dots & 0 \\ b_{n1} & b_{n2} & \dots & b_{nn} \end{bmatrix} \quad \text{..... (12)}$$

The matrix $\boldsymbol{BB}^{T}$ was assumed to be equal to matrix ***C*** ,where ***C***(I,J)=***C***(J,I) with number of stations equal to two ,then :

$$\boldsymbol{BB}^{T}= \begin{bmatrix} b_{11} & 0 \\ b_{21} & b_{22} \end{bmatrix}\begin{bmatrix} b_{11} & b_{21} \\ 0 & b_{22} \end{bmatrix}=\begin{bmatrix} b_{11}^2 & b_{11}b_{21} \\ b_{21}b_{11} & b_{21}^2+b_{22}^2 \end{bmatrix}=\begin{bmatrix} c_{11} & c_{12} \\ c_{21} & c_{22} \end{bmatrix}$$

..... (13)

The elements of matrix ***B*** can be determined as (**Jayarami Reddy, 1997**):

$$b_{11}=(c_{11})^{1/2}\ ,\ b_{21}=c_{21}/b_{11}\ ,\ b_{22}=(c_{22}-b_{21}^2)^{1/2}$$

..... (14)

After estimating the matrices ***A***, ***B***, M_0 and M_1, the model can be applied for generating the required time series for any period.

Model application and discussion:

SARIMA model was applied as a single site model by using program MINITAB ver 13.2 for the time series (maximum and minimum daily series).Matalas model was also applied as a multisite model for the time series mentioned above for the two stations by using a developed computer program modified in this study in FORTRAN 2000.

The recorded data for Tigris and Khabur Rivers at Tusan and Zakho stations respectively were used for the available recorded period ,which were obtained from the references from the Iraqi publication and documentation, like Iraqian publications of the general directorate of irrigation at 1976, publications of the office of the state organization for maintenance and operation of irrigation projects at 1983 and publications of the directorate of operating the irrigation projects at 1989.

In order to check the normality of the time series of the two stations under study, Kolmogrov-Smirnov test should be used, which was present in the MINITAB computer program ver. 13.2 by comparing the studied time series with a theoretical time series which has the normal distribution. **Figure 2 and Figure 3** show the non- normality of the maximum daily time series for Zakho and Tusan stations while **Figure 4 and Figure 5** show the non- normality of the minimum daily time series ,because the skewness coefficient (C_S) for each one was not equal to zero, so the time series for Zakho and Tusan stations must be converted to a normal distribution series as a first step before analyzing the data .

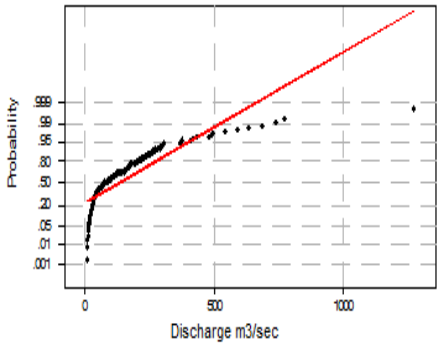

Figure 2 Testing the Normal Distribution of max., daily flow series for Zakho station by Kolmogrov-Smirnov test

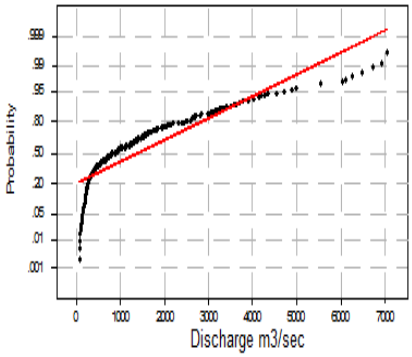

Figure3 Testing the Normal Distribution of max, daily flow series for Tusan station by Kolmogrov- Smirnov test

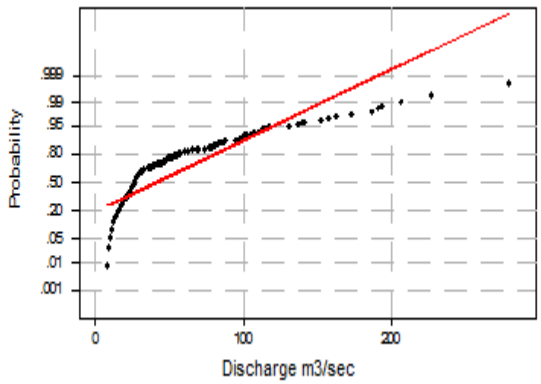

Figure 4 Testing the Normal Distribution of mim., daily flow series for Zakho station by Kolmogrov-Smirnov test

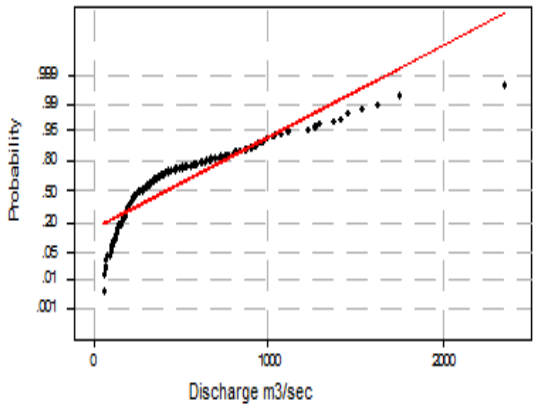

Figure 5 Testing the Normal Distribution of mim, daily flow series for Tusan station by Kolmogrov-Smirnov test

To transform the data to normal distribution, the power transformation of Box-Cox was applied, the value of λ (Box-Cox coefficient) was found to be -0.0685 and -0.03535 for the series of maximum and minimum flow of Zakho station while the value of λ (Box-Cox coefficient) was found to be 0.04491 and -0.1462 for the series of maximum and minimum flow of Tusan station. Applying the λ values in equation 15 the time series of the two station were converted to normal distribution with skewness coefficient equal to zero. (**Salvator Grimaldi, 2004**):

$$Y_t = \frac{X_t^{\lambda} - 1}{\lambda} \qquad \text{…….(15)}$$

where

Y_t:Recorded time series after transforming to normal distribution.

X_t : Recorded time series values.

λ : Box-Cox coefficient. λ lies within the range (+1,-1) but not equal to zero.

Figures 6 and **Figures 7** show the Kolmogrov-Smirnov test after transforming the maximum daily flow time series to the normal distribution. The same procedure were carried out to the minimum daily flow time series for the Zakho and Tusan stations as shown in **Figure 8** and **Figure 9 .**

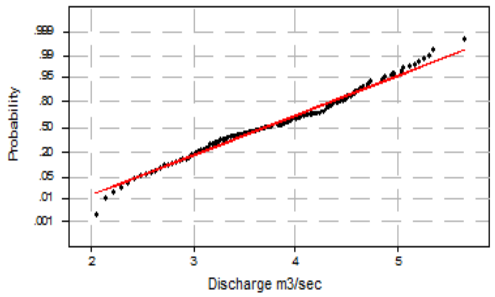

Figure 6 Testing the Normal Distribution of Max.daily Flow Series for Zakho Station Using Kolmogrov-Smirnov Test

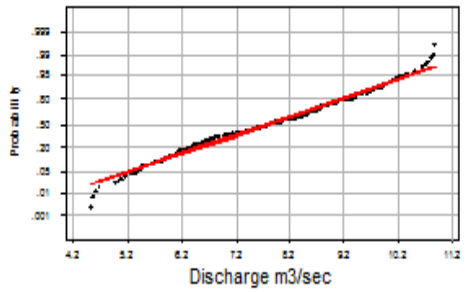

Figure 7 Testing the Normal Distribution of Max.daily Flow Series for Tusan Station Using Kolmogrov-Smirnov Test

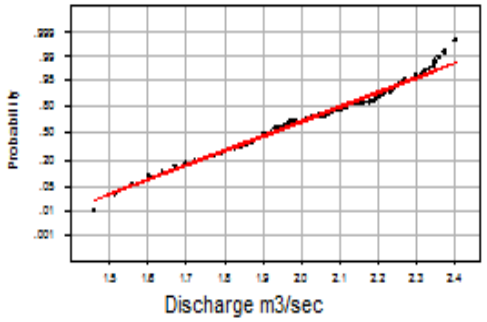

Figure 8 Testing the Normal Distribution of Mim..daily Flow Series for Zakho Station Using Kolmogrov-Smirnov Test

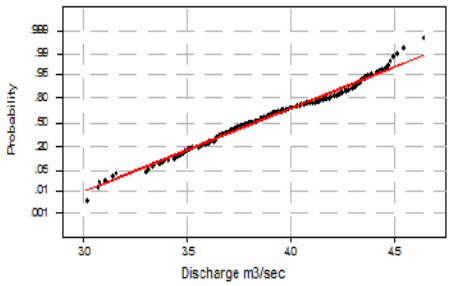

Figure 9 Testing the Normal Distribution of Mim..daily Flow Series for Tusan Station Using Kolmogrov-Smirnov Test

Test for jump component was made using the split sample method, to certify whether or not the difference between the means and standard deviations of two sub-samples is significantly different from zero at 95% probability level of significant. Each time series for the two stations was divided in two equal sub-samples. The critical t-value (tabulate value) was found to be equal to 2.086 . **Tables 1** show the result of the test. The calculated t-values are less than the critical t-value mentioned above for the time series, which indicate that all the time series were free from the jump component.

Table1 t-test results for jump component of Zakho and Tusan Station

Time series	t-calculated for Mean	t- calculated for Standard deviation
Maximum Daily Flow(Zakho)	3.617827E-01	2.852455E-01
Maximum Daily Flow(Tusan)	5.374522E-01	1.335627E-01
Minimum Daily Flow(Zakho)	9.410736E-02	1.253069E-01
Minimum Daily Flow(Tusan)	4.079877E-01	3.474163E-02

The existence of the trend component in the time series of the two stations must be checked. As far as the correlation between the discharges and time scale are concerned, **Figure 10** to **Figure13** show that there was no trend component in the time series for the two stations and the slope of the trend equation was found to be very small as shown in **Tables 2**

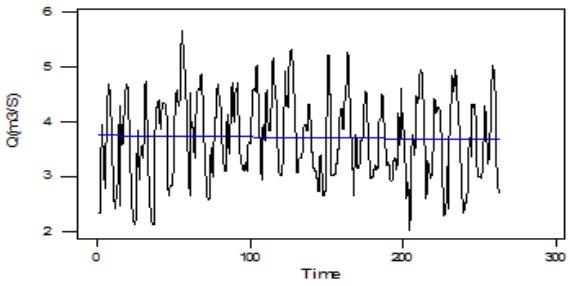

Figure 10 Linear Trend of Max. Daily Flow Series for Zakho Station

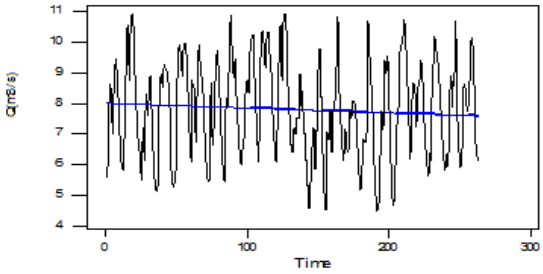

Figure 11 Linear Trend of Max. Daily Flow Series for Tusan Station

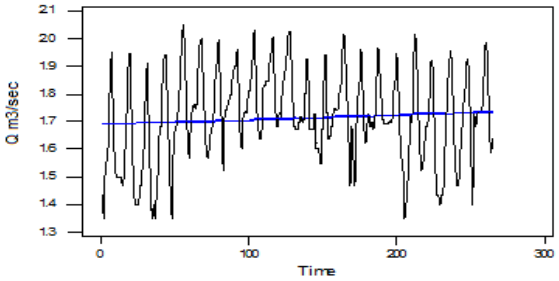

Figure 12 Linear Trend of Mim. Daily Flow Series for Zakho Station

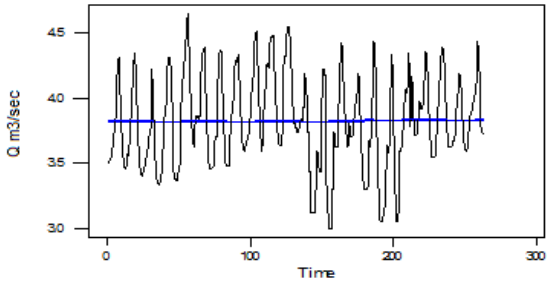

Figure 13 Linear Trend of Mim. Daily Flow Series for Tusan Station

Table 2 Linear Trend for the Time Series of Zakho and Tusan Stations**.**

Time Series	Trend Equation
Maximum Daily Flow(Zakho)	Yt = 3.74869 - 3.02E-04*t
Maximum Daily Flow(Tusan)	Yt = 8.01789 - 1.58E-03*t
Minimum Daily Flow(zakho)	Yt = 1.68821 + 1.85E-04*t
Minimum Daily Flow(Tusan)	Yt = 3.17900 + 1.83E-05*t

The plots of the Autocorrelation Coefficient (ACF) and Partial Autocorrelation Coefficients (PACF) for a series indicate the primary estimation of SARIMA model for the series. **Figure 14** to **Figure 21** show the plots of ACF and PACF for all the maximum and minimum daily flow time series of Zakho and Tusan stations. All the Autocorrelation Coefficient plots for the mentioned time series indicated that they were non random series due to the values of ACF which were not within the confidence limits.

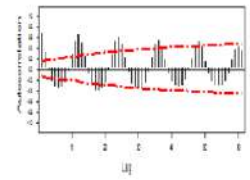

Figure 14 Autocorrelation Function of Max.Daily in Month Flow Series for Zakho Station

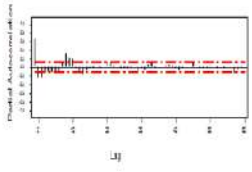

Figure 15 Partial Autocorrelation Function of Max.Daily in Month Flow Series for Zakho Station

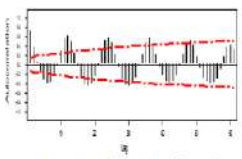

Figure 16 Autocorrelation Function of Max.Daily in Month Flow Series for Tusan Station

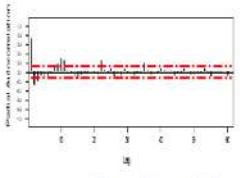

Figure 17 Partial Autocorrelation Function of Max.Daily in Month Flow Series for Tusan Station

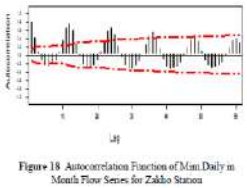

Figure 18 Autocorrelation Function of Min.Daily in Month Flow Series for Zakho Station

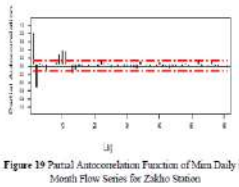

Figure 19 Partial Autocorrelation Function of Min.Daily in Month Flow Series for Zakho Station

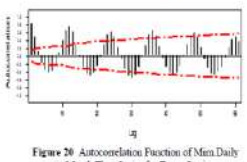

Figure 20 Autocorrelation Function of Min.Daily in Month Flow Series for Tusan Station

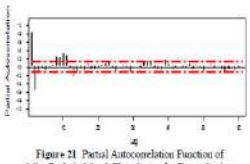

Figure 21 Partial Autocorrelation Function of Min.Daily in Month Flow Series for Tusan Station

After determination of the ACF and PACF of the time series, the parameters of SARIMA for several model were calculated and the parsimony models were selected according to the smallest value of AIC test as (**Kadri, 2004**) :

$$AIC(p,q)=N.Ln(\sigma^2)+2(M) \quad \text{..... (9)}$$

where

$$M = p + q + P + Q$$

Table 3 and **Table 4** shows the SARIMA model for maximum and minimum daily flow time series of Zakho and Tusan station, the seasonal and non-seasonal parameters of the models were evaluated by applying MINTAB program ver 13.2.

Table 3 Parameters of SARIMA Model for Maximum and minimum Daily Flow Series for Zakho Station and the t-test Results

time series	Seasonal			Non-seasonal		
	t-test	SAR Coef.(Φ)	SMA Coef (Θ)	t-test	AR Coef (ϕ)	MA Coef (θ)
Maximum daily series during the month $(1,0,0)(0,1,1)_{12}$	27.55	-	Θ_1 = .928	7.28	ϕ_1 = 0.418	-
Minimum daily data during the month $(1,0,0)(0,1,1)_{12}$	24.91	-	Θ_1 =0.898	20.92	ϕ_1 =0.898	-

Table 4 Parameters of SARIMA Model for Maximum and Minimum Daily Flow Series for Tusan Station and the t-test Results

time series	Seasonal			Non-seasonal		
	t-test	SAR Coef.(Φ)	SMA Coef (Θ)	t-test	AR Coef (ϕ)	MA Coef (θ)
Maximum daily series during the month $(1,1,1)(0,1,1)_{12}$	23.03	-	Θ_1 = .917	5.74 25.11	ϕ_1 = 0.419	θ_1=0.896
Minimum daily data during the month $(1,0,0)(0,1,1)_{12}$	30.81	-	Θ_1=0.939	21	ϕ_1=0.805	-

The model is considered suitable for forecasting process when the residuals Autocorrelation Coefficients are not significant i.e., the series of the residuals is random and they are within the confidence limits. **Figure 22** and **Figure 23** show that the ACF of the residuals of SARIMA models for Zakho station were considered random and not significant, the same result was obtained for Tusan station as shown in **Figure 24** and **Figure 25**, which indicate that all models were accepted and can be used for forecasting process.

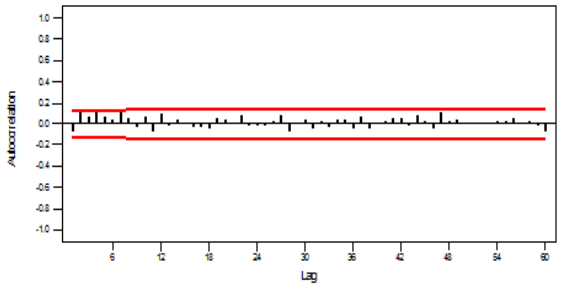

Figure 22 Residual Autocorrelation Function against Lag for SARIMA Model$(1,0,0)(0,1,1)_{12}$ of Max.Daily Flow Series for Zakho Station

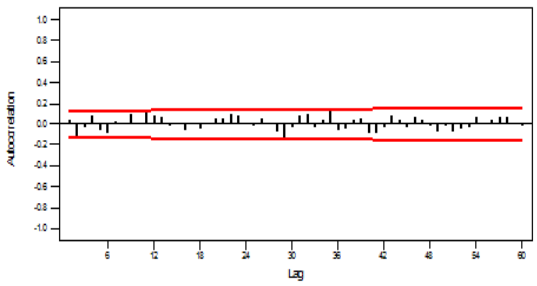

Figure 23 Residual Autocorrelation Function against Lag for SARIMA Model$(1,0,0)(0,1,1)_{12}$ of Mim.Daily Flow Series for Zakho Station

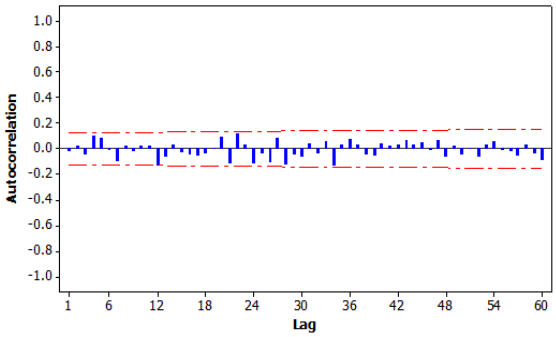

Figure 24 Residual Autocorrelation Function against Lag for SARIMA Model$(1,1,1)(0,1,1)_{12}$ of Max.Daily Flow Series for Tusan Station

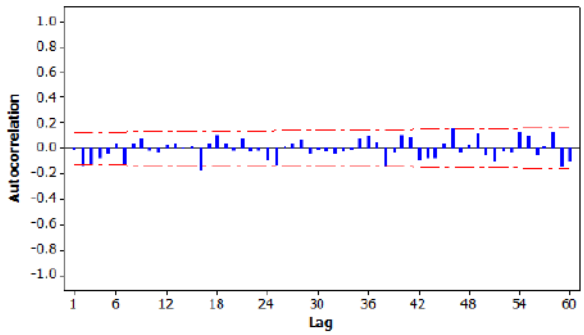

Figure 25 Residual Autocorrelation Function gainst Lag for SARIMA Model$(1,0,0)(0,1,1)_{12}$ of Min.Daily Flow Series for Tusan Station

The best model which described each time series for the two stations was used for forecasting the series for two water years for comparison purpose with the recorded two water years (1981,1982) (which were not entered in any previous calculations). **Figure 26 to Figure 29** show the recorded and forecasted hydrograph for the two water years mentioned above for the time series of the two stations, generally, these figures display the high convergence between the forecasted and recorded hydrograph for the time series, the acceptability of each model was checked by applying different statistical tests(RMSE, MAE, χ^2 and K-S)(**Wen Wang, 2006**) as shown in **Table 5** and **Table 6** , the results show that the series passed the χ^2 and K-S test where the calculated value of each series is less

than the tabulated one. The test and figures show that the best ARIMA model described in each series can be used efficiently for forecasting the flow series, ,taking into consideration the results of RMSE and MAE which had the largest value for the maximum daily flow time series and smallest value for the minimum daily flow time series.

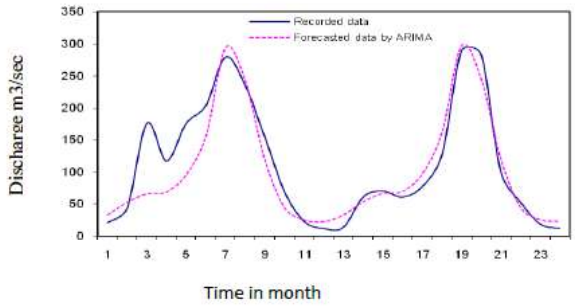

Figure 26 Hydrograph of Recorded and Forecasted Max.Daily Flow Series for Zakho Station using SARIMA Model$(1,0,0)(0,1,1)_{12}$

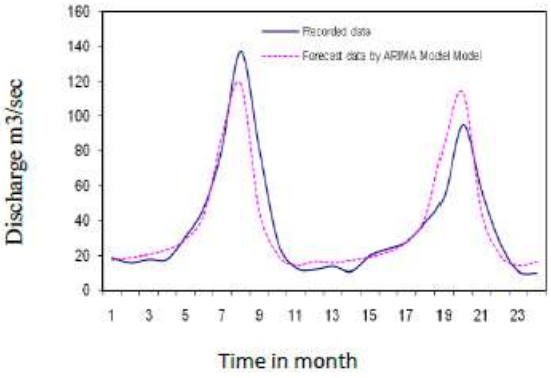

Figure 27 Hydrograph of Recorded and Forecasted Mim.Daily Flow Series for Zakho Station using SARIMA Model(1,0,0)(0,1,1)12

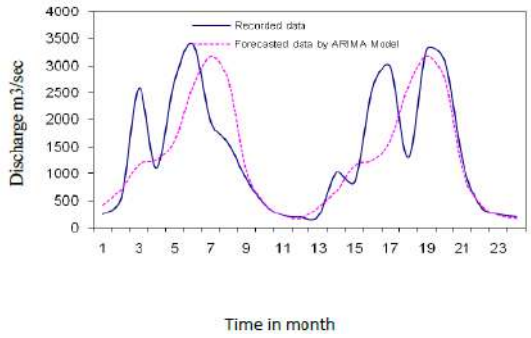

Figure 28 Hydrograph of Recorded and Forecasted Max.Daily Flow Series for Tusan Station using SARIMA Model$(1,1,1)(0,1,1)_{12}$

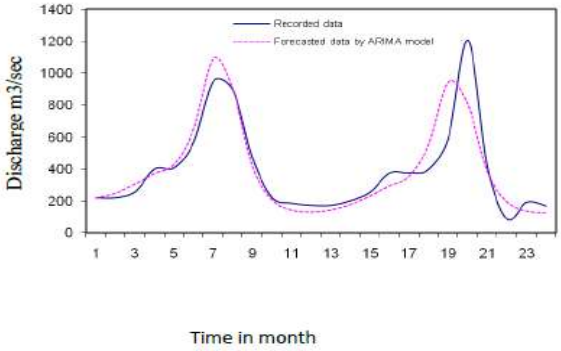

Figure 29 Hydrograph of Recorded and Forecasted Min.Daily Flow Series for Tusan Station using SARIMA Model$(1,0,0)(0,1,1)_{12}$

Table 5 Results of the Statistical Tests for Zakho Station by SARIMA Model

Time Series	RMSE*	MAE**	χ^2		K-S***	
			Cal.	Tab.	Cal.(Δ)	Tab.(Δ_0)
Maximum Daily	35.243	24.516	1.167	9.488	0.083	0.274
Minimum Daily	11.955	7.766	0.313	7.815	0.042	0.274

(*Root Mean Square Error(RMSE), ** Mean Absolute Error (MAE), *** Kolmogrov-Smirnov (K-S) Test)

Table 6 Results of the Statistical Tests for Tusan Station by SARIMA Model

Time Series	RMSE	MAE	χ^2		K-S	
			Cal.	Tab.	Cal.(Δ)	Tab.(Δ_0)
Maximum Daily	728.572	499.578	2.405	9.488	0.083	0.274
Minimum Daily	125.084	75.927	3.544	7.815	0.167	0.274

(*Root Mean Square Error(RMSE), ** Mean Absolute Error (MAE), *** Kolmogrov-Smirnov (K-S) Test)

Table 7 and **Table 8** shows the matrices (M_0), (M_1), (***A***) and (***B***) for all time series of the two stations. The first two matrices were calculated by using MINITAB software ver.13.2, and the other matrices were calculated using MathCAD software ver.10.

Matalas model was applied for all the time series in the present study for both Zakho and Tusan stations for forecasting the flow for the two water years 1981 and 1982 by applying a program modified in this study written in FORTRAN 2000 .As in the estimation of ARIMA models, the same time series with the same length of records were used to estimate the parameters of the Matalas model and the records of the two years 1981, 1982 were used for comparison purposes between the recorded and forecasted discharges.

Table 7 Matrices for Multisite Model (M_0, M_1, ***A***, ***B***) for Maximum Flow Series of the two Stations

Type of Matrix	Station	Zakho	Tusan
Matrix M_0	Zakho	1.000	0.554
	Tusan	0.554	1.000
Matrix M_1	Zakho	0.500	0.399
	Tusan	0.329	0.638
Matrix *A*	Zakho	0.402	0.176
	Tusan	0.035	0.658
Matrix *B*	Zakho	0.854	0.000
	Tusan	0.362	0.679

Table 8 Matrices for Multisite Model (M_0, M_1, ***A***, ***B***) for Minimum Flow Series of the two Stations

Type of Matrix	Station	Zakho	Tusan
Matrix M_0	Zakho	1.000	0.402
	Tusan	0.402	1.000
Matrix M_1	Zakho	0.772	0.350
	Tusan	0.358	0.776
Matrix *A*	Zakho	0.753	0.047
	Tusan	0.055	0.754
Matrix *B*	Zakho	0.634	0.000
	Tusan	0.151	0.610

In order to check the adequacy of the model, the hydrographs of the recorded and forecasted series for the mentioned two water years were drawn to notice the degree of approximating between them. **Figure 30** to **Figure 33** shows the forecasted and recorded hydrograph for the maximum and minimum time series for the two stations. Generally, the above mentioned figures show a high conform between the two hydrographs for the time series. In order to study the effect of the data type on the model adequacy for these two water years, the statistical tests (RMSE, MAE, χ^2 and K-S) were evaluated for the data of the mentioned two water years. **Table 9** and **Table 10** show the results of these tests for both stations, the χ^2 and K-S tests for the time series of the two stations were passed where the calculated value of each series is less than the tabulated one.. The RMSE and MAE tests show that the biggest values were for the maximum daily flow time series, while the smallest values were for the minimum daily flow time series, from comparing the results of the RMSE and MAE of the two models (SARIMA and Matalas) for the two station it was noted that the SARIMA model was more accurate in the forecasting than the Matalas model due to the lowest values of the obtained results from the statistical tests in SARIMA model.

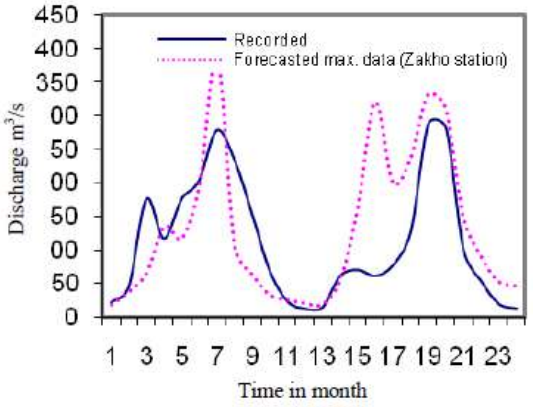

Figure 30 Hydrograph of Recorded and Forecasted Max.Daily Flow Series for Zakho Station using Matals model

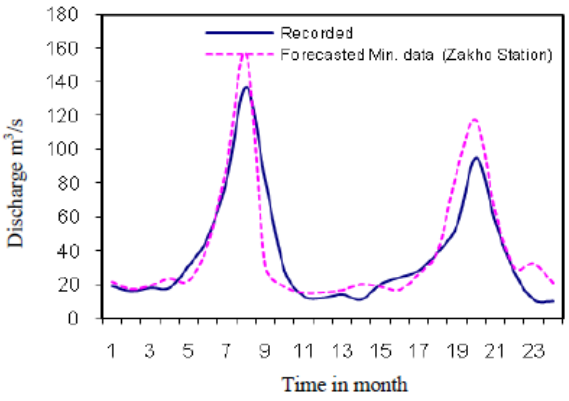

Figure 31 Hydrograph of Recorded and Forecasted Min..Daily Flow Series for Zakho Station using Matals model

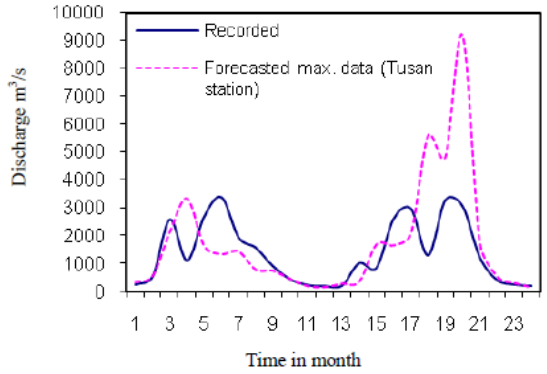

Figure 32 Hydrograph of Recorded and Forecasted Max.Daily Flow Series for Tusan Station using Matals model

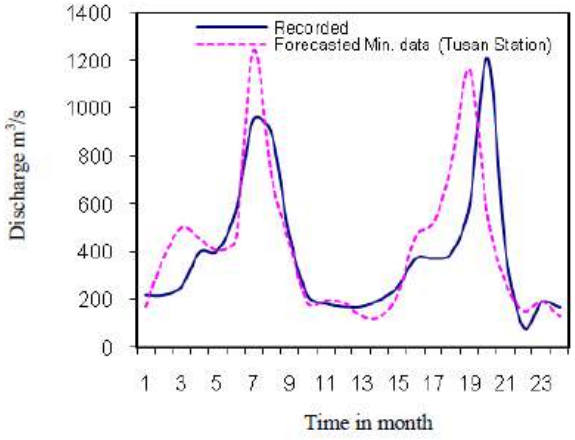

Figure 33 Hydrograph of Recorded and Forecasted Min..Daily Flow Series for Tusan Station using Matals model

Table 9 Results of the Statistical Tests for Zakho Station by Matalas Model

Time Series	RMSA	MAE	χ^2		K-S	
			Cal.	Tab.	Cal.(Δ)	Tab.(Δ_0)
Maximum Daily	83.320	58.574	4.389	9.488	0.208	0.274
Minimum Daily	15.198	9.703	3.600	7.815	0.125	0.274

(*Root Mean Square Error(RMSE), ** Mean Absolute Error (MAE), *** Kolmogrov-Smirnov (K-S) Test)

Table 10 Results of the Statistical Tests for Tusan Station by Matalas Model

Time Series	RMSA	MAE	χ^2		K-S	
			Cal.	Tab.	Cal.(Δ)	Tab.(Δ_0)
Maximum Daily	1745.379	987.497	1.071	5.991	0.083	0.274
Minimum Daily	221.567	142.579	5.905	7.815	0.083	0.274

(*Root Mean Square Error(RMSE), ** Mean Absolute Error (MAE), *** Kolmogrov-Smirnov (K-S) Test)

Conclusions:

In the present study, the following conclusions may be conducted:

1. The time series of the two station for maximum and minimum daily flow were transformed to a normal distribution using the Box-Cox transformation method with values of λ (Box-Cox coefficient) equal to -0.0685 and -0.03535 for the series of maximum and minimum flow of Zakho station while the value of λ (Box-Cox coefficient) was equal to 0.04491 and -0.1462 for the series of maximum and minimum flow of Tusan station .
2. The time series were found to be free from the jump and trend components and also it was found to be stationary in mean and variance.
3. The best SARIMA model was found according to the smallest value of Akakie Information Criterion (AIC) .
   - For maximum daily flow in a month at Zakho station the best model was SARIMA$(1,0,0)(0,1,1)_{12}$.
   - For minimum daily flow in a month at Zakho station the best model was SARIMA$(1,0,0)(0,1,1)_{12}$.
   - For maximum daily flow in a month at Tusan station the best model was SARIMA$(1,1,1)(0,1,1)_{12}$.
   - For minimum daily flow in a month at Tusan station the best model was SARIMA$(1,0,0)(0,1,1)_{12}$.
4. In Matalas model, the time series should be standardized then the model was built using first order Markov process.
5. The performance of the two models was calculated according to the results of RMSE, MAE, χ^2 and K-S tests, and the performance of ARIMA model was

found to be more efficient than that the Matalas model .

References:

Al-Suhaili R.H., 1985. "Stochastic Analysis of Daily Streamflow of Tigris River". M.Sc. University of Baghdad.

Al-Mousawi Eman Mehdi, 2003. "Multisite Stochastic Model of Hydrochemical Properties at Selected Region". M.Sc. Thesis ,College of Civil Engineering, University of Babylon.

Jayrami Reddy, 1997. "Stochastic Hydrology". Second edition, Delhi.

Kadri Yurekli and Ahmet Kurunc, 2004 . "Preforemance of Stochastic Approach in Generating Low Stream Flow Data for Drought Analysis". Journal of Special Hydrology, Spring Vol.5 No. 1 pp 20-32.

Linsley, Kolher and Paulhus, 1982." Hydrology for Engineering ". McGraw-Hill Series in water Resources and Environmental Engineering, United State of America.

Salvatore Grimaldi, 2004. "Linear Parametric Models Applied on Daily Hydrological Series ". Journal of Hydrologic Engineering, pp 1- 9.

Wen Wang, 2006. "Stochasticity, Non linearity and Forecasting of Stream flow Processes". Doctorate thesis submitted to the Technical University of Delft.

Wen Wang, Pieter H. A. J. M. Van Gelder, and J. K. Vrijlingb, 2008 ." Measuring Predictability of Daily Streamflow Processes Based on Univariate Time Series Model ". International Environmental Modeling and Software Society (iEMSs), Delft ,Netherlands , pp 1

Young G.K. and Pisano, W. C, 1968. "Operational of Hydrology Using Residuals". Journal of Hyd. Div ASCE, Vol. 94. HY4, pp 909-923.

ZANCO Journal of Pure and Applied Sciences
The official scientific journal of Salahaddin University-Erbil
ZJPAS (2018) **30**(s1)s62-s69
http://dx.doi.org/10.21271/ZJPAS.30.s1.7

Evaluation of Hydraulic Performance of Nazanin Dam Side Channel Spillway

Shahin S. Ahmed[1] **and Yaseen W. Aziz**[2]

[1] Asst. prof. Department of Dams and Water Resources, College of Engineering, University of Salahaddin, Erbil, Kurdistan Region, Iraq.

[2] M.Sc. Department of Dams and Water Resources, College of Engineering, University of Salahaddin, Erbil, Kurdistan Region, Iraq.

ARTICLE INFO

Article History:
Received: 14/05/2017
Accepted: 12/04/2018
Published:01/06/2018

Keywords:
Spatially Varied Flow
Side Channel Spillway
Physical Model
1D solution

**Corresponding Author:*
Email:
yaseen90aziz@gmail.com

ABSTRACT

Flow in the side channel spillway is very complex due to discharge changing along the side channel called spatially varied flow (SVF). A physical model for Nazanin dam side channel spillway, which has been designed by Hidroconstructia company with scale ratio 1:40 constructed in the laboratory to evaluate the flow characteristics in the spillway. The flow depth at several locations along centerline, right and left side of the spillway were measured for discharges ranging from (2.56 – 33.45) l/s. The performance of the spillway includes determination of discharge coefficient of the side weir, height of side walls for the spillway components and energy dissipation at the downstream of stilling basin. Furthermore, water surface profile was computed in the trough channel using one dimensional (1D) solution. The analysis of the data collected from physical model showed that at higher flow rates the discharge coefficient was reduced and side weir can pass extra 18% of the discharge presented in the design report. Overtopping was observed clearly over transition, chute channel and stilling basin side walls. The stilling basin could not dissipate energy efficiently. It also observed that the percentage of energy dissipation rate was inversely proportional with the discharge. Furthermore, it was found that the 1D solution adequately predicted the water surface profile in the trough channel.

INTRODUCTION

Spillway is a hydraulic structure provided at the dams to release flood discharge and consequently to prevent over-topping.
Side channel spillway has been commonly used with earth dams and dams that constructed in narrow gorges. Flow in this type of spillway is SVF with increasing discharge.
Side channel spillway includes six parts namely; side weir, trough channel, control section channel, transition section channel, chute channel and stilling basin. The simplest form of the side channel spillway is to have a straight weir perpendicular to the axes of the dam (Etheridge, 1996 and Knight 1989). Sometimes L and U shapes side weir are used in order to reduce the cost of excavation. Physical model is an essential tool for constructing model in the laboratory with a suitable scale ratio to show complex flow features, hydraulic performance and ensuring safe operation of the structure. SVF was

initially investigated by Hinds (1926) who introduced the general equation of SVF with excluding friction loss. He proposed the concept of equivalent critical depth channel to determine the location of critical control point. Hager (1985) Analyzed flow in trapezoidal side channel spillway and derived relations to determine the location of singular point for trapezoidal channel with moderate bottom slope. Bremen and Hager (1989) experimentally investigated flow characteristics in rectangular side channel spillway. They showed that due to the effect of jet of water over the weir the axial flow depth at side wall opposite to the side weir is greater than the flow depth at the centerline. Discharge coefficient of side channel spillway is different from normal spillway; it reduced as the discharge increased (Mandegaran, 1998). To ensure that the critical depth occurs within the channel length both dimensionless parameters (design capacity (F_q/S_o) and channel roughness (N/S_o)) should be less than unity (Guo, 1999). (Machajski and Olearczyk ,2011) used physical model with 1:40 scale ratio to investigate hydraulic performance of side channel spillway. They observed that discharge coefficient reduced as side weir submerged and suggested deepening of the channel to improve its performance. For side channel with mild slope and vertical drop face side weir two vortex spiral flow observed at low discharges while a single vortex created at high discharges. This causes increase of water level in the channel at opposite side of the weir (Lucas et al. 2015). There is a limited experimental published research in this field. The present study deals with the evaluation of hydraulic performance of Nazanin dam side channel spillway. A physical model with scale ratio 1:40 was constructed to represent Nazanin dam side channel spillway at the hydraulic laboratory of Dams and Water Resources Engineering Department- College of Engineering at University of Salahaddin. Nazanin dam is a rockfill dam located at 71 km north east of Erbil city in Kurdistan region at the coordinate (459088 – 4010378) WGS_1984_UTM_Zone 38 N (Figure 1). The characteristics of Nazanin dam and the spillway are shown in table 1.

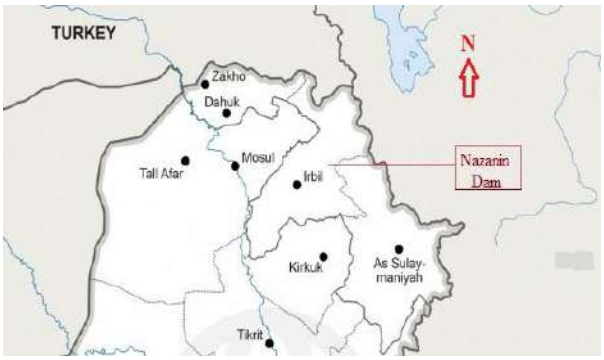

Figure 1 Location of Nazanin Dam project.

Table 1 Characteristics of Nazanin dam and the spillway

Dam and Reservoir Characteristics	Type	Rock fill
	Crest Elevation	730.2 m.a.s.l
	B.L. of River	709.2 m.a.s.l
	M.W.L	725.84 m.a.s.l
	dam Height	21 m
	Crest width	7 m
	Total storage	1864760 m3
Spillway	Type	S.C.S
	Design discharge	342 m3/sec
Trough channel	Length	67.65 m
	Width	29.65 m
Side weir	Type	Vertical Drop
	Length	81 m
	Width	0.5 m
Control channel Transition channel	Length	10 m-18.71m
	Width	25 m
Chute channel	Length	100 m
	Width	15 m
	Slope	8.4 %
Stilling basin	Type	Type II
	Length, width	20

MATERIALS AND METHODS

Physical Model

The physical model for the present study with scale ratio 1:40 was constructed in the hydraulic laboratory of Dams and Water Resources Engineering Department (Figure 2a). The model constructed from high density

plastic Perspex sheets (acrylic). According to the recommendation due to Chanson 2004, for scale ratio 1:40 the roughness of plastic is almost equal to the roughness of concrete in the prototype. A large reservoir tank constructed upstream of the model to permit a steady water to flow over the model of spillway. The side weir consists of three segments, like L shape water comes into the trough channel at the upstream and its left side (Figure 2b). The physical model is similar to the prototype in terms of geometric, kinematic and dynamic. The gravitational force in modeling of the free surface flow is dominant. Therefore, Froude criterion of similitude is applied to calculate all the forces which occur in the model and the prototype. The Froude number of both the model and the prototype should be the same (Durgaiah, 2002, p.636). Froude's law of similitude is used in modeling spillways, weirs, and sluice gates and in general for all free surface flow when the effect of viscous and surface tension forces are relatively small which can be neglected. The scale ratio is the ratio between model and prototype dimensions. The relations derived from Froude's law of similitude as shown in table 2. Flow depths were measured using point gauge with the accuracy 0.05 mm. all measurements were taken when steady state achieved. The steady state condition achieved where the flow depth over V notch weir, side weir and all parts of the spillway does not changed with respect to time.

a) Flow in trough channel

b) physical model components

Figure 2 Physical model of side channel spillway.

Table 2 Froude law relationships for similitude

Parameter		**Ratio**
Length	L_r	L_r
Velocity	V_r	$L_r^{0.5}$
Area	A_r	L_r^{2}
Discharge	Q_r	$L_r^{2.5}$

Hydraulics of Side Channel

When lateral inflow enters the side channel, it causes a considerable energy loss in the channel, due to turbulent mixing of water that enters the channel and water flowing in the channel (French, 1985). Flow in side channel is more complex due to variation of discharge along its length. Therefore, momentum equation is used to develop dynamic equation of spatially varied flow (Chow, 1959).

A. Dynamic Equation of SVF With Increasing Discharge

The equation of SVF with increasing discharge can be obtained based on the assumption of conservation of linear momentum. Subramanya (2009) suggested the following assumptions to apply momentum to the control volume:

1. The streamlines are parallel, hydrostatic pressure distribution prevail with excluding locations of highly curvature in the analysis.

2. The momentum correction factor is used to represent the effect of non-uniformity of velocity distribution.
3. Manning formula used to estimate the friction losses.
4. The effect of air entrainment on forces involved in the momentum equation is neglected.
5. The inflow rate is constant and it does not contribute to any momentum in the stream wise direction.
6. The flow is steady and channel is prismatic with small slope.

The dynamic equation of SVF with increasing discharge as presented in (Chow, 1959) is:

$$\frac{dy}{dx} = \frac{S_o - S_f - (\frac{2\beta Q q}{gA^2})}{1 - \beta \frac{Q^2 T}{A^3 g}} \quad \ldots\ldots\ldots\ldots\ldots 1$$

Where: S_o is the longitudinal bed slope of the trough channel, S_f is the frictional slope, q is the lateral inflow (m^2/s), Q is the total discharge (m^3/s), A is the cross sectional area of the trough channel (m^2), T is the flow top width (m), g is the gravitational acceleration (m/s^2), β is the momentum correction factor, x is the horizontal distance along the channel and y is the depth of flow.

The above equation is hardly to be integrated. Therefore, to draw the water surface profile in the side channel the numerical integration form using trial and error technique can be used as presented in (Chow, 1959).

$$\Delta y = \frac{\alpha Q_1 (V_1 + V_2)}{g(Q_1 + Q_2)} \left(\Delta V + \frac{V_2}{Q_1} \Delta Q \right) + S_f \, \Delta x \ldots\ldots\ldots 2$$

B. Control Section

Computation of water surface profile starts at a point which has a known depth and location. In SVF the critical depth is a curved line due to change of the discharge along the channel. For subcritical flow the control section located at the downstream of the channel while, for supercritical flow the control section located at the upstream of the channel (Chow, 1959). Smith (1967) proposed the concept of transitional profile to find the critical control point (CCP) (A point where Froude number is unity).

$$x_t = \frac{2}{\left(\frac{S_o T}{A} - \frac{gA^2}{\beta K^2}\right)} - \frac{Q_o}{q} \quad \ldots\ldots\ldots\ldots\ldots 3$$

$$x_c = \frac{1}{q} * \sqrt{\frac{gA^3}{\beta T}} \quad \ldots\ldots\ldots\ldots\ldots\ldots\ldots 4$$

Where: x_t is the distance to the transitional depth (m), Q_o is the discharge at the upstream of the trough channel (m^3/s), K is the conveyance factor, x_c is the distance to the critical depth (m).

The intersection point between transitional profile with the critical depth line is the critical control depth.

Discharge Equation

The discharge over the side weir of the spillway can be calculated using the equation of sharp crested weir adopted by Subramanya (2009) as follows:

$$Q = \frac{2}{3} C_d \sqrt{2g}\, L h_o^{3/2} \quad \ldots\ldots\ldots\ldots\ldots\ldots 5$$

Where: C_d is the discharge coefficient, L is the length of the weir, h_o is the water depth over the weir.

At most discharges the weir acts as a sharp crested weir.

RESULTS AND DISCUSSION

Water Surface Profile (WSP)

The WSP was obtained from the physical model by measuring flow depth at

various sections along the spillway including centerline, right and left side walls for eight discharges. In the trough channel the transitional profile and critical depth line did not intersect each other (Figure 3) for this reason the critical control point was fixed at the end of the control channel. Furthermore, the WSP was computed in the trough channel using equation (2).

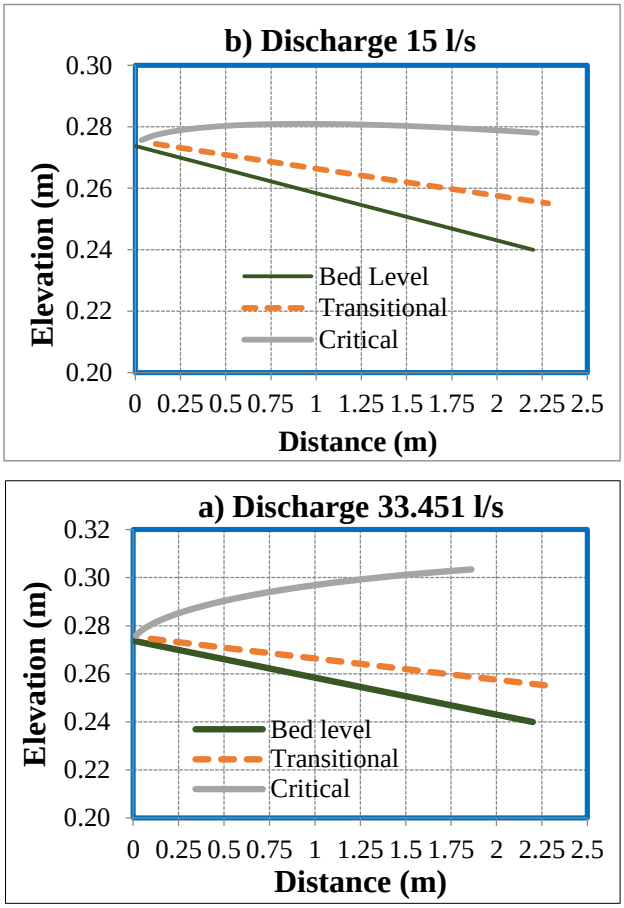

Figure 3 Critical and transitional profile in trough channel for different discharges.

The results obtained from the physical model and calculated WSP are outlined in the following parts:

Trough Channel

In the trough channel the computed, design report and observed WSP are very close to each other (Figure 4). However, the WSP for the design report is only drawn for the maximum discharge as it represents the design discharge on which the structure has been designed accordingly. This reveals that equation (2) adequately predicted WSP. Only there are some deviations between them at the beginning of the channel, which might be due to falling jet of water over the weir caused reduction of flow depth. This phenomenon cannot be handled by one dimensional equation. All results indicated that flow in the trough channel is subcritical, Froude number was increased along the flow direction and approaches unity at the outlet (Table 3). Type of flow is type (A) according to the classifications made by Li 1955 (presented by Chow, 1959). Furthermore, at the design discharge (33.451 l/s) the side weir approaches to the submergence condition. In all discharges flow depth at the opposite of the side weir is greater than the flow depth at its centerline.

Table 3 Calculated Froude number in the trough channel

Distance from US (m)	Froude Number
0.5	0.25345
0.75	0.30684
1	0.36448
1.3	0.42585
1.6	0.62026
1.69125	0.72788

Transition and Chute Channel

Flow in the transition channel is highly non-uniform. Due to shape of the transition and contraction of width of the channel from 0.625 m to 0.375 m cross waves observed in the transition channel and traveled into the chute channel (Figure 5). Therefore, raising water level occurred near boundaries of the transition and chute channel. Furthermore, extreme overtopping observed at the transition and middle of the chute channel. While, at end of the chute channel intensity of waves reduced and raising water level diminished and the flow approximately become uniform. The results of

WSP observed from the physical model are higher than that presented in the design report at the transition and start of the chute channel. The side wall height of the chute channel should be increased from 2m to 2.5m (according to the prototype) to prevent overtopping.

Stilling Basin

The hydraulic jump observed at the outlet of the stilling basin this causes high overtopping at both sides. The result of sequent depth obtained from the physical model is less than that presented in the design report. This can be attributed to the fact that in the design report Blenger momentum equation for rectangular channels has been used to calculate the jump sequent depth, whereas the stilling basin of the structure isn't of rectangular shape. Due to the absent of the chute and baffle blocks, the flow for higher discharges was continuous until reaches end of the basin then the jump was formed (Figure 4a, b). For lower discharges a part of the hydraulic jump comes into the chute channel (Figure 4d) and causes overtopping at both sides of the chute channel.

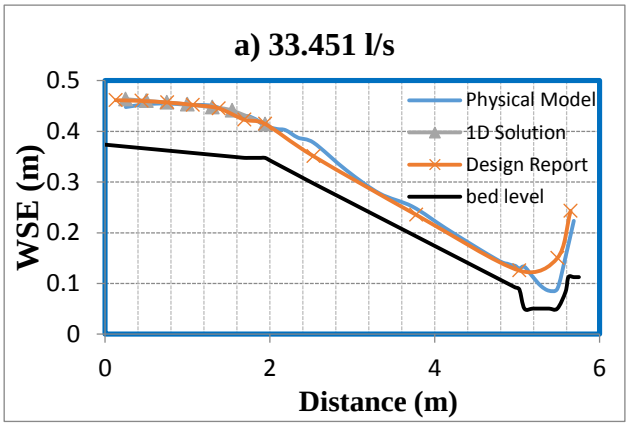

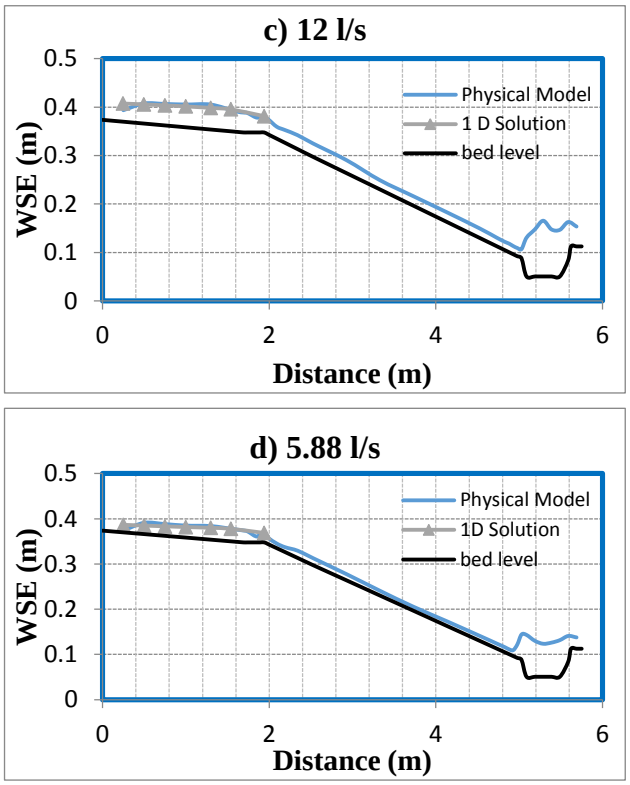

Figure 4 Comparison of physical model, and 1D Solution water surface profile in side

Figure 5 Cross waves in the transition and rising water level at side wall.

Discharge Coefficient

The discharge coefficient for the present was calculated in two conditions:

1. Discharge coefficient when velocity head is neglected from the calculation. In spillways at lower value of the ratio of (h_o/p) the velocity head is very small that cannot affect the results. The discharge coefficient increase as the discharge increase but at higher discharges the discharge coefficient decreases this related to the flow condition in the side channel when the

weir crest approaches to submergence condition (Figure 6a). The results showed that C_d at the design discharge is 0.7228, while in the design report C_d = 0.60975, so the weir can pass extra discharge by 18%.

2. Discharge coefficient when velocity head is considered from the calculation. The results are shown in Figure 6 b, which seems the same behavior as in previous case. From both results it is evident that the velocity head is very small so that it can be neglected.

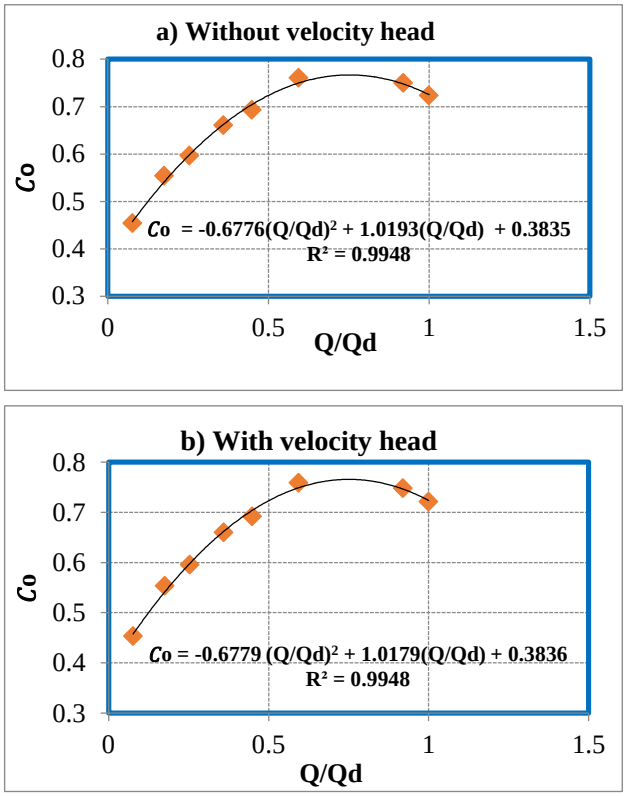

Figure 6 Discharge coefficient versus discharge without and with velocity head

Energy Dissipation

The percentage of energy dissipation is calculated using the following equations.

$$H_1 = h_o + \frac{{V_O}^2}{2g} \quad \ldots\ldots\ldots\ldots\ldots\ldots\ldots \quad 6$$

$$H_2 = y_2 + \alpha\frac{{V_2}^2}{2g} \quad \ldots\ldots\ldots\ldots\ldots\ldots\ldots \quad 7$$

$$\%\ \text{Energy Dissipation} = \frac{H_1 - H_2}{H_1} * 100 \quad \ldots\ldots\ldots\ldots \quad 8$$

H_1 is the total upstream head, H_2 is the residual head at the downstream of the stilling basin, V_o is the average velocity in the reservoir, V_2 is the average velocity at the downstream of the stilling basin, it was calculated using continuity equation (Q/A).

The energy correction factor (α) is assumed be equal to unity, since the channel cross section is regular.

Figure 7 shows the relationship between percentage of the energy loss and the discharge. It is clear that the percentage of energy dissipation decreases as the discharge increases. Percentage of the energy dissipation is equal to 57.5% at the design discharge. This value is very close to the percentage of energy dissipation calculated from the design report which is equal to 56.6%. According to the value of the percentage energy dissipation it is clear that the stilling basin cannot dissipate energy sufficiently, so the river bed is likely prone to scouring. As mitigation measures against such damage, chute and baffle blocks should be added at the end of the stilling basin.

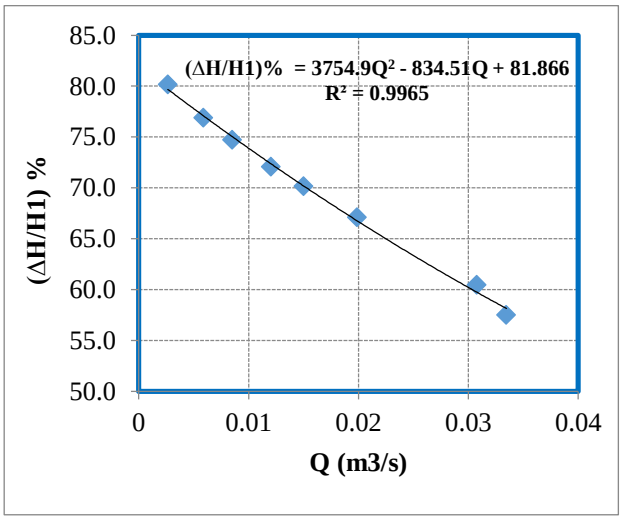

Figure 7 Percentage of energy dissipation at the end of the stilling basin versus discharge.

CONCLUSION

In the present study the hydraulic performance of Nazanin dam SC Spillway was evaluated. The physical model was used to determine water surface profile in the spillway

for discharges ranging from (2.56 – 33.45) l/s. In addition, the discharge coefficient and the energy dissipation at the downstream of the stilling basin were studied. The results of analysis of data obtained from the physical model can be outlined in the following conclusions.

1. Effect of water jet over the weir on the water surface in trough channel at opposite side of the weir is small. Because the channel is wide and shallow.
2. It was found that the dynamic equation for SVF with increasing discharge equation (2) can be used to predict 1D water surface profile in trough channel for L shaped weir, since it gave reasonable results.
3. Flow is subcritical along the entire length of the trough channel according to the location of CCP; this was approved by the physical model results.
4. The shape of the alignment and contraction width of the channel are main factors for generating cross waves in transition and chute channels.
5. The discharge coefficient is very sensitive to the flow condition in trough channel. Its value decreased when the weir approaches to the submergence.
6. The percentage of energy dissipation varied inversely with the discharge.
7. The stilling basin is hydraulically inefficient, it needs extra elements to dissipate energy of flowing water.

REFERENCES

BREMEN, R. and HAGER, W. H. (1989) Experiments in side channel spillways. Journal of hydraulic Engineering, 115 (5). p.617-635.

CHANSON, H. (2004) The Hydraulics of Open Channel Flow: an Introduction. Second Edition, Butterworth-Heinemann.

CHOW, V. T. (1959) Open Channel Hydraulics. New York, McGraw-Hill Company.

DURGAIAH, D. R. (2002) Fluid Mechanics and Machinery. First Edition, New Delhi.

ETHERIDGE, M.J. (1996) The Hydraulic Analysis of Side-Channel Spillways as Reservoir Outlets. Water and Environment Journal, 10(4). p.245-252.

FRENCH, R. H. (1985) Open Channel Hydraulics. International Edition, McGraw-Hill Book New York.

GENERAL DIRECTORATE OF DAMS AND RESERVOIRS (2013) Design Report of Nazanin Dam.

GUO, J. C.Y. (1999) Critical Flow Section in Collector Channel. Journal of Hydraulic Engineering, 125(4). p. 422-425.

HAGER, W. H. (1985) Trapezoidal Side - Channel Spillways. Canadian Journal of Civil Engineering, 12(4). P. 774-781.

HINDS, J. (1926) Side channel spillways: Hydraulic theory, economic factors, and experimental determination of losses. Trans. Am. Soc. Civ. Eng., 89(1), 881–927.

KNIGHT, A. C. (1989) Design of Efficient Side - Channel Spillway. Journal of Hydraulic Engineering, 115(9). p.1275-1289.

LUCAS, J., LUTZ, N., LAIS, A., HAGER, W. H. and BOES, R. M. (2015) Side - Channel Flow: Physical Model Studies. Journal of Hydraulic Engineering, 149(9). p. 05015003.

MACHAJSKI, J. and OLEARCZYK, D. (2011) Model Investigations of Side Channel Spillway of the Złotniki Storage Reservoir on the Kwisa River. In Experimental Methods in Hydraulic Research (p. 189-202). Springer Berlin Heidelberg.

MANDEGARAN, M. A. (1998) Investigation of flow through Overflow and Side Channel Spillways. PhD thesis, Civil Engineering Department, East London University.

SMITH, K. V. H. (1967) Control point in a lateral spillway channel. *J. Hydr. Div.*, ASCE, 93(3), 27-34

SUBRAMANYA, K. (2009) Flow in Open Channels. Third edition, New Delhi,Tata McGraw-Hill Education.

ZANCO Journal of Pure and Applied Sciences
The official scientific journal of Salahaddin University-Erbil
ZJPAS (2018) **30**(s1)s70-s75
http://dx.doi.org/10.21271/ZJPAS.30.s1.8

Experimental Study of Hydraulic Jump Characteristics in Trapezoidal Channels

[1]Shahin S. Ahmed [2]Othman K. Mohammed* [3]Alan A. Ghafoor

1 Department of Dams and Water Resources Engineering, College of Engineering, Salahaddin University-Erbil
2 Department of Civil Engineering, College of Engineering, Salahaddin University-Erbil
3 Department of Soil and Water, Faculty of Agricultural Science, University of Sulaimani- Sulaimani

ARTICLE INFO

Article History:
Received: 14/05/2017
Accepted: 12/04/2018
Published:01/06/2018

Keywords:
Open Channel.
Hydraulic Jump
Sequent depth
Energy Dissipation
Trapezoidal section

**Corresponding Author:*
Email:
othman.mohammed@su.edu.krd

ABSTRACT

In the presented study, the hydraulic jump in a trapezoidal channel has been studied experimentally. Trapezoidal channel sections of bed width 20 cm, and side slopes (1H: 1.5V) and (1H: 1V) was fixed D/S a control sluice gate. For each side slope, the discharges ranging from 5 lit/sec to 25 lit/sec were passed in the channel to form hydraulic jump. The obtained results were analyzed and compared to determine the effect of side slopes and incoming Froude number of the flow on relative energy dissipated in the jump. Empirical equations and curve relations between sequent depths, relative energy lost in the jump and incoming Froude numbers were obtained.

INTRODUCTION

Hydraulic jump is a phenomenon well known to hydraulic engineers as a useful means of dissipating excess energy and thereby prevent scour and erosion downstream of spillways, chutes, power houses and other appurtenances. It has also been used to raise the water level on the downstream to provide the requisite head for diversion into canals and rivers etc. for irrigation purpose. Hydraulic jump is a phenomenon caused by change in flow regime from supercritical to subcritical flow with energy dissipation and rise in depth of flow. Hydraulic jump serves as an energy dissipater to dissipate excess energy of flowing water downstream of hydraulic structures, such as weirs, spillway, sluice gates etc. This excess energy, if left unchecked, will have adverse effect on the banks and the bed of the channel. The below Eqns. has been widely used to study the hydraulic jumps formed on rectangular, smooth and horizontal channel beds and not much theories have been established for trapezoidal channels.

$$\frac{y_2}{y_1} = \frac{1}{2}\left(\sqrt{1 + 8\,Fr_1^2} - 1\right)$$

$$\Delta E = \frac{(y_2 - y_1)^3}{4\,y_2\,y_1}$$

In this study, the properties of a hydraulic jump and energy dissipation has been studied downstream sluice gate in trapezoidal channels.

LITERATURE REVIEW

A review of literature has shown that earlier researcher concentrated more on rectangular channel while very little information is available on trapezoidal channels. The hydraulic jump in trapezoidal open channel has not received much attention. Thus, relatively scarce literature on hydraulic jumps in trapezoidal channels is available to date. (Chow VT 1959) declared that the hydraulic jump first investigated by Bidone, an Italian, in 1818. He mentioned that Belanger obtained the explicit solutions of sequent depth ratio for rectangular and prismatic channels without bed friction. Massey and Thiruvengadam 1961 (Terry W. Sturm 2001) presented two simple charts for obtaining the change in depth of water passing through a hydraulic jump trapezoidal and circular channels. In 1987, Hager and Wanoschek (Rashwan I. Mohamed 2013) declared that, regarding the sequent depth ratio and the relative energy dissipation, trapezoidal and particularly triangular channels are much more effective than rectangular channels, provided the inflow Froude number Fr1 is fixed. (Rashwan I. Mohamed 2013) presented an Analytical solution to problems of hydraulic jump in horizontal triangular channels. (M. Debabeche, S. Cherhabil, A. Hafnaoui and B. Achour 2009) were studied Hydraulic jump in a sloped triangular channel, they obtained an empirical relation for determination of the sequent depth ratio, knowing the inflow Froude number, and the bed slope of the channel for right angle triangle channels. (Sadiq S. Muhsun 2012) were analyzed theoretically the hydraulic jump in the trapezoidal channels using Newton Raphson method.

THEORETICAL ANALYSIS

The hydraulic jump in open channels is a transitional state from an upstream supercritical to downstream subcritical flow. In this transition, water surface rises abruptly, surface rollers are formed, and intense mixing occurs, air is entrained and usually a large amount of energy is dissipated as shown in Fig. 1.

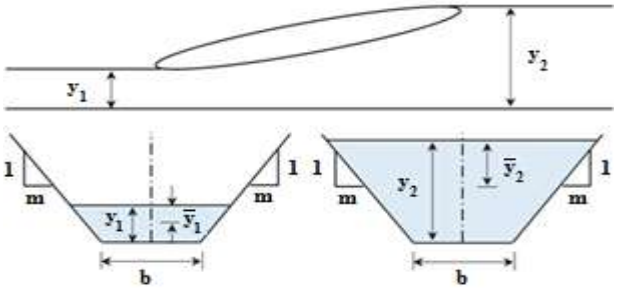

Fig 1: Definition sketch for a hydraulic jump in Trapezoidal channel.

Applying the momentum equation to a short horizontal reach of a prismatic Trapezoidal open channel, the external force of friction and weight effect of water can be ignored. Thus, the momentum equation for uniform velocity distribution becomes:

$$\frac{Q^2}{g\,A_1} + A_1\bar{y}_1 = \frac{Q^2}{g\,A_2} + A_2\bar{y}_2 \qquad \ldots\ldots(1)$$

Where Q = discharge; A_1 and A_2 = water areas at Sections 1 and 2, respectively; $\bar{y}_1$ and $\bar{y}_2$ = the depths from the water surface to the centroids of the Sections 1 and 2, respectively; and g = the acceleration due to gravity. For trapezoidal sections:

$$A = y\,(b + my)$$

and $$A\bar{y} = \frac{by^2}{2} + \frac{my^3}{3} \qquad \ldots\ldots(2)$$

Substituting equations (2) in (1),

$$\frac{Q^2}{g\,y_1(b + my_1)} + \frac{b{y_1}^2}{2} + \frac{m{y_1}^3}{3} = \frac{Q^2}{g\,y_2(b + my_2)} + \frac{b{y_2}^2}{2} + \frac{m{y_2}^3}{3} \qquad \ldots\ldots(3)$$

If we define new functions as:

$$\left(\lambda = \frac{y_2}{y_1} \quad , \quad \delta = \frac{m\,y_1}{b} \quad , \quad K^2 = \frac{Q^2 m^3}{g\,b^5} \right) \ldots\ldots(4)$$

Substituting equations (4) in (3), and simplifying:

$$K^2 = \frac{\delta^3(1.5\,\lambda^2 + \delta\,\lambda^3 - \delta - 1.5)}{\left[\frac{3}{(1+\delta)} - \frac{3}{\lambda(1+\lambda\delta)}\right]} \qquad \ldots\ldots(5)$$

For trapezoidal sections, squared Froude number is given by:

$$F_{r1}^2 = \frac{v^2}{g\left(\frac{Area}{T}\right)} = \frac{Q^2\,T}{g\,Area^3}$$

$$= \frac{Q^2(b + 2\,m\,y_1)}{g(b\,y_1 + m\,y_1^2)^3} \quad \ldots\ldots(6)$$

Substituting equations (4 and 5) in (6) and simplifying:

$$F_{r1}^2 = K^2\,\frac{(1 + 2\delta)}{\delta^3(1 + \delta)^3} \quad \ldots\ldots(7)$$

Relative Energy Dissipation:

Specific energy may be interpreted as the sum of potential and kinetic energy of fluid with respect to the bottom of the channel. Specific energy before the jump can be written as:

$$E1 = y_1 + \alpha_1\frac{v_1^2}{2g}$$

Where E1 = specific energy at Section 1 and α1 = energy coefficient at Section 1.

Specific energy after the jump expressed as:

$$E2 = y_2 + \alpha_2\frac{v_2^2}{2g}$$

For uniform velocity distribution, $\alpha_1 = \alpha_2 = 1$. The Relative Energy Dissipation by the jump can be written as:

$$\frac{\Delta E}{E1} = \frac{E1 - E2}{E1}$$

$$= 1 - \frac{(y_2 + v_2^2/2g)}{(y_1 + v_1^2/2g)} \quad \ldots\ldots(8)$$

Substituting equations (4) and (6) in (8), and simplifying:

$$\frac{\Delta E}{E1} = 1 - \frac{[2\lambda^3\,(1 + 2\delta)(1 + \lambda\,\delta)^2 + (1 + \delta)^3\,F_{r1}^2]}{\lambda^2(1 + \lambda\,\delta)^2[2(1 + 2\delta) + (1 + \delta)F_{r1}^2]}$$

$$\ldots\ldots(9)$$

As seen in eq. (6), the squared of approached Froude number is a function of (λ and δ) and from eq. (9) the relative energy dissipation is a function of (F_{r1}^2, λ and δ), since F_{r1}^2 is a function of (λ and δ), then we can say that the relative energy dissipation is a function of (λ and δ) also.

DIMENSIONAL ANALYSIS

A dimensional analysis is applied to correlate the different factors affecting phenomena under study and the following functional relationship is obtained:

$$F_{r1}^2 = f(\lambda, \delta) \quad \ldots\ldots(10)$$

$$\Delta E/E1 = f(\lambda, \delta) \quad \ldots\ldots(11)$$

EXPERIMENTAL WORK

The experimental work was carried out in the Fluid Laboratory of the College of Engineering, Salahaddin University. The experiments were carried out in a horizontal recirculating laboratory flume 50 cm wide, 50 cm deep with a 12 m working length as shown in Fig. 2. The discharge was measured using a pre-calibrated V-notch weir ($Q = 0.0195\,h^{2.398}$, Q in lit/sec and h in cm) (Othman K. Mohammed 2010), located at the end of the overhead tank. Water drawn from the underground storage tank by an electrically driven centrifugal pump through a 6 inch diameter Steel pipe to the overhead tank providing a maximum discharge of (45 lit/sec). Trapezoidal channel sections of bed width 20 cm, and side slopes (1H: 1.5V) and (1H: 1V) was fixed D/S a control sluice gate. For each side slope, the discharges ranging from 5 lit/sec to 25 lit/sec were passed in the channel to form hydraulic jumps. The parameters y1, y2, and flow rate were measured in each experimental run.

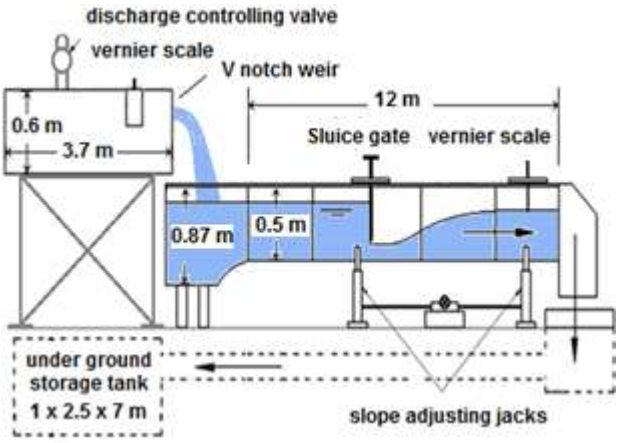

Fig 2: Schematic diagram of the experimental set-up

RESULTS AND DISCUSSION

The variation of different hydraulic jump characteristics such as sequent depth ratio, relative energy loss with approach Froude number and side slope of the channel is given below.

1. Variation of Sequent Depth Ratio with approach Froude number and Side slope of the Channel

Fig. 3 shows a linear variation of sequent depth ratio (y2/y1) against the Froude number $(Fr1)^2$ varying from 5 to 30, for two different side slopes. The R^2 value of the linear fit shows that linear variation holds well within y2/y1 and $(Fr1)^2$ among the possible regression types. The plot of data shows that points of lower side slope (1H: 1V) lies above the that of higher side slope (1H: 1V), this means that lower side slope produces higher sequent depth ratio (y2/y1) for the same squared Froude number.

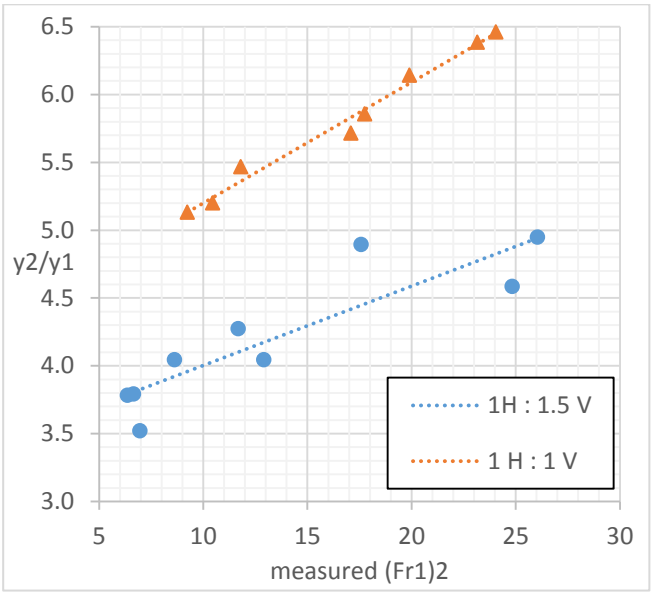

Fig. 3: Sequent depth ratio (y2/y1) verses(F_{r1}^2)

2. Variation of Relative Energy loss with Approach squared Froude number and Side slope of the Channel

Fig. 4 shows a second order polynomial variation of relative energy loss (ΔE/E1) against the Froude number (F_{r1}^2) varying from 5 to 30. The R^2 value of the second order polynomial variation fit shows that its variation holds well within (ΔE/E1) and (F_{r1}^2) among the possible regression types. The plot of data shows that points of higher side slope (1H: 1V), lies above the that of lower side slope (1H: 1V), this means that higher side slope produces higher relative energy loss (ΔE/E1) for the same squared Froude number.

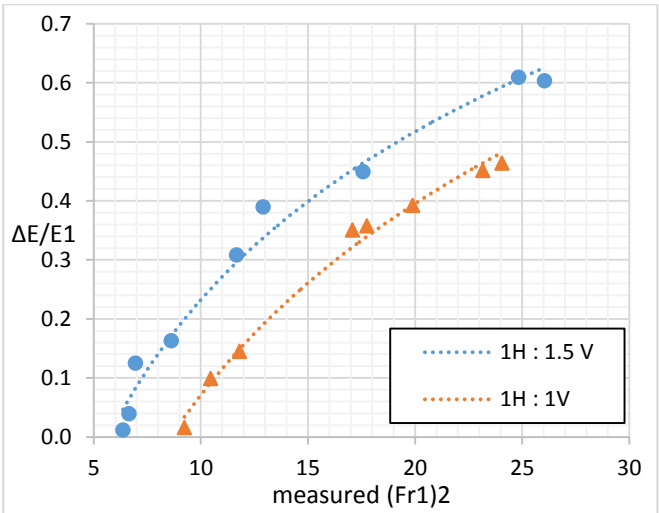

Fig. 4: Dissipated Energy ratio (ΔE/E1) verses (F_{r1}^2)

3. Variation of Relative Energy loss with Sequent Depth Ratio and Side slope of the Channel

Fig. 5 shows a linear variation of relative energy loss (ΔE/E1) against the sequent depth ratio (y2/y1), for two different side slopes. The plot of data shows that points of higher side slope (1H: 1V), lies above the that of lower side slope (1H: 1V), this means that higher side slope produces higher relative energy loss (ΔE/E1) for the same sequent depth ratio (y2/y1).

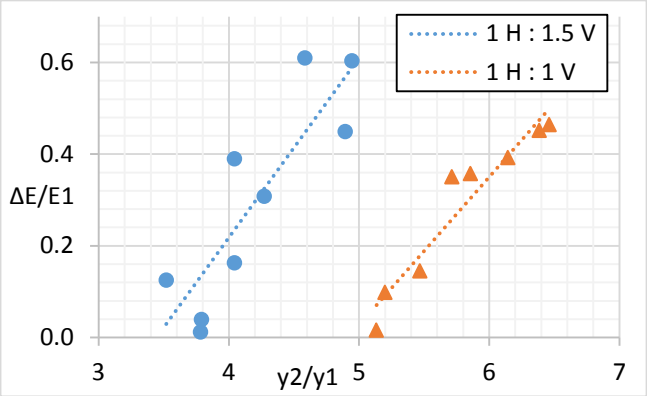

Fig. 5: Dissipated Energy ratio (ΔE/E1) verses (y2/y1),

Empirical Computational Models

To obtain empirical equations for (F_{r1}^2) and (ΔE/E1), (SPSS22) statistical software was used for obtaining two types of regressions between (F_{r1}^2) and dimensionless parameters obtained by dimensional analysis were tested to find the best one, they are:

1. Relationship between (F_{r1}^2) and the rest of the parameters:

linear regression

$$F_{r1}^2 = 79.17 + 0.73\left(\frac{y_2}{y_1}\right) - 939.813\left(\frac{m\,y_1}{b}\right)$$

$$R^2 = 0.814 \qquad \ldots(12)$$

power regression

$$F_{r1}^2 = 0.000187\left(\frac{y_2}{y_1}\right)^{0.538}\left(\frac{m\,y_1}{b}\right)^{-3.938}$$

$$R^2 = 0.802 \qquad \ldots\ldots(13)$$

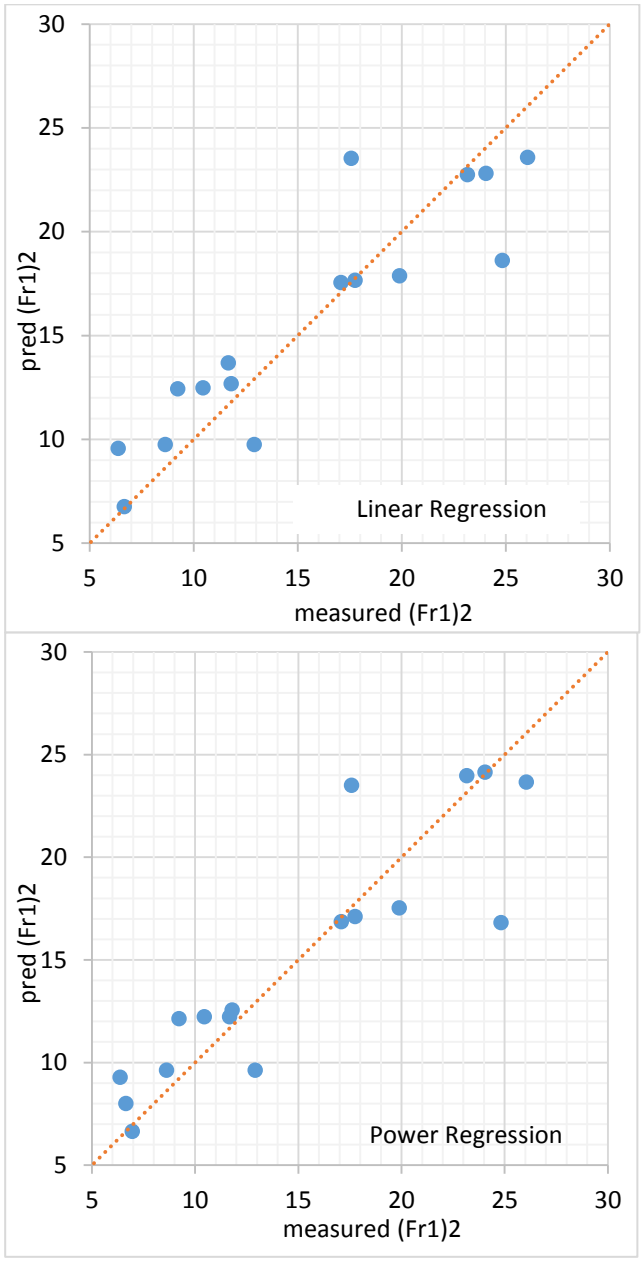

Fig. 6: (F_{r1}^2) measured verses (F_{r1}^2) predicted

2. Relationship between (ΔE/E1) and the rest of the parameters:

linear regression

$$\frac{\Delta E}{E1} = 2.855 - 0.049\left(\frac{y_2}{y_1}\right) - 32.186\left(\frac{m\,y_1}{b}\right)$$

$$R^2 = 0.652 \qquad \ldots(14)$$

power regression

$$\frac{\Delta E}{E1} = 0.000000015\left(\frac{y_2}{y_1}\right)^{-0.095}\left(\frac{m\,y_1}{b}\right)^{-6.016}$$

$R^2 = 0.64$ ...(15)

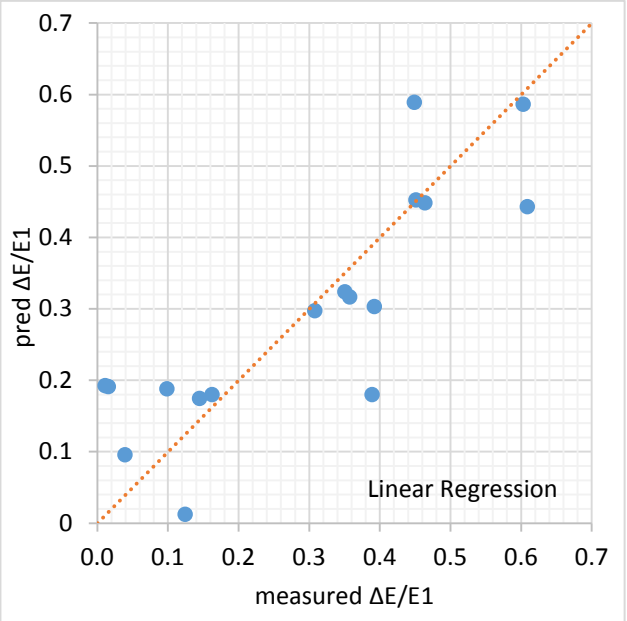

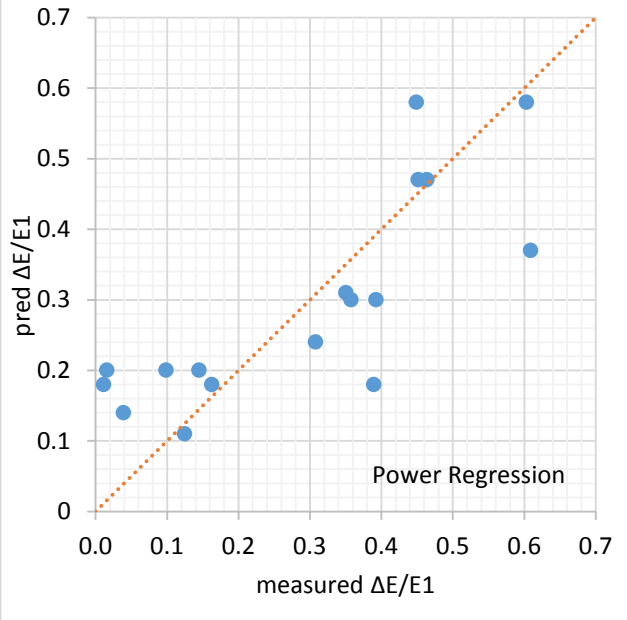

Fig. 7: (ΔE/E1) measured verses (ΔE/E1) predicted

CONCLUSIONS

The results of the experimental and theoretical study on the hydraulic jump are presented. The discussion and analysis of the results highlighted the following conclusions:

1. Sequent depth ratio and relative energy loss increases with increase in approach Froude number. Fig. 3 and Fig. 4
2. For constant Froude number, sequent depth ratio of the jump increase with increase in side slope of the channel. Fig. 3
3. For constant Froude number, relative energy loss through the jump increase with decrease in side slope of the channel. Fig. 4
4. For constant sequent depth ratio, relative energy loss through the jump decrease with increase in side slope of the channel. Fig. 5
5. Analysis of the experimental data showed that the linear regression provides the best fit based on the measured $(F_{r1})^2$ versus predicted $(F_{r1})^2$ plots and the (R^2) values, which has a value of (0.814). Fig. 6 and eq. (12).
6. For the relative energy dissipation, the linear regression provides the best fit based on the measured ΔE/E1 versus predicted ΔE/E1 plots and the (R^2) values, which has a value of (0.652). Fig. 7 and eq. (14).
7. The applicability range of squared Froude number for proposed equations cover 2.5 - 5 and side slopes (1H: 1.5V) and (1H: 1V). Further experiments are recommended to study the applicability of proposed equations for other Froude numbers and different side slopes.

REFERENCES

Chow VT. "Open channel hydraulics". McGraw Hill; 1959.

Hager WH, Wanoschek R. Hydraulic jump in triangular channel. J Hydraulic Res 1987; 25 (5):549–65.

M. Debabeche, S. Cherhabil, A. Hafnaoui and B. Achour " Hydraulic jump in a sloped triangular channel" NRC Research Press, Can. J. Civ. Eng. 36: 655–658 (2009)

Othman K. Mohammed "Flow Characteristics through Pipe Culvert Combined with Broad Crested Weir" MSc Thesis College of Engineering Salahaddin University Erbil 2010 pp 52.

Rashwan, Ibrahim M. H. Analytical solution to problems of hydraulic jump in horizontal triangular channels. Ain Shams Engineering Journal (2013) 4, 365–368

Sadiq Salman Muhsun "Characteristics of the Hydraulic Jump in Trapezoidal Channel Section" Journal of Environmental Studies [JES] 2012. 9: 53-63

Terry W. Sturm "Open channel hydraulics". McGraw Hill; 2001, pp 63.

ZANCO Journal of Pure and Applied Sciences
The official scientific journal of Salahaddin University-Erbil
ZJPAS (2018) **30**(s1)s76-s82
http://dx.doi.org/10.21271/ZJPAS.30.s1.9

Numerical Investigations of Downpull Forces for leaf gate in high dams

Bashir Thabit Mohammed*

*Professor in Department of Dam and Water Resources Engineering, College of Engineering, Salahaddin University-Erbil

Binahi Mohammad Amin Said Ali**

**Lecturer in Department of Dam and Water Resources Engineering, College of Engineering, Salahaddin University-Erbil

ARTICLE INFO

Article History:
Received: 14//05/2017
Accepted: 12/04/2018
Published:01/06/2018

Keywords:
Bottom downpull coefficient Leaf gate ANSYS FLUENT v14 Pressure contours
Velocity vectors
Streamlines velocity

**Corresponding Author:*
Email:
alkadibashir@hotmail.com
binahimuhamad@yahoo.com

ABSTRACT

Determination of hydrodynamic forces is a serious problem on the design of leaf gates in high head dams. Hence, this study aims to estimate and study the downpull coefficients for leaf gate in high dams by the solution of two and three dimensional Navier-Stokes equations using Standard k-ε turbulence model. The equations were solved by ANSYS FLUENT V14 software using finite volume techniques. The simulation revealed the effects of many geometric and hydraulic parameters on downpull coefficient. Moreover, the results appeared that considering the presence of gate well in the model caused slight effects on the bottom downpull coefficients considering two-dimensional flow state. While, in the state of a three-dimensional model, it was noted that there were some differences for the bottom downpull coefficients values between the cases of the gate with and without well. Finally, the numerical model was also used to determine the general characteristics of pressure contours, velocity vectors, and streamlines velocity plots for the flow field profile.

INTRODUCTION:

Downpull forces are defined as the unbalanced vertical hydrodynamic forces resulting from the difference between the downward force on the gate top due to the flow passing over the top gate surface through the upstream and downstream clearance and the upward force results from pressure exerted on the bottom gate surface by the flow issuing beneath the gate. The net force is termed downpull when it is in the downward direction and uplift when it is in the upward direction.

Many studies are conducted to determine the magnitude of downpull and investigated some relevant parameters. The turbulent condition near separation points on the gate bottom by using a laser Doppler-Anemometry was specified. The study concluded that the variation of downpull and discharge coefficient was influenced by the sensitivity of the separated flow pattern near bluff bodies to free stream turbulence and to changes in the mean flow incidence,(Thang et.al.,1983).A one-dimensional of the discharge passing under a tunnel gate and of the hydraulic downpull acting on it was presented and shown that the downpull force was significantly affected not only by the geometry of the gate bottom but also by the rate of flow passing over the top of

the gate through the gate well, (Naudascher et.al.,1986).one-dimensional analyses was presented for estimating the discharge passing over the gate top, the total discharge, top downpull coefficient, the effective piezometric head on the gate top, and predicting the flow condition downstream the gate shaft. Downpull forces acting on the bottom were estimated by predicting the mean pressure and the velocity distribution using two finite element models, one with constant eddy viscosity, and the other of variable eddy viscosity,(Alkadi ,1997).a two-dimensional CFD model was applied to predict a downpull coefficient. The results illustrate that the inclined gate lip shape with an angle of (θ =35°) gave minimum positive values of downpull force. Moreover, the downpull coefficient depends mainly on the magnitudes and the distribution of (kb) for a given value of gap width ratio. A general statistical model was built to predict the bottom downpull coefficient for any gate lip geometry as well,(Almaini, Al-Kifae and Alhashimi ,2010).Finite volume multiphase flow model using standard (k-ε) turbulence model for the case of high Reynolds number was used. The model was verified by backward-facing step flow and results had been compared with experiments founded by (Durst and Schmitt, 1985), on the other hand, air demand ratio had been determined as a function of Froude number at contracted section, (Shmsai and Soleymanzadeh ,2006). The pressure distribution around the outlet channels was evaluated and calculated the hydrodynamic forces. The physical model results were compared with numerical model results by "Fluent" software based on finite volume method, (Naderi and Hadipour ,2013). two and three dimensional "FLUENT" software were applied .The simulation revealed the effects of many geometric and hydraulic parameters on downpull coefficient and Experimental investigations at the hydraulic laboratory were also conducted so as to calibrate and verify the numerical results. The evaluated model was used to predict the distributions of piezometric head on the inclined gate lip surface, top and bottom tunnel walls, and predict the distributions of bottom downpull coefficient in the gate lip,(Alkadi and Ali,2015). In the current study, the water flow controlled by leaf gate in dams under high pressure had been modeled using "FLUENT" software to estimate the effects of the gate well on downpull coefficients.

2. THEORETICAL CONSIDERATIONS

2.1. Hydraulic downpull Force

The downpull force is influenced by various parameters, which may be classified into three groups,(Sagar ,1978). The first group: The flow characteristics which include the operating head on the gate, flow conditions which contain whether free or submerged flow exists, and aeration downstream the gate. The second group: Includes the flow properties such as the specific weight of water, dynamic viscosity, and vapor pressure. The third group: Is the geometry of gate installation, including conduit height upstream the gate shaft, gate opening, gate thickness, gate shaft dimensions, angle inclinations of gate bottom with horizontal, geometry of other lip shapes, and location and thickness of the skin plate. See Fig. (1).

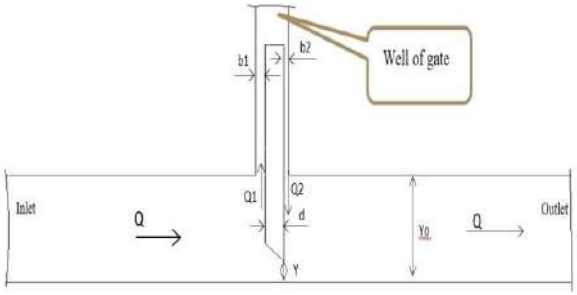

Fig.(1).General Sketch of the Welled gate.

2.2. Bottom Downpull and Discharge Coefficient

The bottom downpull coefficient along the gate width(k_b) that can be computed by following equation:

$$k_b = \frac{H_i - Y_s}{\frac{v_j^2}{2g}} \text{ , and } \frac{v_j^2}{2g} = H_u - Y_s + \frac{v_\circ^2}{2g} \qquad (1)$$

Where

H_i = Piezometric head at specific points on the bottom surface of gate,

Y_s = Piezometric head downstream the gate at contracted jet,

V_j =Velocity of the contracted jet issuing from underneath the gate, which is obtained from the results of model,

H_u, H_d= Piezometric head upstream and downstream of the gate, respectively, and

$V_\circ$ = Average velocity of the flow in the conduit upstream the gate, (Naudascher ,1964).

3. GOVERNING EQUATIONS

In the present study, the numerical model is based on the time-averaged conservation equations (mass and momentum) for two-dimensional (2D), turbulent, steady and incompressible flow. The governing conservation equations of continuity and momentum for an incompressible flow with constant viscosity can be expressed as (in tensor form), Piradeepan, (2002):

1. Continuity equation

$$\frac{\partial}{\partial xi}(\rho U_i) = 0 \qquad (2)$$

2. Momentum (Navier-stokes) equation

$$\frac{\partial(\rho U_i)}{\partial t} + \frac{\partial}{\partial x}\left(\rho U_i U_j - \tau_{ij}\right) + \frac{\partial p}{\partial x_i} - S_{ui} = 0 \qquad (3)$$

Where S_{ui} is a source term. The time-averaged form of these equations for turbulent flows can be derived by substituting the mean and fluctuating component of flow variables, e.g. $U = \bar{U} + \acute{u}, \text{and } P = \bar{P} + \acute{p}$. Eq. (5) can rewritten in terms of the time averaged terms as

$$\frac{\partial}{\partial xi}(\rho \bar{U}_\imath) = 0 \qquad (4)$$

and the time –averaged momentum equation can be derived as

$$\frac{\partial}{\partial x_j}\left(\rho \bar{U}_\imath \bar{U}_j - \bar{\tau}_{ij}\right) + \frac{\partial \bar{p}}{\partial x_i} - \bar{S}_{ui} = \frac{\partial}{\partial x_j}\left(-\rho \overline{\acute{u}_\imath \acute{u}_j}\right) \qquad (5)$$

3.1. The General Form of the Navier Stokes Equations

Turbulent stresses in Reynolds-averaged Navier Stokes equations can be closed using any of several exiting turbulence models. The simple and most widely used two-equation turbulent model is (k-ε) model that solves two separate equations to allow the turbulent kinetic energy and dissipation rate to be independently determined, (Ferzieger and Peric, ,1996).

1. The turbulent kinetic energy, k, is modeled as:

$$\frac{\partial uk}{\partial x} + \frac{\partial vk}{\partial y} = \frac{\partial}{\partial x}\left(\left(\nu + \frac{\nu_t}{\sigma_k}\right)\frac{\partial k}{\partial x}\right) + \frac{\partial}{\partial y}\left(\left(\nu + \frac{\nu_t}{\sigma_k}\right)\frac{\partial k}{\partial y}\right) + G - \varepsilon \qquad (6)$$

2. The dissipation rate of k is denoted, ε, and modeled as

$$\frac{\partial u\varepsilon}{\partial x} + \frac{\partial v\varepsilon}{\partial y} = \frac{\partial}{\partial x}\left(\left(\nu + \frac{\nu_t}{\sigma_\varepsilon}\right)\frac{\partial \varepsilon}{\partial x}\right) + \frac{\partial}{\partial y}\left(\left(\nu + \frac{\nu_t}{\sigma_\varepsilon}\right)\frac{\partial \varepsilon}{\partial y}\right) + C_1\frac{\varepsilon}{k}G - C_2\frac{\varepsilon^2}{k} \qquad (7)$$

The term G, representing the production of turbulent kinetic energy, is modeled identically for the standard, RNG, and realizable (k-ε) models. From the exact equation for the transport of k, this term may be defined as:

$$G = -\rho \overline{\acute{u}_\imath \acute{u}_j}\frac{\partial u_i}{\partial x_j} = \left[\mu_t \frac{\partial u_i}{\partial x_j}\left(\frac{\partial u_i}{\partial x_j} + \frac{\partial u_j}{\partial x_i}\right)\right] \qquad (8)$$

The "eddy" or turbulent viscosity μ_t is computed by combining k and ε as follows

$$\mu_t = c_\mu \rho \frac{k^2}{\varepsilon} \qquad (9)$$

The two dimensional CFD modeling is used to solve a steady state incompressible Reynolds averaged Navier Stokes equations with (k-ε) turbulence closure model which is expressed as :(Douglas and Matthews, 1996)

$$u\frac{\partial u}{\partial x} + v\frac{\partial u}{\partial y} = \frac{F_x}{\rho} - \frac{1}{\rho}\frac{\partial p}{\partial x} + \frac{\partial}{\partial x}\left(\nu_e \frac{\partial u}{\partial x}\right) + \frac{\partial}{\partial y}\left(\nu_e \frac{\partial u}{\partial y}\right) \qquad (10)$$

$$u\frac{\partial v}{\partial x} + v\frac{\partial v}{\partial y} = \frac{F_y}{\rho} - \frac{1}{\rho}\frac{\partial p}{\partial y} + \frac{\partial}{\partial y}\left(\nu_e \frac{\partial v}{\partial x}\right) + \frac{\partial}{\partial y}\left(\nu_e \frac{\partial v}{\partial y}\right) \qquad (11)$$

The 2-D continuity equation for incompressible fluid of steady flow can be expressed as:

$$\frac{\partial u}{\partial x} + \frac{\partial v}{\partial y} = 0 \qquad (12)$$

Equations (10 and 11) with continuity equation (12) complete the set of equations necessary to

predict the turbulent flow, always providing that the eddy viscosity is evaluated.

3.2 Defining Boundary Conditions

Different types of boundary conditions are used for modeling inlet, outlet and walls. Generally, defining boundary conditions includes identifying the location of the boundaries and providing required information at the boundaries. The information required at any boundary usually depends upon the boundary condition type and the physical models used. A fluid boundary is an external surface of a fluid domain and supports following boundary conditions (ANSYS Help, 2011):

- Inlet: Fluid predominantly flows into the domain.
- Outlet: Fluid predominantly flows out of the domain.
- Wall: Impenetrable boundary to fluid flow.
- Symmetry Plane: A plane of both geometric and flow symmetry.

4. RESULTS AND DISCUSSIONS

4.1. Comparisons between the leaf gate with and without well

Fig. (8). illustrates a slight difference between Bottom downpull coefficient (kb) of gate with and without well that computed by ANSYS FLUENT models.

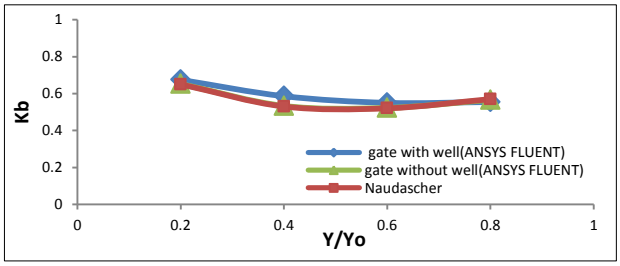

Fig. (8): Variation of bottom downpull coefficient k_b with relative gate opening ratios for the gate with and without well

Different profiles of velocity streamline, velocity vector, and pressure contour estimated by ANSYS FLUENT program for a tunnel with (41m) length, (6m) height, (1m) gate thickness with Well and lip angle (θ=45°) ,(b2/b1=0.2) with gate opening (YY0⁄=0.2) are plotted in Fig. (9) and the following conclusions can be obtained:

a. Maximum velocity reaches to 9.716 m/s.

b. The pressure head distribution appears to be uniform at upstream and non-uniform under the gate and at the gap (b2).

c. The streamline shows contraction and separation for the flow field around and near the gate. Moreover, it appears the shape of submerged hydraulic jump D/S of the gate.

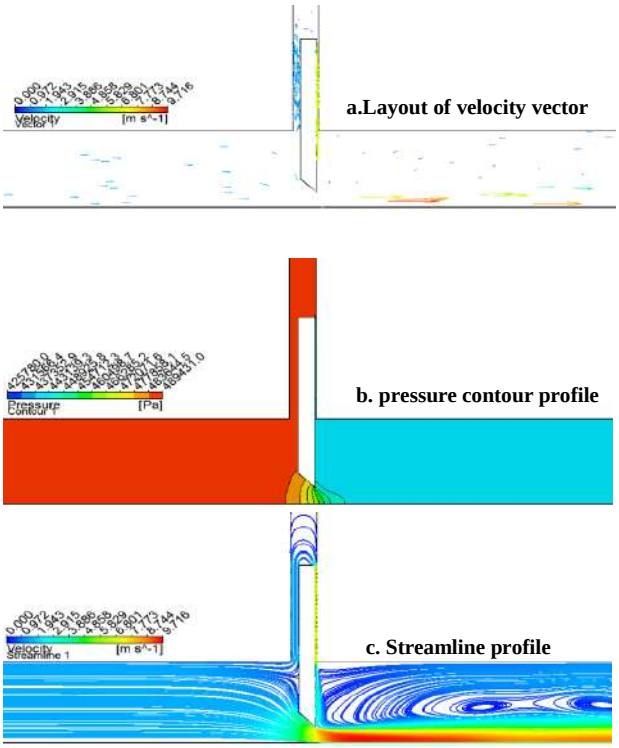

Fig. (9): Layout of velocity vectors, pressure contour lines profile and streamline profile obtained by ANSYS FLUENT model for the gate with well and the gap width ratio (b_2/b_1=0.2)

4.2. The effects of gap widths on bottom downpull coefficients

Fig. (10) illustrates bottom downpull coefficients (kb) computed by ANSYS FLUENT program for tunnel length (41m), lip angle (θ=45°), pressure head (Δh/H = 10%), gap width ratio ((b_2/b_1) = 0.2, 0.5, 1) and reveals an increase for kb values with increase of gap width ratio. The figure also shows different shape for (kb) distribution for the case of (b_2/b_1=1). This phenomenon appears due to the reattachment of separated water at Y/Y_0=0.6.

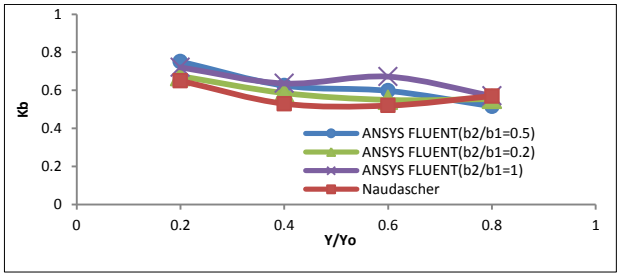

Fig. (10): Variation of bottom downpull coefficient k_b with relative gate opening ratios for the gate with well and different gap width ratio

Different Layouts of velocity streamline, velocity vector, and pressure contour estimated by ANSYS FLUENT program for different gap width ratio, Δh/H =10%, and gate opening (Y/Y0=0.2) in 2D are plotted in Figs. (11) and (12). From these figures, one can obtain the followings:

a. Maximum velocity reached to 9.922m/s and 9.799 m/s for (b_2/b_1=0.25 and 1) respectively.

b. The piezometric head distributed non-uniformly around the gate due to change the pressure head above and contraction of the streamline along the gate lip for both (b_2/b_1=0.5 and b_2/b_1=1).

c. The streamline separates under the gate and then contracted downstream of the gate. The figure also shows a difference in turbulence shape of hydraulic jump for (b_2/b_1=0.5 and b_2/b_1=1).

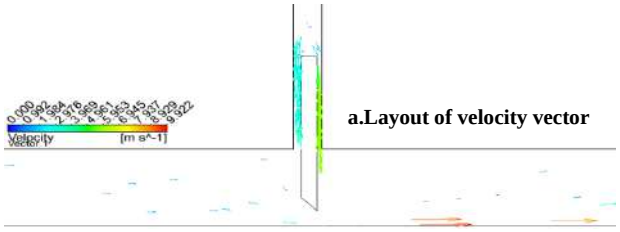

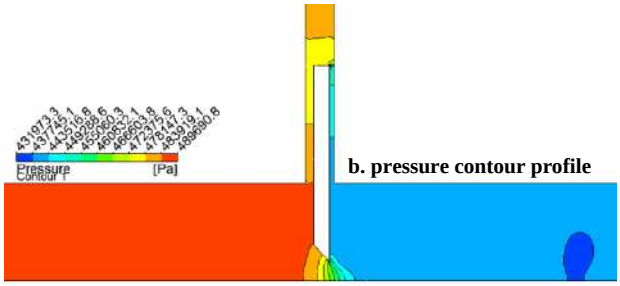

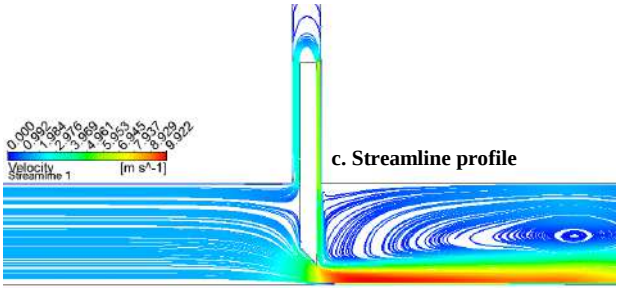

Fig. (11): Layout of velocity vectors, pressure contour lines profile and streamline profile obtained by ANSYS FLUENT model for the gate with well and the gap width ratio(b_2/b_1=0.5)

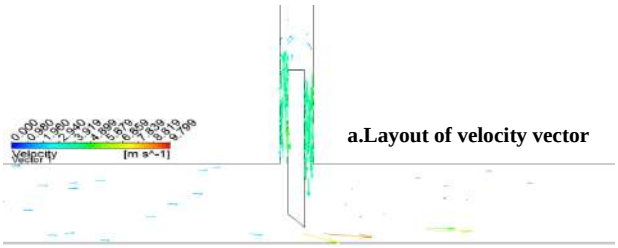

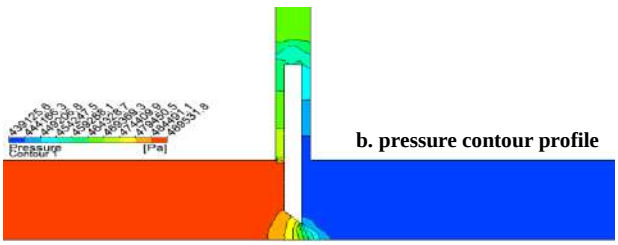

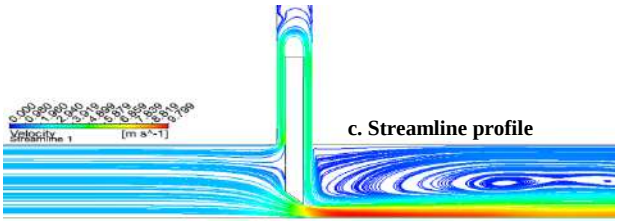

Fig. (12) Layout of velocity vectors, pressure contour lines profile and streamline profile obtained by ANSYS FLUENT model for the gate with well and gap width ratio(b_2/b_1=1)

4.3. A Comparisons between the leaf gate with and without well with 3D Simulation by ANSYS FLUENT Program

Bottom downpull coefficient (k_b) computed by ANSYS FLUENT program for three-dimensional simulation are shown in figure (13). The figure illustrates that there are some differences between the (k_b) values for the cases of gate with and without well computed by 3D ANSYS FLUENT models especially at (Y/Y_o=0.4). One can conclude that that the three-dimensional analyses are not efficient since it is sensitive and needs a

specific size and shape of the elements to reach the stability especially for the case of welled gate.

Different profiles of velocity streamline, velocity vector, and pressure contour estimated by ANSYS FLUENT program for a tunnel with (41m) length, (6m) height, (1m) gate thickness with and without well and with lip angle ($\theta = 45^{\circ}$),considering three-dimensional model and gate opening ($Y/Y_0 = 0.2$)with (b_2/b_1=0.2) are plotted in figures (14 and 15), and the following conclusions can be obtained:

a. Maximum velocity reaches to 12.022m/s and 9.897m/s for gate without well and with well respectively.

b. The pressure head distribution appears to be uniform at upstream and non-uniform under the gate and at gab (b_2).

c. The streamlines reveal contraction and separation for the flow field around and near the gate. Moreover, it illustrates the submerged hydraulic jump D/S of the gate for two cases.

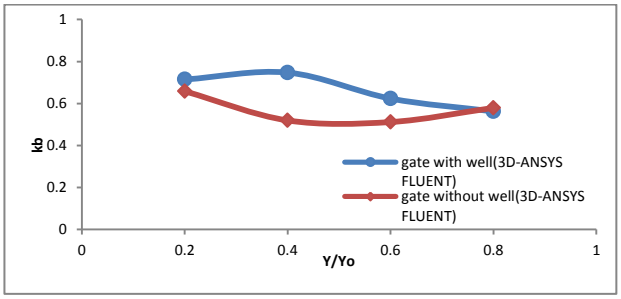

Fig. (13): Variation of bottom downpull coefficient k_b with relative gate opening ratios for the gate with and without well by considering three dimensional simulations.

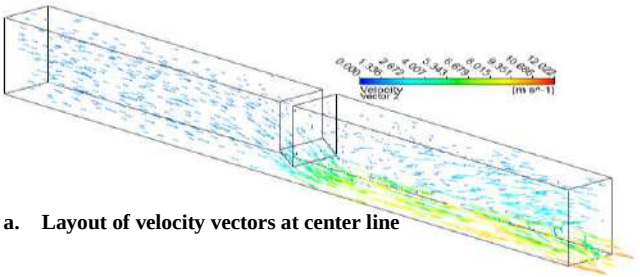

a. Layout of velocity vectors at center line

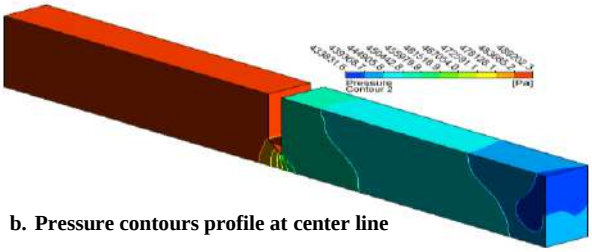

b. Pressure contours profile at center line

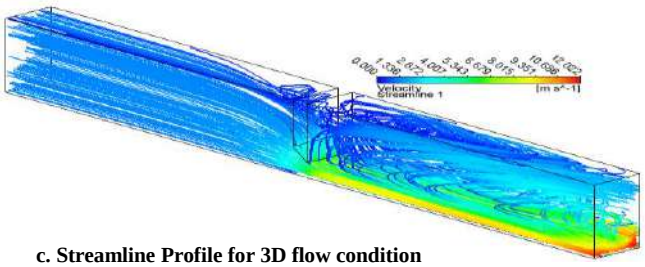

c. Streamline Profile for 3D flow condition

Fig. (14): Layout of velocity vectors, pressure contour lines profile and streamline profile obtained by ANSYS FLUENT model considering three dimensional simulations.

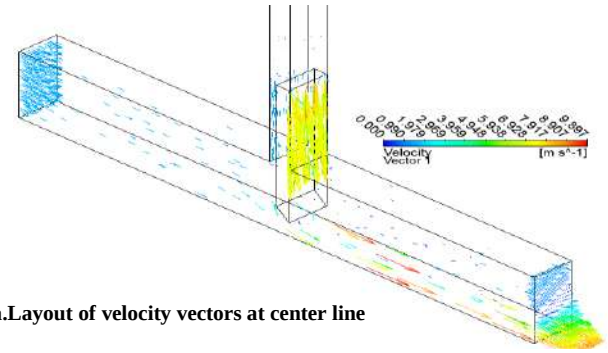

a.Layout of velocity vectors at center line

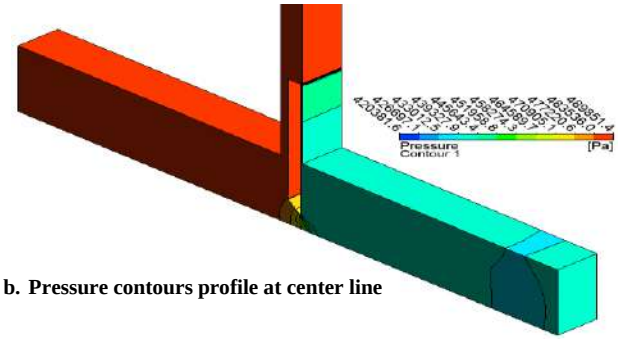

b. Pressure contours profile at center line

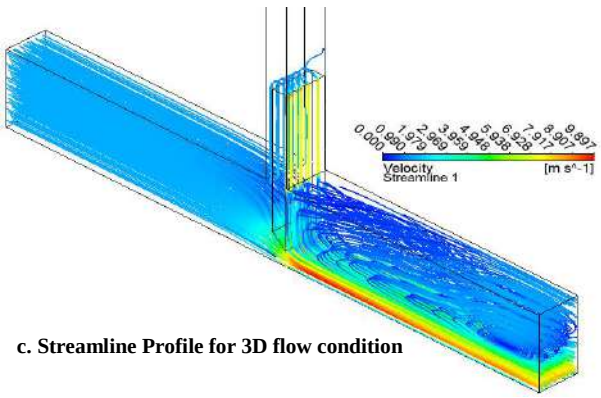

c. Streamline Profile for 3D flow condition

Fig. (15): Layout of velocity vectors, pressure contour lines profile and streamline profile obtained by ANSYS FLUENT model considering three dimensional simulations and the gate with well.

5. CONCLUSIONS

The following conclusions can be outlined:

1.A comparison between bottom downpull coefficient (k_b) for the gate with and without

well computed by ANSYS FLUENT Program showed a slight difference between of them.

2.An increase of gab width ratio from 0.2 to 1 showed an increase of bottom downpull coefficient (k_b) values from 0.46 to 0.62 at gate opening ratio 0.4.

3.A comparison between bottom downpull coefficient (k_b) computed by 3D simulation of ANSYS FLUENT Program showed some difference between them especially at(Y/Y_o=0.4).

REFERENCES

- Al-Kadi, B. 1997. *Numerical Evaluation of Downpull Force in Tunnel Gates*. Ph. D Thesis Submitted to the College of Engineering, University of Baghdad.
- Almaini, R.., Al-Kifae, M., and Alhashimi, S. 2010.*Prediction Downpull Force on Tunnel Gate with Different Gate Lip Geometry*. Journal of Kerbala University, Vol. 8, No.4.
- Ansys Help, 2011.
- Al-Kadi, B. and SaidAli,B. 2015.*Simulation of Downpull Forces of Leaf Gate in High Dams*.Thesis Submitted to Department, dams and water resources Engineering and Salahaddin University -Erbil.
- Douglas, J., and Matthews, R., 1996.*Solving Problems in Fluid Mechanics*.Longman Group Limited.
- Durst, F., and Schmitt ,F.1985.*Experimental Studies of High Reynolds Number Backward-Facing Step Flows*. in Proc. Fifth Symp. Turbulent Shear Flows, Cornell University, Pp.5.19-5.24.
- Ferzieger, J., and Peric, M.1996. *Computational Methods for Fluid Dynamics*.Springer- Verlag, Heidelberg.
- Naderi, M., and Hadipour,E.,2013.*Numerical Simulation of Flow in Bottom Outlet of Narmashir Dam for Calculating of Hydrodynamic Forces*. European Journal of Applied Engineering and Scientific Research, Vol. 2, No. 2, Pp. 33-40.
- Naudascher, E., Rao, P., Richter, A., Vargas, P., and Wonik, G., 1986. *Prediction and Control of Downpull on Tunnel Gates* Hydraulic Engineering, Vol. 112, No. 5, Pp. 392-416.
- Naudascher, E., Kobus, H., and Rao, R.1964.*Hydrodynamic Analysis for High- Head Leaf Gates*.,ASCE, Journal of the Hydraulic Division. Vol. 90, No. 3, Pp. 155-192.
- Piradeepan, N.2002. *An Experimental and Numerical Investigation of a Turbulent Airfoil Wake in* 90°*Curved Duct.* Ph.D , Thesis Submitted to Department, Mechanical Engineering and University of Brunel.
- Shamsai, A., and Soleymanzadeh, R.,2006 .*Numerical Simulation of Air-Water Flow in Bottom Outlet*. International Journal of Civil Engineering. Vol.4, No .1, March.
- Thang, N. D. and Naudascher, E.1983.*Approach Flow Effect on Downpull of Gates*. ASCE, Vol. 109, No. 11, November.

ZANCO Journal of Pure and Applied Sciences
The official scientific journal of Salahaddin University-Erbil
ZJPAS (2018) **30**(s1)s83-s93
http://dx.doi.org/10.21271/ZJPAS.30.s1.10

Numerical Modeling of Flow in Side Channel Spillway Using ANSYS-CFX

Shahin S. Ahmed[1] **and** [*]**Yaseen W. Aziz**[2]

[1] Asst. prof. Department of Dams and Water Resources, College of Engineering, University of Salahaddin, Erbil, Kurdistan Region, Iraq.

[2] M.Sc. Department of Dams and Water Resources, College of Engineering, University of Salahaddin, Erbil, Kurdistan Region, Iraq.

A R T I C L E I N F O

Article History:
Received: 14/05/2017
Accepted: 12/04/2018
Published:01/06/2018

Keywords:
Side Channel Spillway
CFD
ANSYS-CFX
Turbulence models

**Corresponding Author:*
Email: yaseen90aziz@gmail.com

A B S T R A C T

Side channel spillway is one of the most common types of spillways provided at earth dams to release flood discharge laterally. Flow in side channel is complex due to discharge changing along its length. Due to rapid advent of computer technology computational fluid dynamics (CFD) is extensively used to model and analyze complex issues in engineering problems. In the present study ANSYS-CFX code has been used to predict flow characteristics in the side channel spillway. Grid dependence study provided to select the optimum grid size that can predict free surface profile accurately with minimum computational time. In addition, various turbulence models such as k- ε and RNG k- ε were used. The capability of each turbulence model to predict flow characteristics in the spillway were tested. The k- ε and RNG k- ε turbulence models gives good results at most parts of the spillway, while RNG k- ε turbulence model needs higher computational time. Furthermore, the ability of the code to predict free surface water profile for various discharges was validated using results of the physical model. The comparisons of water surface profile predicted by ANSYS-CFX with the physical model show good agreement. Unlikely, at the location of hydraulic jump in the stilling basin for higher discharges which characterized by strong aeration ANSYS-CFX with k- ε turbulence model failed to give accurate predicts of the free surface water profile.

INTRODUCTION

Side channel Spillway (SCS) is one of the types of spillway that is usually provided at earth dams in order to release flood discharge from the reservoir to prevent overtopping and damage of the dam. Therefore, spillway is an important structure in the dam. Thus, great attention should be paid to study the hydraulic characteristics of the structure. SCS consists of six parts namely; side weir, trough channel, control section channel, transition section channel, chute channel and stilling basin. Flow in the side channel is very complex called spatially varied flow (SVF), resulting from added of water along the length of the weir (Subramanya, 2009). Computation fluid dynamics (CFD) is a branch of fluid

mechanics that can simulate real fluid by using numerical methods to solve the governing equations. Nowadays CFD is extensively used by the researchers to model and analyze complex problems in engineering due to rapid advent of high performance computers and parallel computation methods. Investigation of dynamic pressure fluctuation in stepped three sided spillway (U shape) using FLOW 3D code was performed by (Taghizadeh *et al*, 2012). A good agreement was found when the results of the numerical model compared with the experimental results. Furthermore, (Gellibert *et al*, 2016) conducted a study to investigate the performance of side channel spillway of a selected dam using ANSYS-CFX code. The result of water surface profile in the spillway compared with results of the original study, the results showed good agreement between them. Flow characteristics in the hydraulic jump investigated using ANSYS-CFX code, Flow-3D and openFOAM by (Castillo et al, 2014), the k-ω turbulence model in the recirculation zone displayed a better agreement and more realistic than *k- ε*. The flow simulation in front of rectangular broad crested weir was carried out by (Zachoval and Rousar, 2015**)** and compared their results with experimental results. The most reliable result was obtained by using RNG k- ε turbulence model but from all two layers turbulence models (SST) provide most reliable results. In the present study the flow characteristics in SCS were investigated using ANSYS-CFX 14. The results of the numerical model were validated against the physical model data of (Aziz, 2016).

MATERIALS AND METHODS

In the current study ANSYS-CFX code has been used for flow simulation in the side channel spillway. The code is based on finite volume method, which discretizes Naiver stokes equations at each computational cell. In turbulent flow, velocity at each point consists of two components, mean ($\bar{U}$) and fluctuating velocities (u'). The mass and momentum equations in the time average form for incompressible flow can be written as:

$$\frac{\partial}{\partial x_i}(\rho \bar{U}_i) = 0 \quad \ldots\ldots\ldots\ldots\ldots\ldots\ldots\ldots\ldots 1$$

$$\frac{\partial}{\partial x_j}\rho \bar{U}_i \bar{U}_j = -\rho g_i - \frac{\partial \bar{P}}{\partial x_i} + \frac{\partial}{\partial x_j}\left(\mu\left(\frac{\partial \bar{U}_i}{\partial x_j} + \frac{\partial \bar{U}_j}{\partial x_i}\right) - \rho\overline{u_i' u_j'}\right) \ldots 2$$

The Naiver - Stokes equations with time average velocity called Reynolds averaged Naiver – Stokes (RANS) equations. This method eliminates turbulent fluctuations by the averaging process. The averaging of nonlinear terms in the Naiver Stokes equations causes additional unknowns called Reynolds stress. Most of commercial CFD codes use time average equations such as RANS equations for modeling turbulent flow. The term ($-\rho u_i' u_j'$) is referred to the Reynolds stresses, in three dimensional (RANS) equations there are six unknown terms, they behave like stresses.

The turbulence modeling is a computational procedure that can close the governing equations by modeling Reynolds stresses (Piradeepan, 2002). Numerous turbulence models are available based on RANS equations. ANSYS-CFX contains numerous turbulence models which can be divided into two groups namely; eddy viscosity and Reynolds stress models.

The k – ε Turbulence Model

This turbulence model is a semi empirical model. It is probably the most common type used than the other types. It gives a good result in many industrial flows. This model has two model equations one for k (turbulent kinetic energy) and other for ε (dissipation rate). In this model the eddy viscosity is linked to the

turbulent kinetic energy and dissipation (ANSYS, 2011a) as:

$$\mu_t = \rho C_\mu \frac{k^2}{\varepsilon} \quad \ldots\ldots\ldots\ldots\ldots\ldots\ldots\ldots\ldots\ 3$$

Where: k is the turbulent kinetic energy, ε is the rate of dissipation of turbulent kinetic energy, C_μ is an empirical constant = 0.09.

The separate transport equations solve for k and ε at a given time. The transport equations for k and ε are as follow (Launder and Spalding, 1974):

$$\frac{\partial(\rho k)}{\partial t} + div(\rho k U) = div\left[\frac{\mu_t}{\sigma_k} grad k\right] + 2\mu_t S_{ij}.S_{ij} - \rho\varepsilon \quad \ldots\ldots\ldots\ldots\ldots\ 4$$

$$\frac{\partial(\rho\varepsilon)}{\partial t} + div(\rho\varepsilon U) = div\left[\frac{\mu_t}{\sigma_\varepsilon} grad\varepsilon\right] + C_{1\varepsilon}\frac{\varepsilon}{k}2\mu_t S_{ij}.S_{ij} - C_{2\varepsilon}\rho\frac{\varepsilon^2}{k} \quad \ldots\ldots\ldots\ldots\ldots\ 5$$

Where:

σ_k: is Prandtl number connect the diffusivity of k to the eddy viscosity, typically the value of 1.0 is used, σ_ε: is Prandtl number connect the diffusivity of ε to the eddy viscosity, typically the value of 1.3 is used. The value of $C_{1\varepsilon}$ and $C_{2\varepsilon}$ are 1.44 and 1.92 respectively.

The standard (k -ε) model equations (4), (5) have been developed for fully turbulent flow which cannot be applied to the near wall that characterized by viscous layer has low Reynolds number, this leads to erroneous results (Abo, 2013).

The Renormalized Group (RNG) k -ε Turbulence Model

The RNG k -ε turbulence model is based on the re-normalization group (RNG) analysis of Naiver – Stokes equations (ANSYS 2011a). The RNG method uses statistical mechanics to extend the k-ε model. This model systematically removes the small scales of motion from the Naiver - Stokes equations by expressing their effects in terms of large scale motions and modified viscosity (Versteeg and Malalasekera, 2007, p.87).

The RNG k-ε model was first derived by (Yakhot *et al.*, 1992), the equations are as follows:

$$\frac{\partial(\rho k)}{\partial t} + div(\rho k U) = div\left(\alpha_k \mu_{eff} grad\, k\right) + \tau_{ij}.S_{ij} - \rho\varepsilon \quad \ldots\ldots\ldots\ldots\ldots\ 6$$

$$\frac{\partial(\rho\varepsilon)}{\partial t} + div(\rho\varepsilon U) = div\left(\alpha_\varepsilon \mu_{eff} grad\, \varepsilon\right) + C_{1\varepsilon}^{*}\frac{\varepsilon}{k}\tau_{ij}.S_{ij} - C_{2\varepsilon}\rho\frac{\varepsilon^2}{k} \quad \ldots\ldots\ldots\ldots\ldots\ 7$$

Where:

$$\tau_{ij} = -\rho\overline{u_i' u_j'} = 2\mu_t S_{ij} - \frac{2}{3}\rho k\delta_{ij}, \qquad C_{1\varepsilon}^{*} = C_{1\varepsilon} - \frac{\eta\left(1-\frac{\eta}{\eta_o}\right)}{1+\beta\eta^3}, \quad \eta = (2S_{ij}.S_{ij})^{0.5}\frac{k}{\varepsilon}$$

Where: C_μ, $\alpha_k, \alpha_\varepsilon$, $C_{1\varepsilon}$, $C_{2\varepsilon}$, β, η_o are constants

C_μ = 0.0845, $\alpha_k = \alpha_\varepsilon$ =1.39, $C_{1\varepsilon}$ = 1.42, $C_{2\varepsilon}$=1.68, $\beta = 0.012$, $\eta_o = 4.377$

Geometry and Mesh Generation

For the present study, three dimensional geometry of the model was created using AutoCAD 2013. The geometry exported from AutoCAD as a file (.sat) and then imported to the ANSYS Design Modeler. To generate mesh for the fluid domain, ANSYS ICEM CFD was used that is a powerful tool for mesh generation which contains numerous techniques. In this tool different element shapes are available such as tetrahedral, hexahedral, prism, and pyramid with different formats such as multi-block, structured, unstructured, and many others. Because the geometry of the spillway is complex, so it is divided into some parts in order to facilitate controlling mesh type and the size. Different mesh methods were used, for sweepable parts such as chute transition and control channel sweep method was used with the manual controlling source and target face. For other parts such as stilling basin where sweep method cannot be applied multi-zone

and tetrahedron method was employed. A finer grid size was selected for those parts were high flow gradient were observed (Figure 1).

Figure 1 typical view of mesh generation for different parts of side channel spillway.

Boundary Conditions

Boundary conditions have an important role in the flow simulation; accurate result can be obtained by specifying an appropriate initial and boundary conditions. ANSYS-CFX code contains several boundary conditions such as inlet, outlet, opening, wall and symmetry (Figure 2). Inlet boundary condition specified at inlet section with the average velocity, water and air volume fraction. Supercritical outlet type was specified at the outlet since the flow is supercritical, opening boundary condition was specified for the top of the spillway. Sides and bottom of the domain were specified as no slip wall boundary condition, the fluid velocity next to the wall immediately is equal to zero (ANSYS, 2011b).

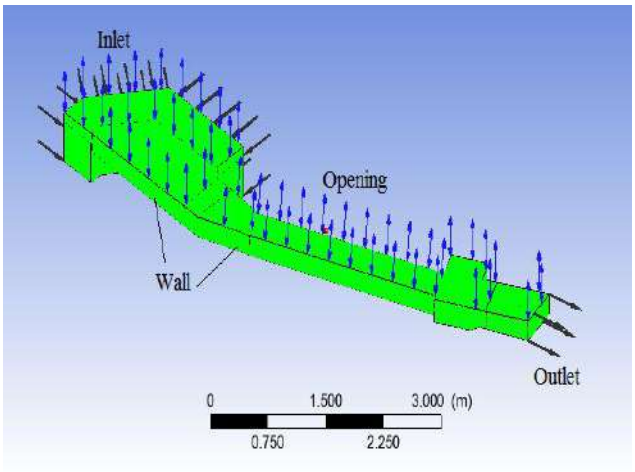

Figure 2 Boundary conditions for model of side channel spillway.

RESULTS AND DISCUSSION

Verification of ANSYS-CFX Results

Because of the numerical models are based on many assumptions which influence the results, these models should be verified in order to assure accuracy of the results. The most important factors that considered in this study are meshing size and turbulence models. . For this purpose the results of water surface profile obtained from ANSYS-CFX were compared with the physical model results.

3.1.1. Mesh size

Three models were simulated with three sets of mesh sizes, coarse, medium and fine meshes, with a number of grids (1300000, 2500000, and 3750000) for the design discharge (33.451 l/s). All models were simulated with the steady state analysis type with using k- ε turbulence model. Total computational time for fine, medium and coarse meshes were (52, 35 and 16) hours respectively. The free surface profile along the centerline and right side wall of the trough, chute channel and stilling basin were taken for comparing the results of numerical models with results of physical model (Figure 3). The percentage error between the physical model

and the ANSYS-CFX was calculated at those sections were flow depths from the physical model are measured. Finally, average percentage of error (APE) computed between ANSYS-CFX and the physical model for each part (Table 1).

a) Trough Channel

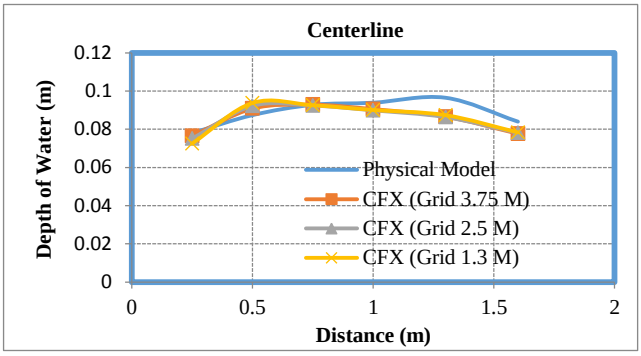

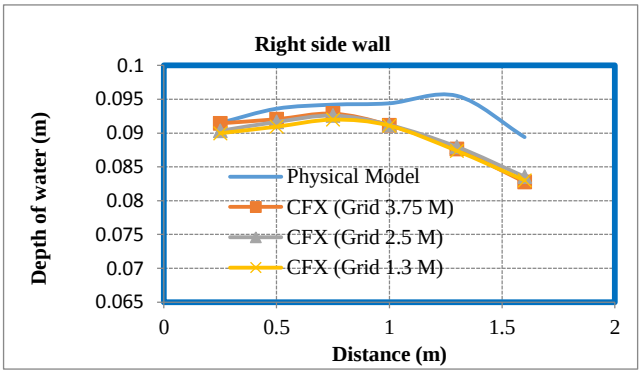

b) Chute Channel

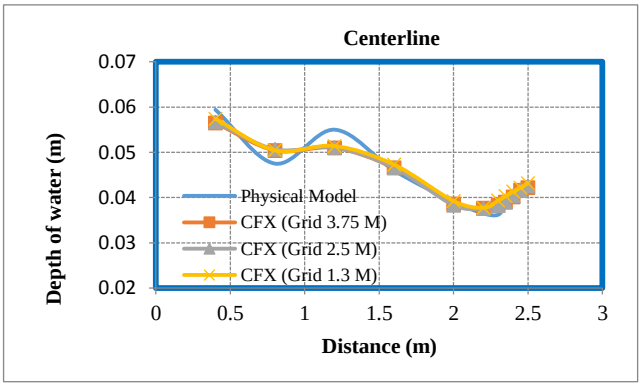

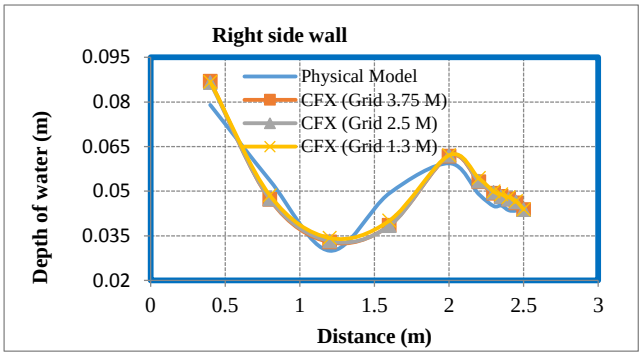

C) Stilling Basin

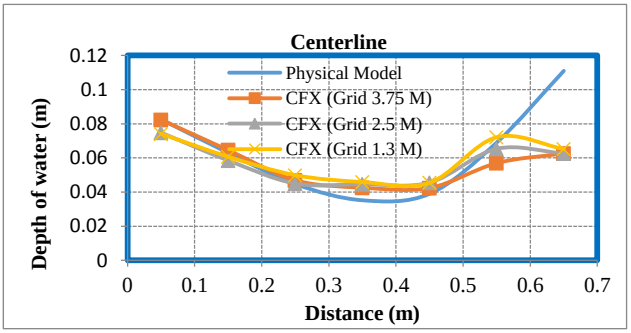

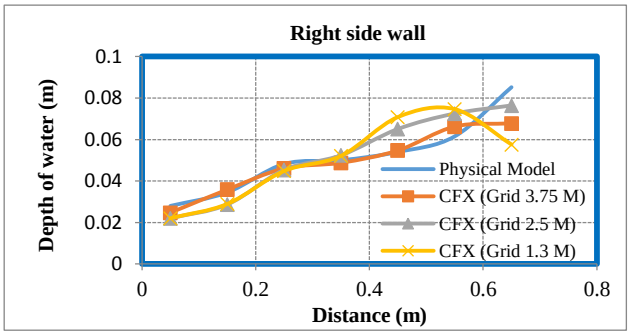

Figure 3 Flow depth obtained from for physical model and numerical models (Grid 3.75 M, Grid 2.5 M and Grid 1.3 M).

Table 1 The APE between physical model and ANSYS-CFX with different grid number along the centerline and right side wall at some parts of spillway

Parts		APE of Grid 3.75 M with P.M.	APE of Grid 2.5 M with P.M.	APE of Grid 1.3 M with P.M.
Trough Channel	C.L.	4.53	5.23	5.79
	R.S.	3.7	3.82	4.3
Chute Channel	C.L.	3.24	3.43	4.1
	R.S.	8.92	9.17	9.59
Stilling Basin	C.L.	14	15.66	16.9
	R.S.	7.4	13.93	19.04

According to the results of tables (1) the following conclusions were made:

1- The accuracy of ANSYS-CFX using 2500000 grids is almost close to that using 3750000 grids, in spite its computational time is less.
2- A noticeable deviation between the results of CFX with the physical model are exist at the end of stilling basin were strong jump occurs. This deviation due to the complexity of the phenomenon rather than mesh density.

3- For the above reasons the numerical model with 2500000 grids can be used for flow simulation in side channel spillway.

Turbulence models

To test the effect of turbulence models on the numerical results of water surface profile, two turbulence models were used for flow simulation in the side channel spillway. The first one is k- ε and the second is RNG k- ε turbulence model. Both simulations were performed for the design discharge (33.451 l/s). The total time required to finish both simulations with k- ε and RNG k- ε were 35, 42 hours respectively. The free surface water profile predicted by ANSYS-CFX using these two turbulence models compared with the physical model results at trough channel, chute channel and stilling basin of the spillway at the centerline and the right side wall of them (Figure 4). The APE between physical model and ANSYS-CFX are shown in Table 2.

a) Trough Channel

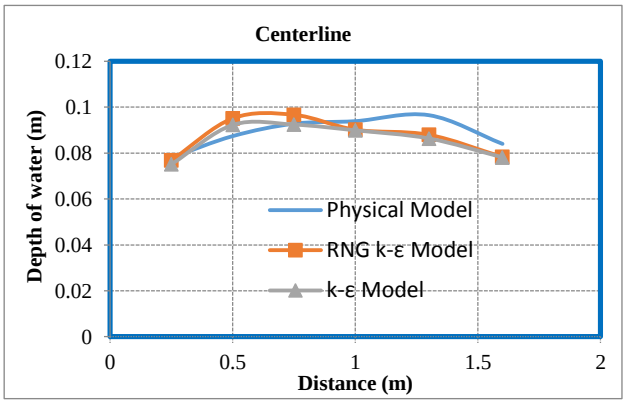

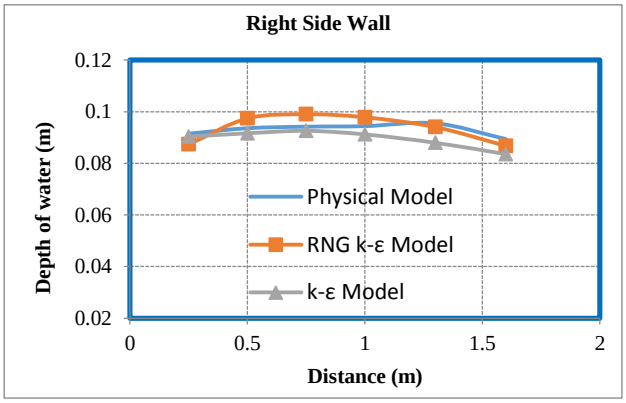

b) Chute Channel

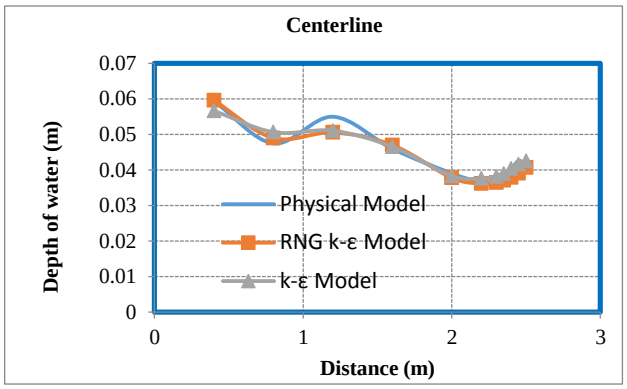

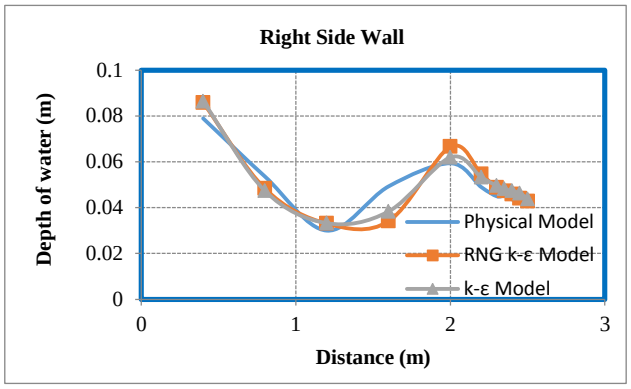

c) Stilling Basin

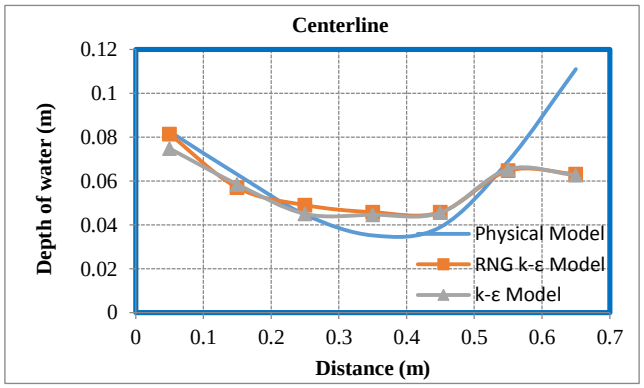

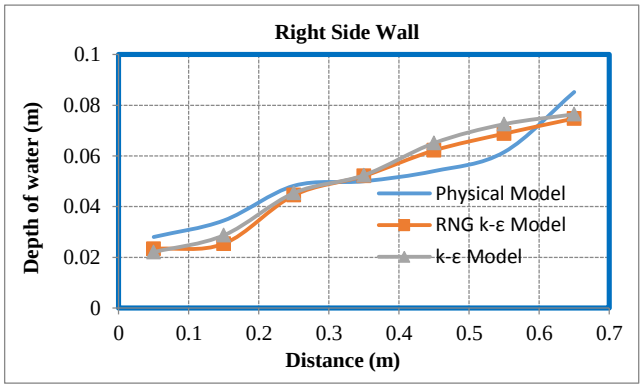

Figure 4 Flow depth obtained from physical model and numerical model (using k- ε and RNG k- ε).

Table 2 The APE between physical model and ANSYS-CFX using (k- ε and RNG k- ε model) at some parts of spillway.

Parts		APE k- ε model with physical model	APE RNG k- ε model with physical model
Trough Channel	C.L.	5.3	5.6
	R.S.	3.8	3.6
Chute Channel	C.L.	3.44	3.4
	R.S.	9.2	9.7
Stilling Basin	C.L.	15.7	16.75
	R.S.	13.95	13.4

The overall percentage of error showed that the k- ε turbulence model can be used for modeling of turbulent flow in the side channel spillway which needs less computational time than RNG k- ε model. Both turbulence models seem fail to predict water surface profile at the location of hydraulic jump. Due to high error percentages at the jump location, it needs an extra study to test the capability of k- ε turbulence model at those locations.

Water Surface Profile (WSP)

The results of WSP along the centerline of the spillway for various discharges predicted by ANSYS-CFX plotted with the corresponding WSP of the physical model as shown in figure 5. There is a good agreement between predicted WSP by CFX with the observed WSP from The physical model at most parts of the spillway. At the chute channel good agreement was found between CFX and physical model results especially at the centerline. While, there is differences between them at the sides of the chute channel this is mostly due to cross waves that created in the chute channel due to sharp alignment of the transition channel. The water level becomes rising and falling near boundaries of the chute channel till the flow reaches its downstream height of waves reduced (Figure 6). At stilling basin the results of ANSYS-CFX can be outlined in the following points:

1- At the beginning of the stilling basin (before jump occurs) the results of ANSYS-CFX are well agreed with results of the physical model.
2- At the jump location which characterized by high streamline curvature and high air concentration, especially for higher discharges there are differences between the flow depth obtained from CFX and that obtained from the physical model. This may be related to:
   a) The complexity of the situation and the turbulence model which cannot well detect air entrainment phenomenon. This well agree with the results obtained by (Zhan *et al*, 2016) (Numerical investigation of air-entrainment in skimming flow over stepped spillway) showing that RANS with k- ε is not suitable for simulation of free surface aeration. Likewise, (Castillo *et al*, 2014) have doubts about the suitability of using k- ε turbulence model to solve hydraulic jumps.
   b) In physical model point gauge is used for measuring flow depth which is not a good instrument for measuring water depth at the location of the hydraulic jump accurately.
3- Furthermore, as it can be observed from figures 5b, c, d, for discharges lower than the design discharge, location of the jump moves to the upstream. Differences between the physical model and ANSYS-CFX results in the stilling basin occurred at the jump location only. This deviation diminishes at very low discharges in which the hydraulic jump is unlikely form or the weak jump may be formed.

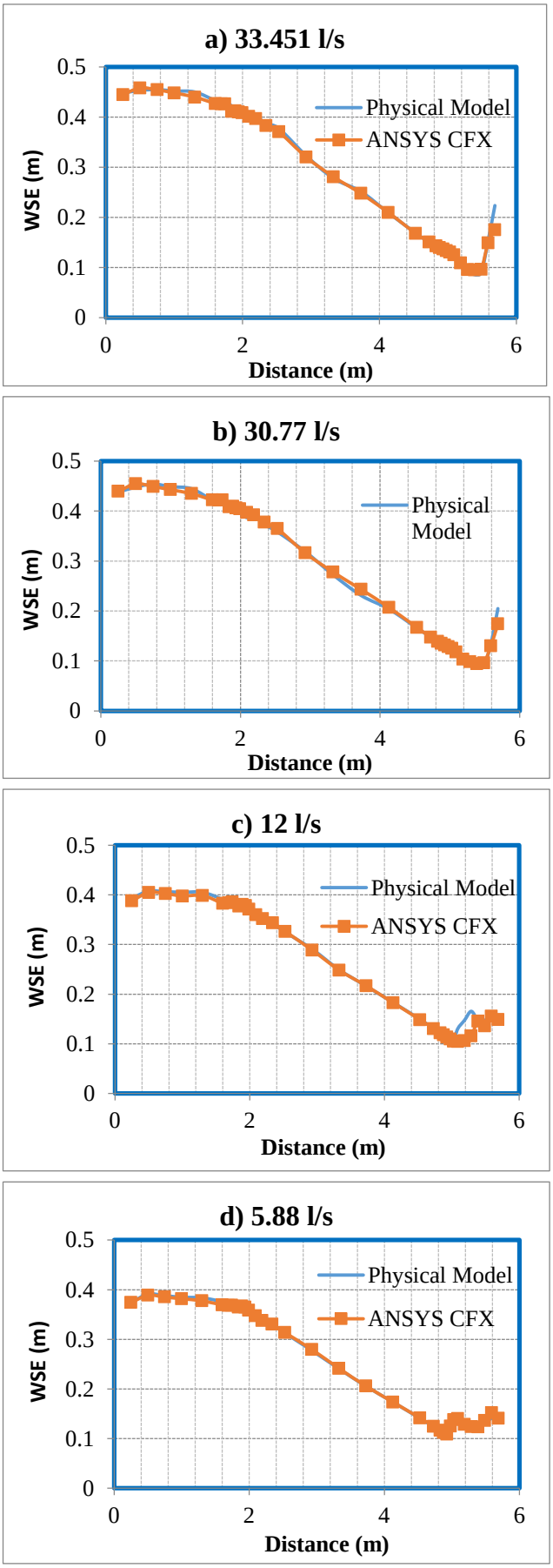

Figure 5 Comparison of ANSYS CFX and physical model water surface profile in side channel spillway for different discharge.

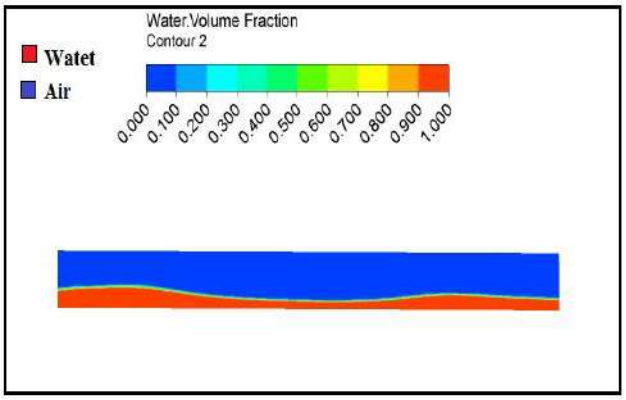

Figure 6 Rising and falling free surface with color-coded values at side wall of the chute channel detected by ANSYS-CFX.

3.3. Velocity Profile

Figure 7 shows velocity distribution along the spillway obtained from CFD code CFX. The vertical velocity profile was taken at some section in the trough channel, chute channel and stilling basin as shown in figure 8, but from the physical model velocity does not measured in order to compare it with CFX. From figure 8a it is clear that the flow is non-uniform at the beginning of the trough channel. This is due to the effect of the jet of water from the crest. At the downstream sections of trough channel the effect of jet reduced, the uniform flow is nearly to achieve. In the chute channel it is clear that the flow is almost uniform, and velocity increases as flow goes downstream. Furthermore, maximum vertical velocity can be observed near the free surface flow (figure 8b). The results of vertical velocity profile in the stilling basin indicated that there is no the recirculation zone at the centerline of the stilling basin. For X* (X/L (length of the channel)) = 0.077 the velocity is decreased to its minimum value as depth of water increased, then it increased till reached maximum value when Y* (y/y_{max}) was equal to 0.75. This is due to separation of incoming jet of water from bottom of the basin when spread into the stilling basin.

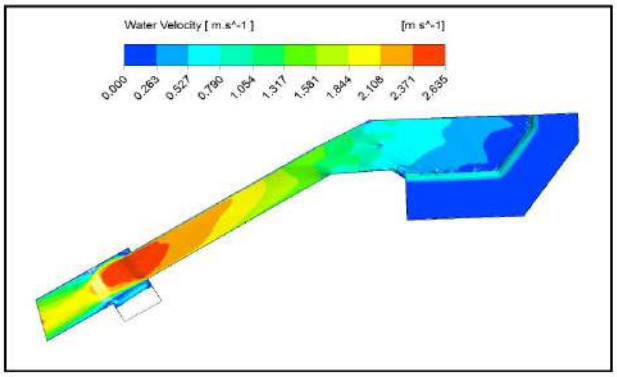

Figure 7 Velocity distribution with color-coded values within the spillway predicted by ANSYS-CFX

a) Trough Channel

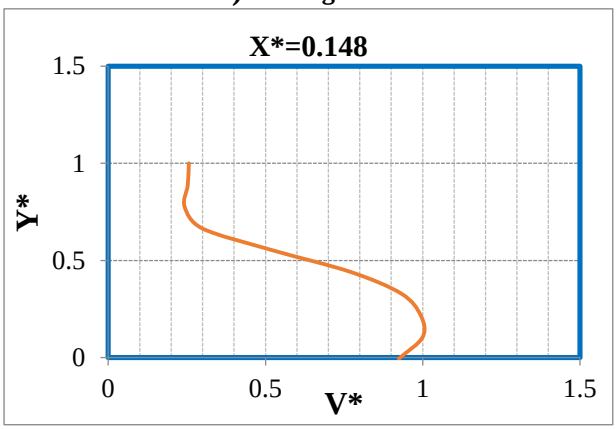

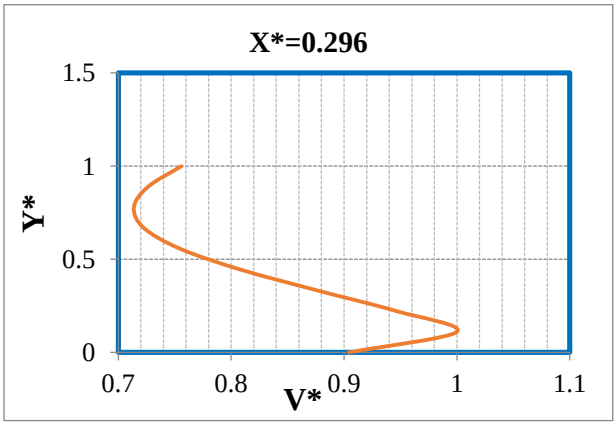

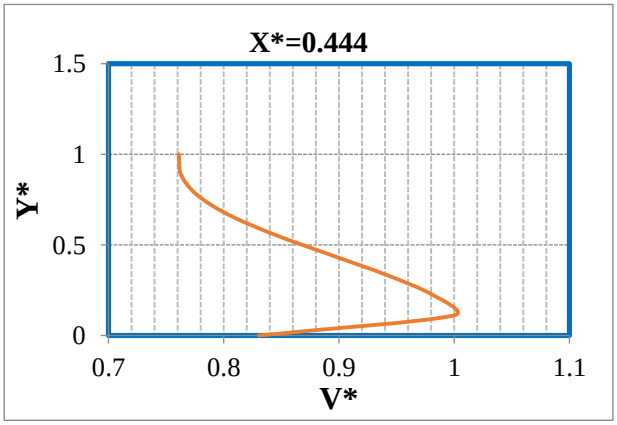

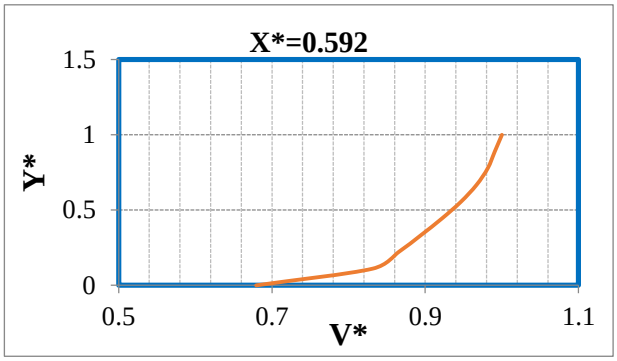

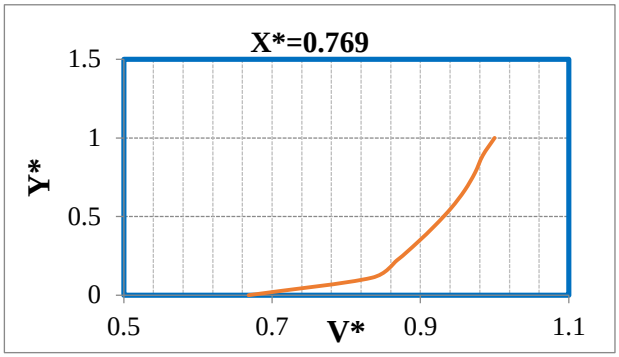

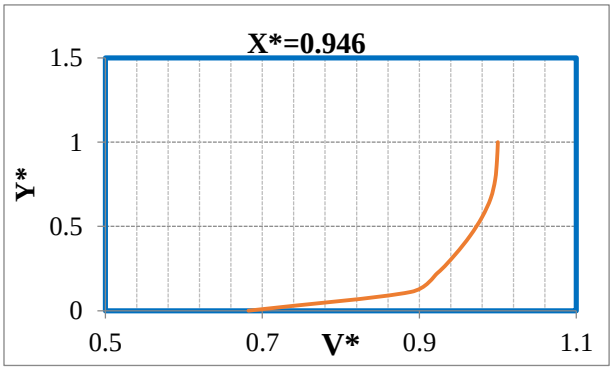

b) Chute Channel

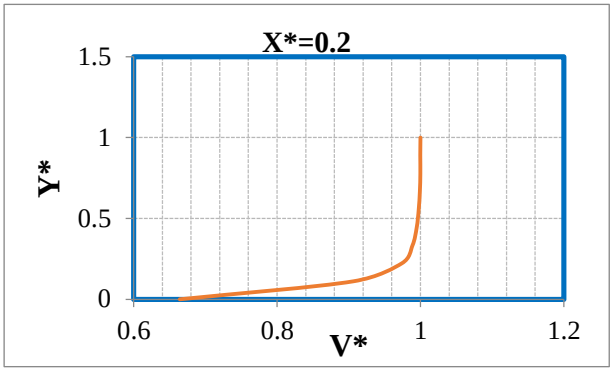

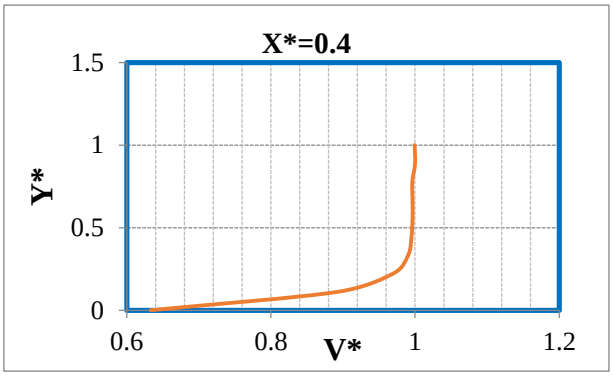

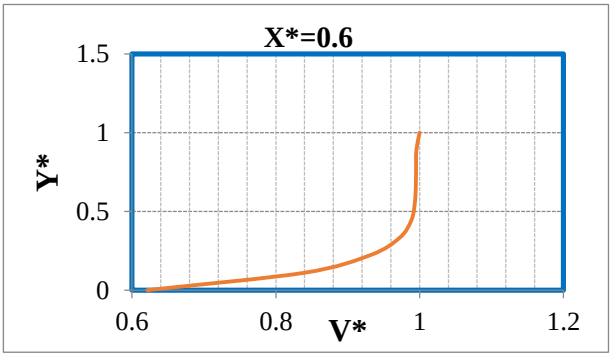

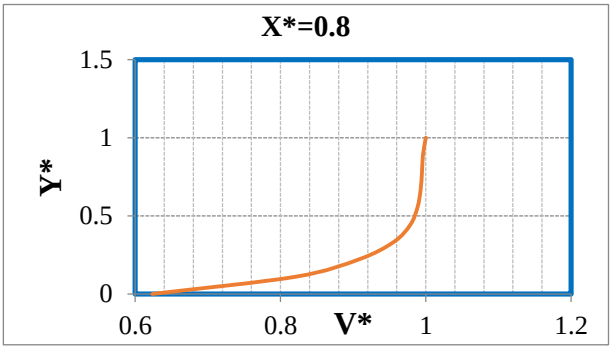

c) Stilling Basin

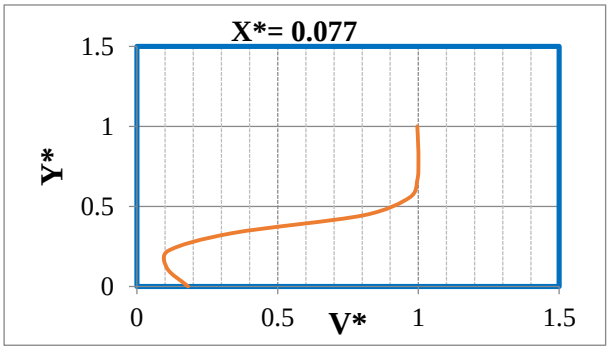

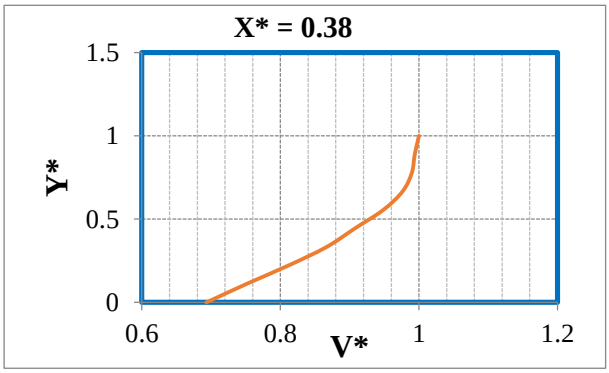

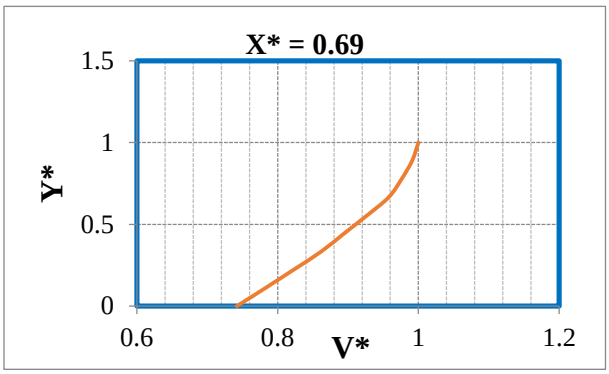

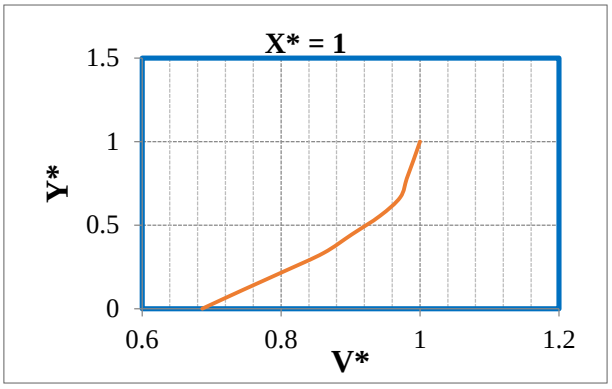

Figure 8 Vertical velocity distributions within the spillway

CONCLUSION

Flow in side channel spillway was simulated using ANSYS-CFX code which is based on finite volume method. The results of water surface profile for different discharges were compared with the physical model results. Velocity distribution predicted by CFX and vertical velocity profile was taken at various sections within the spillway. The following conclusion was established.

1. The results of k- ε and RNG k- ε turbulence models relatively close to each other at most parts of the spillway compared to the physical model results.
2. 2. The predicted WSP by ANSYS-CFX at the center of chute channel is better agreeing with the physical model compared at the boundaries due to cross waves.
3. The ANSYS-CFX code with k- ε turbulence model could well predict the free surface water profile in the SC spillway components. Unlikely, it failed to give accurate predicts of WSP at the hydraulic jump when strong aeration occurred.
4. For lower discharges ANSYS-CFX code gave good predict of WSP in the stilling basin because the hydraulic jump is relatively weak.
5. Flow in the chute channel was almost close to uniform compared with the flow in trough channel and stilling basin.

REFERENCES

ABO, A. A. (2013) A three dimensional flow model for different cross section high velocity channels. PhD thesis, faculty of marine sciences and engineering, Plymouth University.

ANSYS (2011a). ANSYS CFX Release 14.0 - Theory Guide. Computer software manual.

ANSYS (2011b). ANSYS CFX Release 14.0 - Modeling Guide. Computer software manual.

AZIZ, Y. W. (2016) Evaluation of Hydraulic Performance of Nazanin Dam Side Channel Spillway. M.Sc thesis, Dams and Water Resources Department, College of Engineering, University of Salahaddin.

CASTILLO, L. G., CARRILLO, J. M., GARCIA, J. T. and VIGUERAS -RODRIGUEZ, A. (2014) Numerical Simulations and Laboratory Measurements in Hydraulic Jumps. 11th International Conference on Hydroinformatics, *HIC* 2014. New York City, USA, Paper 345. http://academicworks.cuny.edu/cc_conf_hic/345

GELLIBERT, A., SAVATIER, J., PEPIN, N. and FULLY, O. (2016) 3D Computational Modeling of the Galaube Dam Spillway. In Advances in Hydroinformatics (p. 361-376). Springer Singapore.

GENERAL DIRECTORATE OF DAMS AND RESERVOIRS (2013) Design Report of Nazanin Dam.

HIRT, C. W. and NICHOLS, B. D. (1981) Volume of Fluid (VOF) Method for the Dynamics of Free Boundaries. Journal of Computational Physics, 39 (1). P. 201-225.

LAUNDER, B. E. and SPALDING, D. B. (1974) The Numerical Computation of Turbulent Flows. Computer Methods in Applied Mechanics and Engineering, 3(2). p. 269-289.

MACHAJSKI, J. and OLEARCZYK, D. (2011) Model Investigations of Side Channel Spillway of the Złotniki Storage Reservoir on the Kwisa River. In Experimental Methods in Hydraulic Research (p. 189-202). Springer Berlin Heidelberg.

MILESI G. and CAUSSE, S. (2014) 3D Numerical Modeling of a Side - Channel Spillway. In Advances in Hydroinformatics (p. 487–498). Springer Singapore.

PIRADEEPAN, N. (2002) An Experimental and Numerical Investigation of a Turbulent Airfoil Wake in a 90° Curved Duct. PhD thesis, Department of Mechanical Engineering, Brunel University.

SUBRAMANYA, K. (2009) Flow in Open Channels. Third edition, New Delhi,Tata McGraw-Hill Education.

TAGHIZADEH, H., NEYSHABOUR, S. A.A. S. and GHASEMZADEH, F. (2012) Dynamic Pressure Fluctuations in Stepped Three - Side Spillway. Iranica Journal of Energy & Environment, 3(1). p.95-104.

VERSTEEG, H. K. and MALALASEKERA, W. (2007) An introduction to Computational Fluid Dynamics. Second Edition, Edinburgh Gate, Harlow, Addison Wesley Longman Ltd.

YAKHOT, V., ORSZAG, S. A., THANGAM, S., GATSKI, T. B., and SPEZIALE, C. G. (1992) Development of Turbulence Models for Shear Flows by a Double Expansion Technique. Physics of Fluids A, 4(7). p.1510-1520.

ZACHOVAL, Z. and ROUSAR, L. (2015) Flow Structure in front of the Broad – Crested Weir. In EPJ Web of Conferences, 92. p. 02117. EDP Sciences. http://dx.doi.org/10.1051/epjconf/20159202117

ZHAN, J., ZHANG, J. and GONG, Y. (2016) Numerical Investigation of Air-Entrainment in Skimming Flow over Stepped Spillway. Theoretical and Applied Mechanics Letters. 6 (3). p. 139-142.

ZANCO Journal of Pure and Applied Sciences
The official scientific journal of Salahaddin University-Erbil
ZJPAS (2018) **30**(s1)s94-s104
http://dx.doi.org/10.21271/ZJPAS.30.s1.11

Validation of a numerical particle based method for free surface flow downstream of sluice gates

Sarhang M. Husain[1], Abdulla, A. Abo[2] and Basil Y. Mustafa[3]

1, 2 Department of Dams and water resources, College of Engineering, Salahaddin University, Erbil, Kurdistan Region, Iraq

3 Department of Civil Engineering, Technical Engineering College, Polytechnic University, Erbil, Kurdistan Region, Iraq

A R T I C L E I N F O

Article History:
Received: 14/05/2017
Accepted: 12/04/2018
Published:01/06/2018

Keywords:
Numerical simulation Particle-based method
SPH
Sluice gates

***Corresponding Author Contact**
Email:
Sarhang.husain@su.edu.krd

A B S T R A C T

This study is a numerical investigation in which a meshfree computational method known as the Smoothed Particle Hydrodynamics (SPH) is applied to examine its efficiency and accuracy in predicting the flow field variables of free surface flow passing a sluice gate. For this purpose, the numerical 2D SPHysics model, as an implementation of the computational SPH method, is adopted. The numerical code is validated against the theoretical and experimental results of previous works. The validation is performed taking into consideration the conjugate flow depths and velocities for different total upstream heads passing under a fixed gate opening height. The quantitative agreement between the results computed by the numerical 2D SPHysics code and the theoretical and experimental results is fairly good confirming that the numerical code is robust in predicting the flow properties in sluice gates. Then, the validated code is used to find the energy dissipation rate for various total upstream heads and Froude numbers. The results obtained in this study are promising, indicating that the numerical model can be considered as an efficient alternative tool for hydraulic engineers to predict and understand the flow behavior in hydraulic structures.

1. INTRODUCTION

Sluice gates have been widely used for flow control and discharge measurement in irrigation and drainage channels. The formation of hydraulic jumps is a natural occurring phenomenon in flowing fluids such as water. The main characteristic is the sudden transition of rapid shallow flow to slow moving flow with rise of the fluid surface better known as a transition from supercritical to subcritical flow. The subcritical flow condition occurs when the value of Froude number is smaller than one, whereas the supercritical flow condition takes place when the value of Froude number is greater than one. However, the critical flow condition occurs when the value of Froude number is exactly equal to one (Chow, 1959). Froude number is commonly defined as the ratio of the inertia and gravitational forces.

Transition between supercritical and subcritical flow are characterized by strong dissipative mechanism, which is favorable when high kinetic energy levels is unwanted such as in spillway flows. Further characteristics of hydraulic jumps are the development of the large-scale highly turbulent zone known as the "roller" where surface waves and spray, energy dissipation and air entrapment is present (Chanson,2004).

Figure (1) presents the most common parameters needed in describing the flow in sluice gates.

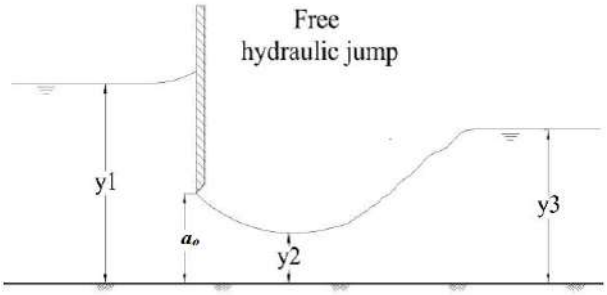

Figure (1): Schematic diagram showing the most important flow parameters passing sluice gates

Following a streamline for frictionless, incompressible and steady flow the Bernoulli equation states that:

$$\frac{v^2}{2g} + \frac{P}{\rho g} + Z = \text{constant} \quad (1)$$

where, v, P, g, Z and ρ are the mean flow velocity, pressure, gravitational acceleration and water density respectively.

For the horizontal and frictionless case depicted in the above figure, the Bernoulli equation can be written as:

$$y_1 + \frac{v_1^2}{2g} = y_2 + \frac{v_2^2}{2g} \quad (2)$$

Applying the principles of continuity, the flow rate per unit width of the channel q must be the same at positions 1 and 2, yielding:

$$q = y_1 v_1 = y_2 v_2 \quad (3)$$

As stated above the hydraulic jump is characterized by a supercritical and a subcritical region where the depths are significantly different. These depths and are referred to as conjugate depths and can be seen in the schematic diagram of Figure 1.

Substituting eq. (2) into eq. (3) and after some manipulations a relationship between the unit flow rate q and the depths y_1 and y_2 can be obtained as:

$$q = C\sqrt{2gy_1} \quad (4)$$

where,

$$C = \frac{y_2}{\sqrt{1+\frac{y_2}{y_1}}} \quad (5)$$

The flow depth at position 2, y_2, can be approximated by:

$$y_2 = C_c a_o \quad (6)$$

where, C_c is the vena contraction coefficient and a_o is the gate opening.

that the most important factors affecting the value of C_c are the total upstream head, sharpness of the gate and the gate opening. However, the same author recommended 0.57 as the average value for the design of hydraulic structures. On the other hand, Henderson (1966) pointed out that the value of C_c is 0.61 for this kind of hydraulic structure. Based on these facts and since that the shape and dimension of the gate used in the current work are kept unchanged for all values of the total upstream head, hence its effect on the value of C_c can be neglected. Following Chanson (2004) the value of C_c is taken as 0.57 in the current work to determine the theoretical value of y_2 for the sake of comparison with the corresponding numerical value for various total upstream heads.

A dimensionless relation between the conjugate depths can easily be derived from continuity, momentum and energy equations for a rectangular channel. Here is assumed hydrostatic pressure distribution and uniform velocity distribution at the up- and downstream end of the control volume. Further, the friction between the bottom and the fluid is assumed to be zero. With these assumptions the conservation equations yield the dimensionless relation between the conjugate depths for a rectangular channel as,

$$\frac{y_3}{y_2} = \frac{1}{2}\left(\sqrt{1 + 8F_{r2}^2} - 1\right) \quad (7)$$

where, F_{r2} is the Froude number upstream of the jump, $F_{r2} = v_2/\sqrt{gy_2}$, which by definition must be greater than one. The upstream Froude number is also used as an indicator of the general characteristics of the jump in a rectangular horizontal channel as different upstream Froude numbers produce different hydraulic jumps (Henderson, 1966).

The importance of the practical implications of sluice gates has drawn the attention of hydraulic researchers to investigate the hydraulics of flow passing under this kind of hydraulic structure. Numerous experimental studies have been conducted to study the hydraulics of flow under sluice gates. While, only few studies are available in the literature concerning the role of numerical approach in identifying the flow characteristics in this type of hydraulic structures. These numerical simulations were conducted using the grid based methods like finite volume and finite difference which may suffer from different numerical difficulties most importantly are the mesh deformation and mesh generation (Liu and Liu, 2003). Khanpour M. et al. (2015) applied the numerical SPH method to characterize the flow field variables downstream of a sluice gate. They developed an innovative method and introduced it to the SPH method to impose the open boundary condition to get the constant inlet discharge. However, in the present work the concept of upstream tank is adopted to simulate the flow behaviour downstream of sluice gates. This technique, which is well-known as semi boundary condition, was initially used by Ferrari (2010) and Husain et al. (2014) to simulate the flow over sharp crested weirs and stepped spillways respectively. This technique allows us to detect the flow properties passing the sluice gate for different total upstream heights at different time by fixing the water depth at the tank which decreases with time. The main objective of this research is to find the efficiency of SPH method as a numerical particle based approach in simulating and predicting the flow properties under sluice gates. Also, it looks at the flow characteristics of the hydraulic jump that would be taken place downstream of the gate. The characteristics include the conjugate depths for various Froude numbers and total heads upstream of the gate. To achieve these, the numerical 2D SPHysics code, as an implementation of the SPH method will be applied.

2. MATERIALS AND METHODS

This section is concentrated on the theory of the SPH method applied in this study. Also, it demonstrates the main features and presents the numerical tools which have been provided by the computational 2D SPHysics code adopted in this study.

2.1 Numerical Smoothed Particle Hydrodynamics Method

SPH is a particle based method initially developed by Lucy (1977) and Gingold and Monaghan (1977) in the field of astrophysics. Since its first application to the simulation of free surface flows by Monaghan (1992), numerous efforts have been made to increase the stability and accuracy of SPH computational results. Over the past two decades this method has been applied with promising outcomes in various free surface flow problems, such as flow in open channels (Lopez and Marivela, 2009; Lopez et al., 2009; Lopez et al., 2010; Federico et al. 2010; Husain, 2013; Husain et al.; 2014, Taban, 2016) and flow over hydraulic structures (Gatti et al., 2007; Lopez et al. 2009b; Ferrari, 2010). In addition, this method has gained considerable interest from industry, for instance Violeau et al. (2007); Violeau (2008) and Lee et al. (2010) for solving a range of difficult problems where the gird-based methods have great difficulty, such as mesh generation for complex geometries and non-linear large deformations (Liu & Liu, 2003).

SPH method is a purely mesh free, Lagrangian and adaptive particle method, in which a set of particles is used to represent the state of a system. Conservation equations can be applied on these particles, which carry fluid properties, and they move accordingly (Liu & Liu, 2003). The approximate expression of the integral interpolant of any function $A(r)$ at any position r located in the space Ω may be written as:

$$A(r) \approx \int_{\Omega} A(r')W(r-r',h)dr' \quad (8)$$

where $W(r-r',h)$ is the kernel function and h is the smoothing length defining the influence area of the kernel function. The value of the smoothing length is commonly taken as 1.3 of the initial distance between the particles.

Equation (8) can be written in the discretized form to estimate a flow field at a desired point, a, using the following summation equation that is carried out over all of the neighboring particles located within its influence area:

$$A(r_a) = \sum_b A_b V_b W(r_a - r_b, h) \quad (9)$$

where the subscript, b, refers to all of the particles residing the desired particle within an area of a circular shape, in 2D fluid flow simulations, of radius characterized by the smoothing length times a scaling factor, kh, known as the compact support of the kernel function, V_b is the volume of that particle and A_b is the value of the function at position r_b. Figure (2) illustrates the influence area of a given particle, a, and the neighboring particles represented by, b, located inside this area.

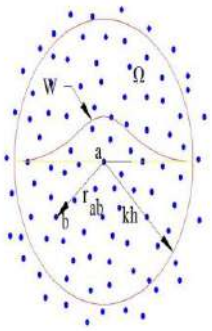

Figure (2). Support domain of particle, a, and its neighboring particles, b, inside a circular area in 2D

The volume V_b can be expressed as the relationship between the mass m_b and mass density ρ_b as follows:

$$V_b = \frac{m_b}{\rho_b} \quad (10)$$

Substituting equation (9) into equation (8) yields:

$$A(r_a) = \sum_b A_b \frac{m_b}{\rho_b} W(r_a - r_b, h) \quad (11)$$

The above equation can be considered as the basic expression of the SPH method which approximates a continuous vectorial or scalar field function.

2.2 Computational 2D SPHysics Code

Since the invention of the smoothed particle hydrodynamics method, many codes have been developed to simulate fluid flow problems. The SPHysics code as an implementation of the SPH method is applied in the current work. It is an open source code which has been developed, and is still under development, via the collaboration of four international institutions: The Johns Hopkins University (USA), Universidade de Vigo (Spain), University of Manchester (UK) and University of Rome, La Sapienza (Italy). This code solves the Naiver-Stokes equations based on the formulations presented in Monaghan (1992) for simulating free surface flows of weakly compressible fluids (Gómez-Gesteira *et al*. 2012). In addition, it implements various techniques which have recently been proposed to improve some numerical issues such as consistency, accuracy and stability. The governing equations and the techniques employed by the SPHysics code are presented below.

The mass and momentum conservation equations in SPH discrete notation are respectively:

$$\frac{d\rho_a}{dt} = \sum_b m_b v_{ab} \nabla_a W_{ab} \quad (12)$$

$$\frac{dv_a}{dt} = -\sum_b m_b \left(\frac{P_a}{\rho_a^2} + \frac{P_b}{\rho_b^2} + \frac{\tau_a}{\rho_a^2} + \frac{\tau_b}{\rho_b^2}\right) \nabla_a W_{ab} + \sum_b m_b \left(\frac{4\nu_o r_{ab} \nabla_a W_{ab}}{(\rho_a + \rho_b)|r_{ab}|^2}\right) v_{ab} + g \quad (13)$$

where ρ, m, v, W, P, τ, ν_o, r and g are the density, velocity, mass, kernel smoothing function, pressure, shear stress, kinetic viscosity of laminar flow, distance between two interactive particles and gravitational acceleration respectively.

Since the flow through most of hydraulic structures is extremely turbulent, the laminar viscosity and sub-particle scale turbulence method SPS is

therefore used in the current work to consider the effect of the turbulent flow field on the numerical results. This method was developed by Dalrymple and Rogers (2006) to introduce the effect of viscosity into the momentum equation. Also, the XSPH variant method (Monaghan, 1989) is adopted to prevent particle penetration through the rigid boundaries as follows:

$$\frac{dr_a}{dt} = v_a + \varepsilon \sum_b \frac{m_b}{\bar{\rho}_{ab}} v_{ab} W_{ab} \quad (14)$$

where ε is a constant ($0 \leq \varepsilon \leq 1$) with a common value of 0.5 and $\bar{\rho}_{ab} = \frac{1}{2}(\rho_a + \rho_b)$.

Equation (14) updates the value of the velocity at the particle under consideration based on the surrounding particles located inside its influence area (Gómez-Gesteira et al. 2012).

As mentioned earlier the SPH model applied in this study considers the fluid to behave as weakly compressible. This significantly reduces the computation time as the pressure term appearing in Equation (13) can be solved explicitly using an equation of state instead of solving a differential equation such as Poisson's equation (Gómez-Gesteira *et al.* 2012). Batchelor (1974) and Monaghan and Kos (1999) modified the equation of state by assuming the pressure-density relationship as:

$$P = B\left[\left(\frac{\rho}{\rho_o}\right)^{\gamma} - 1\right] \quad (15)$$

where P is the pressure, ρ_o is the reference fluid density (for water ρ_o= 1000 kg/m^3), γ is the polytrophic constant and B is the bulk modulus elasticity of the fluid defined by:

$$B = \frac{c_o^2 \rho_o}{\gamma} \quad (16)$$

where c_o is the speed of sound defined in terms of the reference density which may be found from:

$$c_o^2 = c^2(\rho) = \frac{\partial P}{\partial \rho}\Big|\rho_o = \frac{B\gamma}{\rho_o}\left(\frac{\rho}{\rho_o}\right)^{\gamma-1}\Big|\rho_o \quad (17)$$

$$c_o^2 = \frac{B\gamma}{\rho_o} \quad (18)$$

It should be noted here that using the actual physical value of sound speed yields exceedingly small time steps and consequently high computational time. To overcome this problem the SPHysics code utilizes an artificial sound speed based on the maximum velocity of the fluid particles. Monaghan (1994) documented that the Mach number should not exceed 0.1, which requires the minimum value for the speed of sound be 10 times greater than the largest velocity scales in the flow. This may keep the variation of the relative density, (ρ/ρ_o) appearing inside the state equation to within nearly 1% and consequently the compressibility effects may reasonably be neglected. In the present study the value of the artificial sound speed for each test case is used based on the maximum expected fluid velocity.

Different kernel functions are available in the literature to carry out the numerical computations. The Spline function is commonly used to simulate free surface problems which can be defined from the following equation:

$$W(r,h) = \alpha_D \begin{cases} 1 - \frac{3}{2}q^2 + \frac{3}{4}q^3, & 0 \leq q \leq 1 \\ \frac{1}{4}(2-q)^3, & 1 \leq q \leq 2 \\ 0, & q \geq 2 \end{cases} \quad (19)$$

where,

$$\alpha_D = \begin{cases} \frac{10}{(7\pi h^2)} & in\ 2D \\ \frac{1}{(\pi h^3)} & in\ 3D \end{cases} \quad (20)$$

In which h is the smoothing length and q is the dimensionless distance between the particles defined by:

$$q = \frac{r}{h} \quad (21)$$

where r is the distance between the particle under consideration and others located within its compact support.

Differential equations appearing in the governing equations of any numerical modelling method need to be integrated numerically with respect to time. Since these equations in a particle based method are ordinary, they can be integrated in a more straightforward way than grid based methods. However, Gómez-Gesteira *et al.* (2010) recommended that the accuracy of the time scheme used in particle methods should be no less than the second order. The Verlet scheme is a second order time integrator, which has been commonly used in many particle based numerical simulations, is implemented in the SPHysics code. The Verlet time integrator scheme is therefore adopted in the current study. Moreover, the variable time step technique is activated in this study which periodically updates the value of the time step based on the minimum time step value provided by the forcing terms and the combined effects of the viscous diffusion term and the CFL number, (Monaghan and Kos, 1999).

In the present work the linked list technique is utilized to search for the fluid particles residing within each particle's influence area. This procedure is performed at each time step to update particle positions and the flow field functions they carry. The reader is referred to (Monaghan and Lattanzio, 1985) for further details.

It should be noted that since the fluid is treated as weakly compressible by the SPHysics code, high pressure fluctuations may be observed with the standard SPH formulations even with a slight variation of the fluid density. Numerous efforts have been made to remove these fluctuations in the pressure field in the SPH scheme and different methods have been proposed such as Shepard, moving least squares and Riemann solver. In the present work the non-conservative Riemann technique employed by the SPHysics code is applied. This approach was initially proposed by Parshikov (1999) and later by Cha and Whitworth (2003) as the Godunov Particle Hydrodynamics method, or GPH.

Particles close to the solid boundaries and interface may produce instabilities in the numerical solution as the compactness condition may not be satisfied. Two techniques are implemented in the SPHysics code to overcome this issue; namely: kernel correction and kernel gradient correction. In the present study the kernel correction method is used. This method is used by Bonet and Lok (1999) to periodically correct the kernel function in such a way that the exact interpolation up to a given degree has to be achieved.

SPHysics code provides two techniques to model solid boundaries: dynamic (Dalrymple and Kino, 2000, Crespo *et al.*, 2007); and repulsive boundary conditions (Monaghan, 1994). The authors observed a number of fluid particles penetrating solid walls when the dynamic boundary condition is applied. Therefore, the repulsive boundary condition is used in the present study. In the case of immobile walls this approach generates one layer of equally spaced boundary particles with zero pressure and velocity. The repulsion mechanism of this technique is based on prescribed boundary forces exerted by boundary particles in the normal direction. The reader is referred to Monaghan and Kos (1999) and Rogers and Dalrymple (2008) for more details.

It is also worth mentioning that the Lagrangian property of the SPH numerical method applied in the present study allows us to estimate the mean velocity and free surface elevations at desired points from a number of successive output files, for instance 3-5 output files.

3. RESULTS & DISCUSSION

Researchers have compared their numerical results with either the experimental observations and/or analytical results to examine the performance of the applied numerical code in predicting the physical quantities of their studies. In the present investigation the 2D SPHysics code is applied to simulate the characteristics of flow under sluice gates. In order to have confidence in the numerical SPHysics model it is important to validate it against the existing published data. To accomplish this, the results of a previously published experimental model for the flow in sluice gates are considered to evaluate the computational results obtained in this study, namely the experimental work of Lopez et al. (2010) for flow under a sluice gate.

Lopez et al. (2010) conducted their experiments to characterize the flow properties down of a sluice gate. The experimental work was performed in a horizontal and rectangular laboratory flume of 12m length, 0.6m width and 1.0m height. The gate was placed at a distance of 1.2m from the flume inlet. The gate had a sharp upstream edge, thickness = 0.03m, height = 0.30m and width matching the entire flume width. To accelerate the jump formation Lopez et al. (2010) placed a broad crested weir at the end of the flume of length 0.2m and height as the same as the gate opening. Figure (3) demonstrates the initial condition for the flow under a sluice gate physical model tested experimentally by Lopez et al. (2010). It is worth mentioning here that in the current work the concept upstream tank is used to represent the fluid particles stored at the upstream and to detect the flow field variables in the flow domain. Although this approach significantly increases the computational time it is used with successful outcomes in a number of free- surface fluid flow cases, namely; Ferrari (2010) for simulating the flow over sharp crested weirs; Husain (2013) Husain et al. (2014) for the flow over broad crested weirs and stepped spillways and Taban (2016) for the flow over stepped spillways.

Normally, the flow condition upstream of sluice gates is subcritical as the flow depth is relatively high and the flow velocity is low, whereas it passes beneath the gate with high velocity with high level of turbulence and hydraulic jump may form at a distance somehow downstream of the gate, depending on the gate opening, due to the change of flow condition to the super critical condition (Chow, 1959; Henderson, 1966; Chanson, 2004).

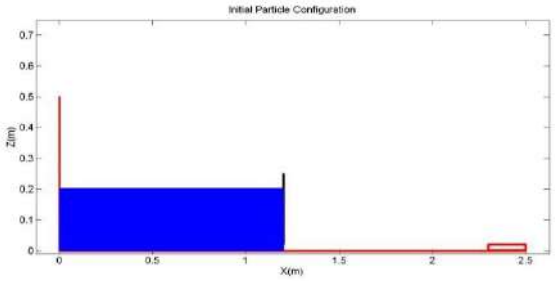

Figure (3): 2D schematic view of the experimental laboratory model used by Lopez et al. (2010) for flow under sluice gates

Figures (4.a) to (4.d) illustrate snapshots depicted by the numerical 2D SPHysics code of flow conditions for the flow under the sluice gate at different time instants. These snapshots demonstrate that the computational results provided by the code are qualitatively in good agreement with the description of flow condition while passing the gate. This indicates that the numerical SPHysics code well captures the physical behavior of the flow under such hydraulic configuration.

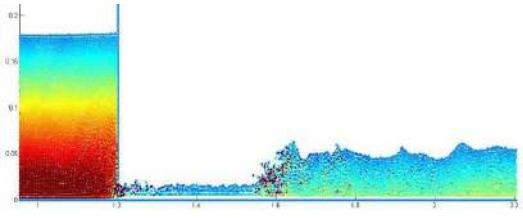

a

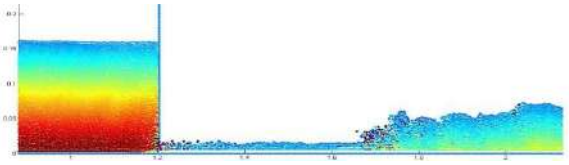

b

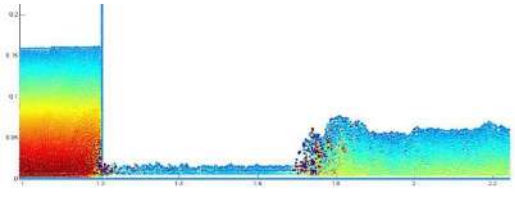

c

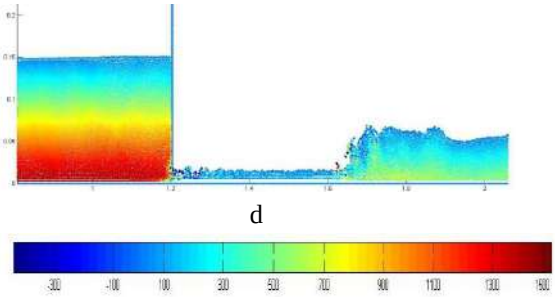

d

Figure (4): Snapshots of free surface profile at: (a) t=0.4s, (b) t=0.55s, (c) t=1.35s and (d) t=4.9s of flow under the sluice gate predicted by the SPHysics code with pressure color-code

Now the quantities of the flow field variables predicted by the numerical SPHysics code will be presented and compared with the experimental and theoretical data. This includes the position of the conjugate depths of the hydraulic jump for various Froude numbers.

Table (1) shows the comparison between the theoretical values of the of the flow depths and flow velocities before *y2theo,V2theo* and after the jump *y3theo, V3theo* and the corresponding ones of the computational results of this work obtained from numerical SPHysics code for different total upstream heads *y1*. The theoretical values of the flow depths are estimated from using equations 6 and 7 respectively, while the continuity equation, equation 8, is used to calculate the theoretical values of the flow velocities before and after the jump.

However, as mentioned earlier in this investigation the position of the highest particle in a given section is taken as the computational flow depth at that section. Also, the mean velocity of the velocity profile in a given section is considered as the flow velocity at that section. As can be observed the agreement between the theoretical and computational flow depths and velocities is fairly good for all total upstream head values tested in this work as the differences between them are relatively small.

Table (1): Comparison between theoretical and numerical values of flow depths and velocities before and after the jump for various total upstream heads

y1	*y2 theo*	*y2 SPHysics*	*V2 theo*	*V2 SPHysics*	*y3 theo*	*y3 SPhysics*	*V3 theo*	*V3 SPHysics*
0.174	0.0114	0.0118	1.870	1.595	0.0846	0.0562	0.2520	0.3266
0.165	0.0114	0.0115	1.815	1.483	0.0820	0.0546	0.2523	0.3057
0.155	0.0114	0.0112	1.760	1.474	0.0793	0.0653	0.2530	0.2453
0.146	0.0114	0.0110	1.698	1.352	0.0764	0.0637	0.2534	0.2288

Figure (5) presents the velocity flow field predicted by the SPHysics code at the time instants measured experimentally by Lopez et al. (2010).

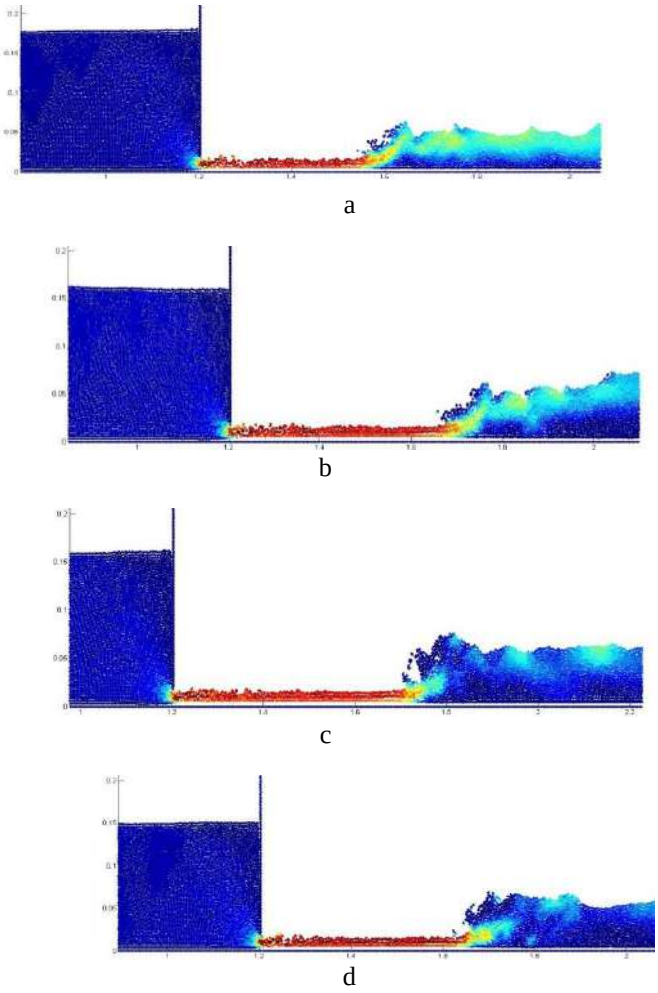

Figure (5): Snapshots of flow velocity at: (a) t=0.4s, (b) t=0.55s, (c) t=1.35s and (d) t=4.9s of flow under the sluice gate predicted by the SPHysics code with color-coded horizontal velocities

Table (2) presents the comparison between the experimental values recorded by Lopez et al. (2010) and the computational results obtained in this study in terms of the flow depths and velocities for various total upstream heads tested in the current work. The flow depths were experimentally measured by Lopez et al. (2010) using digital point gauges and the flow velocities were measured by an advanced pitot tube. It is clear from this Table that the computational results obtained in this study are close to the corresponding experimental values revealing the capability of the SPHysics code as an implementation of the SPH method to efficiently simulate and estimate the flow under sluice gates.

The following section presents and discusses the effect of various flow parameters on the energy dissipation for the flow under sluice gates. These include the relative ratio of gate opening with respect to the total upstream head and Froude number. Also, focuses on the variation of the position of free surface with the Froude number values tested in this study.

Figure (6) is the plot of the variation of the relative gate opening with respect to the total upstream head *y1/ao* with the percentage of the

amount of energy dissipation through the jump *100(E2-E3)/E2* caused by the sluice gate. In this figure *y1* is the total upstream head, *ao* is the gate opening, which is fixed to 0.02m through the whole work of this project, *E2* and *E3* are the energy upstream and downstream of the jump. As it can be seen from this figure the energy dissipation increases as the relative ratio of the gate opening is increased. This indicates that the energy dissipation rate is high when the total head of water stored upstream of the sluice gate is high. This can be attributed to the effect of the flow turbulence, which is considered to have significant role on the energy dissipation in hydraulic structures (Chanson, 2004), which may be increased as the upstream head is high.

Table (2): Comparison between the experimental and numerical values of flow depths and velocities before and after the jump for various total upstream heads

y1	*y2 exp.*	*y2 SPHysics*	*V2 exp.*	*V2 SPHysics*	*y3 exp.*	*y3 SPhysics*	*V3 exp.*	*V3 SPHysics*
0.174	0.0120	0.0118	1.614	1.595	0.0573	0.0562	0.3371	0.3266
0.165	0.0117	0.0115	1.506	1.483	0.0552	0.0546	0.3165	0.3057
0.155	0.0113	0.0112	1.494	1.474	0.0661	0.0653	0.2609	0.2453
0.146	0.0111	0.0110	1.375	1.352	0.0642	0.0637	0.2451	0.2288

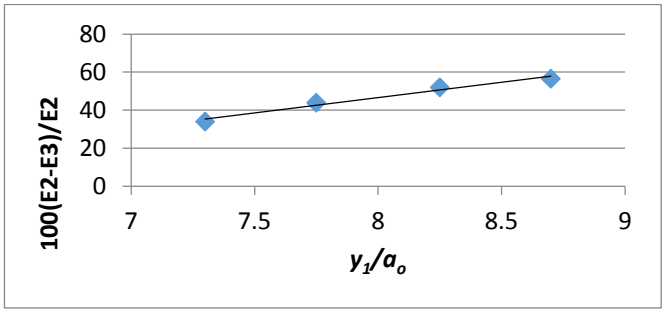

Figure (6): Variation of energy dissipation rate with the relative gate opening with respect to the total upstream head

Variation of the percentage of the energy dissipation *100(E2-E3)/E2* with Froude number due to the pre-jump flow depth *Fr2* is plotted in Figure (7). One can notice that the energy dissipation increases as the Froude number is increased. The increase of the Froude number is associated with the increase of the total head of water stored upstream of the sluice gate.

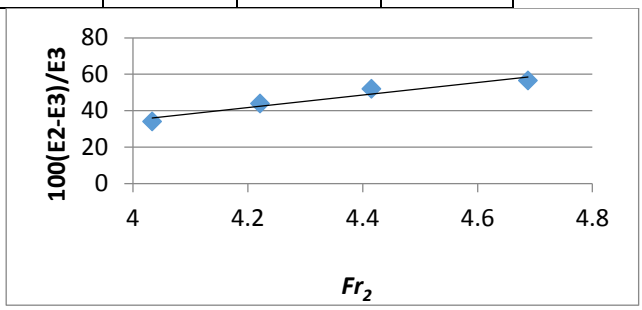

Figure (7): Variation of energy dissipation rate with the pre-jump Froude number

In Figure (8) the variation of pre-jump Froude number Fr2 is plotted versus the percentage of the height of the hydraulic jump *Hj*, which can be defined as relative of the difference between the conjugate depths (Hj= 100(y3-y2)/y3 to the flow depth after the jump. This figure shows that the height of the hydraulic jump increases with the decrease of the Froude number.

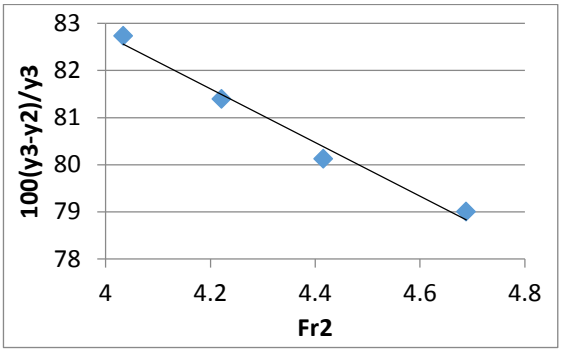

Figure (8): Variation of relative hydraulic jump height with the pre-jump Froude number

4. CONCLUSION

The upstream tank approach is adopted in this study to examine the capability of the numerical 2D SPHysics code, as an implementation of the Smoothed Particle Hydrodynamic method, in detecting the flow field variables in sluice gates qualitatively and quantitatively. Also, the effect of flow parameters such as upstream flow depth, gate opening and Froude number on the amount of energy dissipation downstream of the gate is investigated. For the sake of validating the numerical code, the results obtained in this study are compared with the theoretical as well as the experimental results gathered in this type of hydraulic structure. The results produced by the numerical code are in close agreement with the corresponding theoretical and experimental results. Also, it is observed that the differences between them are insignificant for different total heads upstream of the gate. This is an indication that the computational code is efficient in predicting the flow properties in free surface flow problems. It is also found that the percentage of the total amount of energy dissipation may increase linearly with the increase of the ratio of the flow depth to the gate opening and Froude number. Conversely, the jump length could decrease linearly with the increase of the increase of the Froude number. Despite the fact that the numerical code applied in this study is performed well in simulating the flow in sluice gates, it is still needed to be applied in other free-surface flow problems to prove its validity.

REFERENCES

Batchelor, G., K. (1974). Introduction to fluid mechanics, UK, Cambridge University press.

Bonet, J. and Lok, T. S. (1999). Variational and momentum preservation aspects of Smooth Particle Hydrodynamics. Journal of Computer Methods in Applied Mechanics and Engineering, 180 (1), 97-115.

Cha, S.-H., and Whitworth, A. P. (2003). Implementations and tests of Godunov-particle hydrodynamics, Mon. Not. R. Astro. Soc., 340, 73-90.

Chanson, H. (2004). The hydraulics of open channel flow: an introduction, 2nd edition, Oxford, UK, Butterworth-Heinemann.

Chow, V., T. (1959). Open channel hydraulics, New York, USA, McGraw-Hill.

Crespo, A. J .C., Gómez-Gesteira, M and Dalrymple, R. A. (2007). Boundary conditions generated by dynamic particles in SPH methods. Journal of Computers, Materials and Continua, 5(3), 173-184.

Dalrymple, R. A. and Kino, O. (2000). SPH modelling of water waves. Proc. Coastal Dynamics, Lund.

Dalrymple, R. A. and Rogers, B. D. (2006). Numerical modelling of water waves with SPH method. Journal of Coastal Engineering , 53(2-3), 141-147.

Federico, I., Marrone, S., Colagrossi, A., Aristodemo, F. and Veltri, P. (2010). Simulating free-surface channel flows through SPH. In Proc. 5th International SPHERIC Workshop, Manchester, UK.

Ferrari, A. (2010). SPH simulation of free surface flow over a sharp crested weir. Journal of Advances in Water Resources, 33 (3), 270-276.

Gatti, D., Maffio, A., Zuccala, D. and Di Monaco, A., (2007). SPH Simulation of Hydrodynamics Problems Related To Dam Safety. 2007. 32nd Congress of IAHR, CD-ROM. Paper 2, SS09. Venice. Italy.

Gingold, R. A., and Monaghan, J. J. (1977). Smoothed particle hydrodynamics, theory and application to non-spherical stars, Mon. Not. Roy. Astr. Soc., 181, 375-389.

Gómez-Gesteira, M., Rogers, B., Dalrymple, R. A. and Crespo, A. J. C. (2010). State-of-the-art of classical SPH for free-surface flow. Journal of Hydraulic Research, 48, Extra issue, 6-27.

Gómez-Gesteira, M., Rogers, B., Dalrymple, R. A., Crespo, A. J. C., and Narayanaswamy, M., (2012). User Guide for the SPHysics Code v2.0, http://www.sphysics.org.

Husain M., Sarhang. (2013). Computational investigation of skimming flow over stepped spillways using the smoothed particle hydrodynamics method. PhD thesis, university of Swansea, Swansea, UK.

Husain, S. M., Muhammed, J. R., Karunarathna, H. U., & Reeve, D. E. (2014). Investigation of pressure variations over stepped spillways using smooth particle hydrodynamics, Advances in Water Resources, 66, 52-69.

Henderson, F. M., (1966). Open Channel Flow. New York, Macmillan Publishing Co.

Khanpour, M., Zarrati, A.R. and Kolahdoozan, M., (2014). Numerical simulation of the flow under sluice gates by SPH model. Scientia Iranica. Transaction A, Civil Engineering, 21(5), 1503.

Lee, E. S., Violeau, D., Issa, R. and Ploix, S. (2010). Application of weakly compressible and truly compressible SPH to 3-D water collapse in waterworks, Journal of Hydraulic Research, 48(extra issue), 50-60.

Liu, M. B. and Liu, G. R. (2003). Smoothed Particle Hydrodynamics-A Mesh free Particle Method, Singapore, World scientific.

Lopez, D., Marivela, R. (2009). Applications of the SPH model to the design of fishways. 33rd Congress of IAHR, Water Engineering for a Sustainable Environment (Vancouvert 9-14 de agosto de 2009). ISBN: 978- 90-78046-08-0.

Lopez, D., Marivela, R. and Garrote, L. (2009b). Calibration of SPH using prototype pressure data from the stilling basin of the Villar del Rey dam, Spain, 33rd Congress of IAHR. Water Engineering for a Sustainable Environment (Vancouvert 9-14 de agosto de 2009). ISBN: 978- 90-78046-08-0.

Lopez, D., Marivela, R. and Garrote, L. (2010). Smooth particle hydrodynamics model applied to hydraulic structures: A hydraulic jump test case, Journal of Hydraulic Research, 48, Extra Issue (2010), 142-158. ISSN: 0022-1686.

Lucy, L. B. (1977). A numerical approach to testing the fission hypothesis. The Astronomical Journal, 82(12), 1013–1924.

Monaghan, J. J. (1989). On the problem of penetration in particle methods. Journal of computational physics, 82(1), 1-15.Monaghan, J. J. 1992. Smoothed Particle Hydrodynamics, Annual Review of Astronomy and Astrophysics, 30(1), 543-574.

Monaghan, J. J. (1994). Simulating free surface flows with SPH. Journal of computational physics, 110, 399-406.

Monaghan, J. J. and Kos, A. (1999). Solitary waves on a Cretan beach. Journal of waterway, port, coastal, and ocean Engineering, 125(3), 145-154.

Monaghan, J. J., and Lattanzio, J. C. (1985). A refined particle method for astrophysical problems. Journal of Astronomy and Astrophysics, 149 (1), 135-143.

Parshikov, A. N. (1999). Application of a solution of the Riemann problem to the SPH method. Computational Mathematics and Mathematical Physics, 39, 1173.

Rogers, B. D., and Dalrymple, R. A. (2008). SPH Modelling of tsunami waves, Advances in Coastal and Ocean Engineering, Vol. 10 Advanced Numerical Models for tsunami waves and runup, World Scientific.

Taban K., Hamad (2016). Hydraulic performance evaluation of Bastora dam spillway. MSc thesis, Salahaddin university, Erbil, Iraq.

Verlet, L. (1967). Computer "experiments" on classical fluids. I. Thermodynamical properties of Lennard-Jones molecules. Journal of physical review,159(1), 98.

Violeau, D., Buvat, C., Abed-Meraiim, K. and de Nanteuil, E. (2007). Numerical modelling of boom and oil spill with SPH, Journal of Coastal Engineering, 54(12), 895-913.

Violeau, D., Issa, R., Benhamadouche, S., Saleh, K., Chorda, J. and Maubourguet, M.-M. (2008). Modelling a fish passage with SPH and Eulerian codes: The influence of turbulent closure, Proc. 3rd SPHERIC International Workshop, 3rd–6th June 2008, Lausanne, (Switzerland), 85-91.

ZANCO Journal of Pure and Applied Sciences
The official scientific journal of Salahaddin University-Erbil
ZJPAS (2018) **30**(s1)s105-s112
http://dx.doi.org/10.21271/ZJPAS.30.s1.12

Effect of Sudden Rise of Water in Stream on Adjacent Land

Abulla[1] A. Abo., Sarhang[2] M. Husain . Saud[3] A. Hussein

1, 2 Department of Dams and water resources, College of Engineering, Salahaddin University, Erbil, Kurdistan Region, Iraq

3 Assistant lecturer, Department of Road Construction, Erbil Technical Institute, Erbil Polytechnic University, Hawler, Iraq.

A R T I C L E I N F O

Article History:
Received: 14/05/2017
Accepted: 12/04/2018
Published:01/06/2018

Keywords:
Mathematical method, Embankment, water table, Darcy's equation, Porous media.

**Corresponding Author Contact Email:*
abdulla.abo@su.edu.krd

A B S T R A C T

This study uses both laboratory and mathematical models to compute water table through an embankment cross section due to sudden rise in stream flow level. The main aim for current study to proof whether a one-dimensional 1D mathematical model can capture the phreatic line through embankment. For this purpose four different identical laboratory sand homogeneous embankment models are constructed in a plywood box by using different sand particle sizes 2mm, 1mm, 0.5mm and 0.25mm to represent very coarse, coarse, medium and fine sand respectively. Experiments are conducted on each model by fixing the upstream water depth to 0.75m; in order steady state in water table prevail. The water table level is measured at different sections inside the model body at the steady state flow condition. The time required to achieve the steady state condition in each model is also recorded. For the mathematical model, the Darcy equation is solved considering the flow in one dimension through the embankment model. Then, the mathematical model is verified against the experimental and numerical results available in the literature. The comparisons show well agreement between the computed results of the mathematical model and the corresponding observed results gathered from the experimental and numerical models. The mathematical model derived in this study can be readily applied to predict water level in porous media of infinite length.

1.INTRODUCTION

The water table through adjacent land of a river is significantly influenced by the stream water depth. Structures built over such land might be affected by a sudden rise of water table elevation, which eventually may cause these structures to fail. This is because the seeping water considerably increases the uplift pressure under these structures due to the increase of water content in soil (Rushton and Redshaw 1979). Many special treatments, most importantly lining both sides of the river, are therefore required to avoid such structural failures, which increase the overall cost. Lining of rivers sometimes may not be feasible due to its cost effectiveness.

In addition, seepage through embankments rises the elevation of the phreatic line, which may result in dam failure due to sliding, piping and sloughing (Middlebrooks, 1953). Therefore, understanding the flow behavior through embankments is crucial to improve the design of such hydraulic structure, especially in terms of the elevation of phreatic line. This is because the maximum allowable wet height at the DS face of embankment dams is nearly one-third of its total height (Justin et al., 1944). This type of flow is analogue to the flow through porous media and is well known as seepage through embankments. In fact, Darcy's law is commonly used to compute the water

surface profile for such flow. This study focuses on this kind of flow to find the phreatic line in an embankment dam. Rising of water table in adjacent land of a river mainly depends on the hydraulic conductivity of soil. The hydraulic conductivity in a relatively small area varies over a broad range as it depends on a number of factors such as water viscosity, particle size, and its distribution, density of the soils, size and continuity of cracks and joins (Cedergren 1988). Also flow through porous media, its paths length and travel time depend on type of soils, stratification and meteorological (climatological) conditions (Winter et al. 2002).

Stello (1987) developed design charts to compute the elevation of the phreatic line and amount of seepage passing through homogenous and zoned dams located on an impervious foundation using a computer program known as fragment method. The study showed that the results of this method were in close agreement with previously published results with an average percent error of about 18%. (Ching 1988) analyzes computation of a phreatic line numerically using the boundary element method (BEM). The numerical model is validated against the experimental results reported by (Kellogg 1941) which is considered a benchmark. The comparison showed a maximum variation of about 10%. The impact of hydraulic conductivity and its effect on fall of phreatic surface per various discharge rates that pass through dam body are studied analytically by (Rezk et al. 2010). Comparisons indicated that the phreatic line computed in the analytical method is agreed well with the phreatic line measured in the laboratory.

In the present study, a one dimensional 1D mathematical model is derived from Darcy's law to calculate the phreatic line in homogenous embankment dam and other cases of identical conditions, and this is a limitation of current study. Also, an embankment model is constructed herein to verify the validity of the proposed equation.

1. MATHEMATICAL MODEL

The parameters required to express the flow through a typical embankment model are shown in Figure 1:

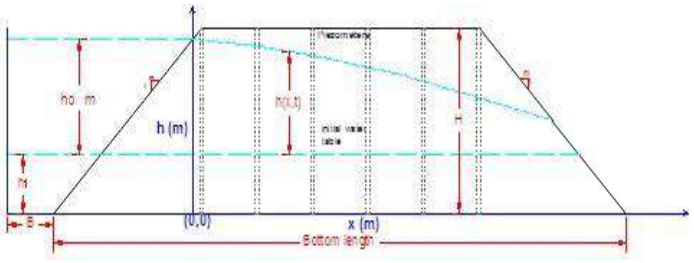

Figure 1 Typical laboratory model.

The flow through saturated porous media is governed by Darcy law:

$$V = KI \quad (1)$$

Where: V Is the velocity of flow through porous media, K is hydraulic conductivity m/s,

$I = \frac{dh}{ds}$ is hydraulic gradient, h is head of flow m, and s is distance along the flow line m.

Equation 1 can be considered only for laminar flow (Reynolds number less than 1).

$$R_e = \frac{VL}{\gamma} \quad (2)$$

Where: V Is the velocity of flow through porous media m/s, L is represents the characteristic length, γ is viscosity of water m^2/s.

Reynolds number in porous media is usually less than one. Hence, the flow through porous media can be considered laminar (Harr M. E. 1962). Darcy's law for three-dimensional flow can be expressed as:

$$u = K_x I_x = -K_x \frac{dh}{dx} \quad (3)$$

$$v = K_y I_y = -K_y \frac{dh}{dy} \quad (4)$$

$$w = K_z I_z = -K_z \frac{dh}{dz} \quad (5)$$

Where u, v, w, K_x, K_y, K_z, I_x, I_y and I_z are velocity, hydraulic conductivity and hydraulic gradient in directions x, y, and z respectively.

Applying continuity equation for incompressible flow in three dimensions yields:

$$\frac{du}{dx}+\frac{dv}{dy}+\frac{dw}{dz}=0 \quad (6)$$

$$\frac{\partial}{\partial x}\left(K_x\frac{dh}{dx}\right)+\frac{\partial}{\partial y}\left(K_y\frac{dh}{dy}\right)+\frac{\partial}{\partial x}\left(K_z\frac{dh}{dz}\right)=0 \quad (7)$$

Assuming that the soil is homogenous and isotropic produces:

$$K_x=K_y=K_z=k \quad (8)$$

Equation 7 can be re-written as below:

$$\frac{\partial^2 h}{\partial x^2}+\frac{\partial^2 h}{\partial y^2}+\frac{\partial^2 h}{\partial z^2}=0 \quad (9)$$

For unsteady state condition, equation 9 can be re-written as follows:

$$\frac{\partial^2 h}{\partial x^2}+\frac{\partial^2 h}{\partial y^2}+\frac{\partial^2 h}{\partial z^2}=\frac{1}{\gamma}\frac{dh}{dt} \quad (10)$$

And for one dimensional flow in x-direction, equation 10 is reduced to.

$$\frac{\partial^2 h}{\partial x^2}=\frac{1}{\gamma}\frac{\partial h}{\partial t} \quad (11)$$

The governing equation of unsteady (Cartesian form) flow through porous media and its boundary and initial conditions in one-dimensional can be set as below.

$$\frac{\partial^2 h}{\partial x^2}=\frac{1}{\gamma}\frac{\partial h}{\partial t} \quad (12)$$

$$h(x,0)=0 \quad (13)$$

$$h(0,t)=h_0 \quad (14)$$

$$h(\infty,t)=0 \quad (15)$$

Where: $h=h(x,t)$ is the rise in water level (Ground water head) caused by the change in stream level at an US face of the model, x-Distance from the US of the models embankment.

For unconfined aquifer $\gamma=\frac{K}{S}$ (Gelhar, L.W. and Axness, C.L., 1983) (6)

Where: γ is hydraulic diffusivity, K is hydraulic conductivity m/s, S is storage coefficient related to compressibility m^{-1}. (7)

Applying Laplace transform with respect to t for equations 12, 14, and 15, provides:

$$L\left[\frac{\partial^2 h}{\partial x^2}\right]=L\left[\frac{1}{\gamma}\frac{\partial h}{\partial t}\right]; \quad (8)$$

$$\frac{d^2\acute{h}}{dx^2}=\frac{1}{\gamma}\left[s\acute{h}-h(x,0)\right]$$

$$L[h(0,t)]=L[h_0]; \quad (16)$$

(9)

$$\acute{h}(0,s)=\frac{h_0}{s} \quad (17)$$

Where:-$L[h(x,t)]=h'(x,s)$

(10) $L[h(\infty,t)]=L[0]$

$$h\acute{}(\infty,s)=0 \quad (18)$$

Equation 16 is a second order differential equation with constant coefficients and can be solved by operator having a general solution:

(11)

$$\acute{h}(x,s)=c_1e^{-x\sqrt{s/\gamma}}+c_2e^{x\sqrt{s/\gamma}} \quad (19)$$

Where; $L[h(x,t)]=\acute{h}(x,s)$ (12)

By applying boundary and initial conditions, particular solution for equation (19) can be obtained by firstly, applying boundary condition (14) in equation (15). Firstly, applying initial (18) in equation (19)

(13)

(14)

yields:

(15)

$$h\acute{}(\infty,s)=c_1e^{-\infty}+c_2e^{\infty}=0$$

$0+c_2e^{\infty}=0$, but e^{∞} not equal to zero, so $c_2=0$

Then equation (19) can be re-written as follows:

$$\acute{h}(x,s) = c_1 e^{-x\sqrt{s/\gamma}} \quad (20)$$

Secondly, applying boundary condition (17) in equation (20)

$$\acute{h}(0,s) = \frac{h_0}{s} = c_1 e^0, \quad c_1 = \frac{h_0}{s}$$

so equation (9) can be re-written as follow:

$$\acute{h}(x,s) = \frac{h_0}{s} e^{-x\sqrt{s/\gamma}} \quad (21)$$

Now the inverse Laplace transform for equation (21) is:

$$L^{-}\left[h'(x,s)\right] = h_0 L^{-}\left[\frac{e^{-x\sqrt{s/\gamma}}}{s}\right]$$

$$h(x,t) = h_0 erfc\left(\frac{x}{\sqrt{4\gamma t}}\right) \quad (22)$$

Where: $erfc$ is complimentary error function which is expressed as below:

$$erfc\ \ (x) = 1 - erf(x) \quad (23)$$

So equation 11 can be re-written:

$$h(x,t) = h_0\left[1 - erf\left(\frac{x}{\sqrt{4\gamma t}}\right)\right] \quad (24)$$

Equation 24 defines the one dimensional phreatic line level along an embankment dam model.

2. MATHEMATICAL MODEL VALIDATION

Equation 24 obtained in section 2 is validated against the experimental data gathered from laboratory models of the current study and a homogenous laboratory dam of Kellogg (1941). The experimental data of Kellogg (1941) were collected on a physical dam of 38 cm high, 68 cm bottom width and identical US and DS side slopes of 1H:1.3V. The dam was constructed from coarse sand of hydraulic conductivity 0.1 cm/s (1*10-3 m/s). This dam configuration is also studied by Ching (1988) numerically using boundary element method (BEM). Figure 2 illustrates schematic diagram of the dam model constructed by Kellogg (1941).

Table 1 presents the results provided by the mathematical model of equation 24, those measured by Kellogg (1941) and those predicted by Ching (1988) in terms of the total head at different stations. The percentage of error due to the difference in results obtained from the experimental and mathematical models (column 5) and the numerical and mathematical models (column 6) for each station is also calculated and shown in Table1. These results are also plotted in Figure 3.

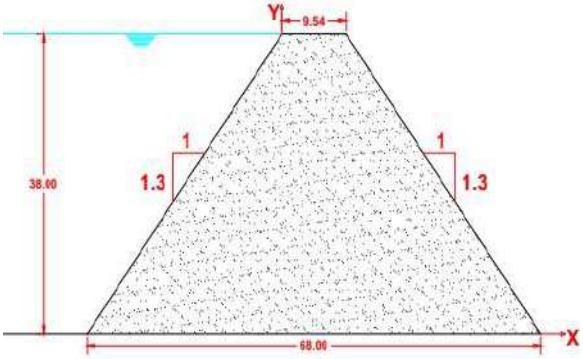

Figure 2 Typical laboratory dam (Kellogg 1941).

From Table 1 and Figure 3 it is clear the results provided by the mathematical model are closer than those computed by the numerical BEM model.

Table 1 Variation in phreatic line height between mathematical and laboratory results of (Kellogg 1941).

Station (x) cm	Total head cm			Error %	Error %
	Exp. Result Kellogg (1941)	Math. result	Ching (1988)		
0.0	38.0	38.0	37.39	0.0	1.6
7.0	34.64	33.97	34.64	1.9	0.0
20.0	27.42	26.79	24.62	2.3	10.2
31.0	21.72	21.13	22.74	2.7	4.7
35.0	20.09	19.63	20.83	2.3	3.8
44.0	15.39	15.31	16.16	0.5	5.0
48.0	14.24	13.76	14.24	3.4	0.0
61.0	9.15	9.39	8.38	2.6	8.4

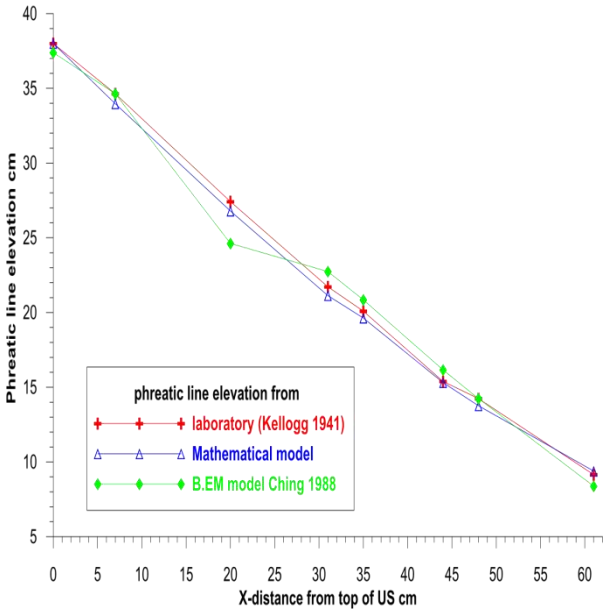

Figure 3 Phreatic line computed mathematically, conducted experimentally by (Kellogg 1941) and computed numerically by (Ching 1988).

3. RESULTS AND DISCUSSION

In this study experiments are conducted on an embankment dam to verify the validity of equation 24. The embankment was initially set horizontally in a plywood box as shown in Figure 4.

The shape of embankment is trapezoidal having dimensions of top width 1.5 m, base width 3.1 m, width 0.5 m, height 0.8 m and DS and US slopes of 1:1. The model is provided with two channels fixed at US and DS having vertical sidewalls and bed width of 0.25 m.

Figure 4 Typical laboratory model.

For different types of soil are prepared according to the particle size distribution determined from sieving procedure. The properties of soil types examined in this study including particle size, hydraulic conductivity and storage coefficient are determined following Domenico and Schwartz (1990) and Morris and Jonhson (1967) as shown in Table 2

Table 2 Particle size limits, hydraulic conductivity and storage coefficients For soil types used in this study.

Station (x) cm	Total head cm			Error %	Error %
	Exp. Result Kellogg (1941)	Math. result	Ching (1988)		
0.0	38.0	38.0	37.39	0.0	1.6
7.0	34.64	33.97	34.64	1.9	0.0
20.0	27.42	26.79	24.62	1.3	10.2
31.0	21.72	21.13	22.74	2,7	4.7
35.0	20.09	19.63	20.83	2.3	3,8
44.0	15.39	15.31	16.16	0.5	5.0
48.0	14.24	13.76	14.24	3.4	0.0
61.0	9.15	9.39	8.38	2.6	8.4

Six artificial screened piezometers are fixed at distances 0.05, 0.35, 0.65, 0.95, 1.25 and 1.55 m measured from the heel of the dam model.

Initially the water table through the embankment is maintained to 0.25 m by providing the water level at both sides of the model 0.25 m and kept constant until the water level reach constant at both sides channel and this is made by blocking the end sides of the model with 0.25 m height plywood.

Then suddenly the water level in the upstream is raised to 0.75 m and maintained constant until the water height in piezometers reach constant. Once the water level in the piezometers gets stable the height of water in piezometers are recorded by using a bar of circular cross-section with diameter 5 mm and length 1 m. Table 3 shows the water level in each of the six piezometers fixed at the distance mentioned above for the four type soils tested in this study. The time required to reach constant water level of each piezometer is also presented in Table 3.

Table 3 Experimental results phreatic line depth.

Models	water level at different stations						
	X=0	X=0.05	X=0.35	X=0.65	X=0.95	X=1.25	X=1.55
Very coarse sand	R equired time for water table reach constant 98 seconds						
	0.75	0.731	0.615	0.525	0.452	0.373	0.334
Coarse sand	R equired time for water table reach constant 212 sec nds						
	0.75	0.734	0.641	0.551	0.475	0.399	0.351
Medium sand	e quired time for water table reach constant 1440 sec nds						
	0.75	0.74	0.662	0.573	0.502	0.426	0.382
Fine sand	e quired time for water table reach constant 4020 sec nds						
	0.75	0.742	0.665	0.615	0.535	0.472	0.421

The mathematical model represented by equation 24 is applied to the same embankment model

constructed in the present work to determine the water level in the model at the same positions where it measured experimentally. The results of the mathematical model are tabulated in Table 4.

Table 4 Explain detail of mathematical model.

Models	water level at different stations						
	X=0	X=0.05	X=0.35	X=0.65	X=0.95	X=1.25	X=1.55
Very coarse sand	Required time for water table reach constant 98 seconds						
	0.75	0.73	0.62	0.525	0.445	0.375	0.33
Coarse sand	Required time for water table reach constant 212 seconds						
	0.75	0.733	0.64	0.545	0.47	0.4	0.35
Medium sand	Required time for water table reach constant 1440 seconds						
	0.75	0.733	0.65	0.57	0.495	0.43	0.375
Fine sand	Required time for water table reach constant 4020 seconds						
	0.75	0.74	0.66	0.59	0.52	0.46	0.41

Table 5 presents the percentage error calculated as a result from the difference between the experimental results measured from each model of this study and the mathematical results at different stations. One can observe that the mathematical model adequately predicted the water level in the piezometers fixed within the embankment model.

Also for each model the mathematical and experimental results are drawn in a Figures 5,6,7 and

8. These figures clearly show that the agreement between these results is fairly good.

Table 5 Comparison between experimental and mathematical results of the phreatic line for different soil types.

		Very coarse sand	
Stations (m)	**Experiment result (Exp. R.)**	**Analytical result (Ana. R.)**	$Error\%$
0.00	0.5	0.5	0
0.05	0.481	0.48	0.21
0.35	0.365	0.37	1.37
0.65	0.275	0.275	0
0.95	0.199	0.195	2.01
1.25	0.123	0.125	1.63
1.55	0.081	0.08	1.23
		Coarse sand	
0.00	0.5	0.5	0
0.05	0.484	0.483	0.21
0.35	0.391	0.39	0.26
0.65	0.301	0.295	1.99
0.95	0.225	0.22	2.22
1.25	0.149	0.15	0.67
1.55	0.101	0.1	0.99
		Medium sand	
0.00	0.5	0.5	0
0.05	0.490	0.483	1.43
0.35	0.412	0.4	2.91
0.65	0.323	0.32	0.93
0.95	0.252	0.245	2.78
1.25	0.176	0.18	2.27
1.55	0.128	0.125	2.34
		Fine sand	
0.00	0.5	0.5	0
0.05	0.492	0.49	0.41
0.35	0.415	0.41	1.20
0.65	0.348	0.34	2.3
0.95	0.278	0.27	2.88
1.25	0.215	0.21	2.32
1.55	0.164	0.16	2.44

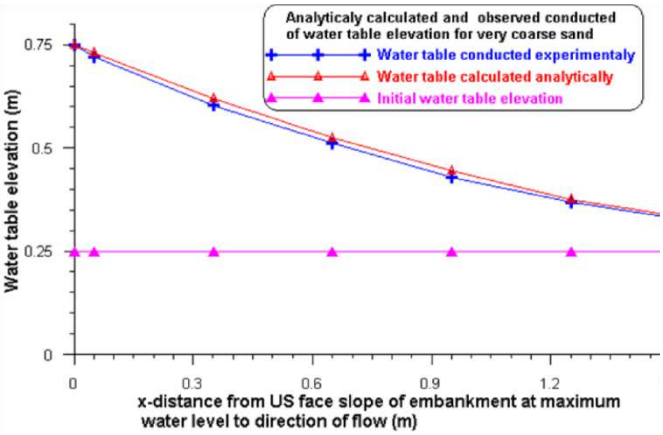

Figure 5 Phreatic line profile computed mathematically and obtained Experimentally for very coarse sand embankment.

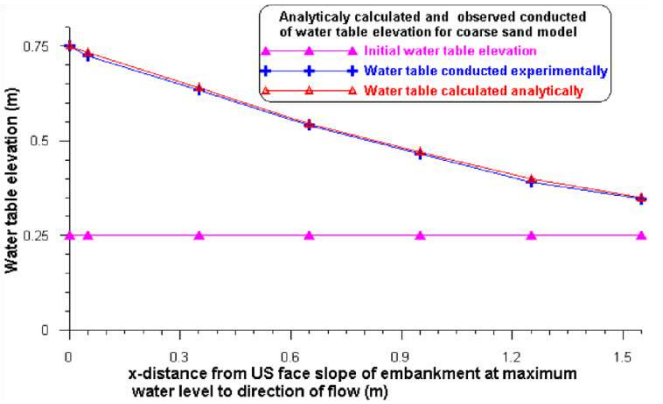

Figure 6 Phreatic line profile computed mathematically and obtained experimentally for coarse sand embankment.

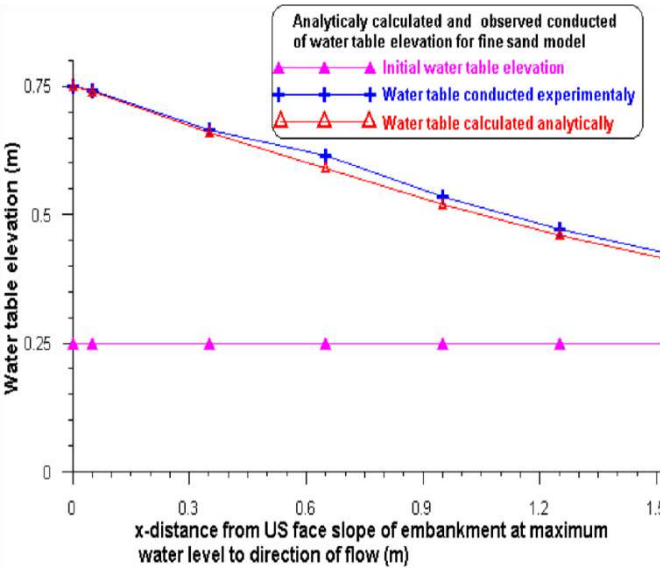

Figure 7 Phreatic line profile computed mathematically and obtained experimentally for medium

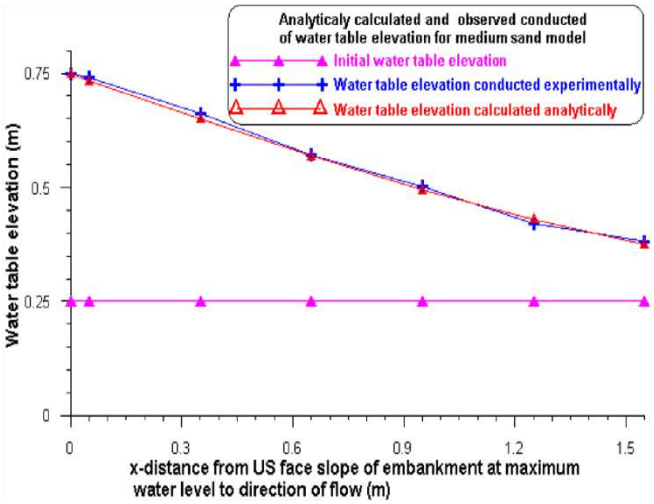

Figure 8 Phreatic line profile computed mathematically and obtained experimentally for fine sand embankment.

4. Conclusion

In the present study, the ability of mathematical model to compute water table elevation is investigated. The study is limited for homogenous embankment. The results demonstrate that a one-dimensional mathematical model is a suitable tool for simulating flow through porous media. The simulation of full-scale flow through porous media is possible using a mathematical modeling in this way, without the cost of producing physical models for a prototype, also with using a mathematical model the scale effect can be overcome.

The methodology used here relies on validation of the mathematical model for a similar flow case using physical experiment data. The study confirmed that the water table situation through porous media studied here could be extensively dependent in porous media particle size.

The results show that the maximum water table elevation can be obtained with greater particle size. The comparison between experimental and analytical result show good agreement, which is, can be considered in future with different media situations. The maximum variation between the analytical and experimental results are found 2.88, while with numerical method was found 10% and with fragment method was 18% as stated in literature.

References

Harr M. E. (1962) “Ground Water and Seepage” Mc-Graw-Hill book company, New York, USA.

Cedergren, H. 1988. Seepage, Drainage, and flow nets – 3erd ed. Wiley-Interscience publication. Norwich, Great Britain. 339 pp.

Ching S. C., “Boundary Element Analysis for Unconfined Seepage Problems” ASCE, J. Geotec. Eng., vol. 114, issue 5, May 1988.

Domenico, P.A. and F.W. Schwartz, 1990. Physical and Chemical Hydrogeology, John Wiley & Sons, New York, 824 p.

Gelhar, L.W. and Axness, C.L., 1983. Three-dimensional stochastic analysis of macro dispersion in aquifers. Water Resources Research, 19(1), pp.161-180.

Justin, J. D., Hinds, J., and Creager, W. P. (1944). Engineering for dams: Earth, rockfill, steel and timber dams, Vol. III, Wiley, New York.

K. R. Rushton and S. C. Redshaw,” Seepage and groundwater flow, numerical analysis by analog and digital methods,” Wiley, New York, 1979. No. of pages: 339

Middlebrooks, T. A. (1953). “Earth dam practice in the United States.” Trans. Am. Soc. Civ. Eng., 118, 697–722

Morris, D.A. and A.I. Johnson. 1967. Summary of hydrologic and physical properties of rock and soil materials as analyzed by the Hydrologic Laboratory of the U.S. Geological Survey 1948-1960. U.S. Geological Survey Water Supply Paper 1839-D. 42 p.

Rezk, M. and Senoon, A. (2010), “Analytical solution of seepage through earth dam whit an internal core.” Alex. Eng. J., Alex. Univ., 50, 111115.

Stello, W. (1987). “Seepage chart for homogeneous and zoned embankment.” Journal of Geotechnical Engineering, ASCE, 13-(9), 996-1012.

ZANCO Journal of Pure and Applied Sciences
The official scientific journal of Salahaddin University-Erbil
ZJPAS (2018) **30**(s1)s113-s121
http://dx.doi.org/10.21271/ZJPAS.30.s1.13

Experimental Investigation to study the Hydraulic Performance of Pressure Flushing in Straight Wall Reservoirs

Bashir T. Mohammad*, Faisal A. Daham and Zina Z. Bilal

Dam and water resources Department, College of Engineering, Salahaddin University-Hawler,

Region-Iraq

A R T I C L E I N F O

Article History:
Received: 14/05/2017
Accepted: 12/04/2018
Published:01/06/2018

Keywords:
Pressure flushing,
Dam Reservoirs,
Sediment,
Bottom outlet.

**Corresponding Author:*
Email:
bashir.mohammed@su.edu.krd
faisal-a-daham@hotmail.com,
zinazakariya@yahoo.com

A B S T R A C T

Sedimentation in reservoirs is considered as a serious problem in dams. Pressure flushing is one of the most effective techniques for removing the deposited sediments from reservoirs as well as it has few local effects and used as a clearing process by removing sediments around the entrance of intakes. Few studies were carried out to cover the gap of studying the hydraulic performance of pressure flushing in straight wall reservoirs. In this study, many laboratory experiments were carried out to find out the effects of many hydraulic and geometric parameters on pressure flushing such as discharge, size and type of sediments, lengths of internal offset, water heights and sediment depths above the bottom outlets. The experimental results demonstrated that the flushed sediment volume increased with the increasing of each of: outlet discharge, sediment depth, and internal offset length of the outlet. On the other hand, the research revealed that the optimal ratio of water to sediment depths that introduced maximum volumes of flushed sediments were found between 2.08 and 2.26. Finally, SPSS21 program and ANN tool integrated with the MATLAB 2011 program were utilized to facilitate the calculations of the regression analysis and the dimensionless equations to be used in estimating the flushed sediment volume and the effective duration time.

INTRODUCTION

Reservoir sedimentation rate in many regions, in Asia, is much higher than other continents and can be annually estimated between 0.5 and 1.0%. Permanent use of existing reservoirs has become an important matter, since building new reservoirs is difficult because of the economy, new environmental rules and lack of appropriate dam locations. Therefore, techniques for reservoir desolation have recently received increasing attention (Meshkati, 2009).

Many important steps have to be implemented to reduces the amount of sediment that entered and settled in the reservoir. These steps include firstly, increasing sediment movements through the reservoir during high discharge and sediment concentration. Secondly, by passing high discharge with high sediment concentration

from inside the Reservoir. Thirdly, flushing sediment from the reservoir by intensity streams. Finally, removing the reservoir sediment by using mechanical methods such as dredging and siphoning.

One of the most active techniques is sedimentation flushing, which the deposited sediment is hydraulically taken away from the bottom outlet. Hydraulic flushing is not a new technique. Flushing method is the oldest technique that has ever been known. It was practiced in Spain in the 16th century as pointed out by D'Rohan (1911). The surplus in shear force of accelerated discharge, which is created by the sudden opening of the bottom outlets of dams, loosens and re-suspends the sediment. If flushing is conducted under a pressurized condition and constant head of water on the bottom outlet, this flushing would be called "pressure flushing" and it would have exact effect only around the outlet. In pressurized flushing, the sediment that is close to the outlet openings is scoured and a cone-shaped crater is created. Figure 1 shows the longitudinal and plan view of the pressure flushing funnel close to the outlet. The hydraulic flushing is considered an efficient technique in narrow reservoirs and strong slopes (Lai and Shen 1996, 1999). Emamgholizadeh (2005 and 2006) proposed by experimental studies that the increasing volume of sediment by increasing the discharge from outlet and decreasing reservoir's water depth and when the changed sediment from coarse to fine the amount of sediment increased. The sediment flushing efficiency changes strongly by many factors like arrange layers of reservoir, elevation of sediment scouring gates, size of sediment, discharge during sediment flushing, duration time of flushing Sumi (2008). Meshkati and et al (2010) proposed an experimental study and they found that the volume of flushing cone was strongly affected by the diameter of bottom outlet and discharge of bottom outlet, also The maximum scour depth of the flushing cone was located very near to the dam wall. Emamgholizadeh (2014), were conducted to laboratory experiments to prove The scour cone of the flushed sediment increases with increase of discharge, and decreases with increase of sediment bulk density(cohesive-soil) and the water level above the sediment. Also, in some dams, the formation of pressure flushing cone has a very important role in preventing sediment entering the power plant intake. Pressurized flushing has been extensively studied and investigation of pressure flushing technique at reservoir outlets has been conducted in wide ranges.

However, studies on the effect of internal bottom outlet offsetting on the flushing cone development are limited. In addition, the loss of water resources and the negative effect of flushing pressure on the environment often make it illogical to finish the flushing process. In this condition, it is necessary to find a balance between removal, discharge of sediments, the limitations of water resources and the impact of the environment. Researches for understanding the volume variations of scouring cone with the discharge bottom outlet, water depth in the reservoir and variations of the height of soil are necessary in order to make a proper design for the bottom outlet. Also, in the planning process of dam operation, it can be right to estimate how much of sediment can be removed, and how much amount of water flushing is required. In the present work experiments are conducted to study the influence of different parameters during pressure flushing operation on the temporal evolution of scouring cone close to the bottom outlet of straight wall dam reservoirs. The purpose of the current work to find how efficient is the mechanism of pressure flushing operation. Also, it aims to describe the evolution of cone formation due to the pressure flushing near the outlet. In addition, it seeks to find the relation between the volume of sediments and all the effective geometric and

hydraulic parameters of the model such as the height of sediment, the height of water, and type of sediment length of internal offset outlet discharge and uniformity coefficient of soil.

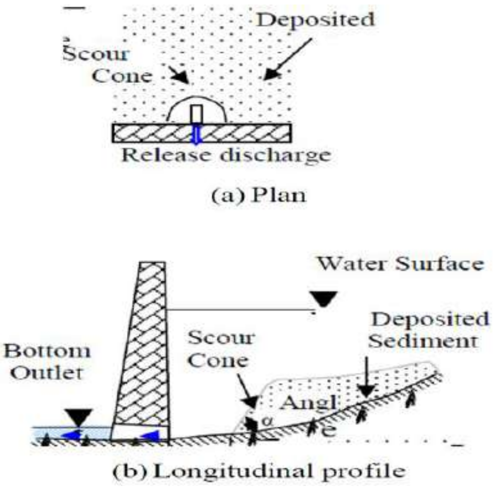

Longitudinal and plan view of the pressure flushing. *(Figure 1)*

Furthermore, the relation between the volume of the sediments and the time the flushing operation takes. See figure (1).

MATERIALS AND METHOD

2.1. Experimental Set-up

The experiments were conducted at the hydraulic laboratory of the Civil Engineering Department at the University of Salahaddin Hawler in the Kurdistan Region of Iraq. The test apparatus consists of four parts:

Water supply system, bottom outlet, settling basin reservoir, and V-notch weir.

Water Supply System: It consists of an underground tank and an electrical pump with capacity 0.018 (m^3/Sec) used to recirculate a desired steady flow. The system is also supported by an adjusting valve and a 5-meter flume upstream of main reservoirs.

Main Reservoir: the Main reservoir was of a rectangular shape of 2-meter length, 0.4-meter-wide and 0.78-meter height. Using two reticulated sheets at the reservoir's entrance, a smooth flow is created. The outlet of the main reservoir includes a valve of the diameter of 2.08 cm with two lengths of internal offsets (2 and 8) cm. Sediment deposits in the main reservoir. The sediment consists of coarse with gravel and coarse sand with a median diameter of d_{50}=1.44 mm and 0.84 mm, and a specific gravity (G_s) 2.63 and 2.64 respectively.

Settling Basin Reservoir: This is the region that the water and sediment were mixed and sediments were settled. The basin is a rectangular flume of 1.52 m long, 0.75 m wide, and 0.6 cm height used to measure the outflow discharge.

Ground tank: A concrete ground tank with 6" opening, internal dimensions of 0.5m length, 2m width, and 0.75m height, to complete the flow recirculation. Photo 1 shows the main parts of the test apparatus used in the current work.

The flume and Main reservoir. *(Photo 1)*

2.2. Dimensional Analysis

The volume of a flashing cone (V) may be written as a function of the following variables:

$$V = f\ (H_w, B, u, L_v, H_s, \rho_w, \rho_s, g, v, d_{50}, C_u, \alpha, D) \quad \ldots\ldots(1)$$

where, u is velocity of flow at the entrance of bottom outlet, D is diameter of bottom outlet, H_w is the height of water above the center of bottom outlet, Hs is the height of sediment deposited above the center of outlet, B is the width of reservoir, d50 is the median size of sediment particles, ρs is the density of sediment, ρw is water density, g is the acceleration due to gravity, v is kinematic viscosity, C_u is uniformity coefficient of

sediment ($C_u = d_{60}/d_{10}$), α is angle of repose, and L_v is length of internal offset. By using Buckingham theorem, and choosing the ρ_s, H_w, and u as repeating variables, the following dimensionless parameters were obtained:

$V/H_w^3 = f\ (H_s/H_w, L_v/H_w, d_{50}/H_w, \rho_w/\rho_s, D/H_w, B, Fr, Re, C_u, \alpha)$ ……..(2)

Where Fr is Froude number and Re is Reynold number. The parameters B, D and g are constants. Hence, the aforementioned dimensionless parameters can be summarized to four parameters. Consequently, the following functional relationship describes dimensionless flushing volume:

V/Hw³ = f (Hs/Hw, Lv/Hw, d50/Hw , ρw/ρs , Fr, Cu, α) ……...(3)

2.3. Experiment Designing

For considering the effect of bottom outlet cross section on dimensions of flushing cone, the experiments were conducted with 3 different values of sediment height (7.46, 20.46, 27.46 cm), six water depths above the center of bottom outlet (32.54, 42.54, 52.54, 57.54, 62.54, 67.54 cm), six different discharges, two length of internal offsets (2, 8 cm) shown in the photo 2, and two different size of sediment with d50 (1.44, 0.84 mm). Table 1 and 2 show the range of variables conducted in this study for measuring experimental data and non-dimensional parameters for dimensional analysis.

a) The internal offset with 2 cm.

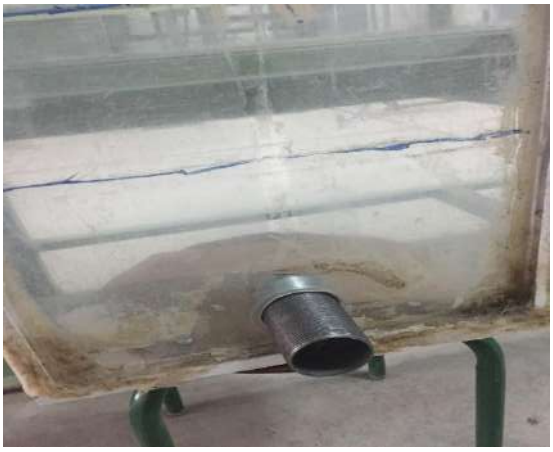

(b) The internal offset with 8 cm.

Bottom outlet valve inside and outside the reservoir. *(Photo 2)*

Q (cm^3/sec)	H_w (cm)	H_s (cm)	L_v (cm)
3. 8 – 6	32.54 – 67.54	7.46 – 27.46	2 - 8

Table 1 Range of variables in this research

Table 2 Range of non-dimensional parameters in this research

V/H_w^3	H_s/H_w	d_{50}/H_w	ρ_w/ρ_s	F_r	L_v/H_w	Cu	α
0.09-0.588	0.11-0.646	0.001-0.004	0.819-0.84	0.833-1.12	0.03-0.246	6.15- 12.03	37.8-38.66

2.4. Experimental Procedure

For running the experiment, the deposited sediment was flattened and leveled firstly to a specific level above the bottom outlet (30 cm), and the model was slowly filled with water until the water surface elevation reached to the desired level. Then, the bottom outlet was manually opened until the steady state flow

condition was attained. Consequently, the sediment was released from the main reservoir. At the beginning of the experiment when the downstream outlet opened, sediment was discharged with high concentration, but the concentration of sediment flushing decreased with time. Experiments were continued until the flushing cone reached to an equilibrium condition in which the sediment concentration was negligible at the end of the experiment. The time required for the formation of the flushing cone depends on an equilibrium conditions. The development of flushing cone was very fast, and the process finished in less than 15 minutes to 25 minutes in the experimental model. In this study, the time for running the experiment was set to 2-3 hour. At the end of each experiment, the flushing outlet was closed and water was carefully and slowly drained from the main reservoir and the measurement of bed configuration was done in a grid system around the bottom outlet. At the end of each experimental test run, the bed level of scour was measured using point gages, and the volume of flushing cone was calculated by Excel sheet, as shown in photo 3 and figure 2 the maximum scours depth of the cone was found very close to the dam wall.

Top view of flushing cone *(Photo 3)*

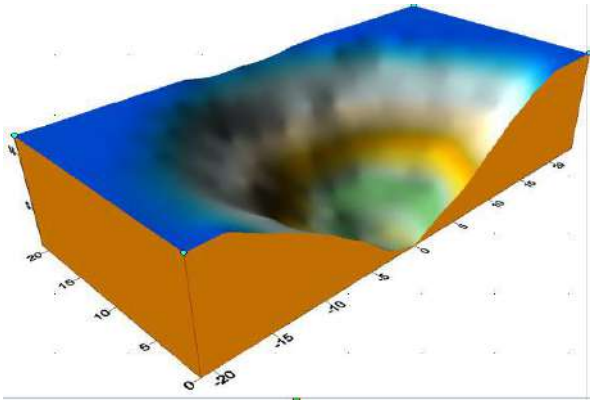

a) Three-Dimensional view

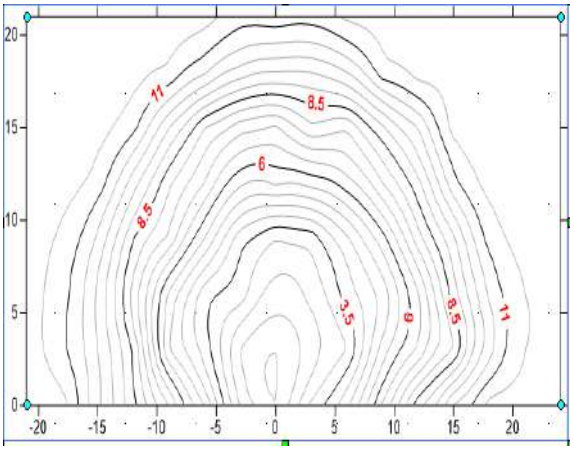

(b) The bed topographic view

Three-dimensional and bed topographic of the flushing cone after the experiment with Q=5.58 lit/s, Hw=60cm, Hs=12cm, Lv=2cm, and d50=1.44mm. *(Figure 2)*

General phases of flushing operation

The flushing process is usually divided into four phases. The first phase the water is slowly released due to the effect of seepage water through the soil, it is represented by lowering the water table down to a few meters above minimum level for power generation. The second phase is the release of high concentration of sediment due to the impact of the pressure of soil and water above the bottom outlet. When concentration increases, the settling velocity decreases, thus the flow can transport with very high concentrations of sediment under a relatively small flow (Lai et al.1993). The third phase is rapid release of the

remaining water, resulting in the release of a free flow water and sediment out of the reservoir due to hydraulic scour. Finally, the fourth phase is the free flow of water out of the reservoir.

3. RESULTS AND DISCUSSION

A funnel shape of scouring is created in the vicinity of outlet gates in the pressure flushing operation. The maximum scouring depth of this cone is found very close to the dam wall. The cone slopes of both longitudinal and side are approximately equal, and also these are similar to the repose angle of the submerged sediment.

3.1 Relation between outlet discharge and volume of flushing cone

To illustrate the effects of volume of flushing cone, the percentage of (V/(VHv=65)∗100) and (Q/Qmax∗100) will be used instead of V and Q directly. The figure 3 shows the relation between volume of sediment ratio and the outlet discharge ratio for different offsets and sizes of sediment particles values. The figure reveals that the maximum volume of sediment ratio which is about 115.5% will happen at 84.7% outlet discharge ratio. Fig. 4 and 5 also present the variation of (V/(VHv=65)∗100) and (Q/Qmax∗100) for 25 and 32 cm depths of sediment above the bed of channel and the maximum volume is 105%, this increasing due to hydraulic mechanism increase. The figures show the same trend for volume release of sediment with the depth of water.

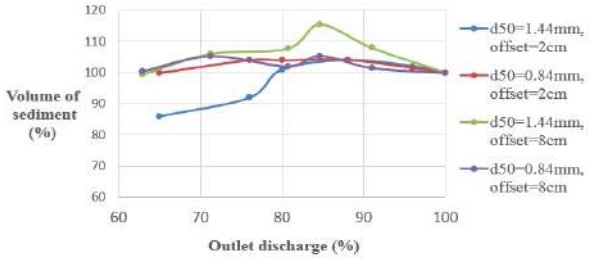

Effect of bottom outlet discharge ratio (Q/Q_{max}) on the volume of flushing ratio (V/V_{Hv}=65) for H_s=12cm above the bed of channel. *(Figure 3)*

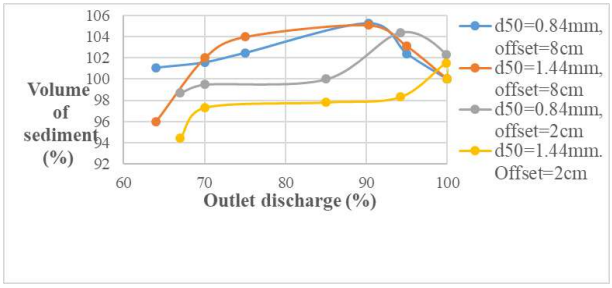

Effect of bottom outlet discharge ratio (Q/Q_{max}) on the volume of flushing ratio (V/V_{Hv}=65) for Hs=25cm above the bed of channel. *(Figure 4)*

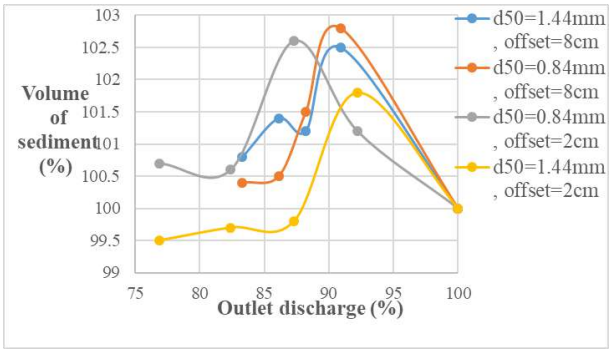

Effect of bottom outlet discharge ratio (Q/Q_{max}) on the volume of flushing ratio (V/V_{Hv}=65) for H_s=32cm above the bed of channel. *(Figure 5)*

3.2 Relation between size of sediment and the volume of flushing cone

Emamgholizadeh (2006) proposed by experimental studies that when the changed sediment from coarse to fine the amount of sediment increased. In the present study as shows in figure 6 the relation between the volume of sediment and size of sediment particles for sediment thickness = 25cm, the same trend for other values of sediment height (12 and 32cm). The figure shows that the sediment flushing cone volume increased when the sediment size is decreased, due to the increase of pressure on the sediment.

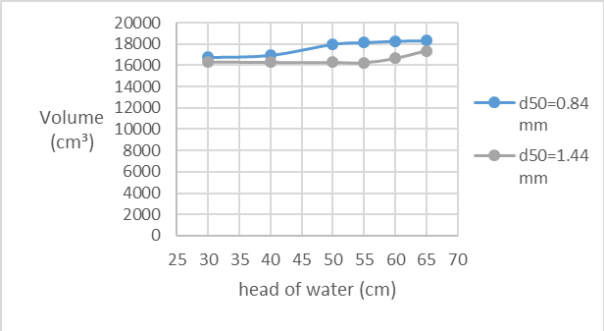

Effect of type of sediment on the volume of the cone when the height of sediment = 25 cm. *(Fig. 6)*

3.3 Relation between length of internal offset and the volume of flushing cone

Figures 7 and 8 show the effect of different length of internal offset on the volume of flushing cone for different size and depth of sediment.

The figures illustrate that increasing the length of internal offset from 2cm to 8cm (30%) causes an increase of the volume of flushing cone about 80%, because this increase in the length of offset leads to increase the distance affected by scouring, and this gets a large amount of sediment flushed.

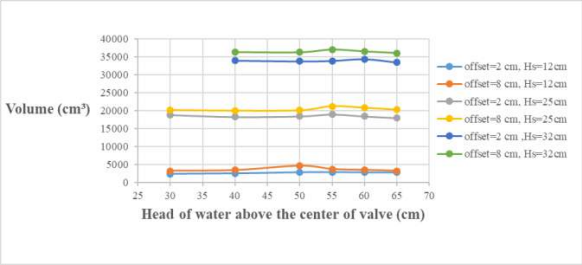

Effect of offset on the volume of cone for the first type of sediment (d50=1.44). *(Fig.7)*

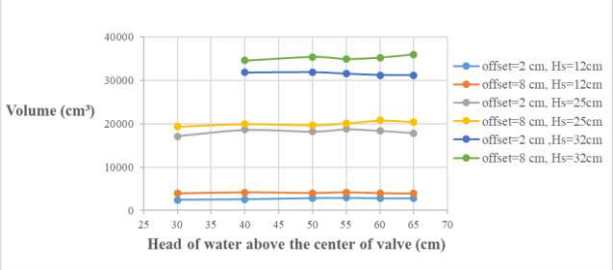

Effect of offset on the volume of cone for the second type of sediment (d50=0.84 mm). *(Fig. 8)*

3.4 Relation between height of sediment and the volume of flushing cone

Figures above 7 and 8 show the effect of height of sediment on the volume of flushing cone for different size of sediment and internal length of offset.

The figures illustrate that increasing height of sediment from 12cm to 32cm causes an increase of the volume of flushing cone about 80%, This increase occurs as a result of increasing the pressure of sediment on the bottom outlet of the reservoir. The upper curve shows the maximum volume of flushing sediment occur when the water depth in the reservoir is 55 and 60cm for Lv is 8cm, d50 is 1.44 and 0.84mm respectively. So, appropriate optimal ratio of water to sediment depths ratios in the reservoir that introduce maximum volumes of flushed sediment are when the ratio of the water depth to the sediment depth in the reservoir is between 2.08 and 2.26 (Hw/Hs=2.26).

3.5 Variation of flushing sediment concentration with time

For a better understanding of the mechanism of flushing processes, the data has been presented graphically. Figure 9 shows the variations of outflow sediment concentration with flushing time for height of sediment 25cm, height of water above the valve 40cm and length of internal offset 2cm. The figure shows that during about the first 10 seconds, the concentration reaches its highest-level due to the pressure flushing mechanism. After that, the concentration level will be damped down rapidly due changing the transport mechanism of the sediment from pressurized flushing process to hydraulic scouring process. The figure also shows that the effective times

(when the flushed sediment reach at equilibrium condition) of flushing is between (60 – 70) secs.

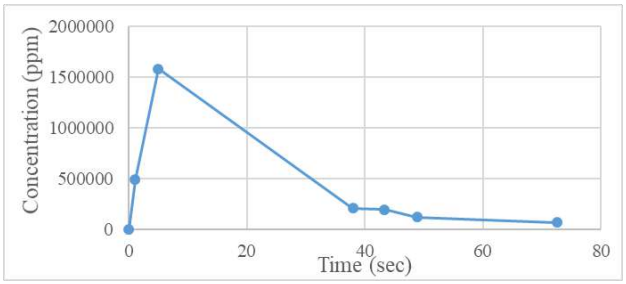

Variation flushing sediment concentration with time of (Hs=25cm, Hw=40cm, Lv=2cm). *(Fig. 9)*

3.6 Statistical analysis for estimating pressure flushing cone volume (V)

In order to obtain a general relationship to all the pi terms that affected the volume of flushing cone (V), SPSS21 and ANN were used to find the correlation coefficient. Many cases of choosing extra pi terms relating to sediment type will be discussed in this section. Table 3 shows the effect of uniformity coefficient and angle of repose on the volume of flushing for straight wall model with a correlation coefficient of 0.944. The table shows it can be used Cu instead of d50, since it is the dimensionless term, in the calculations of the volume of sediment. Fig.10 shows the comparison between the calculated flushing cone parameters using below equations and observed values.

Table 3: Summary of statistical equations with the correlation coefficient for different cases of Straight wall model.

case	parameters	Equations	R^2
A	$V=f(H_w,H_s,d_{50},\rho_s,\rho_w)$	$V/H_w^3=3.784(\frac{Hs}{Hw})^{1.776}(\frac{d50}{Hw})^{0.686}(\frac{\rho w}{\rho s})^{23.463}(Fr)^{0.017}(\frac{Lv}{Hw})^{0.156}$	0.944
B	$V=f(H_w,H_s,d_{50},\rho_s,\rho_w,Cu)$	$V/H_w^3=0.716(\frac{Hs}{Hw})^{1.774}(\frac{d50}{Hw})^{0.687}(\frac{\rho w}{\rho s})^{-5.145}(Fr)^{0.018}(\frac{Lv}{Hw})^{0.158}Cu^{-1.837}$	0.944
C	$V=f(H_w,H_s,\rho_s,\rho_w,Cu)$	$V/H_w^3=-1.28(\frac{Hs}{Hw})^{1.91}(\frac{\rho w}{\rho s})^{-1.477}(Fr)^{-10.8}(\frac{Lv}{Hw})^{0.044}Cu^{0.22}$	0.93
D	$V=f(H_w,H_s,\rho_s,\rho_w,\alpha)$	$V/H_w^3=0.17(\frac{Hs}{Hw})^{1.91}(\frac{\rho w}{\rho s})^{10.8}(Fr)^{0.044}(\frac{Lv}{Hw})^{0.22}\alpha^{0.79}$	0.93

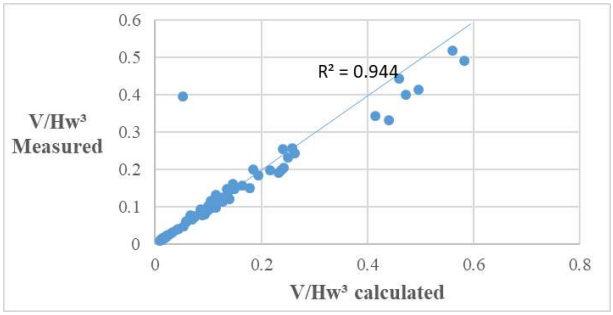

Multivariable power regression yielded for straight wall model. *(Fig. 10)*

Conclusions

The analysis of the experimental data in this study leads to the following findings:

1. The results of the present study revealed that in order to maximize the pressurized sediment flushing efficiency should be made to increase outflow discharge to an optimum value.

2. The optimal ratio of water depths to sediment depth in the reservoir was introduced when a maximum volume of flushed sediment was set 2.26 (Hw/Hs = 2.26).

3. The flushing volume increased with the increasing of the sediment layer thickness in reservoirs, due to the impact of sediment pressure.

4. The maximum scours depth of the cone was found very close to the dam wall.

5. Increasing the internal offset length from 2cm and 8cm caused an increase in flushed sediment volume to about 80%.

6. The effective time of flushing for the two models was found between 60 and 70 sec.

7. One can use Cu instead of d50 to estimate the sediment volume.

REFERENCES

- Emamgholizadeh, S., Borojeni, H. S. And Bina, M. (2005) *"The flushing of the sediments near the power intakes in the Dez Reservoir"*. WIT Transactions on Ecology and the Environment, Vol 83, ISSN 1743-3541 (on-line) http://www.witpress.com.
- Emamgholizadeh, S., Bina, M., Fathi-Mohadam, M. And Ghomeyshi, M. (2006) *"Investigation and Evaluation of Pressure Flushing through Storage Reservoir"* ARPN Journal of Engineering and Applied Sciences, 1 (4). ISSN 1819-6608, http://www.arpnjournals.com.
- Emamgholizadeh, S. And Fathi-Moghdam, M. (2014) *"Pressure Flushing of Cohesive Sediment in Large Dam Reservoirs",* Journal of Hydrologic Engineering, p.674-681.
- Meshkati, M. E., Dehghani, A. A., Naser, G., Emamgholizadeh, S. And Mosaedi, A. (2009) *"Evolution of Developing Flushing Cone during the Pressurized Flushing in Reservoir Storage"*. International Science Index, 3 (10), p.1067-1071. Science Explorer Publications. Available online at https://www.researchgate.net.
- Meshkati, M. E., Dehghani, A. A., Sumi, T. And Mosaedi, A. (2010*)," Experimental Investigation of Pressure Flushing Technique in Reservoir Storages".* Water and Geoscience, ISSN: 1790-5095.
- Shen, H. W. (1999). *"Flushing Sediment through Reservoirs"*. Journal of Hydraulic Research, 37(6): p.743 – 757, online at http://dx.doi.org.
- SHEN, H.W., And LAI, J.S., (1996), "*Sustain Reservoir Useful Life by Flushing Sediment"*. International Journal of sediment Research, IRTCES, Vol. 11, No 3. December.
- Shen, H.W., Lai, J.S. And Zhao, D. (1993), *"Hydraulic de-siltation for non-cohesive sediment".* Proceeding of the 1993 Annual ASCE Hydraulic Engineering Conference, San Francisco, H.W Shen, S.T. Su, and F. Wen, eds, pp. 119-124.
- Sumi, T. (2008) *"Evaluation of Efficiency of Reservoir Sediment Flushing in Kurobe River".* http://www.ecohyd.dpri.kyoto-u.ac.jp.
- Zina, B. (2017). *"Experimental Investigation to study the Hydraulic Performance of Pressure Flushing in Reservoirs"*. MSc thesis, Science in Water Resource-Hydraulics and Dam Engineering, Department of Dam and water resources, Salahaddin University.

ZANCO Journal of Pure and Applied Sciences
The official scientific journal of Salahaddin University-Erbil
ZJPAS (2018) **30**(s1)s122-s134
http://dx.doi.org/10.21271/ZJPAS.30.s1.14

Characteristics and potential treatment technologies for different kinds of wastewaters

Shuokr Qarani Aziz [1] and Sazan Mohamemd Ali [2]

١- Department of Civil Engineering, College of Engineering, Salahaddin University–Erbil, Iraq,

٢- Department of Dams and Water Resources Engineering, College of Engineering, Salahaddin University–Erbil, Iraq

ARTICLE INFO

Article History:
Received: 14/05/2017
Accepted: 12/04/2018
Published:01/06/2018

Keywords:
Wastewater
Characteristics
Treatment
Standards
Process
Reuse

***Corresponding Author:**
Shuokr Qrani Aziz
shuokr.aziz@su.edu.krd
shoker71@yahoo.com
H/P: 00964 750 462 5426

ABSTRACT

The current work was aimed to characterize and defining appropriate treatment processes for various types of raw wastewaters. The fresh wastewater samples were collected from slaughterhouse (SWW), tannery (TWW), municipal (MWW), municipal landfill leachate (MLL), and dairy (DWW). The collected samples were analyzed for temperature, pH, electrical conductivity, turbidity, total alkalinity, total hardness, biological and chemical oxygen demands, suspended and dissolved solids etc. Commonly, MLL contained low biodegradability ratio; while SWW, MWW, and DWW had high biodegradability ratio of greater than 0.5. TWW regarded as strong alkaline because pH values were greater than 10. Physical, chemical and biological treatment processes were explained and suitable treatment methods were complemented with the wastewater type. It can be concluded that generally physical-chemical techniques were fit with old landfill leachate and tannery wastewaters; whilst biological treatment methods with adsorption were adequate for SWW, MWW, and DWW and the effluents match the quality of irrigation water quality.

1. INTRODUCTION

Commonly, the quality of wastewater is characterized by physical, chemical and biological analysis. The concentration of wastewaters depends on the source of the wastewater, function and the activity of particular industries. Wastewaters produced from houses, businesses, schools and public buildings have different characteristics compared to industrial wastewaters. Industrial wastewaters (for instance produced wastewaters from tannery industry, food processing industries, steel factory, dairy factory etc.) contain high amount of organic, inorganic constituents and heavy metals(Aziz and Ali, 2016. On the other hand, municipal landfill leachate (MLL) contains high concentrations of organic and inorganic materials, colour, ammonia-nitrogen, phenols etc. (Aziz et al., 2010; Aziz and Maulood, 2015). Industrial wastewaters and MLL regard as strength wastewaters (Aziz et al., 2010; Metcalf and Eddy, 2014). Typical characteristics of some industrial wastewaters are shown in Table 1.

Selection of appropriate treatment techniques for wastewater is related to its characteristics and the purpose for the treatment process (Aziz and Ali, 2016). Bustillo-Lecompte and Mehrvar, (2015) concluded that slaughterhouse wastewater (SWW) are commonly pre-treated by screening, settling, blood collection, and fat separation, followed by physicochemical treatment, including dissolved air flotation, coagulation/flocculation and/or secondary biological treatment. Tannery wastewater (TWW) contain high amount of pollutants with alkaline range; physical-chemical processes are most suitable for this kind of wastewater. Normally, municipal wastewater (MWW) from Erbil City-Iraq regards as weak waste water with biodegradability ratio of more than 50 (Amin and Aziz, 2005). Practically, primary with secondary treatment processes are useful for MWW and later it can be used for irrigation. Additionally, wetlands, sequencing batch reactor, oxidation ditch etc. are applicable for treatment of MWW and reusing for irrigation purpose (Surampalli et al., 1997; Aziz, 2011). According to the study done by Bashir et al. (2012), the electro-oxidation treatment for stabilized municipal landfill leachate (MLL) can result in removing of a considerable amount of non-biodegradable matters (COD), color and ammonia-nitrogen. The electro-oxidation is a powerful technology, mainly for low BOD_5/COD or high toxic landfill leachate which is hard to be treated biologically). In literature, different treatment methods such as coagulation-flocculation, dissolved air flotation, SBR, ion exchange, adsorption, filtration etc. were applied for treatment of MLL (Bahsir, 2010, Aziz 2011; Mojiri et al., 2014).In contrast, dairy wastewater (DWW) which characterized by high organic matter content and recommended by many researchers to be treated biologically (Dawood et al., 2011; Deshannavar et al., 2012; Lateef et al., 2013; Shahriari and Shokouhi, 2015). Ali (2017) conducted numerous laboratory experiments for treatment of DWW using activated carbon added to trickling filters; natural rock, disposed plastic caps, and useless PVC pipes with different sizes and depths were used as trickling filter media (Ali, 2017).

As known that the effluents of the industries contain huge amounts of both inorganic and organic chemicals and their byproducts (Bougherira et al., 2014). Nowadays, most of industries in Erbil City are in small scale sector and are there is not appropriate and scientific treatment plants and discharge industrial effluents through unlined channels and streams to the environment which causing huge contamination of air, water and soil (environmental pollution). The present study was focused on the characterization of various kinds of wastewaters in Erbil City-Iraq. Produced wastewaters from SWW, TWW, MWW, MLL, and DWW were collected and analyzed for 15 wastewater quality parameters. On the other hand, discussion of wastewater treatment processes and identifying appropriate treatment technology for each type of the collected wastewaters and reusing for irrigation purpose was another goal of current work.

Table 1: The average characteristics of four industrial wastewaters (Hammer and Hammer Jr, 2014; Cristian, 2010)

Constituent	Unit	Milk Processing	Meat Packing	Synthetic Textile	Chlorophenolic Manufacture
BOD5	mg/L	1000	1400	1500	4300
COD	mg/L	1900	2100	3300	5400
Total solids	mg/L	1600	3300	8000	53000
TSS	mg/L	300	1000	2000	1200
Nitrogen	mg/L	50	150	30	0
Phosphorus	mg/L	12	16	0	0
pH	mg/L	7	7	5	7
Temperature	mg/L	29	28	-	17
Grease	mg/L	-	500	-	-
Chloride	mg/L	616	382.6	-	27000
Phenols	mg/L	-	-	-	140

.

2. MATERIALS AND METHODS

2.1. Description of the sites

In this work, the produced wastewaters from five different sites in Erbil City-Iraq were collected. The formed wastewaters at all locations are discharged directly to the natural environment without any prior necessary treatment processes.

2.1.1. SWW (Slaughterhouse wastewater)

The SWW generated from slaughterhouse in Erbil City-Iraq, Fig.1. Erbil Slaughterhouse located in the right side of Erbil-Makhmoor main road and approximately 20 km far from Erbil City Centre. The formed wastewater at Erbil Slaughterhouse is composed of blood of animals from slaughtering and cleaning, washing waters, black water from toilets or urinals and storm water during rainfall periods. Number of slaughtered big size animals such as cow varied from 700 to 800; while for goat and sheep are ranged between 6500 and 9300. Because of increase in population, growth of economy, and the current situation in the area, the number of slaughtered animals will increase. A small wastewater treatment-plant was built in the slaughterhouse campus. But, during the sample collection period the treatment plant was out of service and the wastewater was discharged directly to the surrounded environment without any treatment.

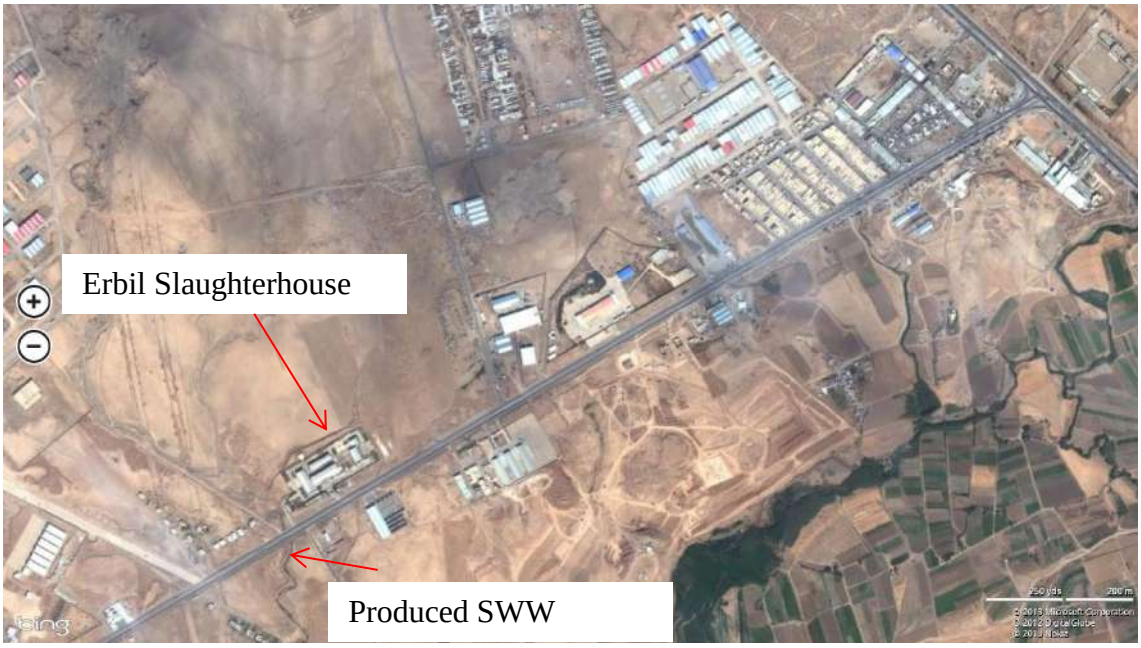

a) Satellite image

b) Discharged wastewater

Fig.1. Slaughterhouse wastewater in Erbil City

2.1.2. TWW (Tannery wastewater)

Tannery factory for cleaning and preparing animal leathers is located in the right side of Erbil-Makhmoor main road. It approximately 12 km far from Erbil City Centre, Fig. 2. It lies in 36 ^{o} 10’ 18”N and 43 ^{o} 54’ 26” E. Preparation of leathers needs numerous processes. In some steps, chemicals used to remove hair and preparation of the leather. Of course, adding chemicals effect on the quality of the wastewater. Currently, TWW collected in the concrete tanks beside of the factory. Later, the collected wastewater

transported by tankers and disposed at Erbil landfill site without treatment.

Fig.2. Tannery wastewater in Erbil City

2.1.3. MWW (Municipal wastewater)

MWWs from Erbil City merge near Turaq Quarter and situated on the left side of Erbil-Mosul main road and approximately 8 km far from Erbil City Centre, Fig. 3. Turaq Quarter lies on 36 ^{o} 10’ 15” N and 43 ^{o} 56’ 12” E. In 2001, the amount of wastewater for Erbil City at Toraq site was ranged from 0.85 m⅜s to 1.7 m⅜s (Mustafa and Sabir, 2001). Nowadays, the flow rate (Q) of wastewater exceeds 2 m^3/s. The wastewater at specified location is composed of: 1) domestic sewage, which originates from kitchens and bathrooms of dwellings, public buildings as well as street wash water, 2) industrial wastewater from Northern and Southern industrial areas, and 3) storm water during rainfall periods (Amin and Aziz, 2005). Sometimes, municipal wastewater in Erbil City used illegally by farmers for irrigation some types of plants. In winter, the wastewater mixed with Greater-Zab River which is one of the tributaries of Tigris River.

2.1.4. MLL (Municipal landfill leachate)

Erbil Landfill Site (ELS) is situated on the left side of the Erbil–Mosul main road (near Kani-Qrzhala Sub-district) in Erbil-Iraq and is approximately 15 km from Erbil City center, Fig. 4. The geographical coordinates are 36°10'23"N and 43°35’32”E. The landfill, which established in 2001, has a total site area of 37 ha. Most of the landfill area has already been used. The site receives more than 3000 tons of MSW daily (based on data obtained from the ELS administration staff). Disposed MSW is mixed without appropriate separation of components. Thus far, studies on the MSW characteristics in Erbil City are limited. A small fraction of recyclable materials, such as plastic, glass, and metals, are separated by scavengers on-site. Because of absence of engineering landfill design and a gas collection system, the fresh MLL is directly disposed to the natural environment and forms gas emission to the atmosphere.

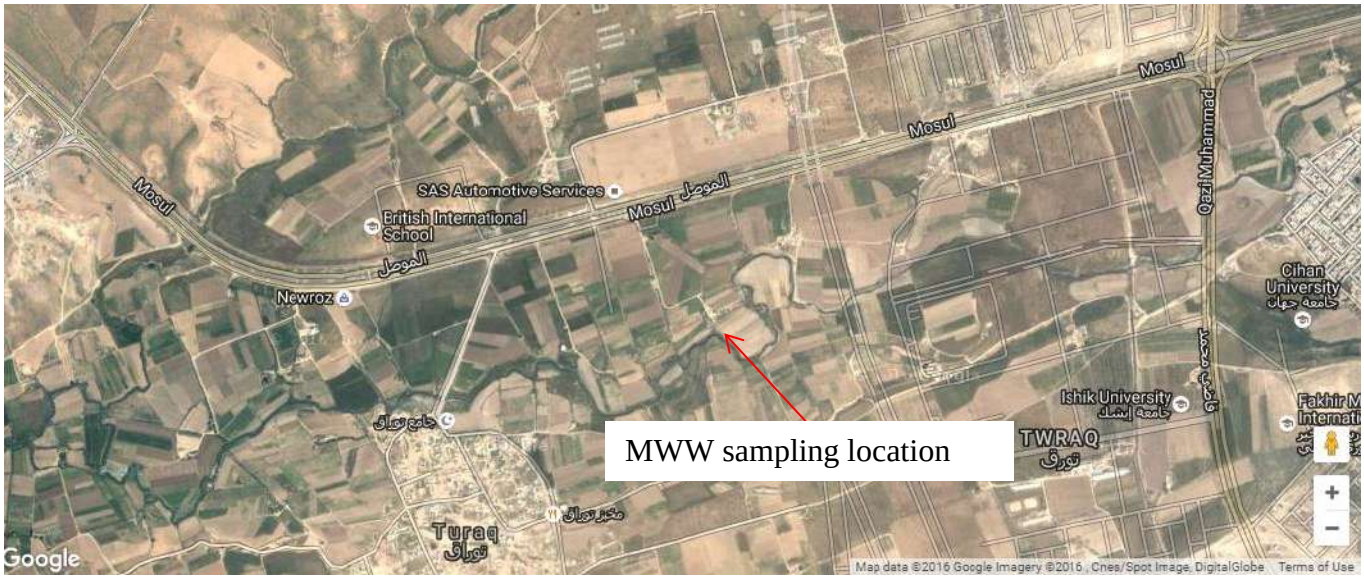

a) Satellite image

b) Municipal wastewater

Fig.3. Municipal wastewater in Erbil City

a) Satellite image

b) Produced landfill leachate

Fig.4. Landfill leachate at ELS

2.1.5. Dairy WW (Dairy wastewater)

DWW produced by a dairy factory (Yoruksut dairy factory YDF) which is one of the Turkish Dairy Factory in Erbil City established since 2010 near Gwer Sub-District. The factory is about 13 km far from the City center and is located at 36° 9' 45" N to 43° 51' 57" E and 371 meter above sea level (Fig.5). It produces approximately 40-50 tons of yoghurt and buttermilk per day (www.yoruksut.com.tr).

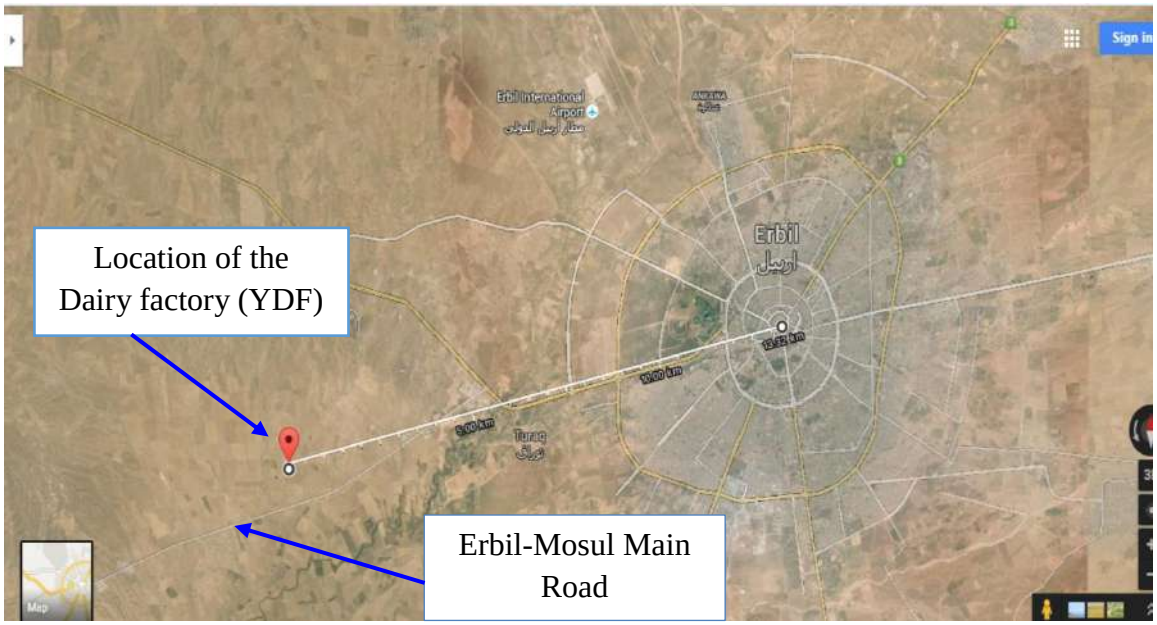

a) Satellite image of YDF

b) Produced wastewater

Fig.5. Produced wastewater from YDF

2.2. Sampling and Analysis

Physico-chemical analyses of wastewaters from the considered regions were conducted in the Sanitary and Environmental Engineering laboratory, Civil Engineering Department, College of Engineering, Salahaddin University-Erbil, Erbil, Iraq. The samples were collected in plastic containers and immediately transported to the laboratory. They were stored in the refrigerator at 4 °C prior to experimental use to prevent biological activities and changes in their characteristics (APHA, 2005). The fresh collected samples were characterized in terms of temperature, pH, turbidity (FTU), electrical conductivity (µmhos/cm), total salts (mg/L), total acidity (mg/L), total alkalinity (mg/L), total hardness (mg/L), chloride (mg/L), five day biochemical oxygen demand (BOD_5) (mg/L), total solids (mg/L), TSS (mg/L), and TDS (mg/L). Measuring of parameter were followed the Standard Method for the Examination of Water and Wastewater (APHA, 2005). Experiments, such as BOD_5, chloride, total hardness, total acidity, and total alkalinity, were determined by titration methods (chemical method). The other experiments, such as pH, EC, turbidity, and TSS were conducted using instruments in the Sanitary and Environmental Laboratory. pH was measured using a pH meter type Hl 8424/HANNA. A turbidity meter type Lp 2000/HANNA was used to measure the turbidity in the samples. EC in the samples was measured using Wissenschaftlich-Teshnischewerkstatten (WTW-LF42). Electrical balance, evaporating dish, filter paper, and oven were also used to measure total and suspended solids in the collected water samples.

3. RESULTS AND DISCUSSIONS

3.1. Characteristics of wastewater samples

The results of physico-chemical analyzes of the collected wastewaters are presented in Table 2. From the results, it can be noted that some of the measured parameters of wastewaters do not meet the standards (Iraqi and EPA effluent standards). There is a variation in the results which showing variations in the degree of pollution from one site to another.

Temperature is a main factor in biological activity rate for microorganism inside the wastewater. Referring to the standards of the EPA (2003) and Iraqi disposal standards (2011), the measured temperature parameter for all types of the wastewaters were below the allowable limits. The temperature variation from one site to another and from one sample to another is due to weather conditions and time of sampling but regional ecosystem may also be involved (Messrouk et al., 2014).

pH is one of the most important parameter which has effect on the biological activity within the wastewater. The highest value of pH was recorded for TWW of 10.2 and considered as strong alkaline. This is due to the chemicals and overdose cleaners which were used to remove hair and predation of the leather. A neutral pH of 7.5 and 7.28 was recorded for the SWW and MLL, respectively. A slightly acidic pH of 6.78 for MWW was recorded. An acidic in pH value for MWW is might due to the degradation of organic matter within the wastewater.

BOD_5 for all wastewater samples were higher than the allowable limits. The highest BOD_5 was recorded for the SWW of 400 mg/L. High BOD_5 value for SWW could be explained by the abundance of organic matter (rumen debris) and the concentration of blood in the effluent (Messrouk et al., 2014). The lowest value of BOD_5 was obtained for MWW of 44 mg/L. according to the literature (Amin and Aziz, 2005). Erbil MWW was classified as moderate to weak wastewater according to its BOD_5 values. In contrast, the BOD_5 for MLL and TWW were 273 and 320 mg/L, respectively. Leachate characterization changes with the climatic regions in addition to the

landfill operational practices. Organic substances (BOD_5 and COD) and ammonia-nitrogen are two main chemical features of environmental concern in landfill leachate (Bashir et al., 2012).

Table 2: Characteristics of different types of wastewaters

Analysis	Unit	Type of wastewater					Standards
		SWW	TWW	MWW	MLL	DWW[+]	
Temperature	^oC	22.6	18.86	21.86	12.58	21.53	<35[*], 40[**]
pH	-	7.5	10.2	6.78	7.28	7.09	6-9.5[*]
Turbidity	FTU	174	289	19.77	9.87	504	
EC	µs/cm	1793.5	12500	582.6	800	800	
Total salts	mg/L	1147.8	8000	372.9	512	512	
Total acidity	mg/L	4000	0	40	60	60	
Total alkalinity	mg/L	3300	4660	206	34.68	260	
Total hardness	mg/L	2000	2600	194	480	620	
Chloride	mg/L	800	6938	30.5	209.9	70	750 [**]
BOD_5	mg/L	400	320	44	273	650	<40[*]
COD	mg/L	600	1207	-	-	951	<100
BOD_5/COD	-	0.67	0.26	-	-	0.68	
Total solids	mg/L	2000	13200	10000	1200	1200	
TSS	mg/L	1200	2000	1800	600	600	60[*], 35[**]
TDS	mg/L	800	11200	8200	600	600	

[*] Iraqi Environmental Standards, Contract No.: W3QR-50-M074, Rev. No.: 03 Oct 2011
[**] (EPA) Environment Protection Agency (EPA), Standards for effluent discharge, Regulations, 2003.
[+] From Ali, 2017

High value of chemical oxygen demand (COD) was recorded for TWW and DWW, namely 1207 mg/L and 951 mg/L, respectively. These values are reflecting the oxidation of these wastewaters which rich in organic matters. According to the results of investigators a COD value of 1700 mg/L obtained for stabilized MLL (Aziz et al., 2010). On the other hand, the value of COD for DWW was 951 mg/L. and exceed the standard limits. Effluents from dairy industry characterized by high concentration of organic compounds (high BOD_5 and COD) (Swati et al., 2012, Ali 2017).

The results of BOD_5 and COD for dairy and slaughterhouse wastewaters were lower than the results obtained by Cristian (2010). Thus, the characteristics of these effluents can be vary dramatically, depending on the type of product being processed, the production program of system and the methods of operation used (Dawood et al., 2011).

Total suspended solids (TSS) is another important quality parameter in characterization of wastewater. For all types of wastewaters, the value of TSS were high and varied depends on the components of wastewater. The highest TSS value was recorded for tannery wastewater of 2000 mg/L. high level of TSS in TWW could be attributed with their accumulation during the processing of finished leather (Islam et al., 2014). Presence of TSS impurities cause high turbidity in the tannery wastewater stream which was 289 FTU. For slaughterhouse and

municipal wastewaters the value of TSS were also high and exceed the standard limits and namely 1200 and 1800 mg/L respectively.

3.2. Potential wastewater treatment methods

The BOD_5/COD referred to biodegradability ratio in the effluent wastewater discharges. It is essential to evaluate and obtain the biodegradability ratio for different kinds of raw wastewaters before selection of appropriate treatment technique, because it is generally considered the cut-off point between biodegradable and non-biodegradable waste (Messrouk et al., 2014). If BOD/ COD is greater than 0.6 then the waste is fairly biodegradable, and can be effectively treated biologically. If biodegradability ratio is between 0.3 and 0.6, then seeding of organic matter is required to treat the wastewater biologically because the biological process is slow. While, if BOD/COD less than 0.3, biodegradation will not proceed, thus it cannot be treated biologically due to the majority existence of toxic and no-biodegradable materials (Abdalla and Hammam, 2014). The result of this study indicated that the biodegradability ratio for SWW was 0.67. This is because the composition of slaughterhouse wastewater contains fats, proteins and fibers, as well as the presence of organics, nutrients, pathogenic and non-pathogenic microorganisms (Bustillo-Lecompte et al., 2016). While the biodegradability ratio for DWW was 0.68; this due to composition of yogurt, butter etc. Therefore, biological treatment include aerobic and anaerobic techniques as a successful technique were frequently used by the researches to treat slaughterhouse effluents (Mrya et al., 2015; Bustillo-Lecompte et al., 2016).

Obtained BOD/COD of greater than 50 % means that biological treatment processes are efficient. Suspended and attached growth biological treatment processes are applicable (Aziz, 2011; Mojiri et al., 2014; Aziz and Ali, 2016; Ali, 2017). For MLL, the BOD/COD average ratios were 0.096, 0.124 and 0.205 have been published by previous researcher for various leachate wastewater sites. The low BOD_5/COD ratio for leachate wastewater indicates that the leachate is stable and difficult to be degraded biologically. Therefore, physico-chemical treatment techniques are particularly recommended for treatment of stabilized leachate. Sequencing batch reactor (SBR) which is a type of biological treatment process and powdered activated carbon were applied for treatment of mature MLL and oil refinery wastewater (Aziz, 2011; Fakhery, 2016).

In addition, the use of coagulation-flocculation treatment technology for removing pollutants in SWW in which the chemicals such as alum, lime, ferric chloride, ferric sulphate and so on were added to the wastewater where the floc is conditioned. Among these coagulants, lime obtained a removal efficiency up to 38.9, 36.1, and 41.9% for BOD, COD and TSS, respectively (Bustillo-Lecompte and Mehrvar, 2015). Furthermore, the application of combined biological and advanced oxidation processes (AOP) is recommended for on-site slaughterhouse wastewater treatment by the researcher Bustillo-Lecompte et al. (2016).

3.3. Reusing of treated wastewater for irrigation purpose

Due to draught, dropping of ground water levels in Erbil City and using drinkable water for irrigation purpose; it is recommended to use treated wastewater for irrigation. Depending on obtained EC and total salts values, fresh TWW is not suitable for irrigation; While MWW has good quality for irrigation (Aziz and Amin, 2005). Depending on chloride values, all kinds of raw wastewaters (SWW, TWW, MWW, MLL, and DWW) cannot be reused for irrigation purpose.

Based on the described treatment methods in the previous section, application of biological treatment process (for example SBR) for treatment of SWW, MWW, and DWW are useful for achieving appropriate irrigation water quality (Surampalli et al., 1997; Azimi et al., 2005, Amin and Aziz). Adding activated carbon to SBR and trickling filters improve the quality of treated wastewater and more suitable for irrigation (Aziz, 2011, Mojiri et al., 2014; Fakhery, 2016; Ali, 2017). Treatment of MLL and TWW by using physical-chemical (coagulation-flocculation, ion exchange etc.), and adsorption added SBR and traditional returned activated sludge will result in acceptable quality of treated wastewater (Aghamohammadi et al., 2007; Ghafari et al., 2009; Bashir 2010, Aziz, 2011).

4. CONCLUSIONS

Fresh wastewater samples (SWW, TWW, MWW, MLL, and DWW) were collected and analyzed for 15 water quality parameters. TWW and MLL had low biodegradability ratio and high amount of total salts. While SWW, MWW, and DWW had high BOD/COD ratio with low amount of contaminants. Physical- chemical treatment techniques are more suitable for TWW and MLL. Biological treatment processes with adsorption are effective for treatment of SWW, MWW, and DWW and the effluent can be used for irrigation purposes.

REFERENCES

Abdalla, K. Z., and Hammam, G., 2014. Correlation between Biochemical Oxygen Demand and Chemical Oxygen Demand for Various Wastewater Treatment Plants in Egypt to Obtain the Biodegradability Indices, 13(1), 42-48.

Aghamohammadi, N., Aziz, H.A., Isa, M.H., and Zinatizadeh, A.A.L., 2007. Powdered activated carbon augmented activated sludge process for treatment of semi-aerobic landfill leachate using response surface methodology, Bioresource Technology, 98, 3570–3578.

Ali, S. M., 2017. Treatment of Erbil Municipal and Dairy Wastewater Using Activated Carbon Added to Biological Filtration Process, M.Sc. Thesis, Department of Dams and Water Resources Engineering, College of Engineering, Salahaddin University-Erbil, Iraq.

American Public Health Association (APHA), 2005. Standard Methods for the Examination of Water and Wastewater, 21st edition, American Public Health Association, Washington, DC.

Amin, K. A., and Aziz, S. Q., 2005. Feasibility of Erbil Wastewater Reuse for Irrigation, J. of Zanco, Salahaddin University-Erbil, 17(2), 63-77.

Azimi, A.A., Hashemi S.H., Bidhendi, G.N., and Mahmoodkhani, R., 2005. Aeration ratio effect on efficiency of organic materials removal in sequencing batch reactors, Pakistan Journal of Biological Sciences, 8 (1), 20–24.

Aziz, S. Q. , 2011. Landfill Leachate Treatment Using Powdered Activated Carbon Augmented Sequencing Batch Reactor (SBR) Process, PhD thesis, School of Civil Engineering, Universiti Sains Malaysia (USM), Malaysia.

Aziz, S. Q., and Ali, S. M., 2016. Performance of Biological Filtration Process for Wastewater Treatment: A review, ZANCO Journal of Pure and Applied Sciences, 28 (2), 554-563.

Aziz, S. Q., Aziz, H. A., Yusoff, M. S., Bashir, M. J. K., Umar, M. 2010. Leachate characterization in semi-aerobic and anaerobic sanitary landfills: A comparative study, Journal of Environmental Management, 91 (12), 2608-2614.

Aziz, S.Q. and Maulood, Y.I., 2015. Contamination Valuation of Soil and Groundwater Source at Anaerobic Municipal Solid Waste Landfill Site, Environmental Monitoring and Assessment. 187(12), DOI: 10.1007/s10661-015-4971-y.

Bashir M.J.K., Aziz, H.A.,Yusoff, M.S., Aziz, S.Q., and Mohajeri S., 2010. Stabilized Sanitary Landfill Leachate Treatment Using Anionic Resin: Treatment Optimization by Response Surface Methodology. Journal of Hazardous Materials, 182, 115-122.

Bashir, M. J. K., Abdul Aziz, H., Aziz, S. Q., and Abu Amr, S. S., 2012. An Overview of Wastewater Treatment Processes Optimization Using Response Surface Methodology (RSM). The 4th International Engineering Conference- Towards engineering of 21st century, p. 1-11.

Bougherira, N., Hania, A., Djabria, L., Toumia, F., Chaffaia, H., Haiedb, N., Nechema, D., Sedratia, N., 2014, Journal of Energy Procedia, 50, 692-701.

Bustillo-Lecompte, C. F. and Mehrvar M. 2015. Slaughterhouse wastewater characteristics, treatment, and management in the meat processing industry: A review on trends and advances, Journal of Environmental Management, 161, 287-302.

Bustillo-Lecompte, C., Mehrvar, M., and Quiñones-Bolaños, E., 2016. Slaughterhouse Wastewater Characterization and Treatment: An Economic and Public Health Necessity of the Meat Processing Industry in Ontario, Canada. Journal of Geoscience and Environment Protection, 4, 175-186.

Cristian, O. 2010. Characteristics of the untreated wastewater produced by food industry, Annals of University of Oradea, Fascicle: Environment, 15, 709-714.

.Dawood, A. T., Kumar, A., and Sambi, A. K., 2011. Study on Anaerobic Treatment of Synthetic Milk Wastewater under Variable Experimental Conditions, International J. of Environmental Science and Development, 2(1), 17-23.

.Deshannavar, U. B., Basavaraj. R. K., and Naik, N. M., 2012. High rate digestion of dairy industry effluent by upflow anaerobic fixed-bed reactor, J. of Chemical and Pharmaceutical Research, 4(6), 2895-2899.

.Environment Protection Agency (EPA) (2003) Standards for effluent discharge Regulations, No. 44.

.Fakhrey, E.S. , 2016. Impact of Resulted Wastewater from Kourkosk Oil Refinery (Erbil-Iraq) on Water Resources and Improvement of the Treatment Process by Adsorption Added to Biological Techniques, M.Sc. Thesis, Department of Dams and Water Resources Engineering, College of Engineering, Salahaddin University-Erbil, Iraq.

Ghafari, S., Aziz, H.A., Isa, M.H., and Zinatizadeh, A.A., 2009. Application of response surface methodology (RSM) to optimize coagulation-flocculation treatment of leachate using poly–aluminum chloride (PAC) and alum, Journal of Hazardous Materials, 163, 650–656.

Hammer, M. J., and Hammer Jr, M. J. 2014. Water and wastewater Technology, 7th edition, Pearson prentice Hall, UK.

http://www.yoruksut.com.tr/en/corporate.

Iraqi Environmental Standards, 2011. Contract No.: W3QR-50-M074, Rev. No.: 03 October.

Lateef, A., Chaudhry, M. N., and Ilyas, S., 2013. Biological treatment of dairy wastewater using activated sludge, J. of Science Asia, 39, 179–185.

.Messrouk, H., Mahammed, M. H., Touil, Y., Amrane, A., 2014. Physico-chemical Characterization of Industrial Effluents From The Town of Ouargla (South East Algeria) Journal of Energy Procedia, 50, 255-262.

.Metcalf and Eddy, 2014. Wastewater Engineering: Treatment and Reuse, 5th edition, Inc., Mc Graw-Hill, New York.

.Mojiri, A., Aziz, H.A., Zaman, N.Q., Aziz, S.Q., and Zahed, M.A. 2014. Powdered ZELIAC augmented sequencing batch reactors (SBR) process for co-treatment of landfill leachate and domestic wastewater, Journal of Environmental Management, 139, 1-14.

.Mustafa, B. Y. and Sabir, S. 2001. Reuse of Erbil City Sewage for Irrigation Purposes, Brayeti Center Erbil -Iraq, 4th year, Vol. 13.

.Myra, T., David, H., Judith, T., Marina, Y., Ricky, B. J., and Reynaldo, E., 2015. Biological Treatment of Meat Processing Wastewater using Anaerobic Sequencing Batch Reactor (ASBR), International Research Journal of Biological Sciences 4 (3), 66-75.

Shahriari, T., and Shokouhi, M. 2015. Assessment of Bio-Trickling Filter Startup for Treatment of Industrial Wastewater, Int. J. of Environ. Res., 9(2), 769-776.

.Surampalli, R.Y., Tyagi, R.D., Scheible, O.K., and Heidman, J.A., 1997. Nitrification, denitrification and phosphorus removal in sequential batch reactors. Bioresource Technolnology, 61, 151–157.

.Swati, B. R., Vedavati, P. R., and Diwan, V. V., 2012. Potential of Phytoremediation for dairy wastewater treatment, J. of Mechanical and Civil Engineering (IOSR-JMCE), Vol. 6, 16-23.

ZANCO Journal of Pure and Applied Sciences
The official scientific journal of Salahaddin University-Erbil
ZJPAS (2018) **30**(s1)s135-s141
http://dx.doi.org/10.21271/ZJPAS.30.s1.15

Darbandikhan Reservoir Operation Optimization Using Ant Colony Optimization Algorithm

[1]Mohammed Nasseh Mohammed, [2]Bnar Faisal A. Daham, [3]Kanar Shukr Mohammed

[1]Department of Surveying, College of Engineering, Salahaddin University-Erbil

[2,3]Department of Software and Informatics, College of Engineering, Salahaddin University-Erbil

A R T I C L E I N F O

Article History:
Received:14 /05/2017
Accepted:12 /04/2018
Published:01/06/2018

Keywords:
Ant Colony Algorithm
Optimization
Reservoir operation

Corresponding Author:
Email:
mohamed_nasseh@yahoo.com

mohammed.mohammed@su.edu.krd

A B S T R A C T

The importance of water resources management has unlimited scope, and from that importance comes the need for optimizing the operation of water reservoirs in terms of achieving hydropower generation demands, irrigation demands, and avoiding flood risks. There were many optimization techniques or methods have been conducted for that purpose.

In this paper we try to bring the operation of Darbandikhan reservoir (located 60 km southeast of Sulaimaniya city) to an optimum level using Ant Colony Optimization (ACO) technique. Thus, the objective is to find a monthly water release plan with least difference from the amount of water demand for that month.

This study covers the operation of the reservoir for one year, sampled into 12 monthly periods. Two methods for pheromone trail update - Iteration Best Path (IBP) and Iteration All Path (IAP) - have been used and tested in the ACO algorithm to find out how fit they are with the reservoir operation problem. Also two levels of reservoir storage discretization have been applied to the problem; 100 and 200 intervals.

Generally, the ACO algorithm showed a high performance in exploring the optimum solutions for the operation of Darbandikhan reservoir. The obtained results of the tests revealed that the IAP outperforms the IBP in finding the optimum solutions. While the tests of the two discretization resolutions showed that the 100 intervals is more efficient than the 200 intervals in getting better results with a certain number of iterations and artificial ants.

1. INTRODUCTION

Water resources planning is the management of water resources under a set of policies and regulations in order to achieve certain goals. Then when we speak of meeting goals, it is clear that we are not dealing with creation of perfection but rather with finding the best possible way of meeting aims within the limitations of resources, and being the meaning of optimization (Serafim, Lorenzo and Miodrag, 1991).

Large dams are usually built for different purposes such as urban water supply, power generation, agricultural, industrial, flood control, and environmental objectives. And recently, much research has been done to achieve certain objectives in optimal reservoir operation. The main research methodologies are about achieving the optimum level of release and optimal storage volume by considering the changes in inflow and needs (D. Nagesh and M. Janga, 2005; Rodrigo and Daniel, 1997).

Optimization techniques applied for finding optimal solutions were mostly limited by the complexities of non linear relationships in model formulation and by increase in the number of variables and constraints. As a

consequent, many heuristic and metaheuristic algorithms have been recently proposed, which can provide quite good and feasible results in an acceptable computation time (Dorian and Keith, 2005; M. R. Jalali, A. Afshar, and M. A. Mariño, 2006).

Ant Colony Optimization (ACO) Algorithm is a relatively new nature-inspired metaheuristic technique. The ACO is used in this paper as a key algorithm to find suitable and optimum operating policy for a multi-purpose reservoir system.

In the rest of the paper; a brief description about ACO and its procedure is presented first. Next, the details of the case study and model formulation for reservoir operation are explained. Finally the results are discussed, followed by the conclusions.

From literature, there is a great potential to apply ACO in the field of water resources problems. D. Nagesh and M. Janga (2005) employed ACO algorithm to derive operation policies for a multi-purpose reservoir system. M. R. Jalali et al. (2007) proposed ACO algorithms to optimize the operation of a water reservoir.

2. ACO ALGORITHM: GENERAL ASPECTS

Ant Colony Optimization (ACO) is a metaheuristic approach proposed by Dorigo (1992). ACO Algorithm is a nature-inspired algorithm and a member in the family of Swarm Intelligence Methods. It is based on the foraging behavior of ants in terms of finding the shortest possible path from their nest to the discovered food source (Marco and Christian, 2005).

Upon finding food, ants of some species return back to their nest while laying down a chemical substance called pheromone. When other ants find such a path, they will not keep scouting and travelling at random, but instead, they follow the trail.

Over time, the more time it takes for an ant to travel down the path and back again, the more pheromones have to evaporate. Whereas on short and more taken paths, pheromone density becomes higher. Thus, pheromone evaporation also has the advantage of avoiding the convergence to a locally optimal solution.

In ACO, a set of software data structures called artificial ants search for desirable solutions to a given optimization problem. To apply ACO, the problem is transformed into a weighted graph to find the best path. Those ants incrementally build solutions by moving on the graph (M. R. Jalali et al., 2007). The probability of an ant movement from state to another depends on the combination of two factors; first, the attractiveness of the move as computed by some heuristic indicating the desirability of that move, and second, the pheromone level or strength of the move, indicating how proficient it has been in the past to make that particular move (Christian, 2005).

```
Begin
Set parameters
        Initialize pheromone
        Do
        Begin
                While remains an ant
                Begin
        Put each ant at an initial state
        While remains unvisited state
        Begin
                Choose next state by applying transition rule
                Find fitness at each state
        End while
        Construct a solution for each ant
                End while
                Update pheromone by applying global pheromone updating
        Till termination condition not satisfied
End
```

Fig. 1. A pseudo-code for ant colony optimization algorithm

A probabilistic decision policy is used by the ants to direct their search towards the most interesting regions of the search space.

Let $\tau_{ij}(t)$ be the total pheromone deposited on path ij at time t, and $\eta_{ij}(t)$ be the heuristic value of path ij at time t, according to the measure of the objective function (R. Moeini and M. H. Afshar, 2009) (Marco, Gianni and Luca, 1999). Heuristic value is a measurement of objective function, which along with the pheromone (τ_{ij}), will determine the transition probability from option i to j, at time period t, as follows:

$$P_{ij}(t) = \begin{cases} \frac{[\tau_{ij}(t)]^{\alpha}[\eta_{ij}(t)]^{\beta}}{\sum_{1}^{no\ of\ classes}[\tau_{ij}(t)]^{\alpha}[\eta_{ij}(t)]^{\beta}} & if\ j \in Allowed \\ 0 & otherwise \end{cases} \quad (1)$$

Where α and β are parameters that determine the relative importance of the pheromone trail against the heuristic value.

When all ants in the colony complete their tour, the pheromone is going to be updated as follows:

$$\tau_{ij}(t) \xleftarrow{iteration} \rho * \tau_{ij}(t) + (1-\rho) * \Delta\tau_{ij} \quad 0 \le \rho \le 1 \quad (2)$$

where ρ = evaporation rate.

One the other hand, there are several ways for finding $\Delta\tau_{ij}(t)$. In this study, we used two approaches:

First Method: Iteration Best Path Pheromone Update (IBP)

In this method, the pheromone update is applied to the edges of only the best path chosen in each iteration.

$$\Delta\tau_{ij}(t) = \begin{cases} \frac{1}{G^{k_{ib}}(m)} & if\ (i,j) \in \text{tour done by ant } k_{ib} \\ 0 & otherwise \end{cases} \quad (3)$$

Where $G^{k}_{ib}\ (m)$ is the value of the fitness function for the ant that took the best tour at iteration *m*.

Second Method: Iteration All Path Pheromone Update (IAP)

In this method, the update of the pheromone is applied to the edges of every path generated during each iteration.

$$\Delta\tau_{ij}(t) = \sum_{k=1}^{M} \tau m_{ij}^{k}(t) \quad (4)$$

$$\tau m_{ij}^{k}(t) = \begin{cases} \frac{1}{G^{k}(m)} & if\ (i,j) \in T^{k}(m) \\ 0 & if\ (i,j) \notin T^{k}(m) \end{cases} \quad (5)$$

Where $G^{k}(m)$ is the value of the fitness function for the tour $T^{k}(m)$ taken by the *k-th* ant at iteration *m* (M. R. Jalali, A. Afshar, and M. A. Mariño, 2006).

3. CASE STUDY DESCRIPTION

Derbendikhan Dam is located on the Diyala Sirwan river approximately 65km south-east of Sulaimaniyah and 230km north-east of Baghdad, situated at latitude 35°6'46"N and longitude 45°42'24"E. It was constructed between 1956 and 1961 for several purposes including: hydroelectric power production, irrigation, and flood control.

Darbendikhan Dam with the 128m high embankment has a total design capacity at normal operating level (El. 485.00m) of 3,000 Mm³, of which 2,500 Mm³ is live storage and 500 Mm³ being dead storage (SMEC International Pty., 2006).

In this paper, the study has been accomplished on the operation of the dam in the year 2015, during which the live storage of the reservoir has a minimum and maximum range from 950Mm^3 to 1500Mm^3 of water, respectively. The monthly inflow and demand data of the dam have also been collected for 2015. So the focus will be on the storage and release amounts, then finding the optimal minimum demand deficit as an objective.

4.1 Model Application

It was observed that the storage capacity in 2015 was ranging between 950Mm^3 and 1500Mm^3, hence, in this study a range from 900Mm^3 to 1700Mm^3 has been taken and discretized into intervals. Two levels of resolution were applied on the intervals, 100 classes; 8Mm^3 per each interval and 200 classes; 4Mm^3 per each interval.

A predefined number of artificial ants as solution makers are placed on random classes in the first period. Then each of them is starting to decide which path to take. They select the transition edge from a storage class in time period *t* to another storage class in time period *t*+1, depending on two main factors:

First: The desirability (heuristic) of that transition edge, in terms of obtaining the minimum difference between the released and the amount of water demand at that period.

Second: The rank (pheromone trail) of that edge, which has been possibly gained from previous successful ants' movement across that edge. There are different strategies for promoting the edges. Figure 2 shows the

discretized graph and an artificial ant when making decisions to find its path.

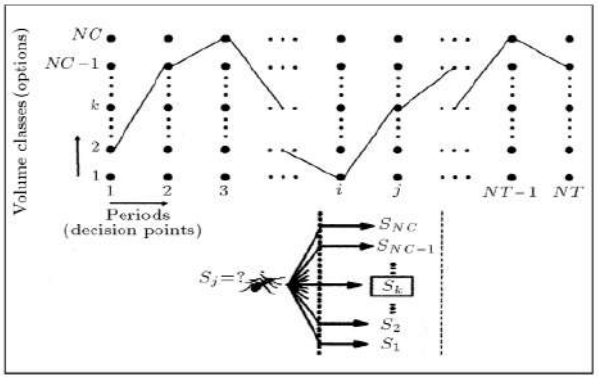

Fig. 2. Discretizaed graph and an artificial ant when making decisions to find its path

4.2 Heuristic Information

The heuristic information η_{ij} (t) of the problem in this paper is determined by considering the criterion as minimum deficit.

$$\eta_{ij}(t) = \frac{1}{\left[\frac{R_{ij}(t)-D(t)}{D(t)}\right]^2 + c} \quad \text{for all } t = 1, 2, \dots, \text{NT} \qquad (6)$$

Where R_{ij} *(t)* = release at period t, depending on the initial and final storage volume at classes *i* and *j*, respectively; *D(t)* = demand of period *t*; and *c* = a constant for irregularity avoiding (i.e. division by zero).

However, the continuity equation expressed below is used to determine R_{ij} *(t)*

$$R_{ij}(t) = S_i - S_j + I(t) \qquad (7)$$

Which is subject to the following constraints:

$$S_{min} \le S_i \le S_{max} \qquad (8)$$
$$S_{min} \le S_j \le S_{max} \qquad (9)$$

Where S_i and S_j = initial and final storage volumes in terms of classes *i* and *j*, respectively. *I(t)* = inflow to the reservoir at time period *t*. S_{min} and S_{max} = minimum and maximum storage allowed respectively.

4.3 Fitness Function

The goodness of the generated solutions is measured according to a defined fitness function. In this paper, the minimum value of the total square deviation (TSD) has been taken as the objective function:

$$TSD^k = \sum_{t=1}^{NT} \left[\frac{(R^k(t)-D(t))}{D(t)}\right]^2 \qquad (10)$$

Where $R^k(t)$ = release at period *t* recommended by ant *k*, and *NT* = total number of periods.

5. TESTS AND RESULTS

For testing this model, several approaches and considerations were conducted. First point to be mentioned is that Java Programming Language is used in writing the source code of this model. Then, two phases of tests have been carried out including Parameters Tune-Up and Ants-Iterations tests.

Furthermore, both of the strategies of pheromone trail update were implemented at each level of the mentioned tests. Those strategies are IBP (promotes the edges of only the best path per iteration) and IAP (promotes the edges of every taken path per iteration).

5.1 Parameters Tune-Up

Hereby, the tests have been accomplished through tuning the main parameters used in ACOA, namely, α (determines the importance of the pheromone trail), β (determines the strength of the heuristic value), and ρ (determines the amount of pheromone increment or evaporation). Those tests have been conducted on only the 100-Class model with the number of ants and iterations being fixed to 5 and 500 respectively. Whereas the parameter were tuned up within the following ranges (α = [1, 2, 3, 4], β = [1, 2, 3, 4], ρ = [0.1, 0.5, 0.9]). The results of each set of parameters as shown in Table 1 have been acquired through 10 runs of the algorithm.

As it could be observed from Table1, the model of 100 classes provided optimum results for the IBP method of pheromone update when the parameters were tuned to (α=3, β=1, and ρ=0.1), resulting in a mean total square deviation of 0.105 units. While for the IAP

method of pheromone update, the optimum mean of total square deviation of 0.043 units was obtained when tuning the parameters to (α=3, β=1, and ρ=0.9). Figure 3 shows mean TSD results for parameters tune-up for both IBP and IAP methods in 100-Class model.

Table 1. TSD results for parameters tune-up for IBP and IAP methods in 100-Class model

	IBP Method				IAP Method			
α, β, ρ	Best	Worst	Mean	SD	Best	Worst	Mean	SD
4,1,0.1	0.053	0.353	0.135	0.086	0.05	0.113	0.08	0.021
4,1,0.5	0.075	0.275	0.183	0.057	0.043	0.108	0.081	0.018
4,1,0.9	0.103	0.62	0.349	0.191	0.04	0.073	0.052	0.011
3,1,0.1	0.06	0.142	0.105	0.027	0.051	0.191	0.127	0.041
3,1,0.5	0.042	0.236	0.157	0.056	0.048	0.147	0.104	0.033
3,1,0.9	0.103	0.61	0.287	0.172	0.026	0.056	0.043	0.010
2,1,0.1	0.077	0.21	0.142	0.039	0.083	0.239	0.171	0.051
2,1,0.5	0.063	0.205	0.147	0.049	0.133	0.245	0.182	0.035
2,1,0.9	0.167	0.61	0.317	0.154	0.036	0.112	0.07	0.028
1,1,0.1	0.051	0.177	0.119	0.044	0.141	0.428	0.252	0.102
1,1,0.5	0.11	0.254	0.166	0.049	0.09	0.322	0.226	0.066
1,1,0.9	0.167	0.612	0.362	0.148	0.037	0.112	0.076	0.029
1,2,0.1	0.087	0.177	0.141	0.031	0.132	0.716	0.332	0.181
1,2,0.5	0.079	0.327	0.17	0.068	0.152	0.401	0.303	0.090
1,2,0.9	0.167	0.498	0.313	0.139	0.073	0.166	0.119	0.028
1,3,0.1	0.066	0.258	0.128	0.058	0.137	0.482	0.318	0.126
1,3,0.5	0.123	0.353	0.226	0.083	0.126	0.284	0.201	0.054
1,3,0.9	0.167	0.612	0.351	0.156	0.091	0.139	0.114	0.016
1,4,0.1	0.054	0.177	0.109	0.042	0.167	0.472	0.282	0.104
1,4,0.5	0.043	0.251	0.146	0.063	0.091	0.544	0.288	0.144
1,4,0.9	0.167	0.61	0.32	0.165	0.111	0.21	0.179	0.027

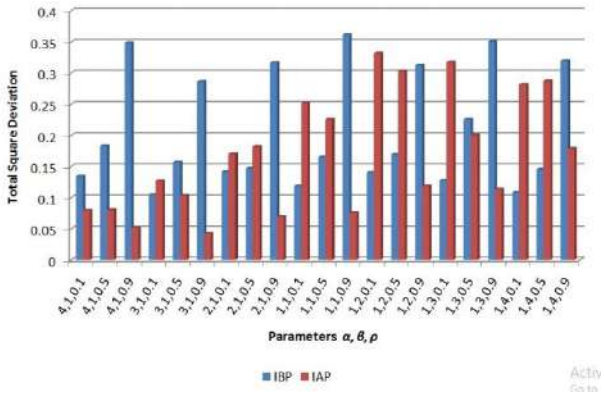

Fig. 3. TSD results for parameters tune-up for IBP and IAP methods in 100-Class model

5.2 Ants-Iterations

In this test the performance of the algorithm has been measured in terms of the number of artificial ants that are generating solutions and the number of iterations or trials they make to find better solutions.

In this phase, the models with both discretization resolutions 100-Class and 200-Class have been tested, and each type of them has been considered with IBP and IAP pheromone updating methods. However, the parameters α, β, and ρ were fixed upon the optimum tunes recorded in the previous test. The numbers of ants and iterations taken for this test were: Ants=[10, 20, 50], Iterations=[50, 100, 500]. The results of each combination of ants and iterations are shown in Table 2 and Table 3, where the best and worst results came out from 10 runs of each combination have been stated, in addition to the mean and standard deviation of the results acquired from those runs.

Table 2. TSD results for different number of ants and iterations using both IBP and IAP methods in 100-Class model

Iterations	Status	Number of Ants (IBP)			Number of Ants (IAP)		
		10	20	50	10	20	50
50	Best	0.167	0.167	0.167	0.088	0.073	0.042
	Worst	0.765	0.472	0.353	0.177	0.116	0.085
	Mean	0.454	0.291	0.216	0.118	0.100	0.065
	SD	0.212	0.137	0.085	0.035	0.019	0.016
100	Best	0.167	0.167	0.167	0.047	0.062	0.042
	Worst	0.61	0.472	0.472	0.073	0.085	0.117
	Mean	0.330	0.279	0.206	0.059	0.072	0.073
	SD	0.160	0.118	0.107	0.010	0.009	0.027
500	Best	0.167	0.167	0.167	0.035	0.03	0.029
	Worst	0.472	0.472	0.472	0.056	0.063	0.066
	Mean	0.278	0.231	0.206	0.045	0.045	0.043
	SD	0.110	0.117	0.107	0.009	0.014	0.014

Table 3. TSD results for different number of ants and iterations using both IBP and IAP methods in 200-Class model

Iterations	Status	Number of Ants (IBP)			Number of Ants (IAP)		
		10	20	50	10	20	50
50	Best	0.348	0.246	0.162	0.089	0.066	0.066
	Worst	0.844	0.76	0.406	0.163	0.202	0.162
	Mean	0.608	0.403	0.283	0.127	0.112	0.103
	SD	0.219	0.219	0.101	0.022	0.041	0.031
100	Best	0.246	0.162	0.162	0.052	0.05	0.04
	Worst	0.605	0.348	0.348	0.115	0.104	0.117
	Mean	0.358	0.251	0.260	0.084	0.082	0.077
	SD	0.143	0.074	0.076	0.027	0.018	0.025
500	Best	0.162	0.162	0.162	0.032	0.028	0.026
	Worst	0.471	0.348	0.295	0.051	0.05	0.059
	Mean	0.279	0.252	0.213	0.040	0.039	0.039
	SD	0.125	0.089	0.057	0.006	0.008	0.009

Table 2 and Table 3 demonstrate that for a certain number of iterations, the more ants were used for searching the solutions the better mean total square deviation is acquired. That means the 50 ants find out better results than 10 ants. Also for a determined number of ants, better value for the mean total square deviation is obtained as the number of iterations used for searching the solutions is increased. This means 500 iterations bring better results than 50 iterations.

On the other hand, the results achieved by IAP method for pheromone update are better than those of IBP method, for a certain number of ants and iterations in both methods.

Also, one can notes that no significant improvements have been made in the results when 200-Class model is used instead of 100-Class model, especially with 500 iterations. Table 4 lists the amounts of water demand of Darbandikhan reservoir for 2015 in terms of 12 months with the optimized release (in million M^3) suggested by the four different approaches applied in this study. Also Figure 4 illustrates the content of Table 4, showing the performance of the four proposed models admitting how optimum results are acquired.

Table 4. Water demand for 2015 with the optimized suggestion of release in million M3 using the four different approaches

	Jan	Feb	Mar	Apr	May	Jun	Jul	Aug	Sep	Oct	Nov	Dec
Demand	163	75	80	65	79	151	247	231	92	67	113	85
100-Class IBP	166	73	79	62	82	127	245	230	92	64	114	75
100-Class IAP	166	73	79	62	74	151	237	214	92	64	114	83
200-Class IBP	166	73	79	74	82	131	245	230	92	68	114	75
200-Class IAP	162	73	79	66	70	147	225	202	92	68	114	83

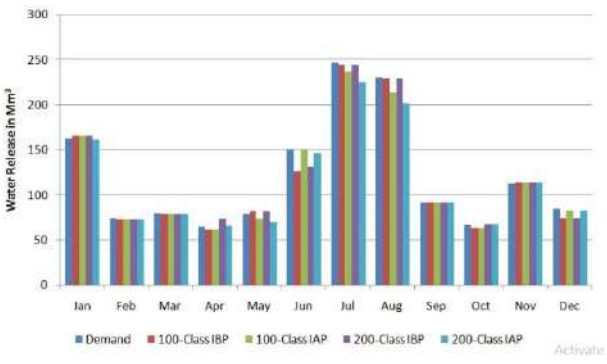

Fig. 4. Optimized water release using the four approaches compared with the demand during the 12-month periods of 2015

6. CONCLUSIONS

After accomplishing this study, there are some notes to be mentioned and some outputs to be remarked and highlighted.

- The key objective of this study is to invest and apply optimization algorithms and techniques on local problems. Darbandikhan dam, being one of the largest three water reservoirs in Kurdistan Region - Iraq, needs to be studied and focused on to get an optimal strategy for its operation.
- Best results for the 100-Class model, were obtained when it is tuned on (α=3, β=1, and ρ=0.1) for IBP method and (α=3, β=1, and ρ=0.9) for IAP method.
- For the 100-Class model the IAP method showed better performance resulting in a mean total square deviation of 0.043 units, while the IBP result was 0.105 units.
- For both the 100 and 200 classes models, increasing the number of ants with a certain number of iterations or the opposite, results in getting better mean total square deviation values.
- Iteration All Path (IAP) method in both 100-Class and 200-Class models of reservoir operation optimization gave better total square deviation results than Iteration Best Path (IBP) method.
- Discretization the reservoir storage into 200 intervals resolution doesn't give better solutions than 100 intervals due to the optimality reached in the last one
- Large number of solutions probabilities (paths) existing in the 200 intervals makes it harder to reach the same results of the 100 intervals with the same number of iterations or ants.
- Generally, the results from all of the four proposed models showed the high level of optimization achieved between the amount of water demand of each month and the suggested amount of water release for the same month.
- Finally, the results of this research work show that ACO algorithm will be an active

approach for establishing optimum reservoir operation and water resources management.

7. RECOMMENDATIONS

The following recommendations are stated:

- Applying different algorithms for reservoir operation of Darbandikhan dam.
- Extending the study to include more data collected of the reservoir (minimum and maximum cases).
- Extending the study for optimizing hydro-electric power generation of the dam.

8. ACKNOWLEDGEMENT

We would like to express our gratitude to Dams and Water Resources Engineering Department specially, assistant professor Faisal A. Daham and Dr. Sarhang Mustafa who gave us the opportunity to accomplish this valuable study and supported us along the way to finish this study.

Also, many thanks to General Directorate of Dams and Reservoirs specially engineer Bery Faisal A. Daham who provided us with the necessary data about Darbandikhan Dam.

9. REFERENCES

Christian Blum (2005) 'Ant Colony Optimization: Introduction and Recent Trends', *Physics of Life Reviews 2*, 353–373, Elsevier B.V. All rights reserved Optimization, *Massachusetts Institute of Technology*, Artificial Life 5: 137–172

D. Nagesh Kumar and M. Janga Reddy (2005) 'Ant Colony Optimization for Multi-Purpose Reservoir Operation', Water Resources Management, No. 20: 879–898, ©Springer 2006

Dorian Gaertner and Keith Clark (2005) '2On Optimal Parameters for Ant Colony Optimization algorithms', Dept of Computing, Imperial College London, 180 Queens Gate, London, SW7 2AZ, UK

M. R. Jalali, A. Afshar, and M. A. Mariño (2006) 'Reservoir Operation by Ant Colony Optimization Algorithms', Iranian Journal of Science & Technology, Transaction B, Engineering, Vol. 30, No. B1, © Shiraz University

M. R. Jalali, A. Afshar, M. A. Mariño, and Hon.M.Asce (2007) 'Multi-Reservoir Operation by Adaptive Pheromone Re-initiated Ant Colony Optimization Algorithm', International Journal of Civil Engineering, Vol. 5, No. 4

Marco Dorigo and Christian Blum (2005) 'Ant Colony Optimization Theory: A Survey', Theoretical Computer Science 344, 243 – 278

Marco Dorigo, Gianni Di Caro, and Luca M. Gambardella (1999) 'Ant Algorithms for Discrete Optimization', Massachusetts Institute of Technology, Artificial Life 5: 137–172

R. Moeini and M.H. Afshar (2009) 'Application of an Ant Colony Optimization Algorithm for Optimal Operation of Reservoirs: A Comparative Study of Three Proposed Formulations', Transaction A: Civil Engineering, Vol. 16, No. 4, pp. 273-285, ©Sharif University of Technology

Rodrigo Oliveira and Daniel P. Loucks (1997) 'Operating Rules for Multireservoir Systems', Water Resources Research, Vol. 33, No. 4, Pages 839-852

Serafim Op., Lorenzo Ec., and Miodrag Is. (1991) 'An Optimization Procedure for Water Reservoir Planning', Yugoslav Journal of Operations Research, No. 2, Pages 225 – 233.

SMEC International Pty. Ltd., (31July 2006) Dokan and Derbendikhan Dam Inspections, World Bank.

ZANCO Journal of Pure and Applied Sciences
The official scientific journal of Salahaddin University-Erbil
ZJPAS (2018) **30**(s1)s142-s151
http://dx.doi.org/10.21271/ZJPAS.30.s1.16

Hydraulic Performance of the Control Butterfly Valves of the Bottom Outlet of Kassa Chai Dam

[1]Riyadh Zuhair Azzubaidi, [2]Ne'emat Mustafa Majeed

1Professor of water resources, Department of Water Resources, College of Engineering University of Baghdad

2 M. Sc. student, Department of Water Resources, College of Engineering University of Baghdad, Bagdad, Iraq

A R T I C L E I N F O

Article History:
Received: 14/05 /2017
Accepted: 12/ 04/2018
Published: 01/06/2018

Keywords:
vibration
hydraulic performance
butterfly valves
negative pressure
Fluent
cone valve

**Corresponding Author:*
Email: azzubaidi@hotmail.com

A B S T R A C T

The bottom outlet of Kassa Chai Dam, Kirkuk, Iraq was designed and constructed to control the storage outflow by using two 1.4m diameter butterfly valves at its end two branches. During the dam commissioning, a series of operation tests were conducted on the bottom outlet under different openings of its valves. Intense noise and vibration were noticed and reported at these valves. To specify the causes of these intense noise and vibration and to propose solutions to eliminate them, the velocity profiles and pressure variations along the bottom outlet of Kassa Chai Dam and at its valves were investigated. A full-scale 3D mathematical model for the bottom outlet was analyzed by using the commercial CFD code Fluent. CFD Fluent based on solving Navier-Stock equations by finite volume method. The standard k-ε turbulence model was selected to deal with turbulence. Simulations were carried out under different operation conditions, including different water levels of the dam reservoir and different angles of the valves opening as well. Outline from study showed that negative pressures developed at the downstream side of the valve especially at small angles of valve openings. To overcome the problem of negative pressure, a suitable solution is suggested to improve the outlet performance by installing a cone valve at the downstream end of the bottom outlet. Results of investigation when using the cone valve showed that no negative pressure developed at the end of the bottom outlet.

INTRODUCTION

Butterfly valves are used to control the outflow of the bottom outlet of Khassa Chai Dam, which is located north-east of Kirkuk City, Iraq. During the dam commissioning, intensive noise and vibrations at these valves were noticed and reported that can affect the safety of the dam. This problem may be due to high flow velocities and negative pressures developed at valves causing cavitation (FEMA, 2010).

Generally, this work aimed at studying the reported problem of the noise and the vibrations at the control valves of bottom outlet of Khassa Chai Dam. The hydraulic performance of the bottom outlet of was investigated. The investigation includes analyzing the profile of the velocities of the flow and the variation of the pressure along the bottom outlet of the dam and at its control valves. This investigation was carried out under different reservoir levels and different valve openings by using Computational Fluid Dynamics, CFD, code Fluent. The investigation helped in understanding and specifying the cause of the noise and vibrations, and suggesting a solution to get rid of the problem.

There exist many studies that were conducted to study the velocities and pressure variations of the flow at butterfly valves by the aid of ANSYS Fluent Computational Fluid Dynamics software, such as Brett et al., 2011, Nazary et al., 2011, Toro, 2012, Dawy et al., 2013, and Elbakhshawangy et al., 2015. These studies indicated that CFD was able to model the general behavior of flow around a butterfly valve for different angles of valve opening.

THE BOTTOM OUTLET OF KHASSA CHAI DAM

The bottom outlet of Khassa Chai Dam consists of an intake with a 13m vertical shaft and a 304.5m steel pipe of 2m in diameter coated with reinforced concrete. The steel pipe is then divided into two identical branches at its end, **Figure 1**. Each branch is a steel pipe of 1.4m diameter provided with two butterfly valves mounted in series. The first butterfly valve is used for emergency and maintenance purposes that is kept fully opened during normal operation. The second valve is used to control the outflow discharges.

Operating one branch of the bottom outlet of Khassa Chai Dam will develop high velocities compared to that when operating two branches. Therefore, the case of operating one branch represents the worst case of the problem of noise and vibration at the butterfly valve and is the case considered in this paper.

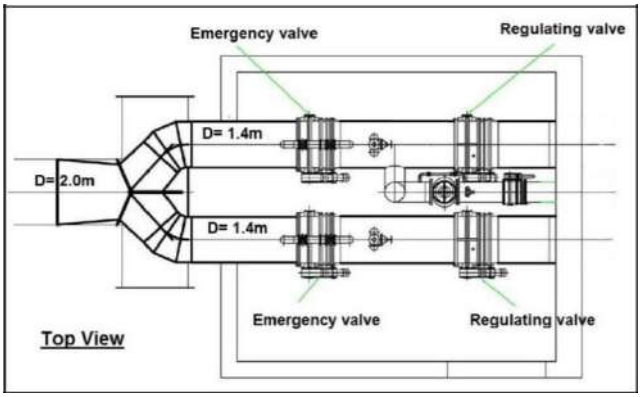

Figure 1. General layout of the chamber of the bottom outlet valves.

THE GOVERNING EQUATIONS

ANSYS Fluent solves numerically the governing equations of steady, incompressible three-dimensional flow. These equations are the continuity and Navier-Stokes equations, which are based on principles of physics mass conservation and Newton's Second Law within a moving fluid. Continuity and Navier-Stokes equations are described by Eq. (1) and (2) respectively:

$$= 0 \quad (1)$$

$$2)$$

In turbulent flow condition, FLUENT provides several turbulent models to solve such as Spalart-Allmaras, k-ε, k-ω, large eddy simulation (LES), and Reynolds stress model (RSM). This study will focus on using the k-ε model which is a semi-empirical two equation model. The simplicity of this model, its robust and reasonable accuracy explains its popularity (Versteeg and Malalasekera, 1995). It relates the turbulent kinetic energy k and its turbulent dissipation rate ε with the turbulent viscosity μ_t. The transport equations for the standard k-ε model are described by the following equations:

$$(3)$$

$$(4)$$

Where is the turbulent viscosity modeled as:

$$= \quad (5)$$

, , 1, 2 *and* are empirical constants having the following default values and their values are:(= 1.0, = 1.3, 1 = 1.44, 2 = 1.92, = 0.09)

And

, = Velocities vectors, m/s.
= Space dimensions, m.

μ= Liquid dynamic viscosity, kg/ms.
k = turbulent kinetic energy, m^2/s^2.
ε = turbulent dissipation rate, m^2/s^3. ρ= Liquid density, kg/m^3.
P= Pressure, N/m^2.

CFD ANALYSIS PROCESS APPLIED TO KHASSA CHAI DAM

The process to perform a CFD analysis generally includes a pre-processing, solver, and post processing. Pre-processing involves the definition of the geometry of the flow domain, mesh generation and definition of the materials and setting appropriate boundary conditions. In the solver process the governing flow equations are solves for flow system. The post processor includes results visualization for appropriate graphical representations, such as vector plots, contour plots, streamlines, or data curves etc.

Operating one branch as the worst case that may cause the vibration. Therefore, one branch was taken into consideration. The flow domain of Khassa Chai Dam was modeled using CAD package, Solidworks. Depending on the angle of the opening of the butterfly valve, seven full scale 3D models were generated. Each of these models have a different opening of the butterfly valve.

The commercial package, GAMBIT 2.4.6, was used to create a high quality unstructured tetrahedral mesh. Tetrahedral mesh can be used with adaptive mesh refinement especially at the complex geometry of the butterfly valve. By using the GAMBIT, the bottom outlet was divided into several segments having different mesh sizes. The smaller mesh size was used at the end of the bottom outlet and at the valves where the flow conditions are highly changed and to increasing the mesh quality. **Figure 2** shows a close-up view of the generated model and the generated mesh at the location of the the butterfly valve. The model meshes consist of about 3 to 4 million cells with gradual elements sizes.

The angles of the butterfly valve opening that were taken into consideration are 5, 15, 30, 45, 60, 75 and 90 degrees. Different values of inlet pressure head were applied for each of the seven models. The applied values of the pressures cover the range of water levels between the minimum to the maximum. Five elevations of reservoir water were considered including the maximum of 495 m.a.m.s.l, the minimum of 466 m.a.m.s.l, and three other levels of reservoir levels of 472, 479, and 486 m.a.m.s.l. The elevation of the inlet of the bottom outlet is 461 m.a.m.s.l. So that the pressure heads at the entrance of the bottom outlet as an upstream boundary condition are 5, 11, 18, 25, and 34 m. Descriptions of the simulations under the different valve openings and reservoir levels are summarized by **Fig. 3**.

The pressure at the end of the bottom outlet was set to be at 1 atmosphere. The valve body and the pipe wall were set as wall boundary condition. The water density ρ is set to 998.2 kg/m^3 and its dynamic viscosity μ is 0.001kg/ms.

Once all the parameters of system of the bottom outlet of Khassa Chai Dam are identified, the system is set to be solved by using CFD code Fluent. A high-performance computer was used for this purpose to handle the large number of the mesh elements. A minimum residual target of 10^{-4} was set as solution convergence criteria.

Appropriate graphical representation of gained results of simulations was used. Vector field plots and shaded contour plots were used for the representation of the profiles velocities and the variation of pressures, respectively.

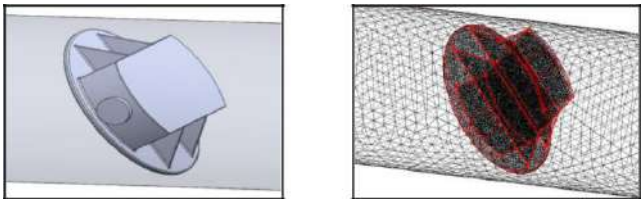

(a) (b)

Fig.2. The model and mesh of the Butterfly valve.

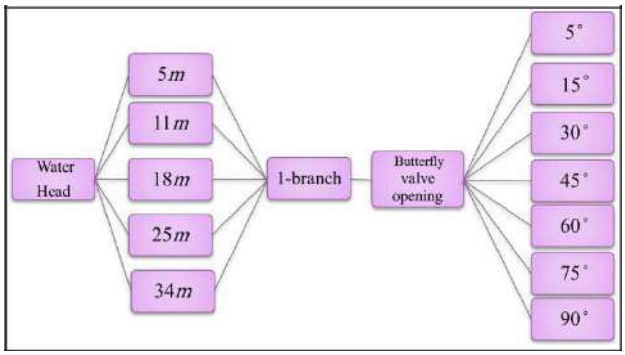

Fig.3. Design of simulation models.

RESULTS AND ANALYSIS

Figures 4 to **8** show the profiles of the flow velocities at the butterfly valve for different angles of valve opening (θ) and different values of pressure at the bottom outlet entrance. The profiles of the flow velocity are affected by changing the valve opening angle much more than changing the pressure at inlet of the bottom outlet. At small opening angles, a flow jet was created because of the small flow area between the pipe and the valve disk edges. As the valve opening is increase, the streamlines at the downstream side of the valve is becoming uniform. This is an indication that the disturbance is greatly reduced when increasing the angle of valve opening. The maximum obtained velocity is 39.23 m/s. This value was obtained with the angle of opening of 75 degree and the pressure at the inlet of 34 m. The maximum velocity value at the valve obtained at this angle of opening at the top edge of disc of the valve, **Figure 9**.

Figures 10 to **14** show the pressure variation at the butterfly valve for different angles of the valve opening and different values of pressure at the inlet of the bottom outlet. It is clear that the angle of opening affects the pressure variation at the valve much more than the pressure at the inlet of the bottom outlet. The highest values of pressure always occur at the upstream side of the valve disc and the pressure values significantly decreased at the valve edges, these results were agreed with the results of (Elbakhshawangy et al., 2015). Low negative pressure values existed in the downstream region immediately behind the valve and then the pressure increased again by getting far from the valve in the downstream region. By increasing the valve opening angel, the pressure difference at both sides of the valve decreases. The minimum negative pressure values at the butterfly valve is about -99 m that was obtained with the angle of opening of 75^{o} and the pressure at the inlet of 34 m.

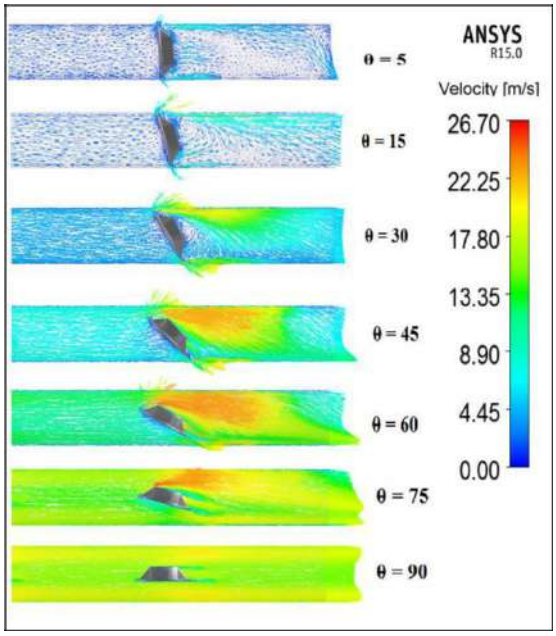

Fig.4. The velocity profiles at the butterfly valve, pressure head at inlet is 5m.

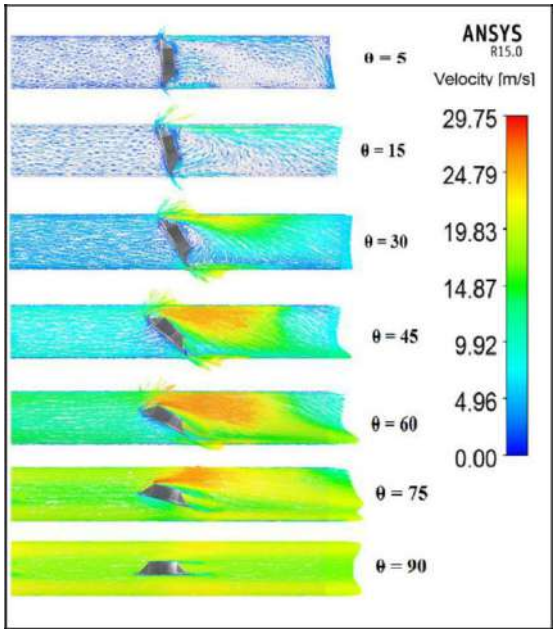

Fig.5. The velocity profiles at the butterfly valve, pressure head at inlet is 11m.

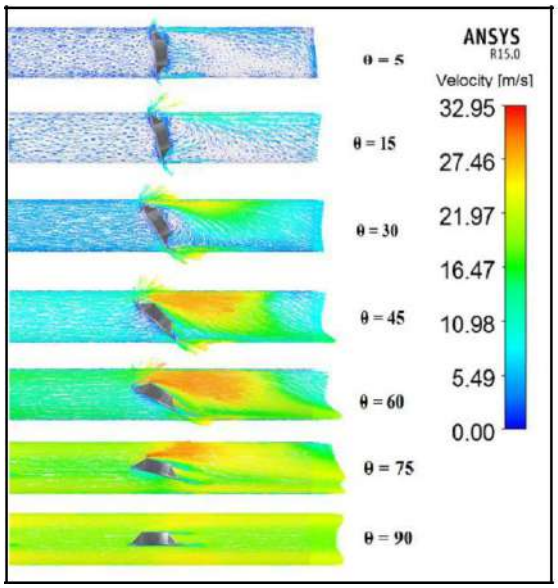

Fig.6. The velocity profiles at the butterfly valve, pressure head at inlet is 18m.

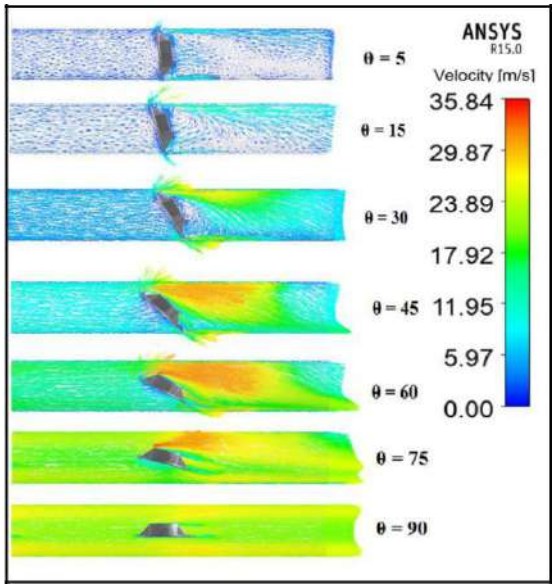

Fig.7. The velocity profiles at the butterfly valve, pressure head at inlet is 25m.

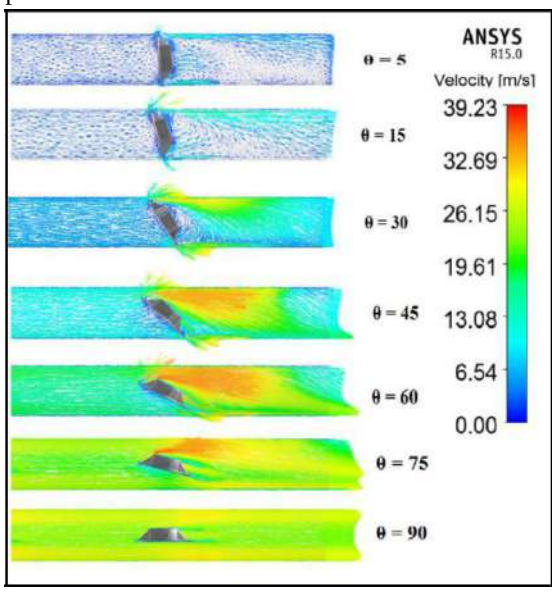

Fig.8. The velocity profiles at the butterfly valve, pressure head at inlet is 34m.

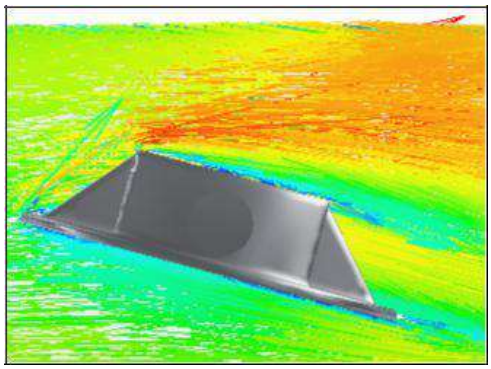

Fig.9. Close up side view, showing the flow velocity at the valve at angle of opening of 75^{o}.

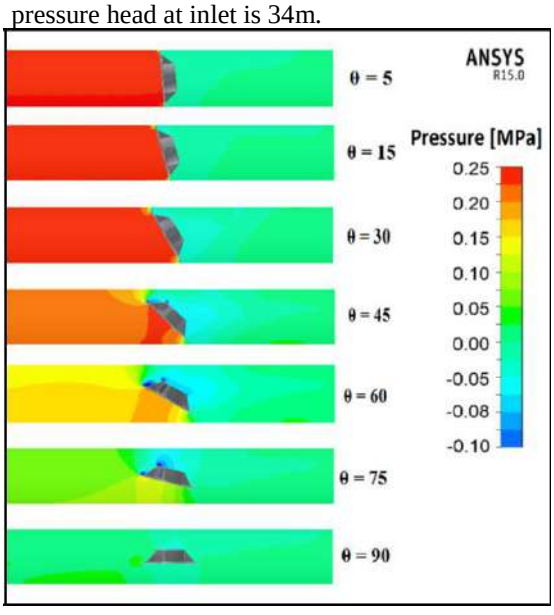

Fig.10. The pressure variation at the butterfly valve, pressure head at inlet is 5m.

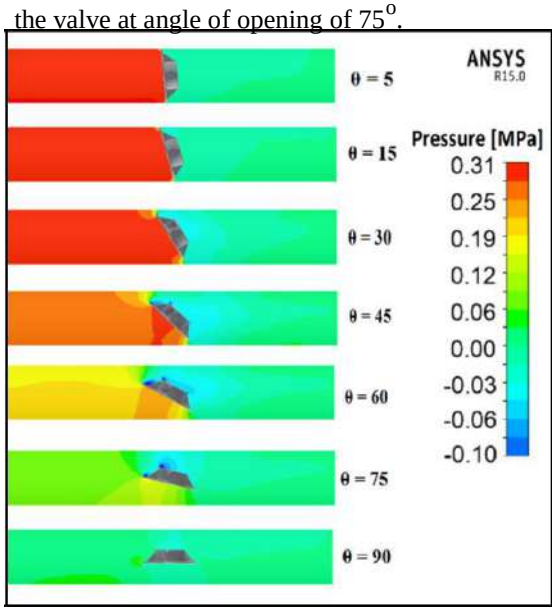

Fig.11. The pressure variation at the butterfly valve, pressure head at inlet is 11m.

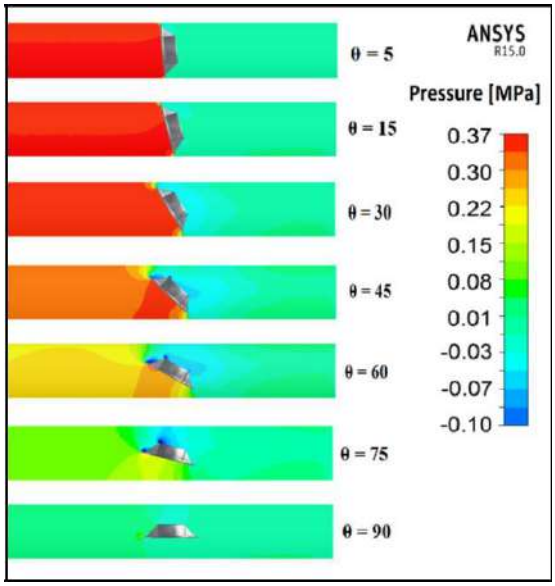

Fig.12. The pressure variation at the butterfly valve, pressure at inlet is 18m.

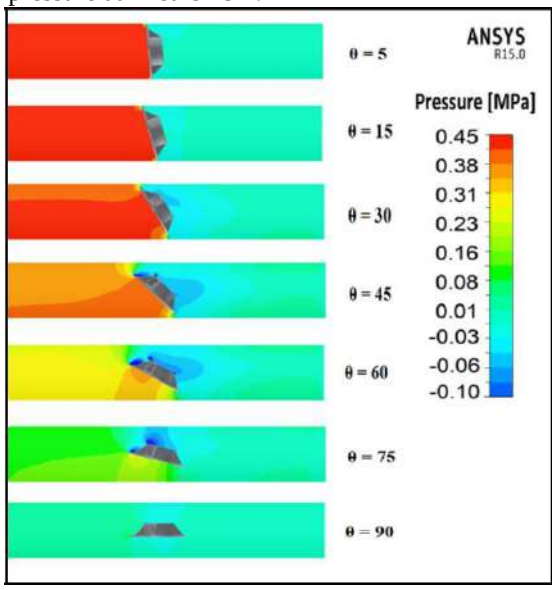

Fig.13. The pressure variation at the butterfly valve, pressure head at inlet is 25m.

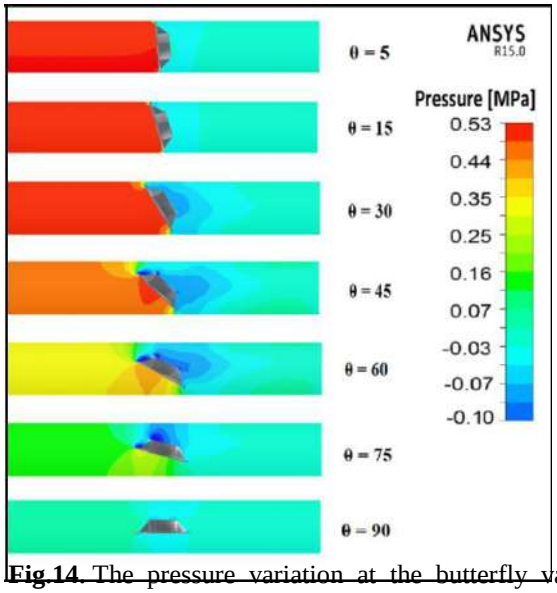

Fig.14. The pressure variation at the butterfly valve, pressure head at inlet is 34m.

Due to the high flow velocities and the development of low negative pressure at the control valves of Khassa Chai Dam, it seems that it was not desirable to use the butterfly valves to control the outflow of the bottom outlet of the dam. "Normally butterfly valves are used as on-off valves and are usually installed in a valve chamber onthe water side of bottom outlet lines in dams or in gravity lines leading to water treatment plants-or hydro power plants. In dam applications, control valves such as needle valves or fixed cone valves are installed after the butterfly valves on the air side. These valves always work as flowregulating or control valves. Unlike butterfly valves or gate valves assuming only shut-off functions in pipeline systems, needle valves and fixed cone valves can meet the requirements of regulating operations" (Oppinger, 2007).

It was suggested to install a fixed cone valve to control outflow of the bottom outlet and to disperse the outflow of water into the atmosphere. This solution minimizes the costs and structural work required to modify the constructed bottom outlet of Khassa Chai Dam. The cone valve consists of a cylindrical shell and a system of equally spaced vanes, and the cone. The vanes are attached radially to the shell and cone. The cylindrical sleeve is opened and closed by means of a pair of hydraulic pistons (Fagerburg, 1983). ROSS VALVE MFG. CO. fixed cone valve model, **Figure 15**, was adopted as the suggested solution to reduce the flow velocities and eliminate negative pressures developed at the end of the bottom outlet. This valve has radially four vanes where there are no horizontal position vanes.

Fig.15. Ross cone valve

The flow of the bottom outlet was reanalyzed when using the suggested cone valve installed at the end of the bottom outlet. The analysis was carried out with different water levels of the reservoir and different cone valve openings, while the butterfly valves were set at fully open position. Descriptions of the simulations under the different valve openings and under different operation condition of pressure head at the entrance of the bottom outlet are summarized by **Figure 16**.

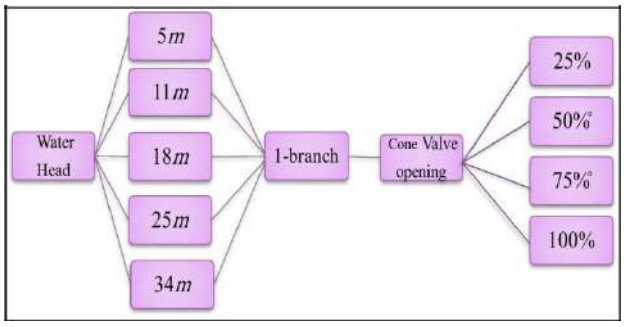

Fig.16. Design of simulation models with the suggested cone valve.

Figures 17 to **21** show the velocity profiles at cone valve region at different cone openings. The velocity profile is uniform. The maximum velocity of the flow is about 31.6 m/s was obtained with the valve of opening of 25% and 50% and the pressure at the inlet of 34 m.

Figures 22 to **26** show the pressure variations at the cone valve at different cone openings. It is clear that the negative pressure is eliminated at end of the bottom outlet except at some points at the edges of the butterfly valve under the condition of large cone openings, **Figure 27**.

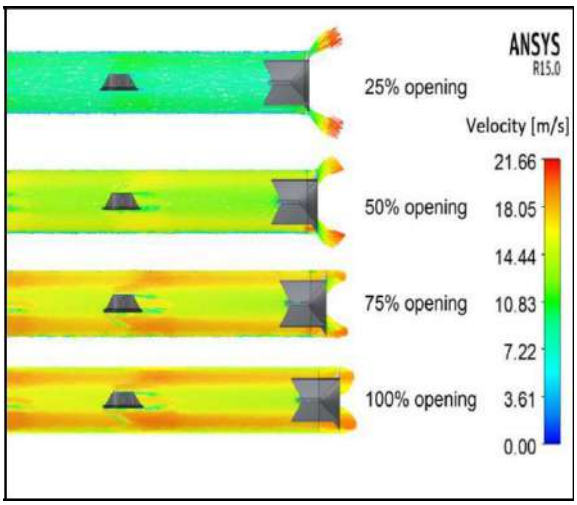

Fig.17. The velocity profiles at the butterfly and cone valves, pressure head at inlet is 5m.

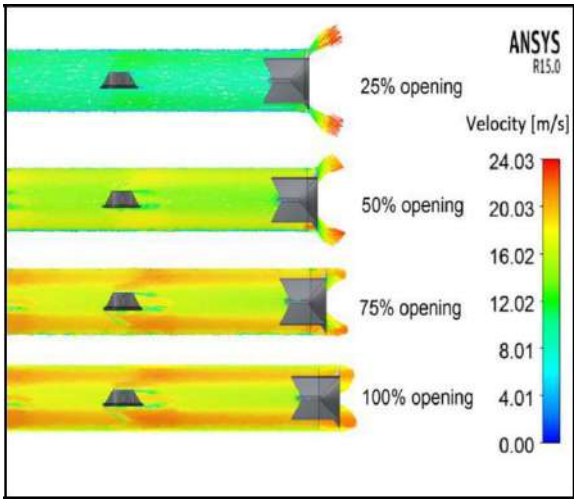

Fig.18. The velocity profiles at the butterfly and cone valves, pressure head at inlet is 11m.

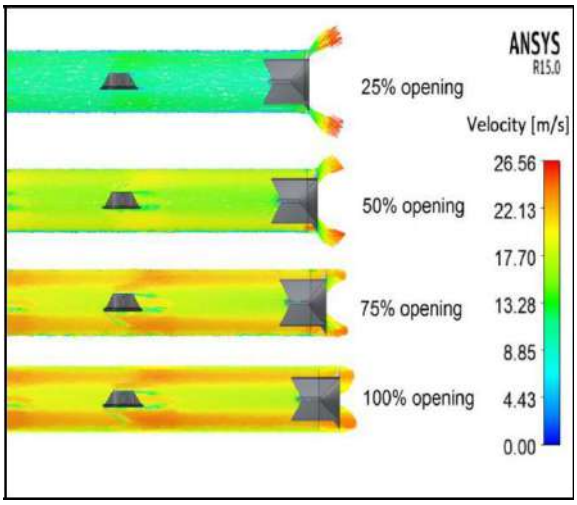

Fig.19. The velocity profiles at the butterfly and cone valves, pressure head at inlet is 18m.

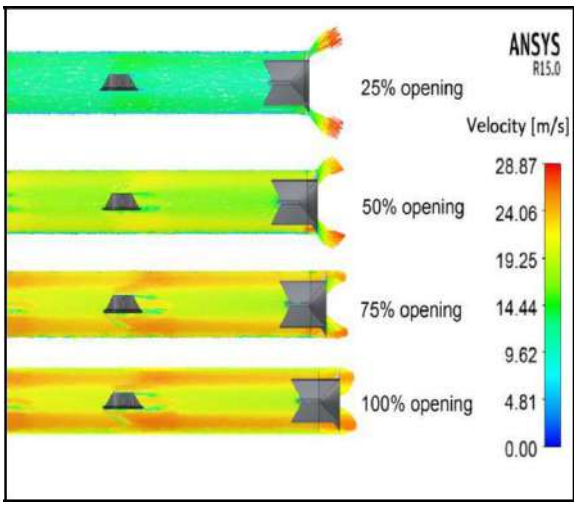

Fig.20. The velocity profiles at the butterfly and cone valves, pressure head at inlet is 25m.

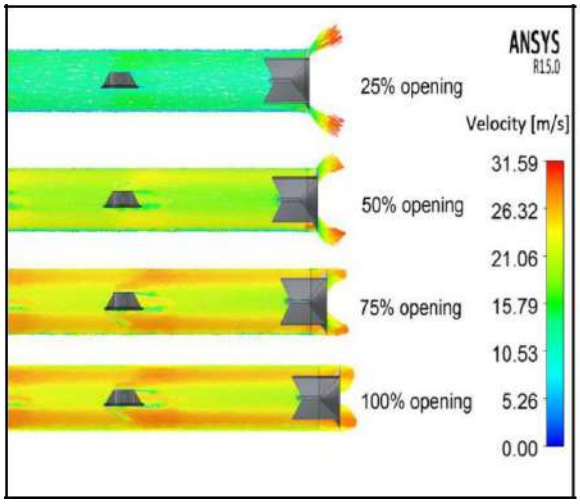

Fig.21. The velocity profiles at the butterfly and cone valves, pressure head at inlet is 34m.

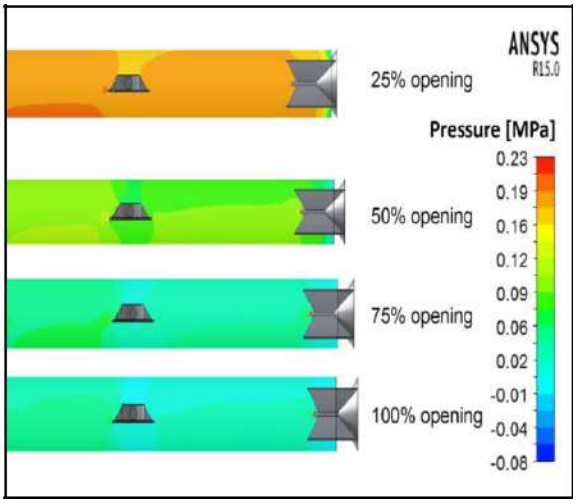

Fig.22. The pressure variation at the butterfly and cone valves, pressure head at inlet is 5 m.

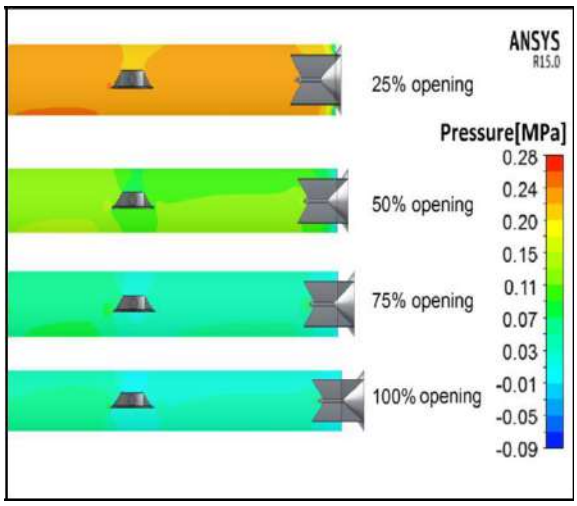

Fig.23. The pressure variation at the butterfly and cone valves, pressure head at inlet is 11 m.

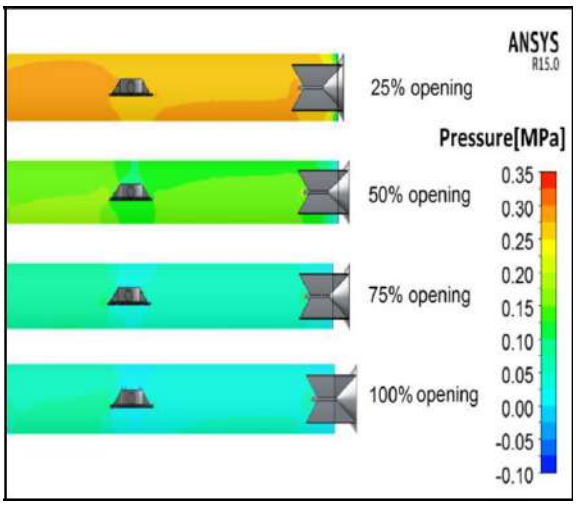

Fig.24. The pressure variation at the butterfly and cone valves, pressure head at inlet is 18 m.

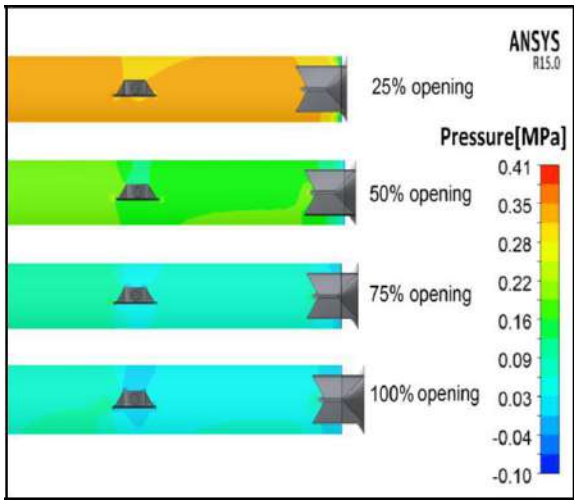

Fig.25. The pressure variation at the butterfly and cone valves, pressure head at inlet is 25 m.

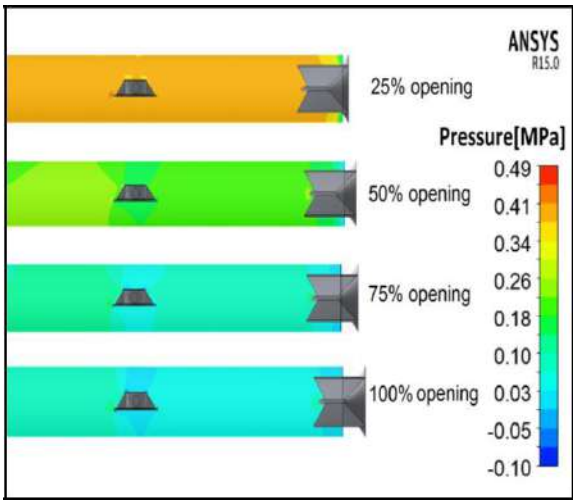

Fig.26. The pressure variation at the butterfly and cone valves, pressure head at inlet is 34 m.

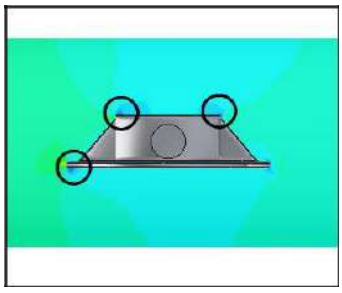

Fig.27. Close up view for the minimum negative pressure at cone openings more than 50%.

It must be noted that at the inside curve of the bottom outlet branching region, the flow velocity is very high and the pressure is always negative, **Figure 28**, during all analysis under all the examined operation conditions especially during large opening of both butterfly and cone valves. This negative pressure may cause local cavitation at this region and needs frequent maintenance.

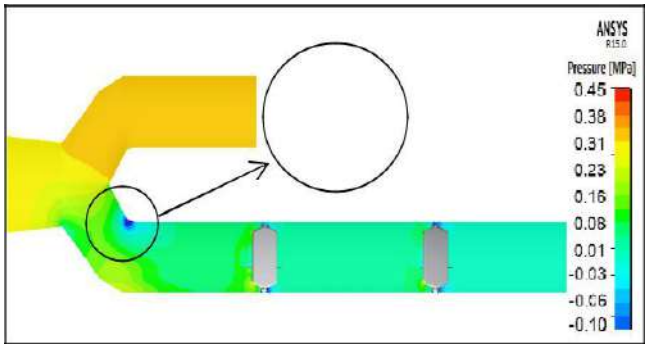

Fig.28. The negative pressure at inside curve of the bottom outlet branching region**.**

CONCLUSIONS

The investigation of the water flow through the bottom outlet of Khassa Chai Dam was conducted. The results of this investigation indicated the following conclusions.

1. Jet is developed at small angles of the butterfly opening.
2. Increasing the angle of the valve opening make the flow smoother and velocity profile more uniform.
3. There is high pressure drop upstream and downstream the butterfly valve especially at the small opening angles. This drop is decreased by increasing the valve opening angle.
4. Low negative pressure values existed in the downstream region immediately behind the valve.
5. It is not desirable to use the butterfly valves to control the outflow of bottom outlets of dams due to high flow velocities and development of negative pressure at the valve.
6. A sound solution of low cost that requires minimum structural modification is to use a cone valve at the end of the existing bottom outlet of Khassa Chai Dam.
7. When using the cone valve, no negative pressures were developed at the valve location, So that the problem of noise and vibration can be solved**.**

REFERENCES

Brett, G., Riveland, M., Jensen, T. C., and Heindel, T. J. 2011. Cavitation from a Butterfly Valve: Comparing 3D Simulations to 3D X-Ray Computed Tomography Flow Visualization, *Mechanical Engineering Conference Presentations*, Papers, and Proceedings, paper 125.

Dawy A., Sharara A., and Hassan A. 2013. A numerical investigation of the incompressible flow through a butterfly valve using CFD, International Journal of Emerging Technology and Advanced Engineering, Volume 3, Issue 11.

Elbakhshawangy, H. F., Abd El-Kawi, O. S., and Sarhan, H. H. 2015. Numerical Study Of Incompressible Flow Characteristics Through Butterfly Valve, Journal of Multidisciplinary Engineering Science and Technology (JMEST), Vol. 2 Issue 7.

Fagerburg, T. L., 1983, Fixed Cone Valve Prototype Tests New Melons Dam, California, Technical report.

Nazary H., Aalipour N., and Alizadeh M. 2011. Investigation of the Flow and Cavitation in a Butterfly Valve, Journal of Mechanical Research and Application, Vol. 3, No. 1.

Neilson, F. M., 1971, Howell-Bunger Valve Vibration Summersville Dam Prototype Tests, Technical report.

Oppinger, P. 2007, Control valves for bottom outlets in dams and in hydro-power plants, International edition of Industriearmaturen, Gremany.

Toro, A. D. 2012, Computational Fluid Dynamics Analysis of Butterfly Valve Performance Factors, M. Sc. thesis, College of Engineering, Utah State University, Logan, Utah .

Versteeg, H.K., and Malalasekera, W. 2007, An Introduction to Computational Fluid Dynamics: The Finite Volume Method.

Federal Emergency Management Agency, 2010,"
Technical Manual: Outlet Works Energy Dissipators: Best Practices for Design, Construction, Problem Identification and Evaluation, Inspection, Maintenance, Renovation, and Repair", FEMA P-679.

ZANCO Journal of Pure and Applied Sciences
The official scientific journal of Salahaddin University-Erbil
ZJPAS (2018) **30**(s1)s152-s158
http://dx.doi.org/10.21271/ZJPAS.30.s1.17

Planning and Operational Flow Forecasting of Lesser Zaab River at Dokan Dam, Kurdistan Region, Iraq

Sarfraz Munir, Sathyendar Sreepada, Bryar Bakr Saeed

Department of Natural Resources Engineering and Management,

University of Kurdistan Hewler-Erbil.

A R T I C L E I N F O

Article History:
Received: 14/05/2017
Accepted: 12/04/2018
Published:01/06/2018

Keywords:
Lesser Zaab River
Markov Model
Forecasting
WaterResources Management
Dokan Dam

**Corresponding Author:*
Email:
s.munir@ukh.edu.krd

A B S T R A C T

Flow forecasting is of paramount importance for efficient management of water resources. Information about availability of flows plays a pivotal role in making efficient decisions in water services operation and planning future water developments. Current study is aimed at understanding the behavior of Lesser Zaab River flows at Dokan Dam and forecast future flows accordingly for planning and operational purposes of water services. Lesser Zaab River is one of the main tributaries in Tigris River Basin. Historical flow series data were collected from dam authorities and it is assumed that data follow normal distribution with no significant trend. The First Order Markov Model for stationary time series was applied for mean annual flow forecasting. The Markov Model with periodicity is also applied for mean monthly flows forecasting. Forecasted data were compared with the observed flow series and found a close match between the two series, both for stationary and periodic flows. Based on the study, it can be recommended that the First Order Markov Model for stationary and periodic hydrologic time series can applied for forecasting with confidence.

INTRODUCTION

Knowledge about availability of future flows is one of the main requirements for all water resources planning, management and modelling projects. It provides basis for the development of any future water project, operation of water facilities, flood control and protection works as well as for other related activities. A variety of hydrologic forecasting models are available which are based on (Box-Jenkin Models, 1970) like Markov Model and Auto Regressive Integrated Moving Average (ARIMA) Models. Other forecasting models are also applied for time series data forecasting like moving average, exponential smoothing, regression analysis and advance computational models using artificial intelligence and data mining techniques.

Time series is defined by (Montgomery *et al.* 2008) as it is a series of time oriented observations on a variable of interest. Classical techniques of flow forecasting are extensively discussed by (Haan 1977 and Gupta 1989). In flow forecasting, the main purpose is to identify the stochastic process that produce the series of data and then forecast accordingly (Akgun, 2003). Analysis of time series is generally performed by determining the auto/serial correlation, which provides the dependence of successive future events on the past events for different lags. Forecasting problems can be classified into short-term,

medium term, and long term forecasting (Montgomery, 2008). Short term may be in the order of days, weeks and months, whereas medium term forecasts can go for one or two years ahead and the long term for serval years. Generally, water system operations are dependent upon the short term forecasts and the long term forecast provides basis for long term planning of water resources. Statistical models are used for water supplies and demand forecasts for short term and long term purposes (Fortin *et al.* 2004). Autoregressive Model of lag-1 (AR(1)) was applied by (Al-Suhaili 1986) for several locations at Tigris River, Iraq. Abed (2007) applied Box-Jenkins seasonal multiplicative model to monthly records of some physical and chemical properties of river water in Babylon, Najaf. Al-Ta'ee (2009) applied ARIMA models to records of rainfall and evaporation at Babylon Governorate. (Muhammad, 2012) compared Markov Model and ARIMA Model for forecasting flow series and found that ARIMA model provided better results.

This study is focused on flow forecasting for operational as well as for planning purposes of Lesser Zaab River at Dokan Dam. First order Markov Model (Haan, 1977) is applied in this study, which depends on lag-1 autocorrelation and first two moments of a time series data, which is assumed to normally distributed and having significant lag-1 autocorrelation. Flows are forecasted on annual basis for next 25 years for planning purposes. At the same time, mean monthly flows are forecasted for next 15 years, which may help in the operation of Dokan Reservoir. These forecasts provide an insight of long term as well short term water availability in the river.

MATERIALS AND METHODS

Study Area

Study was conducted at Lesser Zaab River at Dokan Dam, which is 65 km northwest of the city of Sulaimani. Coordinates of the gauging station are given as 36º 05' 33" N and 44º 56' 09" E. Dokan Dam was commissioned in 1959 at Lesser Zaab River. Dokan Dam is a multipurpose dam, primarily for irrigation purpose and also for hydropower and flood control purposes.

Data Collection

Lesser Zaab River inflow data at Dokan Dam were collected for last 17 years (1999-2015) from Dokan Dam Authority. Data on reservoir inflows, releases and hydropower generation was also collected for last five years' period. Data were collected on daily basis and then the monthly and annual means, standard deviations and other parameters were calculated.

Generating Missing Data Values

There were some values missing in data in the month of February 2002 for two weeks and then in the whole month of September 2003. The missing data were generated by assuming that data follow normal distribution. Values of normally distributed data can be generated by using Equation (1) (Haan, 1977):

$$X = \mu_x + R_N \sigma_x \quad \text{.....1}$$

Where X is generated value, μ_x, σ_x are the mean and standard deviation of variable X respectively, R_N is standard normal deviate. Standard normal deviate is a random observation from the standard normal distribution. Numerically generated tables of standard random normal deviates are available from Rand Corporation, 1965 (Haan, 1977). This is a classical method of finding random numbers. Now-a-days several computer programmes, including Excel ® have inbuilt functions of generating random numbers as well as random standard normal deviates.

Random Numbers

A random number is defined as a number selected at random from a population of

numbers in such a fashion that every number in the population has an equal chance of being selected. Many large tables of random numbers are available (Rand Corporation, 1965). Computer routines for generating random numbers are included as a part of the programme libraries for most computers. They generally generate random numbers in interval (0, 1). A random number Y, in the interval (a,b) can be generated from random numbers in the interval (0,1), R_u, by following relationship:

$$Y = (b - a)R_u + a \quad \ldots\ldots\ldots\ldots\ldots\ldots\ldots\ldots 2$$

First Order Markov Model

Markov Model for stationary and periodic flow series is adopted from (Hann, 1977).

Most of the hydrologic time series exhibit significant auto correlation. That is, the value of the random variable under consideration at one time period is correlated with the values of the random variable at earlier time periods. The correlation of a random variable X at one time period with its value k time periods earlier is denoted by ρ_k and is called k^{th} order auto correlation. If ρ_k can be approximated by $\rho_k = \rho_1$, then the time series of the random variable X might be modelled by a first order Markov Process (Haan, 1977).

The first order Markov Process might also be used for a model if serial correlation for lags greater than 1 are not important.

First order Markov Process is given by (Haan, 1977):

$$X_{i+1} = \mu_x + \rho_1(X_i - \mu_x)\varepsilon_{i+1} \quad \ldots\ldots\ldots\ldots\ldots 3$$

Where X_i is the value of the process at time i, μ_x is the mean of X, ρ_1 is the first order serial correlation and ε_{i+1} is a random component with E(ε) = 0 and Var(ε) = σ_ε^2. The model states that the value of X in one time period is dependent only on the value of X in the preceding time period plus a random component. It is also assumed that ε_{i+1} is independent of X_i. The variance of X_i is given by σ_x^2 and can be shown to be related to σ_ε^2

$$\sigma_\epsilon^2 = \sigma_x^2[1 - \rho_1^2] \quad \ldots\ldots\ldots\ldots\ldots\ldots\ldots\ldots 4$$

If the distribution of X is N(μ_x, σ_x^2) then the distribution of ε is N(0, σ_ε^2). Random values of X_{i+1} can now be generated by selecting ε_{i+1} randomly from a N(0,σ_ε^2).

Thus a model for generating X's that are N(μ_x, σ_x^2) and follow the first order Markov Model is:

$$X_{i+1} = \mu_x + \rho_1(X_i - \mu_x) + t_{i+1}\sigma_x\sqrt{1 - \rho_1^2} \quad \ldots 5$$

In order to generate values of X_{i+1}, the μ_x, σ_x and ρ_1 are estimated by $\bar{X}$, S_x and r_1 respectively. Then value of t_{i+1} is selected at random from a N(0, 1) distribution. Since t is N(0, 1), it is possible to generate values of X that are less than zero. If this occurs, it is recommended that the negative X be used to generate the next value for X and then discarded. If occurrence of negative X's is common in the generation process, it may indicate that X is not normally distributed. In this even some other distribution of ε must be used.

In order to generate values using Equation 5, it needs to find autocorrelation for lag-1. Note that if ρ_1 = 0, Equation 5 reduces to the independent process of selecting a random observation from N(μ_x, σ_x^2). On the other hand if ρ_1 = 1, Equation 5 is completely deterministic in that X_{i+1} is completely specified by

X_i ($X_{i+1} = X_i$).

Serial correlation with lag-k is given by:

$$r_k = \frac{\frac{1}{n}\sum_{i=1}^{n-k}(X_i - \bar{X})(X_{i+k} - \bar{X})}{S_x S_x} \quad \ldots\ldots\ldots\ldots\ldots\ldots 6$$

First Order Markov Process with Periodicity

First order Markov model of the previous section assumes that the process is stationary in its first three moments (mean, standard

deviation and skewness). It is possible to generalize the model so that the periodicity in hydrologic data is accounted for to some extent. The main application of this generalization has been in generating monthly stream flow where pronounced seasonality in the monthly flows exist. Looking at the plot of mean monthly flow series of Lesser Zaab River at Dokan Dam it is evident that the data in some months are much higher than the other months, in general. The periodicity may affect all of the moments of data as well as the first order auto correlation.

To generalize the Markov Model, the notations are adopted in such a way that subscript i refers to the year under consideration and the subscript j refers to the season within the year. Thus j may run from 1 to 4, if 4 seasons are being considered, 1 to 12 if monthly data are being considered, 1 to 52 for weekly data, etc. In general j is taken as to run from 1 to m, the number of seasons in the year.

With this notation, $\mu_{i,j}$ referes to the mean of X in the j[th] season and $\mu_{x,j}$ is estimated by $\bar{X}_j$ where

$$\bar{X}_j = \sum_{i=1}^{n} \frac{X_{i,j}}{n} \quad \text{.....7}$$

With n equal to the number of years of data and $X_{i,j}$ the data value in the j[th] season of the i[th] year. Similarly, $\sigma^2_{x,j}$ is estimated by $S^2_{x,j}$, $\gamma_{x,j}$ is estimated by $Cs_{x,j}$ and $\rho_{1x,j}$ is estimated by $r_{1x,j}$. Note that $\rho_{1x,j}$ is the first order serial correlation between values in successive seasons. If monthly stream flow is being considered, $\rho_{1x,j}$ would be the first order serial correlation between flows in months 4 and 5. $\rho_{1x,j}$ would be estimated as:

$$r_{1,x,j} = \frac{\frac{1}{n}\sum_{i=1}^{n}(X_{i,j} - \bar{X}_{i,j})(X_{i,j+1} - \bar{X}_{i,j+1})}{S_{x,j}S_{x,j+1}} \quad \text{.....8}$$

First order Markov Model for normally distributed flows becomes:

$$X_{i,j+1} = \mu_{x,j+1} + \rho_{1,x,j}\frac{\sigma_{x,j+1}}{\sigma_{x,j}}\left(X_{i,j} - \mu_{x,j}\right) + t_{i,j+1}\sigma_{x,j+1}\sqrt{1 - \rho^2_{1,x,j}} \quad \text{.....9}$$

In any application the population parameters are estimated by the corresponding sample statistics.

Validation of Forecasted Values

Forecasted values are validated by comparing their statistical properties like mean and standard deviation of observed data. Furthermore, several trials were conducted and based on the minimum root mean square error (RMSE) and mean absolute error (MAE) the current models parameters were selected. Then the validity of the model is decided based on the minimum values of RMSE, MAE and closeness of mean and standard deviations between observed and forecasted values. RMSE and MAE are given as:

$$RMSE = \sqrt{\frac{1}{n}\sum_{i=1}^{n}(X_i - \hat{X}_i)^2} \quad \text{.....10}$$

and

$$MAE = \frac{1}{n}\sum_{i=1}^{n}\left|X_i - \hat{X}_i\right| \quad \text{.....11}$$

where X_i *and* $\hat{X}_i$ are the observed and forecasted values of the flow series, n is the total number of observations.

RESULTS

Filling Missing Data

Data during months of February 2002 and September 2003 were missing. The missing values were generated by using Equation 1. Standard normal deviates were generated by using Excel ® Software. Random numbers in excel provides cumulative standard normal distribution values, then by taking the inverse of random numbers, the values of random standard normal deviates, R_N, were generated.

Generated values of flow series were compared with the observed data in the same duration of other hydrologic year and found good proximity in generated and observed values of similar durations.

Annual Flow Series

Figure 1 presents mean annual flow of Lesser Zaab River at Dokan Dam for 17 years from 1999 to 2015.

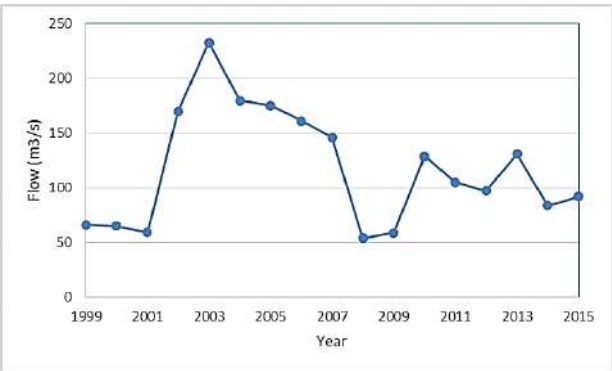

Fig. 1. Mean annual flow series of Lesser Zaab River at Dokan Dam from 1999 to 2015.

Figure shows at first sight a decreasing trend in the data, but it is quite difficult to establish this statement, based on the limited data. Therefore, it is assumed that the data have no significant trend either decreasing or increasing flows. Furthermore, it is assumed that the mean annual flow series data follow a normal distribution.

Flow Forecasting for Mean Annual Flow

Mean annual flows are forecasted using Equation 5 of First Order Markov Model. The model needs lag-I autocorrelation (AC) in addition to first two moments of the distribution (mean and variance). The lag-1 AC is found to be 0.52 for the given flow series data. It also needs standard normal deviates, which are generated using Excel ® Software's inbuilt function to generate random numbers and then taking inverse standard normal distribution of the random numbers. Figure 2 presents a comparison of mean annual flow's forecasted values with the observed values. A close proximity is found in the observed and forecasted values.

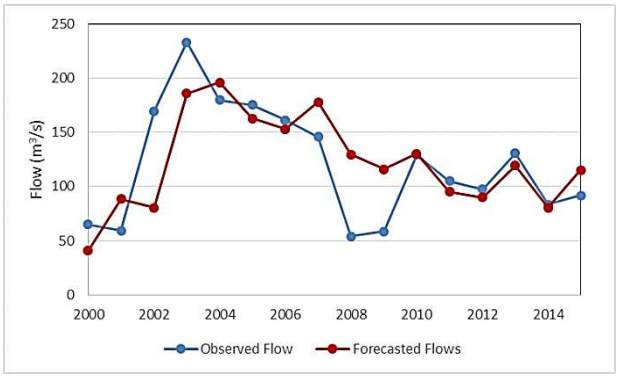

Fig. 2. Comparison of observed and simulated annual flow series.

The mean, standard deviation, MAE and RMSE of the observed and forecasted data are given in the Table 1.

Table 1. Mean, standard deviation, MAE and RMSE of the observed and forecasted data.

Parameter	Unit	Observed Data	Forecasted Data
Mean	m^3/s	118	123
Standard Deviation	m^3/s	53	43
MAE	m^3/s	28	
RMSE	m^3/s	55	

Based on the comparison of validation parameters presented in Table 2, the First Order Markov Model can be used for forecasting flow series for future for long term purposes. Fig. 3 presents the 25 year annual flow series based on the above given parameters.

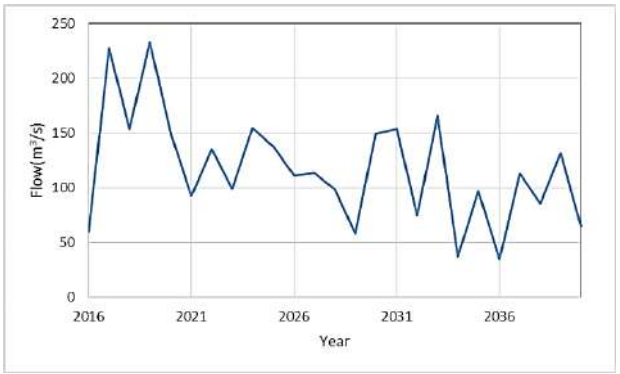

Fig. 3. Forecasted flows series for 25 years of Lesser Zaab River at Dokan Dam.

Lag-I Autocorrelation for Monthly Flows

Table 2 presents the values of monthly means, standard deviations and lag-1 autocorrelations for 17 year data (1999 to 2015) of Lesser Zaab River at Dokan Dam.

Table 2. Monthly mean, standard deviation and lag-1 autocorrelation of Lesser Zaab River at Dokan Dam.

Month	Mean (m^3/s)	Standard Deviation (m^3/s)	Lag-1 Autocorrelation
October	34	32	-0.143
November	88	136	-0.026
December	112	125	-0.483
January	160	206	-0.232
February	269	265	0.361
March	322	258	-0.425
April	332	226	-0.157
May	203	123	0.379
June	84	51	0.980
July	42	21	0.965
August	30	14	0.890
September	25	13	0.321

Forecasting Monthly Flows

Forecasts about monthly flows help operation managers to take efficient decisions regarding operation of water facilities. In this case, the one month ahead forecasts may be useful for dam authorities to manage reservoir operation. Monthly flows are forecasted using lag-1 autocorrelation. Figure 4 presents a comparison of forecasted flows with observed flows, which provide a satisfactory closeness between the two flow series.

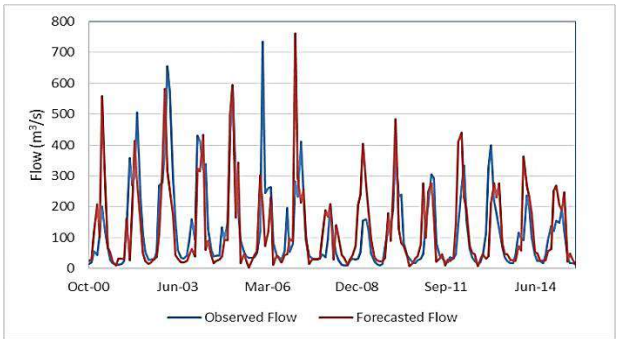

Fig. 4. Comparison of mean monthly observed flow and forecasted flows of Lessser Zaab River at Dokan Dam.

Based on the satisfactory closeness between the observed and forecasted flow series, the mean monthly flow series for next 15 years are forecasted based on the parameters given in Table 2. Figure 5 presents the mean monthly forecasted flow series of Lesser Zaab River at Dokan Dam for next 15 years.

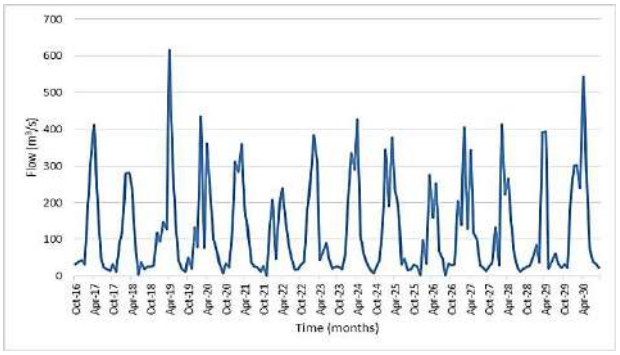

Fig. 5. Mean monthly forecasted flows of Lesser Zaab River at Dokan Dam

DISCUSSION

It is observed from the results that First Order Markov Model provides acceptable long term and short term flow forecasting. The first two moments (mean and variance or standard deviation) of observed flows and forecasted flows have no significant difference. It provides a basis for reliable flow forecasting using this model. In addition, the MAE and RMSE are also found acceptable. The long term forecasting of mean annual flows for 25 years, provides a basis for planning activities for better management of river water.

In addition to planning activities, the operation of water facilities is also one of the main activities in water resources management. The operation decisions are strengthened by having a good idea about water availability in near future. In this case, it is assumed that the decisions are taken on monthly basis, so monthly flows were forecasted. It was observed that Markov Model with periodicity also fits well to the periodic data with lag-1 autocorrelation. Mean monthly flows were forecasted for 15 years in future.

It is found in the study that application of this model can greatly help in better operation and planning of water facilities.

Two main assumptions are made in this study that the data follows normal distribution and have no significant trend.

CONCLUSIONS

Flow forecasting is one of the basic requirement for efficient planning and decision making in water resources management. Keeping this in view, this study has been performed where flows of Lesser Zaab River at Dokan Dam were forecasted for long term and short term purposes. The long term flows are required for long term strategic planning, whereas short term forecasting is required for improved operation of water facilities, like reservoirs and water supply schemes. A variety of techniques are available for time series data forecasting, which required certain number of parameters and somehow computationally intensive. In this study, the First Order Markov Model for stationary data series as well as data with periodicity has been applied. This model needs the first two moments of distribution and depends upon lag-1 autocorrelation for stationary and periodic data. Required parameters for flow forecasting were estimated and the flow series was forecasted accordingly. After that, the flow series were validated by comparing the observed and forecasted series in terms of means, standard deviations, MAE and RMSE. Satisfactory closeness of the observed and forecasted series was found. Based on that the series was forecasted for mean annual flow for next 25 year. Furthermore, the flow series was also forecasted for mean monthly flows for next 15 years. It is concluded that the Markov Model with given parameters can successfully be applied for future flow forecasting for any given duration. The Markov Model was found to be computationally simple and depends only upon lag-1 autocorrelation and at the same time, it provides reasonable good results. The other time series forecasting models may provide better results, but are computationally intensive, especially for data with periodicity.

ACKNOWLEDGEMENTS

We highly acknowledge the support provided by Dokan Dam Authority, Ministry of Agriculture and Water Resources, Kurdistan Regional Government, Iraq for providing the required data of river flow series including reservoir operation. Sincere thanks are extended to Dr. Hamed M. Jassim for his valuable comments and suggestions for the improvement of scientific and presentation quality of this research paper.

REFERENCES

Abed, Z., Al-Ridah, A. (2007). *Stochastic Models of Some Properties of water in the middle of Euphrates Region in Iraq*. M.Sc. Thesis, College of Engineering, University of Babylon.

Akgun, B. (2003). *Identification of Periodic Autoregressive Moving Average Models*. Middle East Technical University.

Ali, S. (2009). *Fitting Seasonal Stochastic Models to Inflow of Bekhme Reservoir*, The Iraqi Journal for Mechanical and Material Engineering, Special Issue(A), College of Engineering, University of Babylon. [online] pp. 1-12. Available at: https://www.iasj.net/iasj?func=fulltext&aId=48846. [Accessed at: 2 May. 2017].

Al-Suhaili, R. (1986). *Stochastic Analysis of Daily Streamflow of Tigris River*. M.Sc. Thesis, College of Engineering, University of Baghdad.

Al-Ta'ee, M. (2009). *Analysis of Records of Rainfall and Evaporation in Babylon*. M.Sc. Thesis, College of Engineering, University of Baghdad.

Box, G. and Jenkins, G. (1970). *Time Series Analysis: Forecasting and Control*. Holden Day, San Francisco. Fifth ed. Wiley., pp. 47.

Fortin, V., Perreault, L. and Salas, J. (2004). *Retrospective Analysis and Forecasting of Stream flows Using a Shifting Model*. Journal of Hydrology, (296), pp.135-163.

Gupta, R. (1989). *Hydrology and Hydraulic Systems*. Fourth ed. Prentice Hal., pp. 423-467

Haan, C. (1977). *Statistical Methods in Hydrology*. 1st ed. The Iowan State University Press., pp. 293-298.

Montgomery, D., Jennings, C., Kulahci, M. (2008). *Introduction to Time Series Analysis and Forecasting*. 1st ed. John Wiley & Sons, Inc., pp.244-261.

Muhammad, M. (2012). *Time Series Modelling Using Markov and ARIMA Models*. MSc. Thesis.

Faculty of Civil Engineering, University of Technology Malaysia.

ZANCO Journal of Pure and Applied Sciences
The official scientific journal of Salahaddin University-Erbil
ZJPAS (2018) **30**(s1)s159-s167
http://dx.doi.org/10.21271/ZJPAS.30.s1.18

Optimizing Reservoir Operation – A Case Study of Dokan Reservoir, Kurdistan Region, Iraq

Sathyendar Sreepada*, Sarfraz Munir, Shirwan Najmadin Jumaa

Department of Natural Resources Engineering and Management,

University of Kurdistan Hewler-Erbil.

A R T I C L E I N F O

Article History:
Received: 14/05/2017
Accepted: 12/04/2018
Published:01/06/2018

Keywords:
Reservoir Operation
Lesser Zaab River
Optimization
Dynamic Programming

**Corresponding Author:*
Email:
s.sreepada@ukh.edu.krd

A B S T R A C T

There has been renewed interest in optimization of reservoir operation for efficient planning and management of water resources. Generally, reservoir operation is based on empirical procedures, including rule curves to a certain range and subjective findings by the operation managers. This study is aimed to design the reservoir operation rule curve, based on optimization principles. The study has been conducted at Dokan Reservoir, which is fed by Lesser Zaab River at Dokan. The reservoir is mainly intended to meet irrigation demands, hydropower generation and flood control. The study proposes opportunity for changing traditional reservoir operation to optimized strategies and taking advantages of the Optimization technique is used to find the optimal solutions and based on that the optimized rule curves are developed for various scenarios of water demand, with different initial conditions rapid development in computational techniques. Dynamic Programing.

INTRODUCTION

Reservoir operation is meant to develop a strategy to fill reservoir during wet season in such a way that it ensures meeting downstream water demands, flood mitigation and dam safety. The objectives of reservoir operation are generally conflicting because water storage reduces the capacity for flood wave mitigation and affects downstream releases to meet the water demands including irrigation, hydropower and environment, etc. It is common in reservoir operation that fulfilment of one objective affects the other. It necessitates to define reservoir operation in such a way that the conflicting objectives should have minimum effects on each other.

One of the way is to devise reservoir operation strategy following optimization principles. (Louks et al., 2005) provide a variety of optimization techniques for water resources planning and management including reservoir operation and capacity expansion.

In general, the optimization techniques can be grouped into the conventional linear, nonlinear, dynamic programming and the emerging evolutionary computations. The conventional optimization techniques are still in practice and are applied extensively in water resources management problems for better solutions. (Rani and Moreira, 2009) stated that the advantage of Linear Programming is its versatility for large water systems, convergence to global optima and supported by many software packages. However, reservoir operation simulation may contain nonlinear

elements in the objective function constrained by reservoir capacity, pump and demand in nonlinear form. Common nonlinear pogramming methods are sequential linear programming (Barros et al., 2003), sequential quadratic programming (Finardi *et al*., 2005), method of multipliers (Fawal *et al.*, 2007) and generalization of reduced gradient method (Peng and Buras, 2000). Stochastic Dynamic Programming (SDP) is another popular optimization method for reservoir operation optimization. (Alaya *et al.*, 2003) studied reservoir optimization by using SDP and applied in Nebhana Reservoir. (Labadie, 2004) presented Dynamic Programming Successive Approximation (DPSA), Incremental Dynamic Programming (IDP) and Discrete Differential Dynamic Programming (DDDP) to manage the dimensionality problem in Dynamic Programming. The emerging group of optimization algorithms comes from computational intelligence which is named as Evolutionary Computations (EC). (Rani and Moreira, 2009) reported that the evolutionary algorithms such as Genetic Algorithm, Simulated Annealing, Tabu Search, Particle Swarm Optimization and Honey Bees Mating Optimization are efficient tools to deal with nonlinear and multi-objective analysis and they can be linked with simulation models. (Chuntian, 1999) applied a fuzzy dynamic programming model for real time operation of multiple reservoirs for flood management. (Chaves and Kojiri, 2007) developed Stochastic Fuzzy Neural Network Model to optimize the operation of Barra Bonita Reservoir in Brazil and concluded that it produced better results. (Ahmad *et al.,* 2014) provides an extensive review of contemporary optimization techniques applied for reservoir operation including conventional optimization simulation techniques as well as some advanced algorithms like Artificial Bee Colony (ABC) and Gravitational Search Algorithm (GSA).

(Celeste and Billib, 2009) investigated the advantages and disadvantages of these optimization techniques. They compared ISO, ESO and Parameterization-Simulation-Optimization (PSO) optimization methods. They conclude that, in general, PSO and ESO produce better results, but the choice of any method depends upon the type of problem and the water system to be optimized. (FANG *et al.,* 2014) proposed a simulation-optimization model of reservoir operation based on target storage curves, where they used improved particle swap optimization (IPSO) to optimize key points of water diversion curves, the hedging rule curves and target multi-reservoir water supply system located in Liaoning Province China, including a water supply project. They concluded that the proposed operating rules are suitable for complex system. The storage allocation rule based on target storage curves shows an improved performance with regard to system storage distribution. (Jahanpour *et al.,* 2014) developed a web-based application for optimization of single reservoir operation. They emphasized the application of computer optimization modelling tools to provide information for their rational operating decisions. Recent improvements in high-speed computers and internet encourage researches to become familiar with and use of modern techniques and tools more frequently. This article presents and tests a set of operational objectives to optimally operate a single reservoir using a web-based platform. All practitioners can use WBA to share their data, findings, and models while simultaneously solving their reservoir operation problems. (Rashid *et al.,* 2007) developed Stochastic Dynamic Programming (SDP) model for Dokan Reservoir and suggested optimal decisions (ending storage levels) as a function of unregulated inflows.

This study is aimed at to improve the Dokan Reservoir's operation by devising a steady state optimized policy. The policy suggests reservoir's improved operation rule curve

based on steady state policy to meet the multipurpose reservoir functions.

MATERIALS AND METHODS

Study Area

Study was conducted at Dokan Reservoir, which is located on the Lesser Zaab River about 65 km northwest of Sulaimaniyah City. The reservoir is impounded by Dokan Dam, which was commissioned in 1959. Reservoir's total design capacity at normal operation level (Elevation 511.00 Above Mean Sea Level (AMSL)) of 6.87 Billion Cubic Meters (BCM) and live storage of 6.14 BCM. Minimum drawdown level is 469 m AMSL. There are five hydropower generation turbines with total installed capacity of the reservoir is 400 Mega Watts (MW), whose installation was completed in 1979. It need 550 m3/s discharge at 95 m head to produce the power at maximum capacity. It is a multipurpose reservoir primarily for irrigation and then for hydropower and flood control. Figure 1 presents reservoir control rule curve (SMEC, 2006)

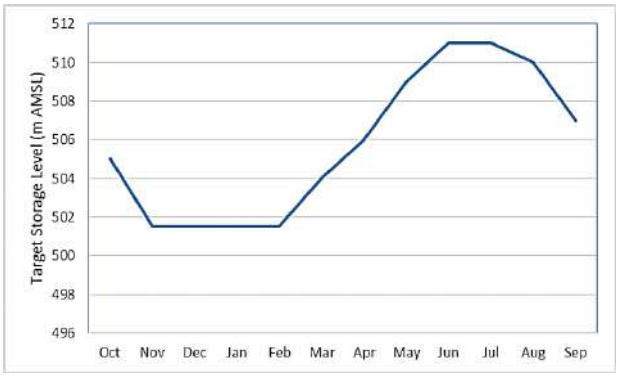

Fig. 1. Dokan Reservoir's control rule curve (Derived from SMEC, 2006).

Data Collection

Lesser Zaab River inflow data at Dokan Dam were collected for last 22 years (1993-2014) from Dokan Dam Authority. Data on reservoir releases and water levels were collected for last five years, whereas the last 5 years data were collected for releases, reservoir water levels and hydropower generation. Downstream water demand data were not available, so the average releases have been considered as bench mark for the downstream water demands. Table 1 provides average monthly inflows to the reservoir for a period of 1993 to 2003 (high flow years) and releases for a period of 2010 to 2015.

Table 1. Mean monthly inflow, release and storage targets of Dokan Reservoir

Month	Inflows (BCM)	Releases (BCM)	Storage Target (BCM)
October	0.146	0.190	5.392
November	0.484	0.223	4.545
December	0.458	0.223	4.545
January	0.905	0.165	4.545
February	1.100	0.184	4.545
March	1.451	0.164	5.135
April	1.677	0.178	5.660
May	0.984	0.216	6.545
June	0.438	0.341	7.207
July	0.201	0.534	7.207
August	0.139	0.575	6.868
September	0.123	0.287	5.941

Dynamic Programming Optimization

Dynamic Programming Optimization (DPO) technique is used in this study adopted from (Louks *et al.*, 2005). Reservoir is mainly meant to meet downstream irrigation water demands, hydropower generation and flood mitigation. Generally, it is not be possible to meet all these objectives by affecting each other. DPO helps to devise reservoir operation strategy by minimizing the effects of one objective on the other by minimize a weighted sum of squared deviations from each of these targets. The weights reflect the relative importance of meeting each target in each season t. Dokan Reservoir's live storage capacity of 6.14 BCM, is divided into 13 units from 0 to 6 for modelling purposes. Initial storage, S_t, can assume any value from 0 to 6 BCM with an interval of 0.3 for all periods t.

Storage volume continuity equation is given as:

$$S_t + Q_t + R_t - L_t(S_t, S_{t+1}) = S_{t+1} \quad \ldots\ldots\ldots\ldots 1$$

where Q_t is mean inflow, $L_t(S_t, S_{t+1})$ the evaporation and seepage losses, and R_t the release or discharge from the reservoir. The hydrologic year is divided into 12 time periods (months), t. Overall four scenarios are simulated as Business as Usual (BAU), Flood Mitigation (FM), Hydropower generation during peak energy demand period (HP-PD) and hydropower generation in all seasons (HP-AS) and increase in downstream future water demands increase by 10%. Table 2 presents the weights associated with each scenario in different time of the year.

Table 2. Weights associated with different scenarios

Month	BAU			Flood Mitigation			HP-PD			HP-AS			Demand 110%		
	ST	FM	DR	ST	FM	DR	ST	FM	DR	ST	FM	DR	ST	FM	DR
Oct	1	0	0	0	1	0	0	0	0	0	0	1	0	0	1
Nov	1	0	0	0	1	0	0	0	0	0	0	1	0	0	1
Dec	1	0	0	0	1	0	0	0	1	0	0	1	0	0	1
Jan	1	0	0	1	0	0	0	0	1	0	0	1	0	0	1
Feb	1	0	0	1	0	0	0	0	1	0	0	1	0	0	1
Mar	1	0	0	1	0	0	0	0	0	0	0	1	0	0	1
Apr	1	0	0	1	0	0	0	0	0	0	0	1	0	0	1
May	1	0	0	1	0	0	0	0	0	0	0	1	0	0	1
Jun	1	0	0	1	0	0	0	0	1	0	0	1	0	0	1
Jul	1	0	0	1	0	0	0	0	1	0	0	1	0	0	1
Aug	1	0	0	1	0	0	0	0	1	0	0	1	0	0	1
Sep	1	0	0	1	0	0	0	0	0	0	0	1	0	0	1

The objective is to minimize the sum of total weighted squared deviations, TSD_t, over all seasons t from now on into the future:

$$Minimize \ \sum_t TSD_t \quad \text{……..2}$$

where,

$$TSD_t = ws_t[(TS_t^R - S_t)^2 + (TS_t^R - S_{t+1})^2] + wfs_t[(ES_t)^2 + (ES_{t+1})^2] + wr_t[DR_t^2] \quad \text{……3}$$

In the above equation, when t = 13, the last period of the year, t +1 = 1, is the first period in the following year. Each ES_t is the storage volume in excess of the flood storage target volume, TS^F_t. Each DR_t is the difference between the actual release, R_t, and the target release TR_t, when the release is less than the target. The excess storage, ES_t, at the beginning of each season t can be defined by the constraint:

$$S_t \leq TS_t^F + ES_t \quad \text{……...……4}$$

for periods t =1 and 2, and the deficit release, DR_t, during period t can be defined by the constraint:

$$R_t \geq TR_t - DR_t \quad \text{……...……5}$$

This constraint applies for all periods t.

The first component of the right side of Equation 3 defines the weighted squared deviations from storage target, TSR_t, at the beginning and end of season t. The weights ws_t associated with the storage component of the objective. The second component of Equation 3 is for flood control. It defines the weighted squared deviations associated with storage volumes in excess of the flood control target volume, TSF_t, at the beginning and end of the flood season, period t+1. Finally, the last component of Equation 3 defines the weighted squared deficit deviations from a release target, TR_t,

This minimum sum of weighted squared deviations for all n remaining seasons t is equal to:

$$F_t^n(S_t, Q_t) = min \sum_t^n TSD_t(S_t, R_t, S_{t+1}) \quad \text{…….6}$$

over all feasible values of R_t , where

$$S_{t+1} = S_t + Q_t - R_t - L_t(S_t, S_{t+1}) \quad \text{……7}$$

and $S_t \leq K$, the carrying capacity of the reservoir.

The policy which is required to be derived is called a steady-state policy. Such a policy assumes the reservoir will be operating for a

relatively long time with the same objectives. This steady-state policy can be found by first assuming that at some time all future benefits, losses or penalties, F_t^0 (S_t, Q_t), will be 0. A steady-state policy will occur if the inflows, Q_t, and objectives, TSD_t (S_t, R_t,S_{t+1}), remain the same from year to year. This steady-state policy is independent of the assumption that the operation will end at some point.

At each stage, or season, the release R_t or equivalently the final storage volume S_{t+1}, are calculated that minimizes

$$F_t^n(S_t, Q_t) = Minimize\{TSD_t(S_t, R_t, S_{t+1}) + F_{t+1}^{n-1}(S_{t+1}, Q_{t+1})\} \; for \; all \; 0 \le S_t \le 6 \quad \ldots\ldots\ldots 8$$

The decision-variable can either be the release, R_t, or the final storage volume, S_{t+1}. If the decision-variable is the release, then the constraints on that release R_t are:

$$R_t \le S_t + Q_t - L_t(S_t, S_{t+1}) \quad \ldots\ldots\ldots\ldots\ldots\ldots 9$$

$$R_t \ge S_t + Q_t - L_t(S_t, S_{t+1}) - 6 \quad \ldots\ldots\ldots\ldots 10$$

and

$$S_{t+1} = S_t + Q_t - L_t(S_t, S_{t+1}) \quad \ldots\ldots\ldots\ldots\ldots 11$$

If the decision-variable is the final storage volume, the constraints on that final storage volume S_{t+1} are:

$$0 \le S_{t+1} \le 6$$

$$S_{t+1} \le S_t + Q_t - L_t(S_t, S_{t+1}) \quad \ldots\ldots\ldots\ldots\ldots 12$$

and

$$R_t = S_t + Q_t - S_{t+1} - L_t(S_t, S_{t+1}) \quad \ldots\ldots\ldots 13$$

The policy differs over each state, and over each different season, but not from year to year for any specified state and season. We have reached a steady-state policy. If we kept on computing the release and final storage policies for preceding seasons, we would get the same results.

RESULTS

Five scenarios are modelled as Business as Usual (BAU), Flood Mitigation (FM), hydropower generation during peak demand period (HP-PD), which are from December to February and June to August, then hydropower generation in all seasons (all months) (HP-AS) and finally downstream water demand increase by 10%. The reservoir operation rule curves are provided for two initial conditions as empty and half-filled reservoir at the beginning of hydrologic year. The steady state policies achieved by modelling are presented in the following sections:

Business as Usual (BAU)

BAU follows the design storage curve and ignores other parameters. Optimized releases and storage volumes are given in the Figure 2a and 2b for two initial conditions as zero and half live storage at the beginning of hydrologic year, in the month of October, respectively. Figures present optimal releases, optimal storages as well as design storage according to rule curve and average releases by the dam authorities in the last five years.

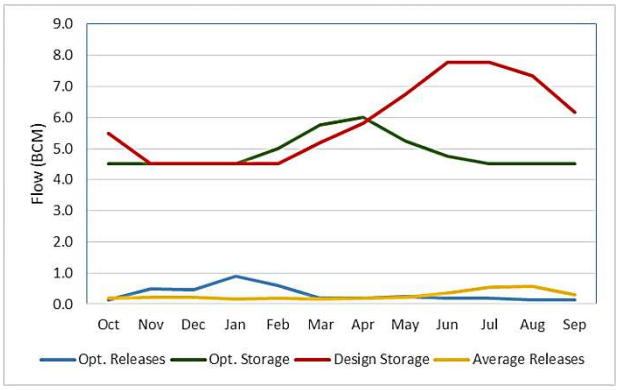

Fig. 2a. Suggested reservoir operation under BAU scenario for zero initial live storage.

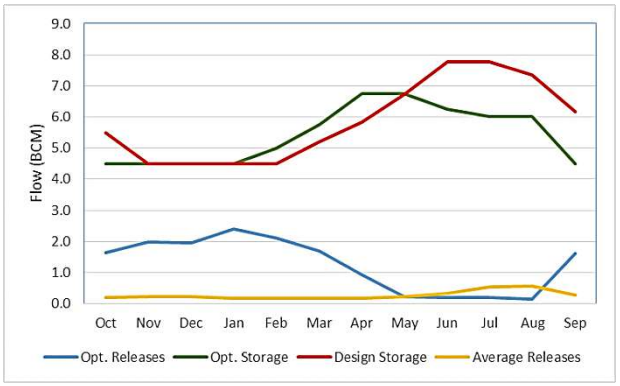

Fig. 2b. Suggested reservoir operation under BAU scenario for half initial live storage.

Flood Mitigation (FM)

Flood mitigation is one of the important objective of reservoir. In the last section, the weightage was given only to storage. In flood mitigation scenario, in the first three months the weightage is given to keep the space for flood storage in the reservoir, in order to mitigate flood peaks. Flood mitigation modelling produces the same results as given under BAU Scenario.

Hydropower Generation in Peak Energy Demand Periods (HP-PD)

Hydropower needs are increasing in the region, which puts pressure on energy sector to produce more sustainable energy. Hydropower generation data show that at Dokan Dam the power generation is directly related to water releases from the reservoir. Therefore, in this scenario, the weightage is given for releases during the peak energy demand months, which are, December to February and then June to August. In other months the weightage is given to storage. Figure 3a and 3b present the hydropower generation in peak demand period.

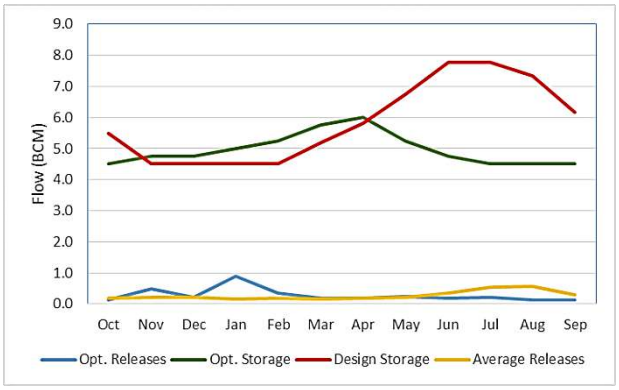

Fig. 3a. Suggested reservoir operation under HP-PD Scenario with zero initial storage.

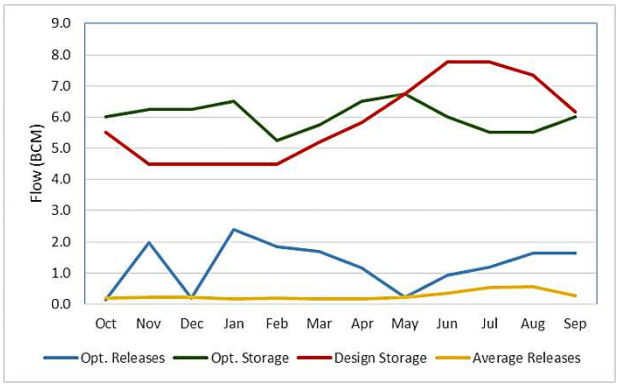

Figure 3b. Suggested reservoir operation under HP-PD scenario with half initial storage.

Hydropower Generation in All Seasons (HP-AS)

In this scenario, the weightage is given for releases to all seasons (months) for hydropower generation. Figure 4a and 4b present the releases and storage volumes for the hydropower generation in all seasons.

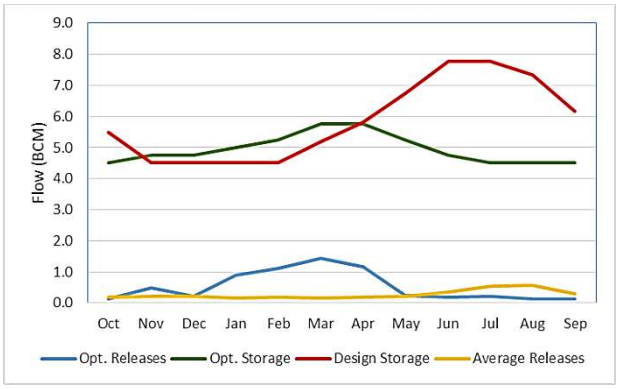

Fig 4a. Suggested reservoir operation under HP-AS scenario with zero live storage.

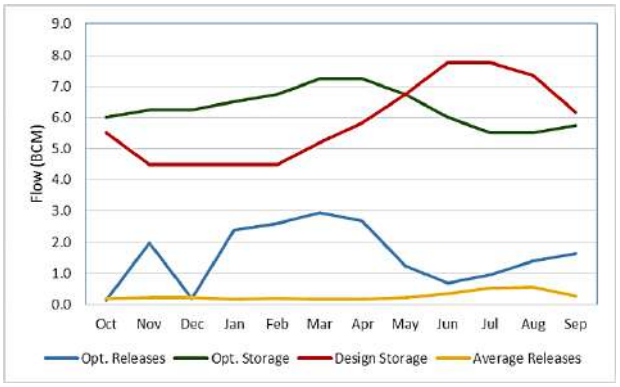

Fig. 4b. Suggested reservoir operation under HP-AS scenario with half live storage.

Increase in Future Water Demands (D10%)

In order to manage the future increase in water demands, a scenario with 10% water demand increase is simulated and the optimized rule curve is presented in the Figure 5a and 5b with two different initial conditions.

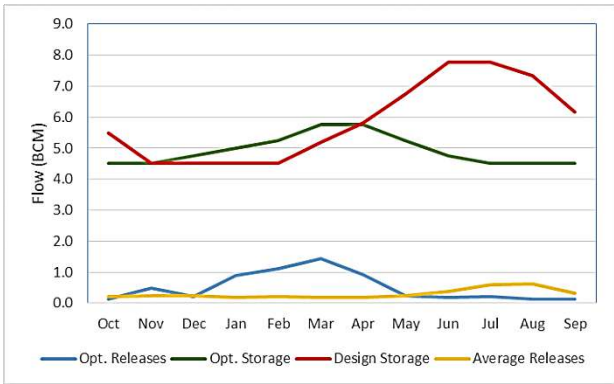

Fig. 5a. Suggested reservoir operation under 10% increase in water demand with zero initial storage.

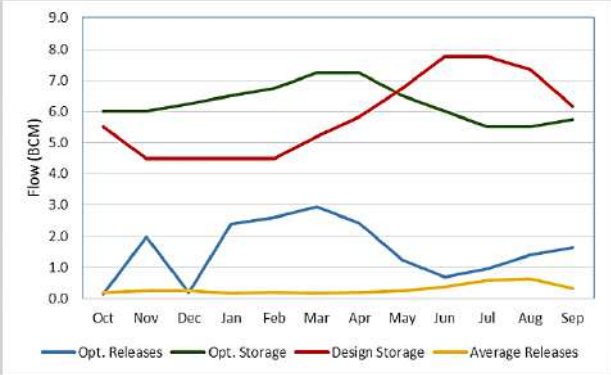

Fig. 5b. Suggested reservoir operation under 10% increase in water demands with half initial storage.

Quantifying the Error

In order to obtain steady state reservoir operation policy, the difference between optimized storage or releases in two consecutive time steps should be zero. It means, the same storage and releases are proposed in two consecutive years. Figure 6 presents the analysis of errors, different between $S_t - S_{t+1}$ and $R_t - R_{t+1}$.

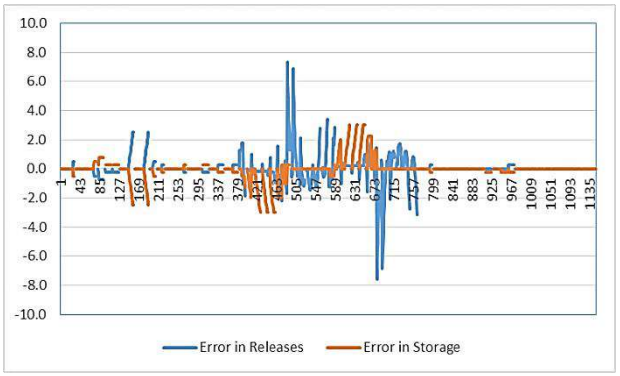

Fig. 6. Errors in optimized storage and releases for two consecutive years.

DISCUSSION

It can be seen in the Figure 6 that error in last two years become zero, which is an indication of achieving steady state policy. Scenarios simulated for different objectives of the reservoir operation suggest different releases and storage volumes as presented in the last section. Weightage given to different scenarios can be seen in Table 2. In general, the reservoir does not seem sufficient to fill the reservoir up to full capacity and meeting the downstream demands simultaneously.

In BAU scenario it can be observed that the optimized storage curve closely match the design storage curve. In HP-PD scenario, the high amount of releases can be seen in the peak demand energy demand months, whereas comparatively low releases are suggested in other months. The storage target in this scenario cannot be met. In HP-AS scenario, the time distribution of suggested releases are different than in the HP-PD scenario. Almost same trend in water releases can be seen in increased demand scenario. These comparisons are shown in Figures 7a to 8b.

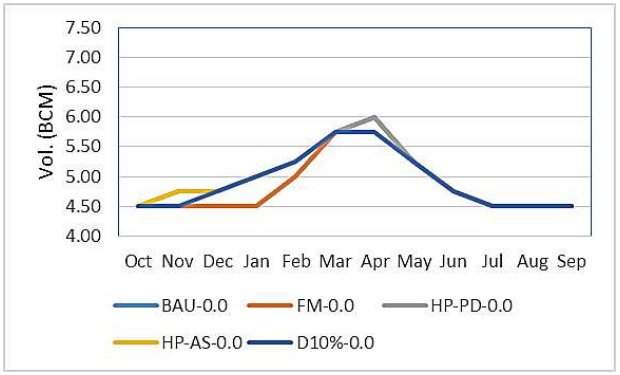

Fig. 7a. Optimized storage volumes for zero initial live storage conditions.

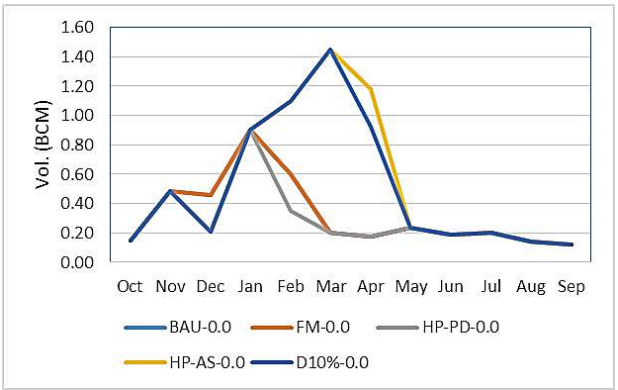

Fig. 7b. Optimized releases for zero initial live storage conditions.

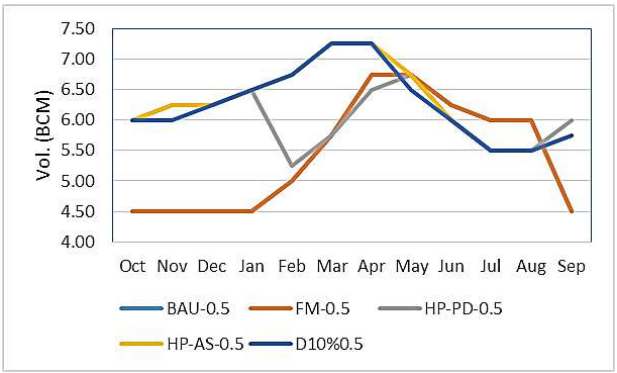

Fig. 8a. Optimized storage for initial half live storage conditions.

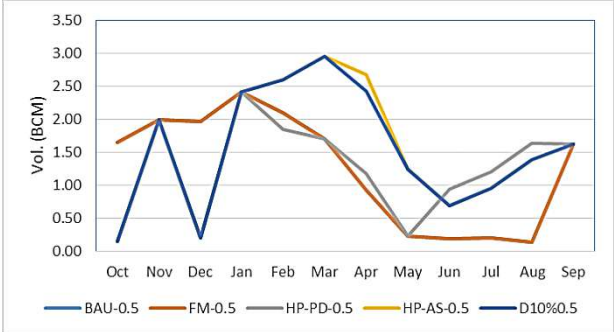

Fig. 8b. Optimized releases for initial half live storage conditions.

CONCLUSIONS

In this study, the Dokan Reservoir's operation has been suggest based on Dynamic Programming Optimization technique on monthly basis. The DP technique solves the discrete optimization problem by minimizing the weighted sum of total squared deviations (TSD). A steady state operation policy is adopted when the error between two consecutive time steps become zero. Although the reservoir was mainly impounded to meet the irrigation water demands. However, growing energy crisis in the region and contribution of hydropower cannot be ignored. Keeping in view these pressing demands, a variety of scenarios has been modelled keeping in view the priorities for reservoir operation. Furthermore, the modelling has been performed for two initial live storage conditions as empty reservoir and half-filled reservoir at the beginning of the hydrologic year, which is start of the October month. The scenarios consist of BAU, FM, HP-PD, HP-AS and 10% increase in future water demand. Based on these scenarios, the study proposes the optimized storages and releases on monthly basis by having minimum effects on other objectives of the reservoir. Figures 7a to 8b present the optimized storages and releases for all the scenarios discussed above. Since downstream water demands are assumed to be equivalent to average releases, the optimized storage and release curves may change when the real data on downstream water demands are used.

ACKNOWLEDGEMENTS

We highly acknowledge the support provided by Dokan Dam Authority, Ministry of Agriculture and Water Resources, Kurdistan Regional Government, Iraq by providing reservoir operation data and other relevant information. Authors are extremely obliged to Dr. Adrian Coad for providing his valuable suggestions in improving the scientific quality of this research paper.

REFERENCES

Ahmad, A., El-Shafie, A., Razali, S. F. M., Mohammad, Z. S. (2014). Reservoir Optimization in Water Resources: a Review. Water Resources Management (28), pp. 3391-3405.

Alaya, A. B., Souissi, A, Tarhouni, J, Ncib, K. (2003) Optimization of Nebhana reservoir water allocation by stochastic dynamic programming. Water Resource Management (17), pp. 259–272.

Barros, M. T. L., Tsai, F. T. C., Yang, S. L., Lopes, J. E. G., Yeh, W. W. G. (2003). Optimization of large-scale hydropower system operations. Water Resources Planning and Management. (129), pp.178–188.

Celeste, A. B., Billib, M. (2009). Evaluation of Stochastic Reservoir Optimization Models. Advance Water Resources. (32), pp. 1429-1443.

Chaves, P., Kojiri, T. (2007) Stochastic fuzzy neural network: Case study of optimal reservoir operation. J Water Resources Planning Management. (133), pp.509–518.

Chuntian, C. (1999) Fuzzy optimal model for the flood control system of the upper and middle reaches of the Yangtze River. Hydrological Sciences. (44), pp.573–582.

Fang, H-B., HU, T-S., Zeng, X., Wu, F-Y. (2014). Simulation-Optimization model of reservoir operation based on target storage curves. Water Science and Engineering. (4), pp. 433-445.

Fawal, H., Georges, D., Bornard, G. (1998) Optimal control of complex irrigation systems via decomposition-coordination and the use of augmented Lagrangian Systems: Man, and Cybernetics, IEEE. pp. 3874–3879.

Finardi, E. C., Silva, E. L., Sagastizábal, C. (2005). Solving the unit commitment problem of hydropower plants via Lagrangian relaxation and sequential quadratic programming. Computer Application Math. (24), pp.317–342.

Jahandpour, M., Sandoval-Solis, S., Afshar, A. (2014). A web-based application for optimization of single reservoir operation. [online] p. E 509-E517. Available at: https://pdfs.semanticscholar.org/2658/74280aa8053ec7ee3b184ffca3e6eb73f5e5.pdf [Accessed 12 April. 2017].

Labadie, John W., "MODSIM: Decision Support System for Integrated River Basin Management" (2006). International Congress on Environmental Modelling and Software. [online] p. 242. Available at: https://scholarsarchive.byu.edu/cgi/viewcontent.cgi?article=3254&context=iemssconference [Accessed 9 May. 2017]

Louks, D. P., Van Beek, E., Stedinger, J, R., Dijkman, J. P. M., Villars, M. T. (2005). Water Resources System planning and Management: An introduction to Methods, Models and Applications, published by (UNESCO) United Nations Educational, Scientific and Cultural Organization, Italy. Available at: http://unesdoc.unesco.org/images/0014/001434/143430e.pdf [Accessed 12 May.2017]

Peng. C-S., Buras, N. (2000). Dynamic operation of a surface water resources system. Water Resources. (36), pp. 2701–2709.

Rani, D., Moreira, M., M. (2009) Simulation–optimization modeling: a survey and potential application in reservoir systems operation. Water Resources Management. (24), pp.1107–1138.

Rashid, K. A., Diacon, Al. G., Popa, B. (2007). Optimal Operation of Large Hydropower Reservoirs with Unregulated Inflows. UPB Sci. Bull, Series C, (69), pp. 2-11.

SMEC, (2006). Consultancy Services for Dokan and Derbendikhan Dam; Final Inspection Report.

ZANCO Journal of Pure and Applied Sciences
The official scientific journal of Salahaddin University-Erbil
ZJPAS (2018) **30**(s1)s168-s172
http://dx.doi.org/10.21271/ZJPAS.30.s1.19

Groundwater vulnerability to pollution assessment using two different models in Halabja Saidsadiq Basin, Iraq.

Twana O. Abdullah[1], Salahalddin S. Ali[2],Nadhir A. Al-Ansari[3] ,Sven Knutsson[4]

[1] Department of Geology, University of Sulaimani, Kurdistan Region, NE. Iraq and Department of Civil, Environmental and Natural Resources and Engineering, Division of Mining and Geotechnical Engineering, Lulea University of Technology, Sweden. Twana.abdullah@ltu.se
[2]President of University of Sulaimani, Kurdistan Region, NE. Iraq, salahalddin.ali@univsul.edu.iq
3&4Department of Civil, Environmental and Natural Resources and Engineering, Division of Mining and Geotechnical Engineering, Lulea University of Technology, Sweden, Nadhir.alansari@ltu.se , Sven.Knutsson@ltu.se

A R T I C L E I N F O

Article History:
Received: 08/04/2015
Accepted: 25/06/2015
Published:01/06/2018

Keywords:
Vulnerability
VLDA
COP
Nitrate concentration
Halabja Saidsadiq Basin (HSB)

**Corresponding Author:*
Email: twana.abdullah@ltu.se

A B S T R A C T

Halabja and Saidsadiq Basin (HSB) considered to be one of the most important basins in Kurdistan Region, NE of Iraq, in terms of groundwater aquifers. The concentration of economic, agricultural and social activities within the basin makes it of prime significance to the region. Therefore, groundwater contamination is of particular concern as groundwater resources are the principal source of water for drinking, agriculture, irrigation and industrial activities. Consequently, the most effective and realistic solution is to prevent the contamination of groundwater through. The current study aims the evaluation of the vulnerability of groundwater aquifers of the study area. Two models were applied, namely VLDA and COP to construct groundwater vulnerability maps for contamination. The VLDA model classified the area into four classes of vulnerability with each covered area: low (2%), moderate (44%), high (53%) and very high (1%).While four vulnerability classes were achieved based on COP model including very low, low, moderate and high vulnerability classes with coverage areas of (1%, 37%, 2% and 60%) respectively. To confirm the suitability of each map for assessment of groundwater vulnerability in the area, it required to be validated of the theoretical sympathetic of current hydrogeological conditions. In this study, nitrate concentration analysis was used as a contamination indicator to validate the result. Significant variations in nitrate concentration on dry to wet seasons had been observed. Accordingly, it can be stating that contaminant can be able to reach to groundwater aquifers in the HSB. Regarding to this validation, the result demonstrates that the vulnerability classes obtained using VLDA model are more consistent.

INTRODUCTION

Halabja and Saidsadiq Basin (HSB) considered to be one of the most important basins in Kurdistan Region, NE of Iraq, in terms of groundwater aquifers. The concentration of economic, agricultural and social activities within the basin makes it of prime significance to the region. Exhaustive agricultural activities are extensive and located close to groundwater wells, which pose

imminent threats to these resources. Moreover, the authoritative structure of Halabja has been changed from a district to governorate in March 2014; this will improve the start of more economic improvement and progression. In perspective of these progressions, there is an expansion of the quantities of human making a beeline for live in this basin and its surrounding areas. This is forcing a developing interest in water which has set significant weights on water resources. Therefore, groundwater contamination is of particular concern as groundwater resources are the principal source of water for drinking, agriculture, irrigation and industrial activities.

Groundwater vulnerability is evaluating the ability of pollutant to transport from the earth surface to reach a productive aquifer. The vulnerability studies can supply precious information about stakeholder working on preventing further deterioration of the environment (Mendoza & Barmen, 2006). To simplify the identification of the groundwater condition and to resist the pollutants in the reservoirs, several methods were recommended such as DRASTIC, VLDA, COP, GOD, SINTACS, etc. These different methods are offered under the form of numerical excerpt systems based on the negotiation of the different factors affecting the hydrogeological system (Attoui and Bousnoubra 2012).

Different vulnerability models were applied previously for the studied area; while it is very important to confirm the computed vulnerability model is reflecting the real vulnerability system for the area. So the main objective of the current study is to compare the achieved vulnerability map from two different models namely VLDA and COP, in order to select more sensible model to be applied for the area.

STUDY AREA

The study basin is located in the northeastern part of Iraq, geographically it is located between the latitude 35” 00 00" and 35" 36’ 00" N and the longitude 45” 36’ 00" and 46” 12’ 00" E (Figure 1). The entire study area is about 1278 square kilometers and its population of early 2015 of about 190,727. This basin divided into two sub-basins by (Ali,2007) including Halabja- Khurmal and Said Sadiq sub-basins. Approximately 57% of the studied area is an arable area due to its suitability for agriculture (Statistical Dtectorate, 2014).

GEOLOGY AND HYDROGEOLOGICAL SETTING

Different geological formations were exposed to the basin, these formations consists of limestone, dolomitic limestone and conglomerate which have an effective role in the vulnerability system in the basin. Alluvial (Quaternary) deposits are the most important unit in the area in terms of hydrogeological characteristics and water supply. The thickness of these deposits as observed by (Abdullah et al, 2015 a) of about nearly 300 m.

Hydrogeologically, different groundwater aquifers exist in the area based on its geological origin, table (1). The mountain series, which surround the basin of the northeast and southeast, are characterized by high depth of groundwater, while toward the center and the southeastern part, the groundwater level has a relatively lower depth. A groundwater movement is usually from high elevated areas at the north , northeast , south and southeast towards southwest or generally toward the reservoir of Derbandikhan Dam.

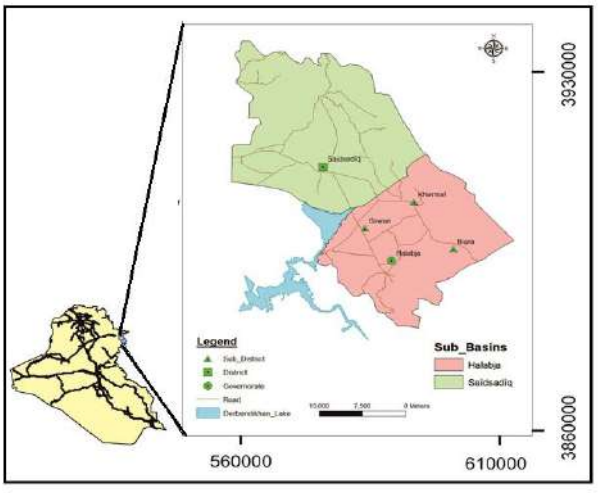

Fig. 1. Location map of study basin.

Table 1. Result of index ratio for all applied models.

Aquifer type	Geological formation	Thickness (m)
Intergranular	Alluvials	>300
Fissured	Balambo,Kometan	250
Fissured-Karstic	Avroman,Jurassic fn.	~200
Aquitard	Tanjero	~2000

METHODOLOGY

Two different models have been applied with the aid of GIS technique in order to map groundwater vulnerability in the study area. The first applied model is VLDA, predominantly it reflect lithology of vadose zone (V), pattern of land use (L), groundwater depth (D), and aquifer characteristics (A), (Zhou et al, 2012). In addition, reliable weight can be assigned to each of the four indexes depending on its impact on groundwater vulnerability.

The vulnerability comprehensive assessment index (DI) is the sum of the above-mentioned weighted four indexes, as computed conferring to the following formula:

$$DI = \sum_{j=1}^{4} (WijRij) \ldots\ldots\ldots\ldots (1)$$ (Zhou et al, 2012)

Where DI is the comprehensive assessment index , Wij is the weight of the j^{th} comprehensive assessment index of the i^{th} sub-system, Rij is the value of the j^{th} assessment index of the i^{th} subsystem; 4 is the quantity of indexes.

The lower the DI signifier to the lower vulnerability of the groundwater system and the superior the stability will be. To assess the groundwater vulnerability, the new corresponding weights in HSB were proposed using sensitivity analysis method (Abdullah 2015 b). Based on the result of sensitivity analysis, the proposed weights used for VLDA model measured as 8.2, 4.8, 5.2 and 4.8, and after normalization, the weight is 0.357, 0.209, 0.226 and 0.209, respectively, (Abdullah 2016 a).

The second applied model is COP; its contraction comes from the three initials of parameters namely flow Concentration(C), Overly layers (O) and Precipitation (P),(Vias et al,2006). The hypothetical basis of this strategy, as indicated by the European Approach (Daly et al, 2002) and (Goldscheider and Popescu, 2004), it is to evaluate the ordinary protection for groundwater (O variable) controlled by the properties of overly soils and the unsaturated zone, and also to measure how this assurance can be adjusted by diffuse, infiltration (C factor) and the climatic conditions (P Factor – precipitation). The COP-Index map was computed from equation 2,(Abdullah et al., 2016 b):

$$\text{COP Index Map} = C*O*P \ldots\ldots\ldots\ldots\ldots 2$$ (Vias et al,2006)

RESULTS AND DISCUSSION

Subsequent to the weighted scores were achieved for all parameters in each model, the GIS technique was used to combine all layers. The vulnerability result based on VLDA model, illustrates that a total of four ranges of vulnerability indexes had been distinguished ranging from low on very high, with vulnerability indexes (2.133-4 , >4-6, >6-8 and > 8), figure (2) . The area of low and very high vulnerability zones to occupy 2% and 1% of the whole study area respectively. The High vulnerability classes covered most of the mountains area that surrounding the area and the central part of HSB. This vulnerability zone covered an area of 53% of whole area. Furthermore, medium vulnerability zones to cover an area of 44% of all studied area and positioned southeast and northwest. Both high and moderate classes that occupied most of the studied basins refer to the exhaustive human activities, good water yield property and lithological composition of existed aquifers.

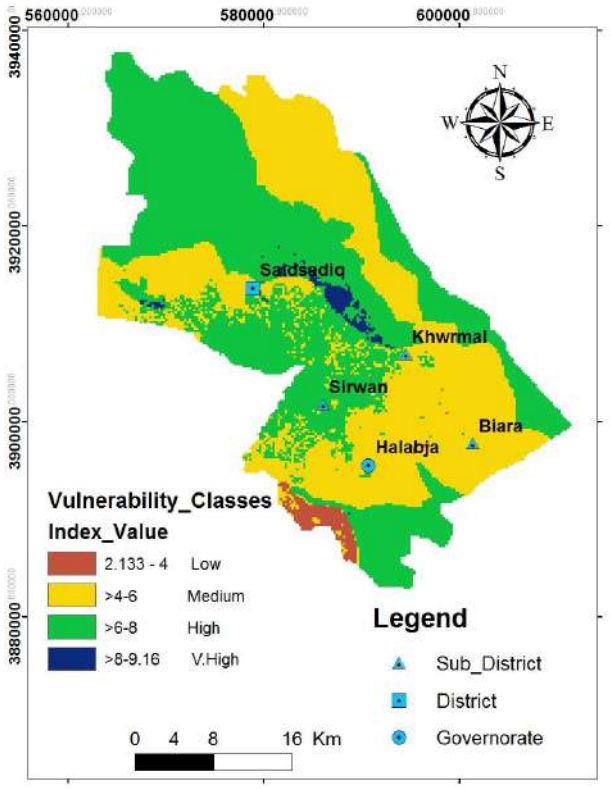

Fig. 2. VLDA Vulnerability Index Map of HSB.

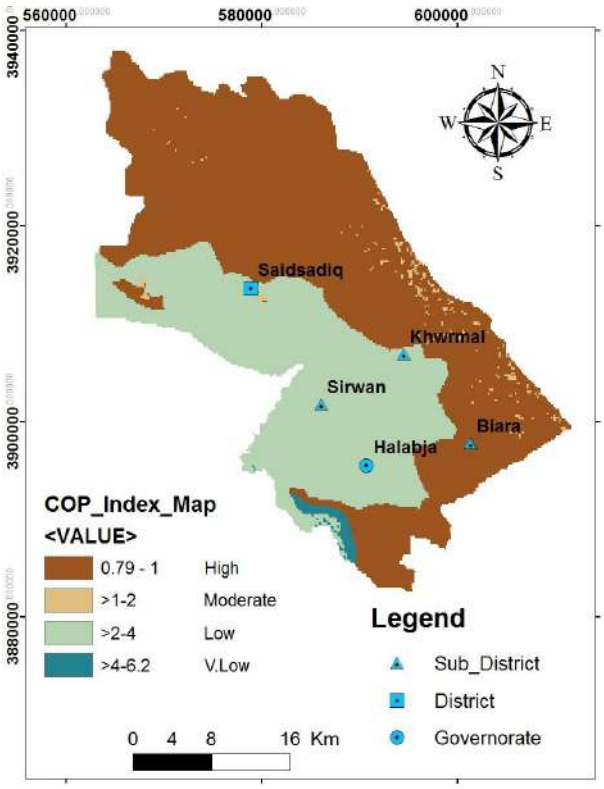

Fig. 3. COP Vulnerability Index Map of HSB.

Four categories of vulnerability ranging from very low to high be achieved according to the COP model, figure (3). High vulnerability areas covering an area of 60% of the entire HSB, geologically includes the fissure zone and minor carbonate karstic rocks. While the low vulnerability class comes in second place and occupies 37% of the entire region, this region is predominantly characterized by alluvial sediments. The area with moderate and very low vulnerable groups covers only 2% and 1% of the total area, respectively.

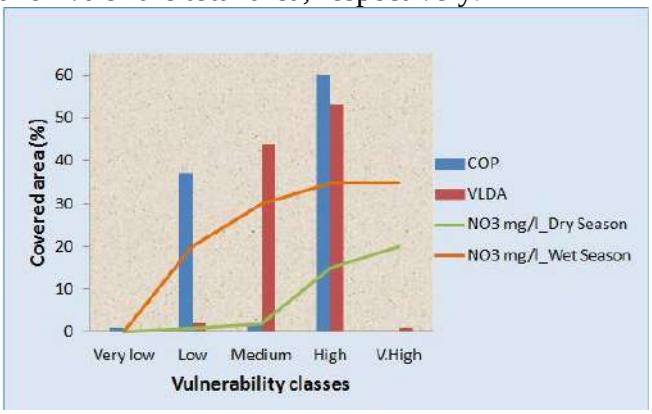

Fig.4. Comparison of all applied models with nitrate concentration

VALIDATION OF THE RESULT

Validation of vulnerability maps for these two models became mandatory because of considerable variation in vulnerability classes illustrated with all applied models. Therefore nitrate concentration analysis as a pollution indicator has been selected. In the exacting study case, the nitrate differences between two following seasons (dry and wet) were analyzed from (30) watering wells. The result exemplifies considerable variations in nitrate concentration on dry to wet seasons, figure (4). Based on this verification, it can be confirmed that aquifers in the HSB are able to receive contaminants because of its suitability in geological and hydrogeolological conditions. On the basis of this verification, the degree and distribution of the acquired vulnerability using a VLDA model is more logical than that of the COP model. With increased concentration of nitrates the levels of vulnerability also increased, because the land use patterns are considered to be one of the most effective factors of VLDA model and this parameter dose not included in the COP model.

CONCLUSION

Two different approaches have been applied to assess the potential groundwater vulnerability of HSB namely VLDA and COP models. The value of the VLDA indexes ranged from (2.133-9.16), and the value of the COP indexes ranged between (0.79-6.2). The high index value of the VLDA models means a higher category of vulnerability, while the value of the lower indicator of the COP model means a higher degree of vulnerability.

The vulnerability classes are clarified in the table (2), all models to clarify four vulnerability classes. COP model comprises (very low to high), while VLDA model embraces (low to very high) vulnerability classes. The noteworthy variation has been observed from all applied models, therefore the results required to be validated. Nitrate as a pollution indicator from agricultural processes can be supportive to distinguish the evolution and changes of groundwater quality. The result illustrates significant variations in nitrate concentration on dry to wet seasons. So it can be confirmed that groundwater in HSB is capable of receiving the pollutant. Based on this confirmation, figure (4) reveals that the degree and distribution of level of vulnerability obtained using the VLDA method is more sensible than that achieved from COP method.

Table 2. Type of aquifers in the study basin.

Vulnerability class	VLDA rate %	COP rate %
Very low	0	1
Low	2	37
Medium	44	2
High	53	60
V.High	1	0

REFERENCES

Ali S. S. (2007). Geology and hydrogeology of Sharazoor - Piramagroon basin in Sulaimani area, northeastern Iraq. Unpublished PhD thesis, Faculty of Mining and Geology, University of Belgrade, Serbia. 317P.

Attoui B, Kherci N, Bousnoubra H (2012). State of vulnerability to pollution of the big reservoirs of groundwater in the region of Annaba-Bouteldja (NE Algeria). Geographia Technica. 2:1-13.

Abdullah T. O. , Ali S.S., Al-Ansari N.A. and Knutsson S. (2015a). Effect of agricultural activities on groundwater vulnerability: Case study of Halabja Saidsadiq Basin, Iraq. Journal of Environmental Hydrology 23(10).The open access electronic journal found at http://www.hydroweb.com/protect/pubs/jeh/jeh2015/AnsariGW.pdf

Abdullah, T.O., Ali, S.S., Al-Ansari, N.A. and Knutsson, S. (2015b). Groundwater Vulnerability Mapping using Lineament Density on Standard DRASTIC Model: Case Study in Halabja Saidsadiq Basin, Kurdistan Region, Iraq. Engineering, 7, 644-667. http://dx.doi.org/10.4236/eng.2015.710057.

Abdullah, T.O., Ali, S.S., Al-Ansari, N.A. and Knutsson, S. (2016a). Assessing the vulnerability of groundwater to pollution using DRASTIC and VLDA models in Halabja Saidsadiq Basin, NE - Iraq.. Journal of Civil Engineering and Architecture 10 (2016) 1144-1159, doi: 10.17265/1934-7359/2016.10.006.

Abdullah, T.O., Ali, S.S., Al-Ansari, N.A. and Knutsson, S. (2016b). Groundwater Vulnerability Using DRASTIC and COP Models: Case Study of Halabja Saidsadiq Basin, Iraq. Engineering, 8, 741-760. http://www.scirp.org/journal/PaperInformation.aspx?PaperID=71681.

Daly D, Dassargues A, Drew D, Dunne S, Goldscheider N, Neale S, Popescu C, Zwhalen F .(2002) Main concepts of the "European Approach" for (karst) groundwater vulnerability assessment and mapping. Hydrogeol J 10(2):340–345.

Goldscheider, N. and Popescu, C. (2004) The European Approach. In: Zwahlen F (ed) Vulnerability and risk mapping for the protection of carbonate (karst) aquifers. European Commission, Brussels, pp 17–21.

Jassim S.Z. and Guff J.C. (2006) Geology of Iraq. Jassim (Eds) D. G. Geo Survey. Min. Invest. Publication. 340p.

Mendoza JA, and Barmen G., (2006): Assessment of groundwater vulnerability in the Rio Artiguas Basin, Nicaragua. Environmental Geology 50: 569_580.

Statistical Directorate in Sulaimaniyah,(2014).Archive Department.

Vias J.M.,Andreo B., Perles M.J. , Carrasco I., Vadillo P. and Jim'enez P., (2006). Proposed method for groundwater vulnerability mapping in carbonate (karstic) aquifers: the COP method. Application in two pilot sites in Southern Spain. Hydrogeology Journal (2006) 14: 912–925. DOI 10.1007/s10040-006-0023-6.

Zhou J. , Li Q. ,Guo Y. , Guo X. , Li X., Zhoa Y. and Jia R. (2012). VLDA model and its application in assessing phreatic groundwater vulnerability: a case study of phreatic groundwater in the plain area of Yanji County, Xinjiang, China. Environmental Earth Science Journal Vol.67 .pp. 1789-1799.